Institute of Physical Chemistry
Polish Academy of Sciences
01-224 Warsaw, Poland

Spin Relaxation in Magnetic Nanostructures

PhD thesis

by

Ehsan Barati

Supervisor: *Dr. hab. Marek Cinal*

A-21-2, A-21-7, A-21-13, K-g-150, K-g-184, H-53
H-69

This dissertation was prepared within the International PhD in Chemistry Studies at
the Institute of Physical Chemistry of the Polish Academy of Sciences in Warsaw.

Warsaw, November 2014

INNOVATIVE ECONOMY
NATIONAL COHESION STRATEGY

FNP
Foundation for Polish Science

EUROPEAN UNION
EUROPEAN REGIONAL
DEVELOPMENT FUND
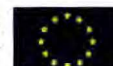
ACKNOWLEDGMENTS

First of all, I gratefully acknowledge the essential guidance of my PhD supervisor Dr. hab. Marek Cinal, who helped me a lot during different stages throughout my PhD. Undoubtedly, I would not have been able to prepare a thesis of this standard without his guidance and help.

I have been very fortunate in being able to meet Professor David Edwards in the Department of Mathematics at Imperial College, London

and

Dr. Andrey Umerski in the Department of Mathematics and Statistics at the Open University, Milton Keynes.

So, I would also like to express my thanks to them for their hospitality during my visits to these two British universities where this project was partly done. They made my stays in England highly enjoyable by providing a very friendly academic atmosphere.

Words cannot express my feelings to my parents: my mother who has always been my symbol of hope

and

my father who was my greatest hero.

My sincerest thanks to them for their unfailing support.

To Leyla

Open the eye of the heart,
to witness what cannot be seen,
to hear what no ear has even heard,
what no eye has ever seen,
cleaving a particle,
it would be observed a sun therein.

Hatef Esfahani (18th A. D.)

ما آزموده‌ایم در این شهر بخت خویش

http://rcin.org.pl

Contents

Abstract

The thesis presents theoretical investigation of spin relaxation in magnetic nanostructures within the quantum-mechanical approach, including novel methods developed in this PhD project. The Gilbert damping constant α which enters the Landau-Lifshitz-Gilbert (LLG) equation describing the dynamics of magnetisation is found for bulk ferromagnetic transition metals and various ultrathin magnetic metallic layered systems employing the torque-correlation model by Kamberský. The expression for α is generalised to an arbitrary direction of magnetisation. Calculations are performed within a realistic tight-binding model including the spin-orbit interaction and their efficiency is remarkably improved by introducing finite temperature into the electronic occupation factors and subsequent summation over the Matsubara frequencies. Furthermore, two alternative formulas, not limited to the TB model, for α in terms of the Green function are derived. The results are reported for bulk ferromagnets, ferromagnetic films, ferromagnet/nonmagnet (Co/NM) bilayers (NM=Cu, Pd, Ag, Pt and Au) as well as NM/Co/NM, Co/NM1/NM2 trilayers, $L1_0$ Co/NM superlattices (ordered alloys) and $[\text{Co/NM}]_N$ multilayers. The obtained dependence of α on the electron scattering rate for bulk Fe, Co and Ni is in good agreement with the previous *ab initio* calculations. The dependence of α on Co and NM thicknesses and the effect of the nonmagnetic caps are investigated and found to be in accord with experiment. The calculated α in Co/NM bilayers and Co/NM1/NM2 trilayers is enhanced due to adding the nonmagnetic caps, particularly in the case of NM, NM2=Pd and Pt. This enhancement is explained by the large spin-orbit coupling of such NMs, combined with their large density of states at the Fermi level ϵ_F. The enhancement in Co/NM1/Pt trilayers is shown to decay with the increasing thickness of the spacer NM1=Cu and Ag. Nonlocal origin of the damping enhancement is proved by visualising large contributions to α from the nonmagnetic part. Contributions to α from individual atomic layers and its $\boldsymbol{k}$-space distribution are determined and analysed in several layered systems. It is revealed that in the Co/NM bilayers including NM metal with the d band crossing ϵ_F the major contributions to the Gilbert damping come from a few atomic layers in the NM close to the Co/NM interfaces, whilst for those with NM d bands below ϵ_F the main contributions originate from the Co part. Investigations in the $\boldsymbol{k}$-space show the existence of hot spots in the Brillouin zone that give the largest contributions to α. Additionally, the nonadiabatic spin-transfer torque coefficient β entering an extended form of the LLG equation is calculated for bulk ferromagnets and ferromagnetic films. Its evaluation method is improved by using the Hellmann-Feynman theorem to calculate the electron velocity. In each case, comparison with results of other theoretical approaches, such as the *ab initio* calculations and the spin pumping theory, as well as experiment is performed.

Streszczenie

W rozprawie zostały przedstawione teoretyczne badania relaksacji spinu w nanostrukturach magnetycznych w oparciu o podejście kwantowo-mechaniczne, zawierające nowe metody opracowane w obecnym projekcie. Stała tłumienia Gilberta α, występująca w równaniu Landaua-Lifszyca-Gilberta (LLG) opisującym dynamikę magnetyzacji, jest wyznaczona dla objętościowych ferromagnetycznych metali przejściowych oraz różnych ultracienkich magnetycznych metalicznych układów warstwowych przy użyciu modelu Kamberskiego wykorzystującego funkcję korelacji momentu siły. Wyrażenie na α zostało uogólnione na przypadek dowolnego kierunku magnetyzacji. Obliczenia zostały przeprowadzone przy użyciu realistycznego modelu ciasnego wiązania uwzględniającego oddziaływanie spin-orbita, a ich efektywność poprawiona przez wprowadzenie skończonej temperatury do czynników obsadzeniowych i sumowanie po częstościach Matsubary. Ponadto otrzymano dwa alternatywne wyrażenia na α zależne od funkcji Greena. Uzyskano wyniki dla objętościowych ferromagnetyków, warstw ferromagnetycznych, dwuwarstw ferromagnetyk/niemagnetyk (Co/NM) (NM=Cu, Pd, Ag, Pt and Au) oraz układów trójwarstwowych NM/Co/NM, Co/NM1/NM2, supersieci $L1_0$ Co/NM (stopów uporządkowanych) i wielowarstw $[\text{Co/NM}]_N$. Otrzymana zależność α od współczynnika rozpraszania elektronów dla objętościowych Fe, Co i Ni jest zgodna z uprzednimi obliczeniami *ab initio*. Zbadano zależność α od grubości Co i NM oraz wpływ warstw niemagnetycznych i stwierdzono ich zgodność z obserwacjami eksperymentalnymi. Obliczona wartość α w układach dwuwarstwowych Co/NM i trójwarstwowych Co/NM1/NM2 ulega zwiększeniu w wyniku pokrycia kobaltu warstwami niemagnetycznymi, szczególnie w przypadku NM, NM2=Pd i Pt. Wzrost ten został wyjaśniony przez silne sprzężenie spin-orbita w tych niemagnetykach, w połączeniu z dużą gęstością stanów na poziomie Fermiego ϵ_{F}. Pokazano, że wzmocnienie tłumienia Gilberta w układzie Co/NM1/Pt ulega zanikowi wraz ze wzrostem grubości warstwy buforowej NM1=Cu i Ag. Nielokalne pochodzenie wzmocnienia tłumienia magnetycznego zostało wykazane przez wizualizację dużego wkładu warstwy niemagnetycznej do stałej α. Wkłady do α pochodzące od poszczególnych warstw atomowych oraz rozkład α w przestrzeni wektora falowego $\boldsymbol{k}$ zostały wyznaczone i analizowane dla różnych układów warstwowych. Stwierdzono, że w dwuwarstwach Co/NM z NM o paśmie d przecinającym ϵ_{F} główny wkład do tłumienia Gilberta pochodzi od kilku warstw atomowych w NM blisko powierzchni międzywarstwowej Co/NM, zaś dla układów z NM o paśmie d leżącym poniżej ϵ_{F} wkład ten pochodzi od warstwy Co. Analiza w przestrzeni $\boldsymbol{k}$ ujawniła istnienie niewielkich „gorących" obszarów strefy Brillouina dających największy wkład do α. Dodatkowo obliczono, dla ferromagnetyków objętościowych i warstw ferromagnetycznych, współczynnik β nieadiabatycznego momentu siły związanego z transferem spinu, wchodzący do rozszerzonej postaci równania LLG. Metoda obliczania tego współczynnika została ulepszona przez zastosowanie twierdzenia Hellmana-Feynmana do wyznaczania prędkości elektronowych. W każdym przypadku otrzymane rezultaty porównano z wynikami innych metod teoretycznych, takimi jak obliczenia *ab initio* i teoria pompowania spinowego, oraz wynikami eksperymentalnymi.

Chapter 1

Introduction

It was the after study of Uhlenbeck and Goudsmit that an intrinsic angular momentum of electron called spin was discovered (1925) [1], although it was already observed in the Stern-Gerlach experiment (1922) [2]. The concept of spin has played a key role in quantum description of physical and chemical phenomena. In particular, the magnetic properties of materials originate from spins of electrons and their orbital motion (nuclear magnetic moments, about 10^3 times smaller than the electron magnetic moment, are usually neglected in solid state physics, though they are at the heart of some physical effects like nuclear magnetic resonance which is used to investigate atomic configurations of molecular systems). Apart from electronic current which is due to the charges of electrons and serves as the basis of electronics, moving electrons can also form spin current which has to be taken into account in theories of electronic transport in magnetic materials. There are two main differences between a spin current and a charge current: unlike charge current, spin current is invariant under time reversal and it is associated with a vector quantity which is the angular momentum. Intensive efforts have been made to employ and manipulate the internal spin degree of freedom giving rise to many applications in spintronics that is a fascinating field which has emerged in the two recent decades [3, 4, 5].

Properties of magnetic materials are mainly determined by the orientation of electronic spins which can exhibit a long-range order as in ferromagnets, antiferromagnets, ferrimagnets and magnetic helical structures or be only locally ordered as in spin glasses. Ferromagnets are materials with spontaneous macroscopic magnetisation (collective magnetic moment per unit volume due to electronic spins) which is present below the Curie temperature T_c whilst above this critical temperature the long-range order is distorted by thermal fluctuations and, as a result, magnetisation vanishes. Ferromagnetism originally results from a compromise between atomic-like exchange interactions and interatomic hybridisation. The former tend to align spins

1

and the latter tends to lower the kinetic energy by reducing the spin polarisation. Magnetisation in ferromagnetic transition metals is formed by spins of localised electrons from the d band. In the absence of external magnetic fields, the equilibrium magnetic configuration of a ferromagnet below T_c has the form of the domain structure where in each domain the nonzero magnetisation is uniform (homogenous) and aligned along one of the directions corresponding to magnetic easy axes, specific to the ferromagnet, its crystallographic lattice and the sample geometry. The domain configuration in equilibrium corresponds to the minimum value of the total energy of the whole ferromagnet which includes terms due to magnetic dipole-dipole interaction, magneto-crystalline anisotropy (MCA) as well as the energy of the domain walls (DWs) which depends on the strength of the exchange interaction. In the presence of an applied magnetic field, the boundaries of magnetic domains change so that some domains grow and others shrink which finally leads to the monodomain state with fully saturated magnetisation along the direction of the field when it becomes very large (of the order of a few Teslas). The magnetisation orientation in magnetic materials, in particular, has the capacity to be used in information technology, in magnetic storage devices like hard-disk drives, in particular.

Conservation of angular momentum results in very interesting phenomena in magnetic materials. As already mentioned above, an electric current (moving charges) passing through a magnetic material can lead to a spin current (moving spins) due to different numbers of conduction electrons with spin up ($\hbar/2$) and spin down ($-\hbar/2$) where $\hbar$ is the reduced Planck constant. Thus, spin currents due to conducting sp electrons can carry a net angular momentum which can be transferred to the magnetisation due to d electrons in other parts of the system. This phenomenon is known as the spin-transfer torque (STT). The total angular momentum of the system remains conserved during such spin transfer process. The physical effect reverse to the STT is the emission of a spin current by precessing magnetisation in a ferromagnet/nonmagnet (FM/NM) system. This effect is predicted by the spin pumping theory [6, 7] which is discussed in more detail below.

Both the STT and spin pumping can have strong effect on the magnetisation dynamics. In particular, in a FM/NM/FM spin-valve structure the direction of magnetisation in the free ferromagnetic layer can be reversed (switched) by passing electric current as long as its density is sufficiently large. The STT effect is also crucial for current-induced motion of magnetic DWs in ferromagnetic nanowires. Such dynamic magnetic processes are profoundly affected by how fast a precessing magnetisation can relax to its equilibrium direction, which depends on magnetic damping phenomena due to either spin-flip scattering or other processes that change spin angular momentum. Magnetic damping is commonly present in real materials since the factors

2

from which it originates, like the spin-orbit (SO) interaction combined with electron scattering on lattice vibrations and defects, are unavoidable. Theoretically, magnetic relaxation in ferromagnetic metallic systems is usually assumed to be governed by the so-called Gilbert damping which enters the phenomenological Landau-Lifshitz-Gilbert (LLG) equation [8, 9] describing the dynamics of magnetisation in such systems. This and some other spin relaxation mechanisms are discussed in more detail below.

Magnetic damping plays a crucial role in magnetic systems, in particular those with layered structures. Such damping is also the mechanism through which energy dissipates in magnetic systems, therefore it is responsible for energy loss (transfer from macroscopic motion of magnetisation to microscopic thermal motion of atomic lattice). The torque due to the damping opposes the macroscopic driving torque due to a time-dependent oscillatory external magnetic field or spin polarised current and then the net energy loss or gain is achieved by the compromise between these two torques. This phenomenon occurs particularly in current-carrying FM/NM/FM spin-valve structures with one ferromagnetic free-layer whose magnetisation precesses around an applied static magnetic field. It has also been proposed that considering the Gilbert damping is the only way to explain the angular dependence of the peak-to-peak ferromagnetic resonance (FMR) spectra linewidth [10].

Controlling magnetic damping in nanostructured materials is of great interest. It has been shown that the presence of magnetic damping is crucial for propagation of DWs along a magnetic nanowire [11]. In particular, it determines the DW velocity in current-carrying domain wall (CCDW) structures where fast propagation of DWs is of great importance for applications in high-speed spintronic devices such as magnetic racetrack memory [12]. One of the key points in application of CCDW structures is the critical (minimum) electric current or critical magnetic field required for depinning the domains. The magnetic damping also determines the operational characteristics of STT-based devices. The switching current in such systems is proportional to the damping constant. Thus, the Gilbert damping is a key factor in understanding magnetisation dynamics in magnetic nanostructures.

Transition metal multilayers built of ferromagnetic and nonmagnetic ultrathin layers (with thicknesses of a few nanometers) have attracted a great deal of interest in recent decades since they have several unique magnetic properties that make them particularly suitable for application in existing and future spintronic devices [13, 14]. It was after discovery of interlayer exchange coupling in 1986 [15] that magnetic layered nanostructures began to attract many scientists to this area. The 2007 Nobel Prize in physics, thereafter, went to Grünberg and Fert for the discovery of the giant magnetoresistance (GMR) which followed the discovery of antiferromagnetic

coupling in an Fe/Cr/Fe system [16, 17]. The GMR effect has also been reported theoretically alongside its discovery in 1988; see Refs. [18, 19, 20] for more details. The interlayer exchange coupling is the coupling between ferromagnetic layers separated by a thin nonmagnetic (or antiferromagnetic) layer like in Co/Cu/Co (or Fe/Cr/Fe) trilayers. As a result the directions of magnetisations in the two ferromagnetic layers can be either parallel or antiparallel depending on the sign of the coupling. The strength of this coupling depends on the nonmagnetic spacer layer and it has been shown to oscillate with its thickness [21, 22]. The GMR effect is referred to as a large change in electrical resistance of FM/NM/FM spin valves as the directions of magnetisations in the two ferromagnetic layers are switched from parallel to antiparallel [23, 24]. The resistivity for the antiparallel magnetic configuration (R_{AP}) is larger than for the parallel configuration (R_P) due to large mismatch of energy bands for majority and minority spins in the FM. The GMR effect is characterised by the ratio (R_{AP}-R_P)/R_P which can be as large as $40 - 60\%$ at room temperature [25, 26, 27].

A similar system built of an ultrathin insulator layer sandwiched between two ferromagnetic metallic layers is known as magnetic tunnel junction (MTJ) in which the magnetisation direction plays a crucial role in the electrical resistivity. The parallel or antiparallel configuration of magnetisations of the two ferromagnetic layers in MTJs results in low or very high resistivity (R_P or R_{AP}), respectively. This is due to different quantum tunneling of electrons through the insulator barrier for the two magnetic configurations and, therefore, it is known as the tunnel magnetoresistance (TMR) effect, discovered in 1975 [28]. In this case, the ratio $\frac{R_{AP}-R_P}{R_P}$ can be very large, more than 1100% at 4.2 K and about 600% at room temperature [29], so that it is much larger than in the GMR effect. The paper by Mathon and Umerski [30] on tunneling properties of an Fe/MgO/Fe system in 2001, reporting over 1000% TMR ratio, also illustrates the point. Thus, the TMR effect is an excellent practical example of electron tunneling predicted by quantum mechanics (see Ref. [31] for a detailed review).

Magnetic layered systems can also exhibit a large perpendicular magnetic anisotropy (PMA) [32, 33, 34, 35, 36] and an enhanced magnetic damping [37, 38, 39]. In particular, this concerns Co/NM bilayers including Co/Pd and Co/Pt bilayers which have been intensively studied [40, 41, 42] due to both their large magneto-optical Kerr rotation and large PMA. The PMA effect corresponds to the out-of-plane orientation of magnetisation, i.e., perpendicular to the film surface. The origin of this effect is the SO interaction combined with the reduced symmetry at FM/NM (and FM/vaccum) interfaces. This can lead to an increase of the MCA term of magnetic anisotropy energy so that it can dominate the shape anisotropy term for ultrathin films. The possible mechanisms of the magnetic damping enhancement and other relevant experimental

reports are discussed in further parts of this introduction as well as in chapter 2.

Employing magnetic multilayers, including combinations of ferromagnetic and nonmagnetic layers, in spintronic devices has lead to a great leap in data storage and data transfer technology. This includes, in particular, the use of GMR-based read heads in computer hard drives. The occurrence of the GMR effect in FM/NM multilayers makes such systems suitable for application even in biochemistry, e.g., as magnetic biosensors [43]. The application of MTJ structures in magnetic random access memory (MRAM) has also made them being of primary interest for data transfer and data storage technology.

Different mechanisms have been assumed to be responsible for the relaxation of magnetisation in magnetic layered systems. Apart from the Gilbert damping [44, 45], the two-magnon scattering [46, 47] and spin pumping [6, 7] are also proposed to account for such a relaxation.

The existence of imperfections in magnetic samples can give rise to scattering of magnons from the uniform mode to two or more nonuniform modes as it can occur in FMR, for instance. In other words, magnons are coupled together by scattering of FMR uniform magnetisation precession mode which is usually called two-magnon scattering. Two-magnon scattering is an extrinsic effect which arises due to lattice imperfections like surface roughness, defects or disorder and it is important in films rather than bulk ferromagnets since such defects are likely to occur in layered systems due to their growth process. This effect is especially remarkable in the case of long-wavelength spin waves for which scattering centres are of atomic scale themselves. Therefore, unambiguously, structural defects and disorder are essential factors in spin relaxation processes. Two-magnon scattering is a common theoretical explanation of spin relaxation in ferrites [48] and has been shown that it can be also utilised for metallic films [49].

It has turned out that the observed FMR linewidth ΔH (due to damping) in magnetic thin films can be accounted for by the two-magnon scattering effect merely at nonzero magnetic field (being shutted off as the field and, subsequently, the FMR frequency approach zero) and for films with in-plane magnetisation (being quenched with magnetisation tipping out of the plane). More specifically, the two-magnon scattering contribution to the FMR linewidth is shown to be completely quenched when the angle between the magnetisation and the film plane is larger than 45° (in particular, for magnetisation perpendicular to the film surface) [47]. Thus, the two-magnon scattering is disregarded for films with out-of-plane direction of magnetisation [50] and in this case the magnetisation dynamics is governed solely by the Gilbert damping, both intrinsic and extrinsic in the spin pumping scenario described below. Although it has been assumed that the two-magnon mechanism can be responsible for the extrinsic damping (extra observed FMR linewidth in comparison with bulk value of ΔH), it has been shown that two-magnon scattering

cannot explain film thickness dependence of the FMR linewidth in magnetic layered systems [51]. Thus, another scenario, namely nonlocal Gilbert damping is of main interest in such systems. Furthermore, it has been shown that considering the nonlocal Gilbert damping, alongside the two-magnon scattering, is indispensable in Co/Pt multilayers to explain the angular dependence of FMR linewidth [52].

The presence of the nonlocal damping in magnetic multilayers was first explained, theoretically, by Berger [45]. The mechanism of damping enhancement proposed by him is based on an idealised picture where conduction sp electrons are coupled by exchange to localised d electrons forming magnetic moments in the ferromagnet and carry spin through the FM/NM interface to the nonmagnet where it is dissipated. As mentioned above, a similar, though partly phenomenological, theoretical description of spin transport in magnetic layered systems that is usually referred to is the spin pumping theory [6, 7]. In this theory, the effective magnetic damping in such systems is assumed to be the sum of intrinsic damping (bulk value) plus a term due to the spin pumping ($\alpha = \alpha_{\mathrm{b}} + \alpha_{\mathrm{pump}}$) [6, 7, 55]. The observed enhanced damping in a magnetic layered system is then explained by the transfer of angular momentum from its ferromagnetic part to the nonmagnetic or antiferromagnetic part, through the interfaces. Interfaces play a crucial role in many phenomena in magnetic layered systems. In particular, magnetisation, as it precesses, pumps a spin angular momentum through the interfaces into adjacent materials. The pumped spin angular momentum is transferred and dissipated in the nonmagnetic part. The rate of dissipation depends on the nature of the adjacent nonmagnetic metal. If the adjacent metal is a perfect spin sink (such as Pt or Pd), the spin accumulation in it is negligible which means that the transferred spin angular momentum is almost totally absorbed in the nonmagnetic part. But, if a poor spin sink (such as Ag or Cu) is used as the adjacent nonmagnetic metal the transferred angular momentum is not fully absorbed and there is a backflow of this momentum into the ferromagnet. That is because of the large spin-diffusion length of such nonmagnetic metals which does not allow the spin angular momentum to be totally absorbed in the nonmagnetic part which gives rise to a substantial spin accumulation and consequently a backflow of spin.

The spin-diffusion length of the nonmagnet is a known major factor in such extrinsic (nonlocal) damping process since to achieve the effective relaxation of magnetisation due to spin pumping in FM/NM bilayers the thickness of the nonmagnetic layer has to be greater than its spin-diffusion length [39]. If two nonmagnetic layers are used to form a FM/NM1/NM2 trilayer, the spin-diffusion length of the spacer layer (NM1) plays the dominant role [53]. The pumped spin current in magnetic multilayers, which gives rise to the damping enhancement, depends on the spin-diffusion length of the nonmagnet as well as it is inversely proportional to the thickness

of the ferromagnetic film [6, 7, 54, 55]. In Ref. [6] the spin pumping model for the enhanced Gilbert damping in an NM/FM/NM system has been proposed and compared with experiment.

The spin pumping theory proposed in Refs. [6, 7] is now commonly used in interpretation and analysis of magnetic damping experimental results [39, 54, 56, 57, 58]. It has also been applied in first-principle calculations of the Gilbert damping in Fe/Au bilayers and trilayers [59] with the nonmagnetic Au layers assumed to be perfect spin sinks. Although the spin pumping theory provides a simple explanation of nonlocal magnetic damping taking place in nonmagnetic metals in contact with ferromagnetic metals, it does not include a quantum description of the SO coupling responsible for spin relaxation in the nonmagnetic part of the system. Instead, the relaxation mechanism is represented only with a phenomenological spin-flip relaxation time. On the other hand, the spin pumping theory accounts merely for the extrinsic damping, and not the intrinsic damping, in magnetic layered systems. Thus, fully quantum calculations including the SO coupling, like the torque-correlation model, should give an insight into the damping processes on a more fundamental level.

Except for the aforementioned theories that account for the spin relaxation in magnetic systems, each with its own limitations, no fully quantum-mechanical calculation in magnetic multilayers has yet been addressed. In this thesis, a quantum-mechanical description is presented and it is found to account for the observed nonlocal magnetic damping in magnetic layered systems, in accordance with experimental measurements and predictions of the spin pumping theory. Thus, calculation of the Gilbert damping constant α is the central topic of this thesis.

A long time ago (1935), a landmark paper by Landau and Lifshitz [60] followed by a later work by Gilbert [8], provided a prototype for phenomenological description of magnetic damping. They proposed a fundamental equation of motion for the magnetisation in magnetic materials, known as the Landau-Lifshitz-Gilbert (LLG) equation. This phenomenological equation, in its original or extended form, is now widely used to describe dynamics of nonuniform magnetisation. In the recent decades, a great effort has been made to use spin-polarised electric current, a current with nonequal numbers of spin up and spin down electrons, in spintronic devices. The properties of such currents have been studied by both theoreticians and experimentalists working in the realm of spintronics. One of these properties is the interaction of a spin-polarised electric current and magnetic DWs in current carrying ferromagnetic metals. Such interaction can be investigated with an extended form of the LLG equation including different terms, each responsible for a different aspect of the magnetisation dynamics, as it will be discussed in detail in the next chapter. The torque due to the magnetic field is followed by the damping term including the Gilbert damping constant α as the prefactor. The torque arising from the Gilbert damping

pushes the magnetisation towards its equilibrium direction. Two other terms in the extended LLG equation are due to the flowing spin current and are known as the adiabatic STT and nonadiabatic STT which is accompanied by the coefficient β [61, 62]. The latter torque appears to be more effective in narrow DWs [63].

As explained above, the two coefficients α and β are present in an extended LLG equation which describes the dynamics of magnetisation in the presence of external magnetic field and electric current flowing through the system. Thus, both coefficients determine the spin relaxation in magnetic metallic structures. In particular, they affect the DW velocity (proportional to β/α) in current-carrying ferromagnetic systems where fast propagation of DWs is desired. Moreover, the nonadiabatic STT, particularly, is one of the main factors which affects the threshold current needed for depinning DWs in such structures. The mutual relation between the two dimensionless coefficients α and β is the subject of yet inconclusive debate. The claim [64, 65] of their equality, $\beta = \alpha$, is seriously challenged by experimental data [66] and few available theoretical results for bulk metals [67, 68]. Calculation of β in magnetic layered systems is the second (minor) topic of this thesis in addition to the evaluation of α.

Experimentally, the Gilbert damping constant can be gained from the peak-to-peak linewidth of the microwave absorption peak, ΔH, measured in the FMR spectroscopy,

$$\Delta H(\omega) = \Delta H(0) + \Delta H_{\text{Gil}} + \Delta H_{\text{2mag}} \tag{1.1}$$

where $\Delta H_{\text{Gil}} = \alpha \frac{\omega}{\gamma}$ (γ is the gyromagnetic ratio). The two-magnon contribution ΔH_{2mag} saturates for larger $\omega = 2\pi f$ and thus the damping constant α is acquired from the slope of ΔH against the resonance frequency f [69, 70]. Alternatively, the so-called effective damping parameter can be found from the relation $\alpha_{\text{eff}} = (2\pi f \tau)^{-1}$ with τ as the relaxation time [71, 72].

The Gilbert damping and its enhancement have been the main subjects of numerous experiments. In Ref. [37], using the FMR technique for tetragonal Ni films on Cu(001) substrate, an enhanced magnetic damping, in comparison to bulk Ni, has been reported. Such an enhancement has also been observed in bcc Fe films on Ag(001) [73] as well as in Cu/Py/Cu/Pt and Cu/Py/Cu layered structures [10]. FMR measurements were also applied to study the magnetisation relaxation in Fe_3Si and $Fe_{20}Si_{80}$ films [74] as well as the Gilbert damping parameter $G = \gamma M_s \alpha$ (where M_{s} is the saturation magnetisation) in $Fe_x Co_{1-x}$ alloy films, and Co/Cu(001) films for the magnetic field applied in the direction of either hard or easy axes of magnetisation [75]. Further, an increase of the Gilbert damping in $[Co/Pt]_N$ multilayer films with increasing stacking number N has been demonstrated using time-resolved magneto-optical Kerr effect (TRMOKE)

[76]. In Ref. [77], the TRMOKE technique has been used to measure the Gilbert damping constant in $L1_0$ ordered-alloy FePdPt films. Experimental reports on the Gilbert damping and its enhancement in some other layered systems with FM/NM interfaces can be found, e.g., in Refs. [39, 55, 57, 58, 78, 79, 80, 81, 82].

Early theoretical work on the Gilbert damping has done by Kamberský and dates back to 1976 [44, 83]. He established a quantum-mechanical approach to the Gilbert damping in magnetic materials by introducing two different models for the damping process, namely the breathing Fermi surface model and the torque-correlation model, which will be discussed in more detail later in this thesis. The two models are based on the usual assumption that the Gilbert damping has origin in the SO interaction. This relativistic effect causes spin-flip scattering of electrons which gives rise to transfer of angular momentum and energy from spin degrees of freedom to the lattice. The SO interaction is also an essential factor in spin relaxation processes in magnetic systems which are of main interest in the present work. It also largely affects the magnetic anisotropy (leading to its magnetocrystalline contribution in thin films which can dominate the shape anisotropy) and it is at the heart of the spintronic effects such as the spin Hall effect or the Rashba effect.

There have been other theoretical methods of investigating spin relaxation, reported later on, such as direct calculation of the spin relaxation torque [84], which includes the effect of the SO coupling on magnetic damping, or determination of spin-wave spectrum within the random-phase-approximation [85, 86]. Also, the expression for the damping constant α in the torque-correlation model has been re-derived [68, 87], or directly applied [88, 89, 90, 91], in several theoretical studies for bulk ferromagnets, half metals [92], transition metal binary alloys [90], $Fe_{1-x}Si_x$ films [93] as well as, very recently, surfaces of ferromagnetic metals [91]. In Ref. [61] considering the solution for a long-wavelength spin-wave in a one-band model, Edwards and Wessely found expressions for various coefficients in an extended LLG equation. Despite all these theoretical reports, the quantum-mechanical approach has hardly been used to study the Gilbert damping and its enhancement in transition metal layered systems (apart from Ref. [91] and recent paper by the present author [94]) and the underlying physics of the enhanced magnetic damping in layered structures is not yet fully understood.

The prime purpose of this PhD thesis is calculation of the Gilbert damping constant α and the nonadiabatic STT coefficient β in bulk ferromagnetic metals as well as various magnetic nanostructures such as metallic films and multilayers. The particular attention is paid to the enhancement of the Gilbert damping in various magnetic layered structures, such as FM/NM bilayers. The research in the present PhD project is focused on two aspects. One is theoretical

contributions to the quantum theory of spin relaxation whilst the other is calculations of the coefficients α and β for different systems and development of methods for analysis of the obtained results.

The Gilbert damping constant α is found with the general expression originally obtained by Kamberský [44]. An alternative derivation of this expression by Edwards [113] is presented in the present work. It is obtained by comparing frequency of the long-wave solution of the LLG equation with complex spin wave energy found within a time-dependent linear-response quantum-mechanical approach. The determination of the nonadiabatic STT coefficient β is based on a quantum-mechanical expression derived by Gilmore *et al.* [67] but slightly modified by employing the Hellmann-Feynman theorem for calculation of electron velocities defined as derivatives of band energies with respect to the wave vector. The calculations of both α and β are performed within a realistic nine-band tight-binding (TB) model [95] with the SO coupling included. The expressions for α and β obtained in the TB model can be utilised at both zero and finite temperature and they are applicable to a wide variety of magnetic structures. The so-called Matsubara frequencies are, particularly, employed for evaluation of α and β at finite temperature. With these expressions established, one is able to investigate α and β in magnetic layered systems, e.g., their dependences on layer thicknesses and the electron scattering rate. The expression for α is presently extended to arbitrary direction of magnetisation. Thus, an explicit quantum-mechanical expression for the damping constant α in bulk and layered magnetic system with arbitrary direction of magnetisation is obtained. Its alternative form in terms Green functions is also determined. Furthermore, an explicit formula for the contributions to the damping constant α from individual atomic layers is found. Taking the advantage of this formula, it is feasible to visualise and explain the nonlocality aspect of the Gilbert damping, related to spin pumping, in magnetic layered systems.

Calculation of α and β for the considered magnetic systems required numerical integration over the Brillouin zone (BZ). The author's own Fortran codes have been developed and applied for calculation of electronic structure (quantum states and their energies), layer-projected density of states as well as coefficients α and β for the considered magnetic layered systems.

The results for Gilbert damping constant α are reported for bulk iron, cobalt and nickel, purely ferromagnetic metallic films, cobalt/nonmagnet (Co/NM) bilayers, NM/Co/NM and Co/NM1/NM2 trilayers, $L1_0$ [Co/NM] superlattices (ordered alloys) as well as [Co/NM]$_N$ magnetic mulilayers. The dependence of α on the electron scattering rate Γ as well as on thicknesses of ferromagnetic and nonmagnetic layers is investigated and compared with recent experiments. The effect of the SO coupling on the Gilbert damping constant in Co/NM bilayers is also stud-

ied by modifying the SO coupling of the constituent NM metals. Finally, to shed light on the obtained results, layer contributions from various atomic layers in a slab as well as $\boldsymbol{k}$-point contributions coming from various $\boldsymbol{k}$-points in the BZ to the Gilbert damping are also analysed.

The present thesis is organised in five chapters as follows:

After chapter 1 with the introductory survey of the thesis' field and its main objectives, chapter 2 reads the basic concepts of the magnetisation dynamics, theoretical framework and mathematical tools whereby the Gilbert damping constant α is calculated. In this chapter an expression for α is derived, which is in fact a re-derivation of Kamberský's formula, and the applied TB model of electronic structure is presented. Moreover, in section 2.7 of this chapter an expression for α in terms of Green functions is obtained. Chapter 3 deals with the calculation of the Gilbert damping constant α in various magnetic nanostructures. The dependence of magnetic damping on the magnetisation direction is also discussed in this chapter. Chapter 4 includes breakdown of the Gilbert damping in real space (atomic layer contributions for which an explicit expression is derived) and momentum space ($\boldsymbol{k}$-point contributions). In chapter 5, based on the results of Ref. [67] an expression for nonadiabatic STT coefficient β is obtained within the TB model and calculations of β for bulk ferromagnets and ferromagnetic films are presented. The thesis is ended with the summary and four brief appendixes.

Chapter 2

Theory

2.1 Spin-transfer torque and domain wall motion

The faster manipulation of spin, lower energy cost than in charge manipulation as well as application in atomic-scale magnetic memories make spin-based (spintronic) systems promising candidates for future electronic devices. Fundamental to these systems are spin currents which have specific properties not found in charge currents. In particular, unlike charge currents $J = J_\uparrow + J_\downarrow$, the spin currents $J_s = J_\uparrow - J_\downarrow$ decay during propagation in current carrying systems ($J_\uparrow$ and $J_\downarrow$ correspond to spin-up and spin-down electrons, respectively). They are retained only within the scale of a few micrometers. Spin currents can propagate through magnetic systems even if there is no net charge current. Beside accompanying charge currents, pure spin currents can also be carried by spin waves or induced in the spin Hall effect (SHE) [96]. Such pure spin currents can be detected, e.g., by the inverse SHE in which an electric current is induced using spin current. Understanding the occurrence and properties of pure spin current is the topic of many recent works [97, 98]. Spin currents are behind many novel magnetic phenomena in layered systems.

In ferromagnetic nanostructures there exist domains with different directions of magnetisation. Regions where the magnetisation changes its direction are known as domain walls. The finite width of DWs is a result of the compromise between exchange energy and magnetic anisotropy, so it is different for different systems. It is usually of the order of 10-100 nm (100-150 atoms) but it can be as thin as a few nm in nanowires [99]. DWs can be moved through a magnetic structure (e.g., a nanowire) by two means: electric current and magnetic field. The velocity of a magnetic DW depends on the magnitude of applied magnetic field or the intensity of the flowing electric current.

When electrons flow through a magnetic DW structure the net spin angular momentum, carried by the spin current, can be transferred to the local magnetisation, a phenomenon known

as the STT. In other words, as the spin-polarised current passes through a magnetic system it exerts a torque on the magnetisation. This torque, perpendicular to the local magnetisation of the ferromagnet and applied by conduction electrons onto the ferromagnet, is the so-called STT. As already mentioned in the introduction the same effect is present in FM/NM/FM trilayers where the electron current passes from a thick ferromagnetic layer through the nonmagnetic metal spacer into a thin ferromagnetic layer. In all these processes there are a few major torques engaged: the precessional torque, due to the effective magnetic field, the STT and the damping torque. Magnetisation reversal (switching) occurs, e.g., in spin-torque-MRAMs, if the STT overcomes the damping torque. Since, the STT is not merely limited to metallic ferromagnets (but can be also present in antiferromagnets and semiconductors) and is subject to interfacial effects in magnetic multilayers like MTJs, its occurrence has opened a new playground for research with applications in the growing field of spintronics. There also exists a phenomenon opposite to the STT, the so-called spin pumping effect in which precessing magnetisation emits a spin current [7].

The occurrence of the STT leads to the following scenario in the case of a DW. As itinerant electrons pass through a DW, the electron spins precess and their angular momentum undergoes a change. The flow of spin angular momentum is changed due to the torque exerted on the flowing spins (spin-polarised current) by the magnetisation. To compensate this effect, an equal but opposite torque must be exerted on the ferromagnet by the flowing charge carriers so that the total angular momentum of the system is conserved. Thus the angular momentum of the traversing electrons is transferred to d electrons localised on magnetic ions and changes the directions of magnetic moments. The change of local magnetisation direction due to this transferring process has an immediate implication on the displacement of the DW known as current-induced DW motion. That is how a DW moves by means of an electric current. DWs motion can be achieved without any applied magnetic field if the density of the applied current exceeds a threshold value known as the Walker breakdown, proportional to the DW width and the Gilbert damping constant. Seeking materials with lowest Walker breakdown (such as magnetic semiconductors) is one of the most interesting objectives in spintronics.

A massive study has been launched in recent years on controlling the DWs' motion [12, 100, 101]. This is due to their ability to be employed in data storage devices in which propagating magnetic DWs (regions of nonuniform magnetisation) can serve as bits of information. In particular, displacement of DWs is the subject of an intensive and promising research on racetrack memories developed by Stuart Parkin's group at IBM. They have been proposed to be competitors for the new high capacity hard disk drives, a GMR based technology that brought Parkin

the 2014 Millennium Technology Prize.

2.2   Damped precession, Landau-Lifshitz-Gilbert equation

The configuration of magnetisation (as a function of position) at equilibrium is given by (nonlinear) Brown's equations which correspond to the condition that at equilibrium there is no torque exerted on magnetisation by the effective magnetic field. These equations arise as a result of minimizing the total energy of the system at equilibrium which leads to formation of stable domain structures.

To get an insight into the magnetisation states out of the equilibrium one can first use the similarity with classical or semi-classical model of spinning top. A spinning charged particle like an electron posseses a magnetic moment which interacts with an applied magnetic field. The equation of motion for such a particle with the total angular momentum $\boldsymbol{J}$ ($\boldsymbol{J} = \boldsymbol{S} + \boldsymbol{L}$, with spin $\boldsymbol{S}$ and orbital angular momentum $\boldsymbol{L}$) is expressed as (in CGS units)

$$\frac{\partial \boldsymbol{J}}{\partial t} = \gamma \boldsymbol{J} \times \boldsymbol{H}_{\text{eff}} \tag{2.1}$$

where $\gamma = \frac{e}{2m_0 c}g = -\frac{|e|}{m_0 c}g = -\frac{g\mu_{\text{B}}}{\hbar} = -|\gamma|$ is the electron gyromagnetic ratio (dependent on the Landé g-factor g) with e as the electron (negative) charge, m_0 as its mass, $\hbar$ as the reduced Planck constant, c as the light velocity in vacuum and μ_{B} as Bohr magneton. $\boldsymbol{H}_{\text{eff}} = \boldsymbol{H} + \boldsymbol{H}_{\text{ex}} + \boldsymbol{H}_{\text{k}}$ is an effective (externally applied $\boldsymbol{H}$, exchange $\boldsymbol{H}_{\text{ex}}$, anisotropy $\boldsymbol{H}_{\text{k}}$) magnetic field, which can be found from the negative gradient of the Gibbs free energy with respect to the magnetisation $\boldsymbol{M}$. Knowing that $\boldsymbol{M} = \gamma N \boldsymbol{J}$ (N is the number of magnetic moments per unit volume in the system), an analogous equation for magnetisation $\boldsymbol{M}$ can be written as

$$\frac{\partial \boldsymbol{M}}{\partial t} = \gamma \boldsymbol{M} \times \boldsymbol{H}_{\text{eff}}. \tag{2.2}$$

According to this equation the change of the magnetisation $\boldsymbol{M}$ in the unit of time t is equal to the torque exerted on $\boldsymbol{M}$ by the effective field $\boldsymbol{H}_{\text{eff}}$. This torque vanishes at equilibrium when $\boldsymbol{M}$ is parallel to $\boldsymbol{H}_{\text{eff}}$. This equation can also be obtained within the quantum-theoretical approach as follows.

In ferromagnetic metals the spontaneous magnetisation comes almost entirely from the spin of electrons since their net orbital moments are quenched due to periodic potential. This quenching is perfect in the absence of the SO interaction whilst its presence restores a small orbital

component of the total angular momentum. If the SO interaction is neglected, the Hamiltonian of an N-electron system is given by

$$H = H_{\text{kin}} + H_{\text{ext}} + H_{\text{ee}} + H_Z \tag{2.3}$$

where $H_{\text{kin}} = \frac{\hbar^2}{2m_0} \sum_{i=1}^N p_i^2$ is the kinetic energy, $H_{\text{ext}} = \sum_{i=1}^N e\, V_{\text{ext}}(\boldsymbol{r}_i)$ represents the interaction of electrons with the electric field $\boldsymbol{E} = -\nabla V_{\text{ext}}(\boldsymbol{r})$ coming from the nuclei and external sources, $H_{\text{ee}} = \frac{1}{2} \sum_i \sum_{i \neq j} \frac{e^2}{|\boldsymbol{r}_i - \boldsymbol{r}_j|}|$ is the Coulomb interaction between electrons, and lastly

$$H_Z = -\gamma \sum_{i=1}^N \boldsymbol{S}_i \cdot \boldsymbol{B} - \frac{1}{2}\gamma \sum_{i=1}^N \boldsymbol{L}_i \cdot \boldsymbol{B} = -\gamma \boldsymbol{S}_{\text{tot}} \cdot \boldsymbol{B} - \frac{1}{2}\gamma \boldsymbol{L}_{\text{tot}} \cdot \boldsymbol{B} \tag{2.4}$$

is the Zeeman term. Here, $\boldsymbol{S}_{\text{tot}}$ and $\boldsymbol{L}_{\text{tot}}$, the operators of total spin and orbital angular momenta, respectively, are composed of individual electronic spins $\boldsymbol{S}_i$ and angular momenta $\boldsymbol{L}_i$. The equation of motion for the spin operator $\boldsymbol{S}_{\text{tot}}(t) = e^{iHt/\hbar} S_{\text{tot}} e^{-iHt/\hbar}$ (in the Heisenberg picture) gives

$$\frac{d\boldsymbol{S}_{\text{tot}}}{dt} = \frac{1}{i\hbar}\left[\boldsymbol{S}_{\text{tot}}, H\right] = \frac{1}{i\hbar}\Big[\sum_{j=1}^N \boldsymbol{S}_j, H_Z\Big] = \frac{1}{i\hbar}(-\gamma) \sum_{i=1}^N \left[\boldsymbol{S}_i, \boldsymbol{S}_i \cdot \boldsymbol{B}\right] \tag{2.5}$$

since only the Zeeman term in the Hamiltonian depends on spins $\boldsymbol{S}_i$. The x-component of the commutator can be expressed as follows [102],

$$
\begin{aligned}
\left[S_i^x, \boldsymbol{S}_i \cdot \boldsymbol{B}\right] &= \left[S_i^x, S_i^x B_x + S_i^y B_y + S_i^z B_z\right] \\
&= \left[S_i^x, S_i^y\right] B_y + \left[S_i^x, S_i^z\right] B_z = i\hbar S_i^z B_y - i\hbar S_i^y B_z \\
&= -i\hbar\, (\boldsymbol{S}_i \times \boldsymbol{B})_x.
\end{aligned} \tag{2.6}
$$

where the commutation rules for the spin operators S_i^x, S_i^y, S_i^z are used. In a similar way, it is found that

$$\left[S_i^y, \boldsymbol{S}_i \cdot \boldsymbol{B}\right] = -i\hbar\, (\boldsymbol{S}_i \times \boldsymbol{B})_y, \tag{2.7a}$$

$$\left[S_i^z, \boldsymbol{S}_i \cdot \boldsymbol{B}\right] = -i\hbar\, (\boldsymbol{S}_i \times \boldsymbol{B})_z \tag{2.7b}$$

so that the equation of motion takes the form

$$\frac{d\boldsymbol{S}_{\text{tot}}}{dt} = \gamma\, \boldsymbol{S}_{\text{tot}} \times \boldsymbol{B}. \tag{2.8}$$
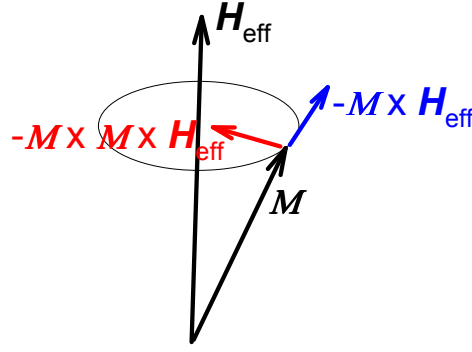
15

Figure 2.1: Damped precession of magnetisation $\boldsymbol{M}$ in the presence of effective magnetic field $\boldsymbol{H}_{\text{eff}}$.

If the total magnetic moment $\boldsymbol{M}_{\text{tot}}$ comes from electron spins, like in metallic ferromagnets, this moment is given by the expectation value $\boldsymbol{M}_{\text{tot}} = \gamma \langle \boldsymbol{S}_{\text{tot}} \rangle$ of the total spin operator $\boldsymbol{S}_{\text{tot}}$. This value is equal to $\langle 0 | \boldsymbol{S}_{\text{tot}} | 0 \rangle$ in the ground state $|0\rangle$ or to the trace $\text{tr}(\rho \text{S}_{\text{tot}})$ including the density matrix ρ at finite temperature. In both cases the classical equation for the precession of magnetisation

$$\frac{d\boldsymbol{M}}{dt} = \gamma \, \boldsymbol{M} \times \boldsymbol{B}, \qquad \boldsymbol{M} = \boldsymbol{M}_{\text{tot}}/V \;\; (V \text{ is the system volume}) \tag{2.9}$$

is now obtained within the quantum-mechanical approach.

To better describe dynamics of the magnetisation in metallic systems, different phenomenological damping terms have been added to the equation of motion (2.9). The first attempt to include damping in modeling magnetisation dynamics in metals was carried out by Landau and Lifshitz in 1935 [60]. Their proposed equation, known as Landau-Lifshitz (LL) equation, reads

$$\frac{\partial \boldsymbol{M}}{\partial t} = -|\gamma| \boldsymbol{M} \times \left(\boldsymbol{H}_{\text{eff}} + \frac{\lambda}{M^2} \boldsymbol{M} \times \boldsymbol{H}_{\text{eff}} \right) \tag{2.10}$$

where λ is the damping parameter which is material specific. The first term of the LL equation describes the torque that leads to the magnetisation precession and the second term is the damping torque in response to this precession. The latter works as a centripetal force that pushes the magnetisation to be aligned with the effective magnetic field (see Fig. 2.1). The LLG equation well describes the magnetisation dynamics when the damping is small, but it appears to be problematic for large damping rates. Thus, providing a more flexible equation was of significant importance.

Later on (in 1955) Gilbert proposed a modified version of the LL equation known nowadays

as the Landau-Lifshitz-Gilbert (LLG) equation

$$\frac{\partial \boldsymbol{M}}{\partial t} = -|\gamma| \boldsymbol{M} \times \left(\boldsymbol{H}_{\text{eff}} + \frac{\alpha}{M^2} \frac{\partial \boldsymbol{M}}{\partial t} \right) \tag{2.11}$$

In this equation, the damping term is modified if compared to the LL equation. However, the LL equation and its version modified by Gilbert (LLG equation) are equivalent and the respective damping parameters are connected with each other by the relation $\lambda = \frac{\gamma \alpha}{1+\alpha^2}$ [9]. The LLG equation is more practical for describing the magnetic damping in metallic systems. Let us note that the LLG equation describes a dynamical magnetic system in which the magnitude of the magnetisation remains unchanged, and therefore the magnetisation vector evolves on a sphere implying that the module $M = |\boldsymbol{M}|$ of the magnetisation is preserved.

Noteworthy is remarking that the LLG equation is a nonlinear differential equation which, in general, can be solved numerically by the finite difference method. However, it can also be solved analytically for some special problems [103, 104, 105]. An example of an analytical solution of the LLG equation is a spin wave, with wave vector $\boldsymbol{q}$, propagating along the x axis (see [61] for details)

$$\boldsymbol{m} = \left(c\, e^{i(qx-\omega t)}, d\, e^{i(qx-\omega t)}, -1 \right) + c.c., \qquad c, d \ll 1\,. \tag{2.12}$$

The parameter $\boldsymbol{m} = \boldsymbol{M}/M_{\text{s}}$ is the magnetisation vector $\boldsymbol{M}$ normalised to its saturation value M_{s} and $c.c.$ denotes the complex conjugate. The spin wave frequency $\omega = \omega_1 - i\omega_2$ is complex when finite damping is present in the LLG equation. The spin wave with infinitely large wave length, i.e., with the zero wave vector $q = 0$, corresponds to uniform precession of magnetisation. In such a case, the real part of $\omega = \omega(q = 0)$ is the Larmor precession frequency $\omega_1 = |\gamma| H_{\text{eff}}$ whilst the imaginary part $\omega_2 = \alpha\, \omega_1$ is proportional to the Gilbert damping constant α. It is seen that according to Eq. (2.12) the m_x and m_y components decay as $e^{-\omega_2 t}$ with time t. Thus, the magnetisation $\boldsymbol{M}$ corresponding to a spin wave relaxes to its equilibrium direction $(0, 0, -1)$ with the lifetime $1/\omega_2 \sim 1/\alpha$. Physically, the relaxation of spin waves in metals can result from the SO interaction. Then, the relation $\alpha = \frac{\omega_2(q=0)}{\omega_1(q=0)}$ can be used to find the damping constant if the complex spin frequency ω is obtained in a quantum-mechanical method with the SO interaction included. This will be performed in the next section where a quantum-mechanical expression for the imaginary part ω_2 of a long-wavelength spin wave is found (see Sec. 2.3).

The knowledge of the spin-wave frequency $\omega(q)$ for small q can also be used to determine other parameters appearing in extended forms of the LLG equation. Such method has been applied in the work by Edwards and Wessely [61] where $\omega(q)$ found in one-band model is compared with a spin-wave solution of an extended LLG equation. They presented a quantum-mechanical

approach in which expressions for various coefficients of the extended LLG equation have been obtained by finding expressions for the real and imaginary parts of the spin wave energies in the long wavelength limit (i.e., small q). In this method, coefficients of different powers in q stand for different aspects of the spin wave propagation. In the lowest order ($q = 0$) the real part of the spin wave energy is given by the Larmor frequency ω_1, but to find the imaginary part ω_2 one needs to calculate the corresponding dynamical susceptibility of the system. The Heisenberg's equation of motion is used to find an explicit expression for the dynamical susceptibility. The poles of the dynamical susceptibility are nothing but the spin wave energies $\omega = \omega_1 - i\omega_2$. In this way, the damping constant can be found as $\alpha = \omega_2/\omega_1$ (at $q = 0$) by comparing the spin wave energies calculated quantum-mechanically and obtained from the spin-wave solution of the LLG equation.

In the presence of the non-uniform magnetisation the usual extension of the phenomenological LLG equation describing the magnetisation dynamics of metallic systems has the following form

$$\frac{\partial \boldsymbol{m}}{\partial t} = -|\gamma|\,\boldsymbol{m} \times \boldsymbol{H}_{\text{eff}} + \alpha\,\boldsymbol{m} \times \frac{\partial \boldsymbol{m}}{\partial t} + 2A\,\boldsymbol{m} \times \frac{\partial^2 \boldsymbol{m}}{\partial x^2} - v_0\frac{\partial \boldsymbol{m}}{\partial x} + \beta v_0\,\boldsymbol{m} \times \frac{\partial \boldsymbol{m}}{\partial x} \quad (2.13)$$

where A stands for the exchange stiffness constant. The first term in Eq. (2.13) describes Larmor precession of magnetisation around the effective magnetic field $\boldsymbol{H}_{\text{eff}}$, applied externally and/or arising due to magnetic anisotropy. This field can be found as $\boldsymbol{H}_{\text{eff}} = -\frac{\partial U}{\partial \boldsymbol{M}}$ where U is the magnetic energy (or the Gibbs free energy at finite temperature). It is followed by the relaxation term proportional to the dimensionless Gilbert damping constant α. This damping term acts as a torque that pushes the magnetisation toward the effective field. The remaining terms in Eq. (2.13) are effective only for non-homogenous magnetisation $\boldsymbol{m}(x)$ (varying with the position x) as in spin waves or DWs. The fourth and the fifth terms, introduced by Zhang and Li [106, 107], describe adiabatic and nonadiabatic STT, respectively. They both arise due to the electric current J, with finite spin polarization P in ferromagnets, and are defined by the parameter $v_0 = g\mu_{\text{B}}PJ/(2|e|M_{\text{s}})$ [108]. Although it is known that the DW velocity is independent of the adiabatic term, it can be controlled by the nonadiabatic term which is known to be more effective for narrow DWs [63]. It can be shown [107] that uniform DW motion can be driven by a current with velocity $v = (\beta/\alpha)v_0$. Both α and β are therefore important in magnetisation dynamics and it is noteworthy that they both depend on the SO coupling. In this thesis, however, the main focus is on the damping constant α, though β is also addressed briefly in chapter 5. Other terms shown in Eq. (2.13) can also be included in further extensions of the LLG equation [61].

Magnetic damping is also the mechanism through which energy (irreversibly) dissipates in

18

magnetic systems. Although it is already known that a moving DW in a magnetic nanowire dissipates energy due to the Gilbert damping [11], there is still no accepted recipe for the relation between the energy dissipation rate and the DW velocity. The energy dissipates solely when the magnetisation is not parallel to the effective magnetic field, i.e., the first term in Eq (2.13) is nonzero. Based on the Walker special mobility formula the energy dissipation rate is inversely proportional to the Gilbert damping constant. On the other hand, there are some other works testifying that DW velocity is proportional to the energy dissipation rate and, therefore, an enhancement of the energy dissipation will speed up the DW propagation [11].

Calculation of the damping constant α is highly desirable since it plays a key role in magnetisation dynamics of magnetic systems. As already discussed in the introduction (chapter 1), there have been a few different approaches to describe the magnetic damping with models based on various physical processes. Some of the proposed mechanisms are intrinsic to the material, such as those due to magnetoelastic scattering, and others are considered extrinsic like two-magnon scattering from lattice imperfections [46, 47] or the spin pumping in FM/NM structures [7]. It has emerged that the torque-correlation model by Kamberský [44], based on electron-hole pair generation due to the SO interaction in the presence of lattice vibrations, describes the dominant source of intrinsic damping in a variety of magnetic systems including the ferromagnetic semiconductors [109] and transition metals [88].

The magnetic damping in magnetic nanostructures can be split into two terms: intrinsic (size-dependent) damping and extrinsic (size-independent) damping. The former is, usually known as the bulk value of the damping, due to the SO coupling and interactions of electrons with magnons or phonons, whilst the latter is due to spin pumping or two-magnon scattering by defects or imperfections in the system. What is measured in experiment as the magnetic damping is the total (intrinsic + extrinsic) damping known sometimes as the effective damping. The extrinsic damping arises basically in layered structures where the damping alters with changing thickness of the system. The extrinsic damping is of particular interest in magnetic layered systems like FM/NM bilayers, since it originates from the nonlocal damping in the nonmagnetic parts of the system. In a FM/NM bilayer, for example, the magnetisation is present in the ferromagnetic part FM, but the relaxation (damping) of this magnetisation can be affected by the presence of nonmagnetic part NM. In other words, the magnetic moment precesses in the FM but it can be damped mainly in the NM. This effect is particularly strong if the NM part is a perfect spin sink, like Pt or Pd. Such nonlocality of the magnetic damping can also be seen in spin valves or trilayer systems with different NM spacer and cap metals, as it will be shown in the present thesis (see Sec. 3.5). According to the spin pumping theory the nonlocal damping in FM/NM

bilayers is related to the spin-diffusion length of the NM part and it is inversely proportional to thickness of the FM layer. To achieve an effective nonlocal damping the thickness of the NM metal has to be comparable to its spin-diffusion length. Further discussion on spin pumping in FM/NM bilayers can be found in Sec. 3.4.

Another possible source of the magnetic damping in layered structures is eddy currents [110]. The contribution to the damping in layered systems caused by the eddy currents is proportional to square of the film thickness and that is why it is assumed to be negligible in ultrathin magnetic films and, therefor, it is disregarded in this thesis. Note also that, the threshold film thickness below which the eddy currents can be neglected varies with metal (about 25 nm for Fe but about 100 nm for Py).

It is also worth mentioning that the Gilbert damping in magnetic layered systems is altered for magnetisation along different crystallographic axes. It is only slightly modified for (001), (110) and (111) surfaces of fcc Co, for instance [91]. Also in Ref. [111] the Gilbert damping has been investigated experimentally in Fe/V multilayer samples with the magnetic field along different crystallographic directions. Therein, it has been shown that the the Gilbert damping is significant for [110] and [001] directions. In this thesis, however, except for Sec. 3.7 that is devoted to the Gilbert damping for arbitrary direction of magnetisation, the Gilbert damping is calculated for bulk cubic metals with magnetisation along the [001] axis and films with out-of-plane magnetisation.

2.3   Quantum mechanical approach to Gilbert damping

The first proposed expression for the Gilbert damping constant dates back to 1976 to the works by Kamberský [44]. He introduced two different models for the magnetic damping process: the breathing Fermi surface model and the torque-correlation model, which lead to the same results in the low scattering rate limit [88]. The breathing Fermi surface model leads to an expression for the damping constant in terms of electron scattering lifetime and derivatives of electron energies with respect to the spin direction. This model correctly predicts the damping at low temperature limit corresponding to low scattering rate. The magnetic damping in the torque-correlation model stems from two types of electron transitions between energy bands: intraband (diagonal) transitions and interband (off-diagonal) transitions. The diagonal (intraband) elements of the SO torque operator, appearing in the torque-correlation model, can be written in terms of the electron energy derivatives appearing in the breathing Fermi surface model. A direct connection between parameters appearing in the breathing Fermi surface model and the torque-correlation

model can be found in [88].

In the torque-correlation model, set up nearly 40 years ago [44], the magnetic damping is attributed to the SO interaction, as the physical factor that does not conserve spin, combined with electron-lattice scattering. The latter turns out to strongly affect the magnetic damping since the scattering of electrons on lattice vibrations (phonons) leads to broadening of electronic quantum energy levels and, thus, a finite lifetime of electron states. Kamberský's original derivation of the expression for the Gilbert damping constant α is based on comparison of the transverse magnetic susceptibility found from the LLG equation with the formula obtained for this susceptibility in the random phase approximation (RPA) within the linear-response theory. The effect of the electron-lattice scattering is included in an approximate way based on the coherent potential approximation (CPA).

Below, Kamberský's formula is rederived in a similar way, but different significantly in details which makes the derivation clearer in the author's opinion. Such derivation was introduced by Edwards and Wessely [61] for one-band model with a spin dependent potential to mimic H_{SO} and later extended by Edwards [113] to a general case of multi-band system with the full SO interaction H_{SO}. It is done by comparing the complex frequency $\omega = \omega_1 - i\omega_2$ of the spin-wave solution of the LLG equation with the frequency of a long-wavelength spin wave propagating in a many-electron quantum system.

A system of N electrons in an external magnetic field $\boldsymbol{B} = (0, 0, -B_{\mathrm{ext}})$ is described with the semi-relativistic many-electron Hamiltonian

$$H = H_{\mathrm{kin}} + H_{\mathrm{ee}} + H_{\mathrm{ext}} + H_{\mathrm{Z}} + H_{\mathrm{SO}} \tag{2.14}$$

where the consecutive terms stand for the kinetic energy, the electron-electron interaction energy, the interaction of electrons with electric field due to nuclei and/or external sources, the Zeeman interaction, respectively, all defined below Eq. (2.3), and finally the SO interaction

$$H_{\mathrm{SO}} = \sum_{i=1}^{N} \xi \boldsymbol{L}_i \cdot \boldsymbol{S}_i \tag{2.15}$$

with the SO coupling constant ξ. The Zeeman interaction, Eq. (2.4), can be written as

$$H_{\mathrm{Z}} = -2\mu_{\mathrm{B}} B_{\mathrm{ext}} S_z - \mu_{\mathrm{B}} B_{\mathrm{ext}} L_{\mathrm{tot}}^z \tag{2.16}$$

and it depends on the z component $S_z = \sum_{i=1}^{N} S_i^z$ of the total spin $\boldsymbol{S}$ composed of individual electronic spins S_i^z (hereafter, in this section and in Appendix B the index "tot" is skipped in $S_{\mathrm{tot}}^z = S_z$ and $S_{\mathrm{tot}}^{\pm} = S^{\pm}$ for simplicity). The SO interaction term, Eq. (2.15), is written here in

a simplified form (its full form is discussed in Sec. 2.5). In the present Hamiltonian (particularly in its Zeeman and SO terms) as well as in the following part of this thesis, it is assumed that the angular momentum is measured in units of the Planck constant $\hbar$ so that the spin and orbital angular momentum operators $\boldsymbol{S}$ and $\boldsymbol{L}$ are dimensionless. The minus sign of the z component of the external field $\boldsymbol{B} = (0, 0, -B)$ is chosen to have the usually assumed positive sign of the total electron spin $\langle S_z \rangle$ in the case of a ferromagnetic electronic system. The total spin magnetic moment $-2\mu_B \langle S_z \rangle$ is then negative due to the negative electron charge e.

The time-dependent transverse component $\boldsymbol{M}_\perp(\boldsymbol{r}, t) = (M_x, M_y, 0)$ of magnetisation in a ferromagnetic spin system subject to a magnetic field $\boldsymbol{B}_\perp(\boldsymbol{r}, t) = (B_x, B_y, 0)$ perpendicular to the magnetisation direction at equilibrium and oscillating in time and space can be determined within the linear-response theory. The corresponding response function is the transverse dynamical susceptibility $\chi_\perp(\boldsymbol{q}, \omega)$ that links the applied transverse field of the frequency ω and the wave vector $\boldsymbol{q}$ to the amplitude of the induced transverse magnetisation $\boldsymbol{M}_\perp(\boldsymbol{q}, \omega) = \chi_\perp(\boldsymbol{q}, \omega) B_\perp(\boldsymbol{q}, \omega)$. The following expression is obtained for this susceptibility within the time-dependent linear-response theory [112],

$$\chi(\boldsymbol{q}, \omega) = \int dt \, \langle\langle S_{\boldsymbol{q}}^-(t), S_{-\boldsymbol{q}}^+(0) \rangle\rangle \, e^{-i\omega_- t} \tag{2.17}$$

with $\omega_- = \omega - i\eta$ $(\eta \to 0^+)$ and the operator $S_{\boldsymbol{q}}^\pm = \sum_n e^{i\boldsymbol{q}\cdot\boldsymbol{r}_n} S_n^\pm$. The factor appearing under the integral in Eq. (2.17) is given by

$$\langle\langle S_{\boldsymbol{q}}^-(t), S_{-\boldsymbol{q}}^+(0) \rangle\rangle = \frac{i}{\hbar} \langle [S_{\boldsymbol{q}}^-(t), S_{-\boldsymbol{q}}^+(0)] \rangle \, \theta(t) \tag{2.18}$$

where $\langle X \rangle$ denotes the average of the operator X defined, at finite temperature T, as the trace $\mathrm{tr}(\rho X)$ with the density matrix operator $\rho = e^{-\beta H}/\mathrm{tr}(e^{-\beta H})$, $\beta = 1/(k_B T)$ where k_B is the Boltzmann constant. At zero temperature $(T = 0)$ this average reduces to the expectation value $\langle X \rangle = \langle 0|X|0 \rangle$ in the many-electron ground state $|0\rangle$.

The transverse dynamical susceptibility corresponding to the uniform magnetisation precession $(\boldsymbol{q} = 0)$ is then given by

$$\chi_\perp(\omega) = \chi_\perp(0, \omega) = \frac{i}{\hbar} \int_0^t dt \, \langle [S^-(t), S^+(0)] \rangle \, e^{-i\omega_- t} \tag{2.19}$$

where $S^\pm = \sum_n S_n^\pm$. This susceptibility satisfies the following relation [61],

$$\chi_\perp(\omega) = \frac{-2\langle S_z \rangle}{\hbar(\omega - b_{\mathrm{ext}})} + \frac{1}{\hbar^2(\omega - b_{\mathrm{ext}})^2} \left\{ \chi_A(\omega) - \langle [A^-, S^+] \rangle \right\} \tag{2.20}$$

where

$$\chi_A(\omega) = \frac{i}{\hbar} \int_0^t dt \, \langle [A^-(t), A^+] \rangle \, e^{-i\omega_- t} \tag{2.21}$$

is the correlation function for the SO torque

$$A^- = [S^-, H_{\text{SO}}], \tag{2.22}$$

$A^+ = (A^-)^\dagger = [H_{\text{SO}}, S^+]$ is its Hermitian conjugate and $b_{\text{ext}} = |\gamma| B_{\text{ext}} = \frac{2\mu_{\text{B}}}{\hbar} B_{\text{ext}}$ denotes the Larmor frequency, following the notation of Refs. [61, 113]. This relation for $\chi_\perp(\omega)$ can be obtained using the general method introduced by Edwards and Fisher [114] and based on the equation of motion for the spin operator $S^-(t)$ in the Heisenberg representation. The detailed derivation is given in the appendix B.

The dynamical susceptibility $\chi_\perp(\boldsymbol{q}, \omega)$ has pole at the frequency $\omega(\boldsymbol{q})$ of the spin wave with wave vector $\boldsymbol{q}$,

$$\chi_\perp(\omega) = -\frac{2\langle S_z \rangle}{\hbar(\omega - \omega(\boldsymbol{q}))}. \tag{2.23}$$

In the presence of SO interaction the spin-wave frequencies $\omega(\boldsymbol{q}) = \omega_1(\boldsymbol{q}) - i\omega_2(\boldsymbol{q})$ are complex that results in damping of the spin waves. The imaginary part of such poles is nothing but the inverse lifetime of the spin wave mode or the FMR linewidth for $\boldsymbol{q} = 0$. In this work, the attention is turned to the energy $\hbar\omega(\boldsymbol{q})$ of a long-wavelength spin wave (very small wave vector $\boldsymbol{q}$), corresponding to the uniform precession of magnetisation in the limit of $\boldsymbol{q} = 0$. Such energy is also found as a solution of the phenomenological LLG equation for a spin wave with zero wave vector $\boldsymbol{q}$ that leads to $\omega_1 = b_{\text{ext}} + \triangle\omega$ and $\omega_2 = \alpha \, b_{\text{ext}}$ as previously discussed in Sec. 2.2. The shift $\triangle\omega$ of the precession frequency b_{ext} is due to an additional term $\triangle B$ in the effective magnetic field arising from the presence of the MCA due to the SO interaction which also yields finite ω_2. The general dependence of the dynamical susceptibility around a spin-wave frequency pole, Eq. (2.23), can then be represented using the formula for the geometric series $(1-x)^{-1} = 1+x+...$,

$$
\begin{aligned}
\chi_\perp(\omega) &= \frac{-2\langle S_z \rangle}{\hbar(\omega - b_{\text{ext}} - \triangle\omega - i\omega_2)} = \frac{-2\langle S_z \rangle}{\hbar(\omega - b_{\text{ext}})} \frac{1}{1 - \frac{\triangle\omega + i\omega_2}{\omega - b_{\text{ext}}} + ...} \\
&= \frac{-2\langle S_z \rangle}{\hbar(\omega - b_{\text{ext}})} - \frac{2\langle S_z \rangle}{\hbar(\omega - b_{\text{ext}})^2}(\triangle\omega + i\omega_2)
\end{aligned} \tag{2.24}
$$

where terms of higher order in $x = (\omega + i\omega_2)/(\omega - b_{\text{ext}})$ are neglected. This equation has the same form as the general relation (2.20). Whilst the first terms in the two relations are identical, the comparison of the second terms leads to the following identification

$$-2\langle S_z \rangle(\triangle\omega + i\omega_2) = \frac{1}{\hbar}\Big\{ \chi_A(b_{\text{ext}}) - \langle [A^-, S^+] \rangle \Big\} \tag{2.25}$$

23

where $\chi_A(\omega)$ has been superseded by the zeroth order term $\chi_A(b_{\text{ext}})$ in the expansion around $\omega = b_{\text{ext}}$. In this way the following formula is obtained for the imaginary part of the spin-wave frequency

$$\omega_2 = -\frac{1}{2\hbar\langle S_z\rangle}\Big\{\operatorname{Im}\chi_A(\boldsymbol{q}, b_{\text{ext}}) - \operatorname{Im}\langle[A^-, S^+]\rangle\Big\}. \tag{2.26}$$

Thus, the calculation of the imaginary part of the spin-wave frequency ω_2, which defines the Gilbert damping, is reduced to evaluation of the SO torque correlation function $\chi_A(b_{\text{ext}})$ and the mean value of the commutator $[A^-, S^+]$.

The correlation function at $T = 0$ can be expressed in terms of the eigenstates $|n\rangle$ of the many-electron Hamiltonian as

$$\chi_A(\omega) = \frac{i}{\hbar}\sum_n \int_0^t dt\,\big\{\langle 0|A^-(t)|n\rangle\langle n|A^+|0\rangle - \langle 0|A^+|n\rangle\langle n|A^-(t)|0\rangle\big\}\,e^{-i\omega_- t} \tag{2.27}$$

where the unit operator $\sum_n |n\rangle\langle n| = 1$ has been used. Using the definition of the time evolution of the operator $A^-(t)$ in the Heisenberg picture, one can calculate the expectation values appearing in (2.27)

$$\langle 0|A^-(t)|n\rangle = \langle 0|e^{iHt/\hbar}A^- e^{-iHt/\hbar}|n\rangle = e^{i(E_0 - E_n)t/\hbar}\langle 0|A^-|n\rangle, \tag{2.28a}$$

$$\langle n|A^-(t)|0\rangle = \langle n|e^{iHt/\hbar}A^- e^{-iHt/\hbar}|0\rangle = e^{i(E_n - E_0)t/\hbar}\langle n|A^-|0\rangle \tag{2.28b}$$

where E_n are the eigenenergies, including the ground state energy E_0. After substituting the matrix elements (2.28) into (2.27) the expression (in the curly brackets) representing $\langle 0|[A^-(t), A^+]|0\rangle$ is found

$$\{...\} = e^{i(E_0 - E_n)t/\hbar}\langle 0|A^-|n\rangle\langle n|A^+|0\rangle - e^{i(E_n - E_0)t/\hbar}\langle 0|A^+|n\rangle\langle n|A^-|0\rangle = ...\tag{2.29}$$

The evaluation of the time integral yields

$$\int_0^\infty e^{i(-\omega \mp \frac{E_n - E_0}{\hbar} + i\eta)\,t}\,dt = \frac{1}{i\left(\omega \pm \frac{E_n - E_0}{\hbar} - i\eta\right)}. \tag{2.30}$$

Thus, using the relation $\lim_{\eta\to 0^+}\operatorname{Im}(x - a - i\eta)^{-1} = \pi\delta(x - a)$, the imaginary part of $\chi_A(b_{\text{ext}})$ is expressed as

$$\begin{aligned}
\operatorname{Im}\chi_A(b_{\text{ext}}) &= \frac{\pi}{\hbar}\sum_n |\langle n|A^+|0\rangle|^2\,\delta(b_{\text{ext}} + \frac{E_n - E_0}{\hbar}) \\
&\quad - \frac{\pi}{\hbar}\sum_n |\langle n|A^-|0\rangle|^2\,\delta(b_{\text{ext}} - \frac{E_n - E_0}{\hbar}).
\end{aligned} \tag{2.31}$$

However, the first term vanishes since $E_n - E_0 \geqslant 0$ whilst $b_{\text{ext}} > 0$. Thus, using the scaling property of the Dirac δ-function, $a\delta(ax) = \delta(x)$, the following formula is finally found from Eq. (2.26),

$$
\begin{aligned}
\omega_2 &= \frac{\pi}{2\hbar\langle S_z\rangle} \sum_n |\langle n|A^-|0\rangle|^2 \, \delta(\Omega - E_n + E_0) \\
&= \frac{\pi}{2\hbar\langle S_z\rangle} \sum_n \langle 0|A^+|n\rangle\langle n|A^-|0\rangle \, \delta(\Omega - E_n + E_0)
\end{aligned}
\tag{2.32}
$$

where $\Omega = \hbar \, b_{\text{ext}}$ is the energy of a spin wave in the uniform precession mode. In this formula for ω_2 it is also assumed that the second term in Eq. (2.26) vanishes. This can be proved as follows.

The imaginary part of $\langle 0|[A^-, S^+]|0\rangle$ can be written as

$$
\text{Im} \, \langle 0|X|0\rangle = \frac{1}{2i}\left\{\langle 0|X|0\rangle - \langle 0|X|0\rangle^*\right\} = \frac{1}{2i}\langle 0|X - X^\dagger|0\rangle
\tag{2.33}
$$

where $X = [A^-, S^+]$ with $A^- = [S^-, H_{\text{SO}}]$. General commutator rule $[[A, B], C] = [A, [B, C]] - [B, [A, C]]$ (valid for arbitrary operators A, B and C) allows us to express X as

$$
X = [S^-, [H_{\text{SO}}, S^+]] - [H_{\text{SO}}, [S^-, S^+]] = [S^-, A^+] + 2\,[H_{\text{SO}}, S_z]
\tag{2.34}
$$

where the relations $A^+ = [H_{\text{SO}}, S^+]$ and $[S^-, S^+] = 2S_z$ have also been used. Thus, one finds

$$
X^\dagger = [A^-, S^+] + 2\hbar\,[S_z, H_{\text{SO}}] = X - 2\,[H_{\text{SO}}, S_z]
\tag{2.35}
$$

which gives finally

$$
X - X^\dagger = 4\,[H_{\text{SO}}, S_z] = 4\,[H, S_z],
\tag{2.36}
$$

since the SO interaction is the only term in the total Hamiltonian H that does not commute with S_z. The obtained relation for the difference $X - X^\dagger$ allows us to immediately prove that the imaginary part of its expectation vale in the ground state $|0\rangle$ vanishes,

$$
\begin{aligned}
\text{Im} \, \langle 0|X|0\rangle &= \frac{2}{i}\langle 0|[H, S_z]|0\rangle = \frac{2}{i}\langle 0|HS_z - S_z H|0\rangle \\
&= \frac{2}{i}\left(E_0\langle 0|S_z|0\rangle - E_0\langle 0|S_z|0\rangle\right) = 0.
\end{aligned}
\tag{2.37}
$$

Extending this proof to show that $\langle X\rangle = tr(\rho X) = 0$ at finite temperature is straightforward.

The obtained expression (2.32) for ω_2 can be evaluated within the Hartree-Fock approximation (HFA), using the singly exited many-electron states $|n\rangle = c_f^+ c_i|0\rangle(1 - n_f)n_i$, represented in the second quantisation picture by the action of the annihilation and creation operators, c_i and

c_f^+ respectively, on the ground state $|0\rangle$. In such ground states, one of initially occupied state by electron, $|i\rangle$, is excited to an originally empty final state $|f\rangle$ whose process is represented by the factor $(1 - n_f)n_i$. The energy difference $E_n - E_0$ is then given by the difference of the one-electron levels $\epsilon_f - \epsilon_i$. Since $\delta(\Omega - E_n + E_0) = \delta(\Omega - \epsilon_f + \epsilon_i)$ vanishes for $\epsilon_f < \epsilon_i$ and $\Omega > 0$, the factor $(1 - n_f)n_i$ can be safely replaced by $n_i - n_f$ (at $T = 0$). The matrix element $\langle n|A^-|0\rangle$ of the one-body operator $A^- = \sum_{k,m}\langle k|A^-|m\rangle\, c_k^+ c_m$, expressed in the second quantisation picture, reduces then to $\langle f|A^-|i\rangle$. In this way, one obtains

$$\omega_2 = \frac{\pi}{2\hbar\langle S_z\rangle}\sum_{i,f}|\langle f|A^-|i\rangle|^2\,\delta(\Omega - \epsilon_f + \epsilon_i)(n_i - n_f). \tag{2.38}$$

After expressing the occupation factors as $n_i = \theta(\epsilon_F - \epsilon_i)$, $n_f = \theta(\epsilon_F - \epsilon_f)$, with the Fermi energy ϵ_F, and introducing an integral over energy ϵ the expression (2.38) can be rewritten as

$$\omega_2 = \frac{\pi}{2\hbar\langle S_z\rangle}\sum_{i,f}|\langle f|A^-|i\rangle|^2\int d\epsilon\,\delta(\epsilon - \epsilon_i)\delta(\Omega - \epsilon_f + \epsilon)\big[\theta(\epsilon_F - \epsilon) - \theta(\epsilon_F - \epsilon - \Omega)\big] \tag{2.39}$$

where ϵ_i, ϵ_f have been superseded by ϵ and $\epsilon + \Omega$, respectively, due to the presence of the two δ-functions. The last part of the integrand (i.e., the difference of the two θ-functions) determines the actual integration interval,

$$\omega_2 = \frac{\pi}{2\hbar\langle S_z\rangle}\sum_{i,f}|\langle f|A^-|i\rangle|^2\int_{\epsilon_F - \Omega}^{\epsilon_F} d\epsilon\,\delta(\epsilon - \epsilon_i)\delta(\epsilon - \epsilon_f + \Omega). \tag{2.40}$$

The leading term in ω_2, linear in $\Omega = \hbar\, b_{\text{ext}}$, proportional to the magnetic field B_{ext} is then given by

$$\begin{aligned}
\omega_2 &= \frac{\pi\Omega}{2\hbar\langle S_z\rangle}\sum_{i,f}|\langle f|A^-|i\rangle|^2\,\delta(\epsilon_F - \epsilon_i)\delta(\epsilon_F - \epsilon_f) \\
&= \frac{\pi b_{\text{ext}}}{2\langle S_z\rangle}\sum_{i,f}\langle f|A^-|i\rangle\delta(\epsilon_F - \epsilon_i)\langle i|A^+|f\rangle\delta(\epsilon_F - \epsilon_f).
\end{aligned} \tag{2.41}$$

In real systems electrons are subject to scattering due to lattice vibrations (phonons), imperfections and other factors. As a result the lifetime τ of electronic states becomes finite and electronic levels like ϵ_i, ϵ_f, infinitely narrow in the absence of scattering, have a finite width. It is described formally by introducing a configuration average $\langle...\rangle_c$ of quantum expressions, like Eq. (2.41) for ω_2. The effect of such averaging can be represented in an approximate way, by broadening of electronic levels, which can be formally justified within the coherent potential approximation (CPA) [115]. Such CPA average has been used in Kamberský's model [116] where

the Dirac δ-functions, like $\delta(\epsilon_{\mathrm{F}} - \epsilon_i)$, are replaced by the Lorentz functions $L(\epsilon_{\mathrm{F}} - \epsilon_i)$. The latter are defined as

$$L(x) = \frac{\Gamma}{2\pi} \frac{1}{x^2 + \Gamma^2/4} \tag{2.42}$$

and characterised with the electron scattering rate Γ which is usually assumed to be state-independent, for the sake of simplicity, and thus it represents the average scattering rate. Mathematically, the parameter Γ is the full width at half maximum (FWHM) of the Lorentz function.

In this way, after using the unit operator $\sum_i |i\rangle\langle i| = 1$ in Eq. (2.41) and the definition of trace, the final expression for the Gilbert damping constant at $T = 0$ is obtained,

$$\alpha = \frac{\omega_2}{b_{\mathrm{ext}}} = \frac{\pi}{2\langle S_{\mathrm{tot}}^z \rangle} \operatorname{tr} \left\{ \mathrm{A}^- \mathrm{L}(\epsilon_{\mathrm{F}} - \mathrm{H_s}) \mathrm{A}^+ \mathrm{L}(\epsilon_{\mathrm{F}} - \mathrm{H_s}) \right\}. \tag{2.43}$$

The index "tot" is now reintroduced, for clarity, in the symbol of the total spin $S_{\mathrm{tot}}^z = S_z$ and H_{s} denotes the Hamiltonian that gives the one-electron states: $H_{\mathrm{s}}|i\rangle = \epsilon_i|i\rangle$. In the calculations, H_{s} and its eigenstates $|i\rangle$ are usually found within the Kohn-Sham approch of the DFT, or in a more approximate way, within the TB model, as done in the present thesis. In the next sections, the index "s" will be skipped for simplicity so that H will no longer denote the many-electron Hamiltonian as it does in the present section. The SO torque operator $A^- = [S^-, H_{\mathrm{SO}}]$, previously defined for N electrons, acts in Eq. (2.43), in a similar way as H_{s}, in the Hilbert space of one-electron quantum states. Accordingly, the same holds for the spin operator S^- and the SO interaction H_{SO} that define A^-. Thus, in all following sections of this chapter (except the appendix B) the spin operators S^-, S^+, S_z and H_{SO} refer to a single electron.

As shown by Kamberský [44] the finite temperature T can be explicitly introduced in the calculations by replacing the value of the trace at $\epsilon = \epsilon_{\mathrm{F}}$ by the integral

$$\alpha = \frac{\pi}{2\langle S_{\mathrm{tot}}^z \rangle} \int_{-\infty}^{\infty} d\epsilon\, \eta(\epsilon) \operatorname{tr} \left\{ \mathrm{A}^- \mathrm{L}(\epsilon - \mathrm{H_s}) \mathrm{A}^+ \mathrm{L}(\epsilon - \mathrm{H_s}) \right\} \tag{2.44}$$

where $\eta(\epsilon) = -df_{\mathrm{FD}}/d\epsilon$ is obtained with the Fermi-Dirac function $f_{\mathrm{FD}}(\epsilon) = [1 + e^{(\epsilon - \epsilon_{\mathrm{F}})/k_{\mathrm{B}}T}]^{-1}$ (where k_{B} is the Boltzmann constant).

2.4 Tight-binding model of electronic structure

This part is divided into five sections. First, the density functional theory as the background for one-electron description of many-electron systems is reviewed and the Kohn-Sham equation

27

is introduced. Then in next two sections, the TB method is presented. It is shown how the TB Hamiltonian can be constructed for the layered structures. This is followed by the description of TB atomic orbital basis. Finally, evaluation of the hopping integrals in terms of the two-centre Slater-Koster parameters is described in a separate section.

2.4.1 Density functional theory as background for one-electron description of many-electron systems

Calculations of electronic properties of molecules, solids and nanostructures are usually based on the density functional theory (DFT) [117]. It is a powerful quantum-mechanical method which has been honoured with the Nobel prize in chemistry in 1998, awarded to its main founder Walter Kohn [118, 119]. In the DFT approach, a many-electronic system is represented with an equivalent system of non-interacting particles (electrons) which has the same electron density $n(\boldsymbol{r})$, or, alternatively, the same densities $n^{\uparrow}(\boldsymbol{r}), n^{\downarrow}(\boldsymbol{r})$ of electrons with spin $\sigma =\uparrow,\downarrow$ as the original interacting system. As a result the non-interacting system is described within the Kohn-Sham (KS) scheme where each electron of spin σ travels in a common effective potential $V_{\mathrm{eff}}^{\sigma}(\boldsymbol{r})$. This potential depends on the spin-up and spin-down electron densities $n^{\uparrow}, n^{\downarrow}$ not only through the total electron density $n(\boldsymbol{r}) = n^{\uparrow}(\boldsymbol{r}) + n^{\downarrow}(\boldsymbol{r})$ (i.e., the charge density) which defines the electrostatic potential $V_{\mathrm{es}}(\boldsymbol{r}) = \int n(\boldsymbol{r})|\boldsymbol{r} - \boldsymbol{r'}|^{-1}dr$, but also through the exchange-correlation (xc) potential $V_{\mathrm{xc}}^{\sigma}(\boldsymbol{r})$. The latter is defined as the functional derivative $\delta E_{\mathrm{xc}}[n^{\uparrow}, n^{\downarrow}]/\delta n^{\sigma}(\boldsymbol{r})$ of the xc energy functional $E_{\mathrm{xc}}[n^{\uparrow}, n^{\downarrow}]$. This energy is the part of the total energy of the interacting system that describes its change (reduction) resulting from correlations of electronic motions due to the fermionic character of electrons (leading to exchange effects) and the repulsive Coulomb interaction between electrons.

In the DFT calculations, the xc energy $E_{\mathrm{xc}}[n^{\uparrow}, n^{\downarrow}]$ and the resulting exchange potential $V_{\mathrm{xc}}^{\sigma}(\boldsymbol{r})$ are usually expressed in the local-spin-density (LSDA) or generalised-gradient (GGA) approximations since the exact form of the $E_{\mathrm{xc}}[n^{\uparrow}, n^{\downarrow}]$ functional is yet unknown. The effective potential $V_{\mathrm{eff}}^{\sigma} = V_{\mathrm{ext}} + V_{\mathrm{es}} + V_{\mathrm{xc}}^{\sigma}$ also contains the external potential V_{ext} coming from the interaction of electrons with the external fields due to the nuclei of atoms forming the system and external sources if present. Additionally, the interaction of electron spin and orbital angular momenta with external magnetic field $\boldsymbol{B}_{\mathrm{ext}}(\boldsymbol{r})$ can be included. However, it is not done in the present calculations since the expression for the damping constant α is evaluated in the limit of $B_{\mathrm{ext}} \to 0$ (taken after small finite B_{ext} is assumed in its derivation).

The quantum states (wave functions) $\psi_{n}^{\sigma}(\boldsymbol{r})$ of non-interaction electrons with energies ϵ_{n}^{σ} are

called KS states or KS orbitals. They are eigenstates of the *one-electron* Hamiltonian

$$H_0^\sigma = -\frac{1}{2}\nabla^2 + V_{\text{eff}}^\sigma(\boldsymbol{r}), \tag{2.45}$$

i.e., they satisfy the KS equation

$$H_0^\sigma \, \psi_n^\sigma = \epsilon_n^\sigma \, \psi_n^\sigma. \tag{2.46}$$

In the DFT approach, the KS equation is solved self-consistently since the occupied (occ) KS orbitals have to yield such spin electron densities $n^\sigma(\boldsymbol{r}) = \sum_n^{occ} |\psi_n^\sigma(\boldsymbol{r})|^2$, $(\sigma = \uparrow, \downarrow)$, that lead to the potential $V_{\text{eff}}^\sigma(\boldsymbol{r})[n^\uparrow, n^\downarrow]$. The self-consistent solution of the KS equation is found iteratively by determining the densities $n^\uparrow(\boldsymbol{r}), n^\downarrow(\boldsymbol{r})$, and the corresponding potential $V_{\text{eff}}(\boldsymbol{r})$ at each step.

If relativistic corrections to the Hamiltonian are included, the external potential contains the SO interaction H_{SO} which is represented by a 2×2 matrix $H_{\text{SO}}^{\sigma\sigma'}(\boldsymbol{r})$ acting in the electron spin space (for further details see Sec. 2.5). As a result, the total one-electron KS Hamiltonian is no longer diagonal in spin,

$$H = H_0 + H_{\text{SO}} = \begin{pmatrix} H_0^\uparrow & 0 \\ 0 & H_0^\downarrow \end{pmatrix} + \begin{pmatrix} H_{\text{SO}}^{\uparrow\uparrow} & H_{\text{SO}}^{\uparrow\downarrow} \\ H_{\text{SO}}^{\downarrow\uparrow} & H_{\text{SO}}^{\downarrow\downarrow} \end{pmatrix} = \begin{pmatrix} H_0^\uparrow + H_{\text{SO}}^{\uparrow\uparrow} & H_{\text{SO}}^{\uparrow\downarrow} \\ H_{\text{SO}}^{\downarrow\uparrow} & H_0^\downarrow + H_{\text{SO}}^{\downarrow\downarrow} \end{pmatrix}. \tag{2.47}$$

Thus, the resultant eigenstates $\psi_n(\boldsymbol{r})$ of the corresponding KS equation

$$H\psi_n = \epsilon_n\psi_n \tag{2.48}$$

do not have a definite spin since they are not eigenstates of S_z, i.e., the z component of the electron spin operator.

In the *ab initio* DFT calculations the KS differential equation is solved in the configurational space (real space) or using a large basis of atomic-like orbitals and/or plane waves. Alternatively, an equivalent equation for the Green function can be solved like in the Korringa-Kohn-Rostoker approximation method (KKR) [120, 121].

2.4.2 Tight-binding model: basics

The TB model was introduced by Slater and Koster back in 1954 [122] and provided a simple yet realistic recipe for calculation of electronic band structure in solids. The TB model is based on one-electron description of physical (many-electron) systems which is currently justified by the DFT and takes the form of the KS equation. This model represents the eigenstates $|n\rangle \equiv \psi_n$ of the KS one-electron Hamiltonian H in a small basis of atomic-like orbital states $|j\mu\sigma\rangle$. The orbital

wave functions $\langle \boldsymbol{r}|j\mu\sigma\rangle = \varphi_{\mu\sigma}(\boldsymbol{r}-\boldsymbol{R}_j)$ are usually of s, p, d spatial symmetry and they are centred on different atomic sites $\boldsymbol{R}_j$ (i.e., the positions of atomic nuclei) in the investigated system. They can be identified with the Wannier functions defined in the solid state theory. Importantly, in the TB model the Hamiltonian is represented only by its matrix elements $\langle j'\mu'\sigma'|H|j\mu\sigma\rangle$ which are usually assumed to be nonzero only if the atomic sites j and j' are the same atom or they are first and second nearest neighbours (n.n.). These matrix elements are usually expressed within the Slater-Koster (SK) formalism by a small set of several two-centre integrals between first and second n.n. as well as the on-site energies corresponding to the elements on the same atomic sites ($j = j'$). The values of these basic parameters are found by fitting the energy bands obtained for bulk materials in the TB model to the energies found in *ab initio* DFT calculations [123].

The TB model is widely used in solid state physics for the study of electronic band structure and related physical properties in various metallic and semiconductor crystal systems. It works particularly well in cases of strongly localised electrons and small band width (i.e., for d-bands and f-bands). The Hubbard model and the Anderson impurity model illustrate this point. The TB model is associated closely with the linear combination of atomic orbitals (LCAO) method which is used in chemistry. The basis functions to be considered are orthonormalised atomic orbitals $|j\mu\sigma\rangle$. If an investigated system has m-dimensional translational symmetry ($m = 1, 2$ or 3) the atomic orbitals can be conveniently replaced by the associated Bloch basis functions dependent on m-dimensional wave vector $\boldsymbol{k}$. The use of Bloch functions reduces the size of the eigenvalue problem and thus makes its solution easier.

2.4.3 Construction of tight-binding Hamiltonian

The TB method, outlined generally above, can be applied to construct the TB Hamiltonian for bulk crystals as well as slabs representing layered systems which are of particular interest in this work (see, e.g., Refs. [95]). In the latter case, the basis functions are orthonormalised atomic orbitals $|lj\mu\sigma\rangle$ where the index j labels different atoms which are located at positions $\boldsymbol{R}_{lj}$ in the l-th atomic layer. The wave function corresponding to a basis state $|lj\mu\sigma\rangle$ is centred at $\boldsymbol{R}_{lj}$ and has the form $\langle \boldsymbol{r}|lj\mu\sigma\rangle = \varphi_{\mu\sigma}(\boldsymbol{r}-\boldsymbol{R}_{lj})$ of an atomic orbital with spin σ and spatial symmetry specified by the index μ. Layered systems, films, have two-dimensional (2D) translational symmetry since they remain unchanged if all atoms are shifted by the same lattice vector $\boldsymbol{R}$ parallel to the film surface. The invariance of the Hamiltonian under the 2D translations, $H(\boldsymbol{r}+\boldsymbol{R}) = H(\boldsymbol{r})$, leads to the Bloch theorem implying that the eigenstates of H satisfy the relation $\psi_n(\boldsymbol{r}+\boldsymbol{R}) = e^{i\boldsymbol{k}\cdot\boldsymbol{R}}\psi_n(\boldsymbol{r})$. Consequently, these states can be labelled with the 2D wave vector $\boldsymbol{k} = (k_x, k_y)$ parallel to the film surface and often also denoted as $\boldsymbol{k}_{\parallel}$. As a result, due to the 2D translational symmetry

the eigenvalue problem for a layered system can be formulated most conveniently using the associated basis of Bloch functions

$$|\boldsymbol{k}l\mu\sigma\rangle = \frac{1}{\sqrt{N_{2\mathrm{D}}}} \sum_j e^{i\boldsymbol{k}\cdot\boldsymbol{R}_{lj}} |lj\mu\sigma\rangle \tag{2.49}$$

constructed from the atomic orbitals $|lj\mu\sigma\rangle$, for each 2D wave vector $\boldsymbol{k}$ from the first 2D BZ. Here, $N_{2\mathrm{D}}$ denotes the number of atoms in each atomic plane (with periodic boundary conditions at its edges) and it is equal to the number of $\boldsymbol{k}$-points in the BZ. The eigenstates $|n\boldsymbol{k}\rangle$ of the Hamiltonian can then be expanded as a linear combination

$$|n\boldsymbol{k}\rangle = \sum_{l\mu\sigma} a_{nl\mu}^{\sigma}(\boldsymbol{k}) |\boldsymbol{k}l\mu\sigma\rangle \tag{2.50}$$

of all Bloch basis states (of both spins σ) with the same wave vector $\boldsymbol{k}$. Thus, each eigenstate is represented by the probability amplitudes $a_{nl\mu}^{\sigma}(\boldsymbol{k}) = \langle \boldsymbol{k}l\mu\sigma|n\boldsymbol{k}\rangle$. These amplitudes can be found by solving the matrix equation obtained by representing the KS equation

$$H|n\boldsymbol{k}\rangle = \epsilon_n(\boldsymbol{k})|n\boldsymbol{k}\rangle \tag{2.51}$$

in the Bloch basis. This can be done by expressing the eigenstates in the orbital basis

$$\begin{aligned}
|n\boldsymbol{k}\rangle &= \sum_{l'\nu\sigma'} a_{nl'\nu}^{\sigma'}(\boldsymbol{k})|\boldsymbol{k}l'\nu\sigma'\rangle = \sum_{l'\nu\sigma'} a_{nl'\nu}^{\sigma'}(\boldsymbol{k}) \left(\frac{1}{\sqrt{N_{2\mathrm{D}}}} \sum_j e^{i\boldsymbol{k}\cdot\boldsymbol{R}_{lj}} |l'j\nu\sigma'\rangle \right) \\
&= \frac{1}{\sqrt{N_{2\mathrm{D}}}} \sum_{jl'\nu\sigma'} a_{nl'\nu}^{\sigma'}(\boldsymbol{k}) e^{i\boldsymbol{k}\cdot\boldsymbol{R}_{lj}} |l'j\nu\sigma'\rangle
\end{aligned} \tag{2.52}$$

using the definition (2.49) of the Bloch basis states $|\boldsymbol{k}l'\nu\sigma'\rangle$. Inserting this expression into the KS equation (2.51) and subsequent application of the bra $\langle l0\mu\sigma|$ to its both sides leads us to the equation

$$\begin{aligned}
\sum_{l'\nu\sigma'} a_{nl'\nu}^{\sigma'}(\boldsymbol{k}) \sum_j e^{i\boldsymbol{k}\cdot\boldsymbol{R}_{lj}} \langle l0\mu\sigma|H|l'j\nu\sigma'\rangle &= \epsilon_n(\boldsymbol{k}) \sum_{l'j\nu\sigma'} a_{nl'\nu}^{\sigma'}(\boldsymbol{k}) e^{i\boldsymbol{k}\cdot\boldsymbol{R}_{lj}} \langle l0\mu\sigma|l'j\nu\sigma'\rangle \\
&= \epsilon_n(\boldsymbol{k}) \sum_{l'j\nu\sigma'} a_{nl'\nu}^{\sigma'}(\boldsymbol{k}) e^{i\boldsymbol{k}\cdot\boldsymbol{R}_{lj}} \delta_{ll'}\delta_{\mu\nu}\delta_{0j}\delta_{\sigma\sigma'} \\
&= \epsilon_n(\boldsymbol{k})\, a_{nl\nu}^{\sigma}(\boldsymbol{k})\, e^{i\boldsymbol{k}\cdot\boldsymbol{R}_{l0}}.
\end{aligned} \tag{2.53}$$

It can be written as

$$\sum_{l'\nu\sigma'} H_{l\mu,l'\nu}^{\sigma\sigma'}(\boldsymbol{k})\, a_{nl'\nu}^{\sigma'}(\boldsymbol{k}) = \epsilon_n(\boldsymbol{k})\, a_{nl\mu}^{\sigma}(\boldsymbol{k}) \tag{2.54}$$

where

$$H_{l\mu,l'\nu}^{\sigma\sigma'}(\boldsymbol{k}) = \sum_j e^{i\boldsymbol{k}\cdot(\boldsymbol{R}_{l'j}-\boldsymbol{R}_{l0})}\langle l0\mu\sigma|H|l'j\nu\sigma'\rangle \tag{2.55}$$

is the matrix element of the Hamiltonian $H = H_0 + H_{\mathrm{SO}}$ in the 2D Bloch basis. This gives the final form of the TB eigenvalue matrix equation for layered systems.

The above procedure can also be applied to bulk systems once the layer index l is skipped and the 2D $\boldsymbol{k}$-vector is replaced by the three-dimensional (3D) wave vector $\boldsymbol{k} = (k_x, k_y, k_z)$. For bulk crystals the TB equation takes the form

$$\sum_{\nu\sigma'} H_{\mu,\nu}^{\sigma\sigma'}(\boldsymbol{k})\, a_{n\nu}^{\sigma'}(\boldsymbol{k}) = \epsilon_n(\boldsymbol{k})\, a_{n\mu}^{\sigma}(\boldsymbol{k}) \tag{2.56}$$

from which the eigenstates $|n\boldsymbol{k}\rangle = \sum_{\mu\sigma} a_{n\mu}^{\sigma}(\boldsymbol{k})|\mu\sigma\rangle$ and their eigenvalues $\epsilon_n(\boldsymbol{k})$, forming bulk energy bands, can be found.

The dominant part of the TB Hamiltonian matrix for a layered system

$$H_{l\mu,l'\nu}^{\sigma\sigma'}(\boldsymbol{k}) = H_{0;\,l\mu,l'\nu}^{\sigma}(\boldsymbol{k})\delta_{\sigma\sigma'} + H_{\mathrm{SO};\,l\mu,l'\nu}^{\sigma\sigma'}(\boldsymbol{k}). \tag{2.57}$$

is diagonal in spin σ. It includes the on-site energies $\epsilon_{l\mu}^{\sigma} = \langle l0\mu\sigma|H_0^{\sigma}|l0\mu\sigma\rangle$ and the hopping integrals $\langle l0\mu\sigma|H_0^{\sigma}|l'j\nu\sigma'\rangle$, i.e., the interatomic Hamiltonian matrix elements between a chosen central atom at position $\boldsymbol{R}_{l0}$ in atomic layer l and neighbouring atoms at positions $\boldsymbol{R}_{l'j}$ in the same layer ($l = l'$) or different layers ($l \neq l'$). The hopping integrals decay quickly with increasing interatomic distance $\boldsymbol{R}_{l'j} - \boldsymbol{R}_{l0}$. For this reason, only first and second n.n. are usually taken into account in the sum (2.55) defining the Hamiltonian matrix elements

$$H_{0;\,l\mu,l'\nu}^{\sigma} = \epsilon_{l\mu}^{\sigma}\delta_{ll'}\delta_{\mu\mu'} + \sum_j^{\mathrm{1st,2nd\ n.n.}} e^{i\boldsymbol{k}\cdot(\boldsymbol{R}_{l'j}-\boldsymbol{R}_{l0})}\langle l0\mu\sigma|H_0|l'j\nu\sigma\rangle. \tag{2.58}$$

For a given atom at position $\boldsymbol{R}_{l0}$, the positions $\boldsymbol{R}_{l'j'}$ of its n.n. depend on the type of the crystal lattice. For the two types of the cubic lattice present in layered systems investigated in this work, the n.n. are at the following positions.

a) In face-centred cubic (fcc) lattice, 16 first n.n. are at $\boldsymbol{R}_{l0}+(\pm a/2, \pm a/2, 0)$, $\boldsymbol{R}_{l0}+(0, \pm a/2, \pm a/2)$, $\boldsymbol{R}_{l0} + (\pm a/2, 0, \pm a/2)$; 6 second n.n. are at $\boldsymbol{R}_{l0} + (\pm a, 0, 0)$, $\boldsymbol{R}_{l0} + (0, \pm a, 0)$, $\boldsymbol{R}_{l0} + (0, 0, \pm a)$.

b) In body-centred cubic (bcc) lattice, 8 first n.n. are at $\boldsymbol{R}_{l0} + (\pm a/2, \pm a/2, \pm a/2)$; 6 second n.n. are at $\boldsymbol{R}_{l0} + (\pm a, 0, 0)$, $\boldsymbol{R}_{l0} + (0, \pm a, 0)$, $\boldsymbol{R}_{l0} + (0, 0, \pm a)$ where in both cases a is the lattice constant.

The hopping integrals $\langle l0\mu\sigma|H_0^{\sigma}|l'j\nu\sigma'\rangle$ depend on the symmetry of orbitals μ, ν and their

orientation with respect to the vector $\boldsymbol{R} = \boldsymbol{R}_{l'j} - \boldsymbol{R}_{l0}$ connecting the two atoms at $\boldsymbol{R}_{l0}$ and $\boldsymbol{R}_{l'j}$. This dependency is given by the SK formulas, discussed in Sec. 2.4.5. The minor part of the TB Hamiltonian matrix is the SO interaction matrix $H_{\mathrm{SO};\,l\mu,l'\nu}^{\sigma\sigma'}(\boldsymbol{k}) = \langle \boldsymbol{k}l\mu\sigma|H_{\mathrm{SO}}|\boldsymbol{k}l'\nu\sigma'\rangle$. It includes both diagonal and off-diagonal spin-pair elements but it does not depend on $\boldsymbol{k}$ and, in fact, is diagonal in l, l' as it is explained in Sec. 2.5.

2.4.4 Atomic orbital basis

The atomic-like orbitals used as the TB basis are products $\varphi_\mu(\boldsymbol{r}) = f_L(r)Y_\mu(\theta,\phi)$ of radial wave functions $f_L(r)$ and functions $Y_\mu(\theta,\phi)$ dependent on the polar θ and azimuthal ϕ angles, where L is the orbital number corresponding to the orbital μ. Such form of orbitals corresponds to solutions of the Schrödinger equation with a spherically symmetric potential which are eigenstates of the square $\boldsymbol{L}^2$ of the orbital angular momentum operator $\boldsymbol{L}$. In atomic physics and quantum mechanical chemistry, the functions $Y_\mu(\theta,\phi)$ are often chosen to be the spherical harmonics

$$Y_L^m(\theta,\phi) = (-1)^m \left[\frac{(2L+1)(L-|m|)}{4\pi(L+|m|)} \right]^{1/2} P_L^m(\cos\theta)e^{im\phi} \tag{2.59}$$

which are also eigenstates (labeled with L and the quantum magnetic number m) of the operator L_z; here P_L^m are the associated Legendre functions.

However, in solid state theory and in the TB model, in particular, the real functions $Y_\mu(\theta,\phi)$ referred to as cubic harmonics and they are usually used instead of $Y_L^m(\theta,\phi)$ which have complex values. The cubic harmonics can be defined as linear combinations of the spherical harmonics Y_L^{-m} and Y_L^m, and they are labeled with index μ describing their spatial symmetry. The cubic harmonics for s, p and d orbitals with $L = 0$ ($Y_\mu = s$), $L = 1$ ($Y_\mu = p_\mu$) and $L = 2$ ($Y_\mu = d_\mu$), respectively, are listed below.

$$
\begin{aligned}
s &= Y_0^0 = N_s\,, \\
p_z &= Y_1^0 = N_p \cos\theta = N_p \frac{z}{r}\,, \\
p_x &= \frac{1}{\sqrt{2}}(Y_1^{-1} - Y_1^1) = N_p \sin\theta \cos\phi = N_p \frac{x}{r}\,, \\
p_y &= \frac{i}{\sqrt{2}}(Y_1^{-1} + Y_1^1) = N_p \sin\theta \sin\phi = N_p \frac{y}{r}\,, \\
d_{3z^2-r^2} &= Y_2^0 = \frac{1}{2\sqrt{3}} N_d(3\cos^2\theta - 1) = \frac{1}{2\sqrt{3}} \frac{3z^2 - r^2}{r^2}\,, \\
d_{xz} &= \frac{1}{2}(Y_2^{-1} - Y_2^1) = N_d \sin\theta \cos\theta \cos\phi = N_d \frac{xz}{r}\,,
\end{aligned}
$$

33

$$
\begin{aligned}
d_{yz} &= \frac{i}{\sqrt{2}}(Y_2^{-1} + Y_2^1) = N_d \sin\theta \cos\theta \sin\phi = N_d \frac{yz}{r}\,, \\
d_{xy} &= \frac{i}{\sqrt{2}}(Y_2^{-2} + Y_2^2) = N_d \sin^2\theta \cos\phi \sin\phi = N_d \frac{xy}{r}\,, \\
d_{x^2-y^2} &= \frac{1}{\sqrt{2}}(Y_2^{-2} - Y_2^2) = \frac{1}{2}N_d \sin^2\theta(\cos^2\phi - \sin^2\phi) = \frac{1}{2}N_d \frac{x^2 - y^2}{r^2}
\end{aligned}
\tag{2.60}
$$

where $N_s = \frac{1}{\sqrt{4\pi}}$, $N_p = \sqrt{3/4\pi}$ and $N_d = \sqrt{15/4\pi}$. Having established these explicit forms of angular dependent atomic-like orbitals which form the TB basis, one can find the SK expressions for the hopping integrals. This is discussed in the following section and the appendix C in detail.

2.4.5   Hopping integrals and two-centre Slater-Koster parameters

The two-centre SK parameters, introduced by Slater and Koster [122], are the key ingredients in the TB model used for calculation of the electronic band structure in solids. They are used in evaluation of the hopping integrals which are the interatomic matrix elements $\langle l0\mu\sigma|H_0^\sigma|l'j\nu\sigma\rangle$ of the one-electron Hamiltonian H_0^σ between orbitals centred on neighbouring atoms. Atomic orbitals are not eigenstates of the Hamiltonian anymore in a crystal system due to their overlap with orbitals on adjacent atomic sites. Therefore, the hopping integrals (bond energies in chemistry) represent an effective interaction between atomic orbitals centred on two neighbouring atoms (though such interpretation is not strict since it is not a physical interaction between different electrons). In the TB model, the hopping integrals are expressed in terms of several two-centre SK parameters (a separate set for each spin in the case of ferromagnets) and angle-dependent trigonometric functions that reflect the relative position of one atom with respect to the other. The two-centre SK parameters are generic matrix elements of the Hamiltonian between pairs of s, p, d orbitals corresponding to orbital angular momentum quantised along the axis joining the two neighbouring atoms. The explicit expressions for the hopping integrals in terms of the two-centre parameters can be found in literature [122, 124, 125]. Here, a derivation of the general formula for these integrals and a few examples of it are presented.

The hopping integrals depend on the distance between atoms, the spatial symmetry of orbitals and their orientation with respect to the vector $\boldsymbol{R}$ connecting these atoms (in the case of s orbitals they only depend on the distance, due to the spherical symmetry). The occurrence of such dependences can be understood as follows. The angular parts of the two orbitals $\varphi_\mu(\mathrm{r}_1), \varphi_\nu(\mathrm{r}_2)$ are cubic harmonics $Y_\mu(\theta_1, \phi_1), Y_\nu(\theta_2, \phi_2)$ which correspond to some orbital numbers L, L', and magnetic numbers m, m', respectively. They can be represented in terms of the spherical harmonics Y_L^m, Y_L^{-m} (or $Y_{L'}^m, Y_{L'}^{-m}$ for Y_ν) as it is shown in the previous section. This
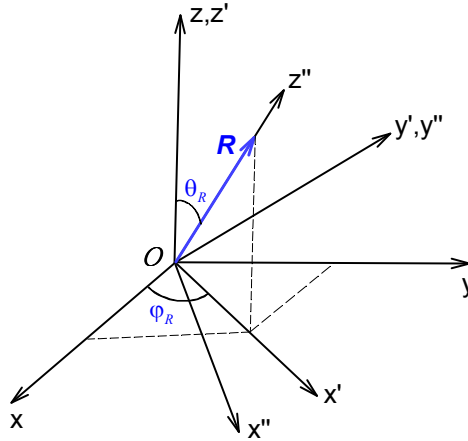
34

Figure 2.2: Passive transformation of cartesian coordinates

relation can be written in the following general form,

$$Y_\mu = C_\mu^m Y_L^m + C_\mu^{-m} Y_L^{-m} \qquad (m = 0, 1, ..., L) \qquad (2.61)$$

where $|C_\mu^m|^2 + |C_\mu^{-m}|^2 = 1$. Similar relation is satisfied between Y_ν and $Y_{L'}^m$, $Y_{L'}^{-m}$. For $m = 0$, $Y_\mu = Y_L^0$ holds so that $C_\mu^0 = C_\mu^{-0} = \frac{1}{2}$ can be assumed in the general relation (2.61).

It is convenient to transform the coordinates from $\boldsymbol{r} = (x, y, z)$ to $\boldsymbol{r}'' = (x'', y'', z'')$ so that the resultant axis z'' is along the interatomic vector $\boldsymbol{R} = \boldsymbol{R}_{l'j'} - \boldsymbol{R}_{l0}$. Such a *passive* transformation can be achieved by the composition of two transformations: the rotation around z axis, leading to $\boldsymbol{r}' = (x', y', z')$ coordinates, and the subsequent rotation around y' axis. The two consecutive transformations (rotations by the Euler angles $\alpha = \phi_{\boldsymbol{R}}$, $\beta = \theta_{\boldsymbol{R}}$) are

$$
\begin{aligned}
x &= x' \cos \phi_{\boldsymbol{R}} - y' \sin \phi_{\boldsymbol{R}}, \\
y &= x' \sin \phi_{\boldsymbol{R}} + y' \cos \phi_{\boldsymbol{R}}, \qquad \text{(rotation around } z) \\
z &= z'
\end{aligned}
\qquad (2.62)
$$

and

$$
\begin{aligned}
x' &= x'' \cos \theta_{\boldsymbol{R}} + z'' \sin \theta_{\boldsymbol{R}}, \\
z' &= -x'' \sin \theta_{\boldsymbol{R}} + z'' \cos \theta_{\boldsymbol{R}}, \qquad \text{(rotation around } y') \\
y' &= y''
\end{aligned}
\qquad (2.63)
$$

where the angles $\theta_{\boldsymbol{R}}, \phi_{\boldsymbol{R}}$ define the direction of $\boldsymbol{R} = R(\alpha_x, \alpha_y, \alpha_z)$ in the original frame of

35

reference O_{xyz} through the direction cosines of $\boldsymbol{R}$,

$$
\begin{aligned}
\alpha_x &= \sin\theta_{\boldsymbol{R}}\cos\phi_{\boldsymbol{R}}\,, \\
\alpha_y &= \sin\theta_{\boldsymbol{R}}\sin\phi_{\boldsymbol{R}}\,, \\
\alpha_z &= \cos\theta_{\boldsymbol{R}}\,.
\end{aligned}
\tag{2.64}
$$

The final transformation has the form

$$
\begin{aligned}
x &= x''\cos\theta_{\boldsymbol{R}}\cos\phi_{\boldsymbol{R}} - y''\sin\phi_{\boldsymbol{R}} + z''\sin\theta_{\boldsymbol{R}}\cos\phi_{\boldsymbol{R}}, \\
y &= x''\cos\theta_{\boldsymbol{R}}\sin\phi_{\boldsymbol{R}} + y''\cos\phi_{\boldsymbol{R}} + z''\sin\theta_{\boldsymbol{R}}\sin\phi_{\boldsymbol{R}}, \\
z &= -x''\sin\theta_{\boldsymbol{R}} + z''\cos\phi_{\boldsymbol{R}}\,.
\end{aligned}
\tag{2.65}
$$

This linear transformation can be written in a concise form as $\boldsymbol{r} = Q\,\boldsymbol{r}''$ where $\boldsymbol{r} = (x'', y'', z'')$, and $Q = Q(\theta_{\boldsymbol{R}}, \phi_{\boldsymbol{R}})$ is the transformation matrix. The coordinates determining the positions of atoms $(l0)$ and $(l'j')$ are transformed as

$$
\boldsymbol{R}_{l0} = Q\,\boldsymbol{R}''_{l0}\,, \qquad \boldsymbol{R}_{l'j'} = Q\,\boldsymbol{R}''_{l'j'}
\tag{2.66}
$$

and the local atomic coordinates $\boldsymbol{r}_1 = \boldsymbol{r} - \boldsymbol{R}_{l0}\,, \boldsymbol{r}_2 = \boldsymbol{r} - \boldsymbol{R}_{l'j'}$ of an electron, in different frames, transform in a similar way

$$
\begin{aligned}
\boldsymbol{r}_1 &= Q\,\boldsymbol{r}'' - Q\,\boldsymbol{R}''_{l0} = Q(\boldsymbol{r}'' - \boldsymbol{R}''_{l0}) = Q\,\boldsymbol{r}''_1\,, \tag{2.67a} \\
\boldsymbol{r}_2 &= Q\,\boldsymbol{r}''_2 \tag{2.67b}
\end{aligned}
$$

where $\boldsymbol{r}''_1 = \boldsymbol{r}'' - \boldsymbol{R}''_{l0}$ and $\boldsymbol{r}''_2 = \boldsymbol{r}'' - \boldsymbol{R}''_{l'j'}$.

The radial parts of the electronic orbitals

$$
\begin{aligned}
\varphi_\mu(\boldsymbol{r} - \boldsymbol{R}_{l0}) &= \varphi_\mu(\boldsymbol{r}_1) = f_L(r_1)Y_\mu(\theta_1, \phi_1)\,, \tag{2.68a} \\
\varphi_\nu(\boldsymbol{r} - \boldsymbol{R}_{l'j'}) &= \varphi_\nu(\boldsymbol{r}_2) = f_L(r_2)Y_\mu(\theta_2, \phi_2) \tag{2.68b}
\end{aligned}
$$

are invariant under the operator Q

$$
\begin{aligned}
f_L(r_1) &= f_L(r''_1)\,, \tag{2.69a} \\
f_L(r_2) &= f_L(r''_2) \tag{2.69b}
\end{aligned}
$$

since $r_i = |\boldsymbol{r}_i| = |Q\,\boldsymbol{r}_{i''}| = |\boldsymbol{r}_{i''}| = r_{i''}$ $(i = 1, 2)$. This is because the rotation Q is an orthogonal

linear operator.

The spherical harmonics $Y_L^m(\theta_i, \phi_i)$, $|m| \leqslant L$ form a subspace of the $(2L+1)$-dimensional representation of the group SO(3) of all rotations around a point. This means that for an arbitrary rotation Q, the function $Y_L^m(\theta_i, \phi_i)$ can be expressed as

$$Y_L^m(\theta_i, \phi_i) = \sum_{m'=-L}^{L} D_{mm'}^{(L)}(\gamma, \beta, \alpha) Y_L^{m'}(\theta_i'', \phi_i''), \tag{2.70}$$

i.e., as a linear combination of spherical harmonics $Y_L^{m'}(\theta_i'', \phi_i'')$ in the rotated frame $Ox_i'' y_i'' z_i''$. Formally, the coefficients of this combination are given by

$$D_{m'm}^{(L)}(\gamma, \beta, \alpha) = \langle Lm' | U_Q(\gamma, \beta, \alpha) | Lm \rangle \tag{2.71}$$

where $U_Q = e^{iL_z\gamma} e^{iL_z\beta} e^{iL_z\alpha} = e^{iL_y\theta_{\boldsymbol{R}}} e^{iL_z\theta_{\boldsymbol{R}}}$ is the rotation operator for the Euler angles $\alpha = \phi_{\boldsymbol{R}}$, $\beta = \theta_{\boldsymbol{R}}$, $\gamma = 0$, and $\boldsymbol{L} = (L_x, L_y, L_z)$ is operator of angular momentum. Thus, it turns out that each cubic harmonic defined by Eq. (2.61), corresponding to the orbital number L and the magnetic numbers $\pm m$, can be expressed as

$$Y_\mu(\theta_i, \phi_i) = \sum_{m'=-L}^{L} \widetilde{D}_{m'\mu}^{(L)}(\theta_{\boldsymbol{R}}, \phi_{\boldsymbol{R}}) Y_L^{m'}(\theta_i'', \phi_i'') \tag{2.72}$$

where $\widetilde{D}_{m'\mu}^{(L)} = C_\mu^m D_{m'm}^{(L)} + C_\mu^{-m} D_{m',-m}^{(L)}$; $i = 1, 2$.

In the two-centre approximation the TB Hamiltonian H_0^σ is approximated, in each of its matrix elements $\langle l0\mu\sigma | H_0^\sigma | l'j\nu\sigma \rangle$, by the kinetic term and two spherically symmetric atomic potentials $V_{\text{at}}^{(l\sigma)}(|\boldsymbol{r} - \boldsymbol{R}_{l0}|) = V_{\text{at}}^{(l\sigma)}(r_1)$, $V_{\text{at}}^{(l'\sigma)}(|\boldsymbol{r} - \boldsymbol{R}_{l'j'}|) = V_{\text{at}}^{(l'\sigma)}(r_2)$ centred at $\boldsymbol{R}_{l0}$ and $\boldsymbol{R}_{l'j'}$, respectively. Thus, the Hamiltonian reads

$$H_0^\sigma \simeq H_{2c}^\sigma = \frac{\boldsymbol{p}^2}{2m_0} + V_{\text{at}}^{(l\sigma)}(r_1) + V_{\text{at}}^{(l'\sigma)}(r_2) \tag{2.73}$$

where $\boldsymbol{p}^2 = -\hbar^2 \nabla_{\boldsymbol{r}}^2$. After change of the coordinates from $\boldsymbol{r}$ to $\boldsymbol{r}_1''$ we have the following relation: $\boldsymbol{r} = \boldsymbol{r}_1 + \boldsymbol{R}_{l0}$ where $\boldsymbol{r}_1 = Q\boldsymbol{r}_1''$ and $\boldsymbol{r}_2 = Q\boldsymbol{r}_2''$ where $\boldsymbol{r}_2'' = \boldsymbol{r}_1'' + \boldsymbol{R}'' = (x_1'', y_1'', z_1'' + R)$. The vector $\boldsymbol{R}'' = (0, 0, R)$ is the interatomic vector $\boldsymbol{R} = \boldsymbol{R}_{l'j} - \boldsymbol{R}_{l0}$ transformed to the rotated frame $O_1 x_1'' y_1'' z_1''$, i.e. $\boldsymbol{R} = Q\boldsymbol{R}''$, $R = |\boldsymbol{R}|$. The two-centre Hamiltonian can be expressed in the rotated frame as

$$H_{2c}^\sigma = \frac{-\hbar^2}{2m_0} \nabla_{\boldsymbol{r}_1''}^2 + V_{\text{at}}^{(l\sigma)}(r_1'') + V_{\text{at}}^{(l'\sigma)}(r_2'') = H_{2c}^\sigma(r_1'') \tag{2.74}$$

(note that $r_1 = r_1''$, $r_2 = r_2''$). In the local cylindrical coordinates $(\rho_1'', z_1'', \phi_1'')$ the radii $r_1'' =$

$|\boldsymbol{r}_1''|$, $r_2'' = |\boldsymbol{r}_2''|$ are represented as

$$r_1'' = \sqrt{(\rho_1'')^2 + (z_1'')^2}\,, \qquad r_2'' = \sqrt{(\rho_1'')^2 + (z_1'' + R)^2} \tag{2.75}$$

and the Laplacian is given by

$$\nabla_{r_1''}^2 = \frac{1}{\rho_1''}\frac{\partial}{\partial\rho_1''}\left(\rho_1''\frac{\partial}{\partial\rho_1''}\right) + \frac{1}{\rho_1''^2}\frac{\partial^2}{\partial\phi_1''^2} + \frac{\partial^2}{\partial z_1''^2}. \tag{2.76}$$

Thus, the operator H_{2c}^σ does not depend on ϕ_1'' which means that it is invariant under rotation by an arbitrary angle around the z_1'' axis.

After such change of variables the matrix elements of $H_0^\sigma \approx H_{2c}^\sigma$ take the form

$$\langle l0\mu\sigma | H_0^\sigma | l'j'\nu\sigma \rangle = \int d\boldsymbol{r}\, f_L(r_1)^* Y_\mu(\theta_1, \phi_1)^* H_{2c}^\sigma(\boldsymbol{r})\, f_{L'}(r_2) Y_\nu(\theta_2, \phi_2)$$

$$= \sum_{m'=-L}^{L} \sum_{m''=-L}^{L'} (\widetilde{D}_{m'\mu}^{(L)})^* \widetilde{D}_{m''\nu}^{(L')} \int d\boldsymbol{r}_1'' f_L(r_1'')^* f_{L'}(r_2'') H_{2c}(\rho_1'', z_1'') Y_L^{m'}(\theta_1'', \phi_1'')^* Y_{L'}^{m''}(\theta_2'', \phi_2''). \tag{2.77}$$

However, $\phi_2'' = \phi_1''$ (since the corresponding axes of the two frames $O_1 x_1'' y_1'' z_1''$ and $O_2 x_2'' y_2'' z_1''$ are parallel to each other) thus the integral $\int d\boldsymbol{r}_1'' = \int_{-\infty}^{\infty} dz_1'' \int_0^{\infty} \rho_1'' d\rho_1'' \int_0^{2\pi} d\phi_1$ expressed in the cylindrical coordinates $(\rho_1'', z_1'', \phi_1'')$ vanishes if $m'' \neq m'$. This is so because

$$Y_L^{m'}(\theta_1'', \phi_1'') \sim e^{im'\phi_1''}\,, \qquad Y_L^{m''}(\theta_2'', \phi_2'') \sim e^{im''\phi_2''} = e^{im''\phi_1''} \tag{2.78}$$

whilst other parts of the integrand do not depend on ϕ_1''. The Hamiltonian matrix elements can then be expressed as

$$\langle l0\mu\sigma | H_0^\sigma | l'j'\nu\sigma \rangle = \sum_{m'=0}^{min(L,L')} F_{\mu\nu}^{LL'm'}(\theta_{\boldsymbol{R}}, \phi_{\boldsymbol{R}})\, T_{LL'm'}^\sigma \tag{2.79}$$

where

$$T_{LL'm'}^\sigma = \int d\boldsymbol{r}_1''\, f_L(r_1'')^* f_{L'}(r_2'') Y_L^{m'}(\theta_1'', \phi_1'')^* Y_{L'}^{m'}(\theta_2'', \phi_1'') \tag{2.80}$$

are two-centre SK parameters corresponding to orbitals which have the same or different orbital numbers L, L' but their angular parts are given by spherical harmonics with the same magnetic number m' with respect to the axis z'' joining the two atoms. The sum in Eq. (2.79) starts with $m' = 0$ since $T_{LL',-m'} = T_{LL',m}$ and the function

$$F_{\mu\nu}^{LL'm'}(\theta_{\boldsymbol{R}}, \phi_{\boldsymbol{R}}) = (\widetilde{D}_{m'\mu}^{(L)})^* \widetilde{D}_{m'\nu}^{(L')} + (\widetilde{D}_{-m'\mu}^{(L)})^* \widetilde{D}_{-m'\nu}^{(L')} \tag{2.81}$$

defined for $m' > 0$ includes also terms with negative m' present in Eq. (2.77). For $m' = 0$ this

38

function is equal to $F_{\mu\nu}^{LL'0}(\theta_{\boldsymbol{R}}, \phi_{\boldsymbol{R}}) = (\widetilde{D}_{0\mu}^{(L)})^* \, \widetilde{D}_{0\nu}^{(L')}$.

In this context, the numbers L, L' and m' are denoted as in molecular quantum chemistry i.e., s for $L = 0$, p for $L = 1$, d for $L = 2$; and σ for $m' = 0$, π for $m' = 1$, δ for $m' = 2$. Thus, there are 10 basic TB two-centre SK parameters $T_{ss\sigma}^\sigma, T_{pp\sigma}^\sigma, T_{pp\pi}^\sigma, T_{dd\sigma}^\sigma, T_{dd\pi}^\sigma, T_{dd\delta}^\sigma, T_{sp\sigma}^\sigma, T_{pd\sigma}^\sigma, T_{pd\pi}^\sigma, T_{pd\pi}^\sigma$ for each spin $\sigma = \uparrow, \downarrow$. Note that here, in the $T_{LL'\sigma}^\sigma$ symbol, σ has different meaning in subscript $(m' = 0)$ and superscript (spin). The parameters $T_{LL'\sigma}^\sigma$ depend on the overlap of the functions

$$f_L(r_1'') = f_L(r_1) = f_L(|\boldsymbol{r}' - \boldsymbol{R}_{l0}|) \tag{2.82}$$

and

$$f_{L'}(r_2'') = f_{L'}(r_2) = f_{L'}(|\boldsymbol{r}' - \boldsymbol{R}_{l'j'}|) \tag{2.83}$$

which quickly decays. This is why the values of $T_{LL'\sigma}^\sigma$ rapidly decrease with increasing interatomic distance $R = |\boldsymbol{R}_{l'j'} - \boldsymbol{R}_{l0}|$ so that the parameters $T_{LL'\mu}^\sigma$ are usually assumed to be nonzero only for the first and second nearest neighbours.

The tabulated two-centre SK parameters $T_{LL'm'}^\sigma$ for 1st and 2nd n.n. can be found for several tens of elements in Papaconstantopoulos' book [123]. They have been obtained by fitting the TB energy bands for bulk solid crystals to energies obtained in *ab initio* DFT calculations. These SK parameters are used in the present TB calculations.

The functions $F_{\mu\nu}^{(LL'm')}(\theta_{\boldsymbol{R}}, \phi_{\boldsymbol{R}})$, entering the expression (2.81) for the matrix elements of the TB Hamiltonian H_0^σ, depend on the orientation $(\theta_{\boldsymbol{R}}, \phi_{\boldsymbol{R}})$ of the interatomic vector $\boldsymbol{R}$ and they can be expressed in terms of its direction cosines $\alpha_x, \alpha_y, \alpha_z$. As already mentioned, the detailed expressions for these functions are given for s, p, d orbitals in the seminal work by Slater and Koster [122]. The angular dependence of the functions $F_{\mu\nu}^{(LL'm')}(\theta_R, \phi_R)$ can be derived using the definition of the cubic harmonics and the explicit form of the coordinate transformation $\boldsymbol{r} = Q \, \boldsymbol{r}''$. A few examples of such derivation are given in the appendix C. A general method for obtaining the two-centre SK formulas and extending them to arbitrary orbital numbers L, L' is given by McMahan in Ref. [124].

2.5 Spin-orbit interaction

Spin of electrons is coupled to their orbital motion. This interaction takes the form of the coupling of spin direction with the electron orbital angular momentum in atomic systems. Such

SO interaction alongside other relativistic corrections gives rise to the fine structure of energy levels in atoms. In crystalline systems with 2D or 3D translational symmetry the SO interaction leads to (partially) removing the degeneracy of energy bands along the symmetry lines in the BZ as well as avoiding crossings of bands with opposite spins. Although the SO interaction is a relatively weak interaction compared to the exchange interaction (about 10-100 times smaller), such an interaction is of great importance in the spintronic domain. In particular, it largely affects the magnetic anisotropy (leading to its magnetocrystalline contribution which can dominate the shape anisotropy) and it is at the heart of the spintronic effects such as the spin Hall effect or the Rashba effect. The SO interaction is also an essential factor in spin relaxation processes in magnetic systems which are of main interest in the present work.

The physical mechanism of the SO interaction can be explained on the grounds of the classical electrodynamics in the following way. As an electron moves with velocity $\boldsymbol{v}$ in electric field $\boldsymbol{E}$, it experiences a magnetic field $\boldsymbol{B}'$ in its rest frame and this field affects the electron spin $\boldsymbol{S}$. According to the transformation rules for electric and magnetic fields between two inertial frames of reference the magnetic field in question is equal to (in CGS units)

$$\boldsymbol{B}' = \frac{\boldsymbol{E} \times \boldsymbol{v}}{c} = \frac{\boldsymbol{E} \times \boldsymbol{p}}{m_0 c} \tag{2.84}$$

where $\boldsymbol{p}$ is the electron momentum. Such transformation of fields results from the Lorentz transformation of coordinates in the special relativity theory.

Due to the interaction of the electron magnetic moment $\boldsymbol{\mu} = -2\mu_{\mathrm{B}}\boldsymbol{S}/\hbar$ with the magnetic field, the following potential energy emerges

$$-\boldsymbol{\mu} \cdot \boldsymbol{B}' = \frac{2\mu_{\mathrm{B}}}{\hbar m_0 c}\, \boldsymbol{S} \cdot (\boldsymbol{E} \times \boldsymbol{p}) = \frac{|e|}{m_0^2 c^2}\, \boldsymbol{S} \cdot (\boldsymbol{E} \times \boldsymbol{p}) \tag{2.85}$$

where the definition of the Bohr magneton $\mu_{\mathrm{B}} = \frac{\hbar|e|}{2m_0 c}$ is used. This energy gives the general form of the SO interaction in an arbitrary electric field $\boldsymbol{E}$

$$H_{\mathrm{SO}} = -\frac{e}{2m_0^2 c^2}\, \boldsymbol{S} \cdot (\boldsymbol{E} \times \boldsymbol{p}) \tag{2.86}$$

if the correct prefactor $1/2$ is introduced as the additional relativistic correction due to the Thomas precession [126]. The latter is a purely kinematic relativistic effect which occurs when the acceleration $\boldsymbol{a} = e\boldsymbol{E}/m_0$ of an electron has a component perpendicular to its velocity $\boldsymbol{v}$ during the curvilinear motion of the electron in the electric field. This effect is the result of the fact that in the special relativistic theory the composition of two Lorentz boosts (i.e., Lorentz

transformations $A(\boldsymbol{\beta})$ and $A(\delta\boldsymbol{\beta})$ where $\boldsymbol{\beta} = \boldsymbol{v}/c$ is not equivalent to a single pure Lorentz boost $A(\boldsymbol{\beta} + \delta\boldsymbol{\beta})$ since an additional rotation of the axes of the electron rest frame, called the Thomas rotation takes place [127]. The angular frequency of this rotation, $\omega_{\mathrm{T}} = \frac{\boldsymbol{a} \times \boldsymbol{v}}{c^2} = \frac{e}{m_0 c^2}\, \boldsymbol{a} \times \boldsymbol{v}$, leads to the reduction of the energy in Eq. (2.85) by $1/2$.

The correct form of the SO interaction as a quantum operator can also be derived from the Dirac equation in the relativistic quantum mechanics. In the semi-relativistic regime, the total Hamiltonian of an electron in an electric field $\boldsymbol{E}$ and a magnetic field $\boldsymbol{B}$ (present in an inertial frame of reference) reads

$$
\begin{aligned}
H \;=\; & m_0 c^2 + \left[\frac{1}{2m_0}\left(\boldsymbol{p} - \frac{e}{c}\boldsymbol{A} \right)^2 - \frac{p^4}{8m_0^3 c^2} \right] + e\phi - \frac{e\hbar}{2m_0 c}\, \boldsymbol{\sigma} \cdot \boldsymbol{B} \\
& - i\frac{e\hbar^2}{8m_0^2 c^2}\, \boldsymbol{\sigma} \cdot \boldsymbol{\nabla} \times \boldsymbol{E} - \frac{e\hbar}{4m_0^2 c^2}\, \boldsymbol{\sigma} \cdot \boldsymbol{E} \times \boldsymbol{p} - \frac{e\hbar^2}{8m_0^2 c^2}\, \boldsymbol{\nabla} \cdot \boldsymbol{E}\,. \qquad (2.87)
\end{aligned}
$$

The quantities appearing here are the familiar Pauli matrices $\boldsymbol{\sigma} = (\sigma_x, \sigma_y, \sigma_z)$ which define the electron spin $S = \frac{1}{2}\hbar\boldsymbol{\sigma}$, the vector potential $\boldsymbol{A}$ and the scalar potential ϕ.

The term in the square brackets in Eq. (2.87) is just the relativistic form of the kinetic energy with the leading corrections ($\sim p^4$). The second and third terms stand for the electrostatic potential and the Zeeman term (its spin part), respectively. The fourth ($\sim \boldsymbol{\sigma} \cdot \boldsymbol{\nabla} \times \boldsymbol{E}$) and fifth ($\sim \boldsymbol{\sigma} \cdot \boldsymbol{E} \times \boldsymbol{p}$) terms together represent the SO interaction. The former vanishes due to the spherical symmetry of the electron static potential ($\boldsymbol{\nabla} \times \boldsymbol{E} = 0$). Thus, one is left with the latter term as the SO interaction given by Eq. (2.86). The last term ($\sim \boldsymbol{\nabla} \cdot \boldsymbol{E}$) is known as the Darwin term and is effective merely for s states ($L = 0$).

The electric field can be expressed as $\boldsymbol{E} = -\nabla\phi = -\frac{1}{e}\nabla V(\boldsymbol{r})$ with the electrostatic potential $\phi(\boldsymbol{r})$ or the corresponding potential energy $V(\boldsymbol{r}) = e\phi(\boldsymbol{r})$ of an electron. It should be noted here that the potential energy $V(\boldsymbol{r})$ is also often called the potential within the quantum theory so that some care is needed to avoid ambiguity in discussion. In the case of solids, the SO interaction results from the periodic crystal potential which can be identified with the effective KS potential within the DFT approach. This potential can be well approximated, e.g., in a layered metallic system, as the sum

$$
V(\boldsymbol{r}) = \sum_{lj} V_{\mathrm{at}}^{(l)}(|\boldsymbol{r} - \boldsymbol{R}_{lj}|) \qquad (2.88)
$$

of atomic-like potentials $V_{\mathrm{at}}^{(l)}$, each of which is spherically symmetric and is centred at one of atomic sites at positions $\boldsymbol{R}_{lj}$. The atomic potential $V_{\mathrm{at}}^{(l)}$ depends on the type of metal that the l-th atomic layer is built of. The gradient of the potential $V_{\mathrm{at}}^{(l)}(r')$, dependent on $r' = |\boldsymbol{r}'|$ where $\boldsymbol{r}' = \boldsymbol{r} - \boldsymbol{R}_{lj}$, gives the electric field $\boldsymbol{E} = -\frac{1}{e}\frac{\boldsymbol{r}'}{r'}\, dV_{\mathrm{at}}^{(l)}(r')/dr'$ which has the radial direction

around each atom. Thus, the SO interaction can be expressed in terms of the orbital angular momentum $\boldsymbol{L}(\boldsymbol{r'}) = \boldsymbol{r'} \times \boldsymbol{p}$ and spin $\boldsymbol{S}$ operators only,

$$H_{\mathrm{SO}} = \sum_{lj} \xi_{\mathrm{at}}^{(l)}(|\boldsymbol{r} - \boldsymbol{R}_{lj}|)\, \boldsymbol{L}(\boldsymbol{r} - \boldsymbol{R}_{lj}) \cdot \boldsymbol{S} \equiv \sum_{lj} h_{\mathrm{SO}}^{(lj)}(\boldsymbol{r} - \boldsymbol{R}_{lj}) \tag{2.89}$$

where the function $\xi_{\mathrm{at}}^{(l)}(r') = \frac{\hbar^2}{2m_0^2 c^2} \frac{1}{r'} \frac{dV_{\mathrm{at}}^{(l)}(r')}{dr'}$ defines the strength of the SO interaction. The form of this function, with $\hbar^2$ (instead of 1), is valid if angular momentum is expressed in units of $\hbar$, i.e., $\boldsymbol{L}$ and $\boldsymbol{S}$ stand for the dimensionless operators $\boldsymbol{L}/\hbar$ and $\boldsymbol{S}/\hbar$, in fact. The largest contributions to the SO interaction come from the atomic regions close to the atomic nuclei where $V_{\mathrm{at}}^{(l)}(r') \simeq -\frac{Ze^2}{r'}$ so that $\xi_{\mathrm{at}}^{(l)}(r') \sim \frac{Z}{(r')^3}$. This proves that the SO coupling is the sum of short-range interactions $h_{\mathrm{SO}}^{(lj)}$ localised around each atom. As a result, the matrix elements $\langle l0\mu\sigma | h_{\mathrm{SO}}^{(l''j'')} | l'j'\nu\sigma' \rangle$ of an atomic contribution $h_{\mathrm{SO}}^{(l''j'')}$ to the total SO Hamiltonian H_{SO} can be assumed to be negligible if one or two of the atomic orbitals $\phi_\mu(\boldsymbol{r} - \boldsymbol{R}_{l0})$ and $\phi_\nu(\boldsymbol{r} - \boldsymbol{R}_{l'j'})$ are located on atoms different than the atom $(l''j'')$, i.e., $\langle l0\mu\sigma | h_{\mathrm{SO}}^{(l''j'')} | l'j'\nu\sigma' \rangle \sim \delta_{ll''}\delta_{l'l''}\delta_{0j''}\delta_{j'j''}$. Thus, the matrix elements of H_{SO} are finite only between orbitals on the same atom,

$$\langle l0\mu\sigma | H_{\mathrm{SO}} | l'j'\nu\sigma' \rangle = \langle l0\mu\sigma | h_{\mathrm{SO}}^{(l0)} | l0\nu\sigma' \rangle \delta_{ll'}\delta_{0j'}. \tag{2.90}$$

Due to the form of the SO atomic interaction, $h_{\mathrm{SO}}^{(l0)} = \xi_{\mathrm{at}}^{(l)}(r')\boldsymbol{L}(\boldsymbol{r'}) \cdot \boldsymbol{S}$, it has nonzero matrix elements only between orbitals $\phi_\mu(\boldsymbol{r'}) = f_L(r')Y_\mu(\theta', \phi')$ and $\phi_\nu(\boldsymbol{r'}) = f_L(r')Y_\nu(\theta', \phi')$ with the same orbital number L. These elements are equal to

$$
\begin{aligned}
\langle l0\mu\sigma | h_{\mathrm{SO}}^{(l0)} | l0\nu\sigma' \rangle &= \left[\int d\boldsymbol{r'}\, \phi_\mu^*(\boldsymbol{r'})\xi_{\mathrm{at}}^{(l)}(r')\boldsymbol{L}(\boldsymbol{r'})\phi_\nu(\boldsymbol{r'}) \right] \cdot \langle \sigma | \boldsymbol{S} | \sigma' \rangle \\
&= \int_0^\infty dr\, r^2 f_L^2(r)\xi_{\mathrm{at}}^{(l)}(r) \int_0^\pi d\theta \sin\theta \int_0^{2\pi} d\phi\, Y_\mu^*(\theta, \phi)\boldsymbol{L}(\theta, \phi)Y_\nu(\theta, \phi) \cdot \langle \sigma | \boldsymbol{S} | \sigma' \rangle \\
&= \xi_{\mathrm{at,L}}^{(l)}\langle \mu | \boldsymbol{L} | \nu \rangle \cdot \langle \sigma | \boldsymbol{S} | \sigma' \rangle \\
&= \xi_{\mathrm{at,L}}^{(l)}\langle \mu\sigma | \boldsymbol{L} \cdot \boldsymbol{S} | \nu\sigma' \rangle
\end{aligned}
\tag{2.91}
$$

where $\xi_{\mathrm{at,L}}^{(l)} = \int_0^\infty dr\, r^2 f_L^2(r)\xi_{\mathrm{at}}^{(l)}(r)$ defines the SO coupling constant (dependent on L) for a metal forming the l-th layer. As it is usually done in TB model, for each metal M, a common SO coupling constant $\xi_{\mathrm{at,L}}^{(l)} = \xi_{\mathrm{M}}$ is taken for all L, corresponding to the d orbitals $(L = 2)$ responsible for magnetic phenomena. Let us note that the SO coupling strength has a constant value in bulk metals M $(\xi_{\mathrm{at}} = \xi_{\mathrm{M}})$ and in monometallic films, $\xi_{\mathrm{at}}^{(l)} = \xi_l = \xi_{\mathrm{M}}$ (equal to the bulk value ξ_{M}), whilst for multilayer systems the SO coupling constant ξ_l alters with the layer index l depending on the type of metal in each atomic layer. This fact has been taken into account in chapter 3 when dealing with magnetic bilayers, trilayers and multilayers which consist of different

metals. The values of the SO coupling for $3d$, $4d$ and $5d$ metals considered in the present thesis: $\xi_{\mathrm{Fe}} = 0.075$ eV, $\xi_{\mathrm{Co}} = 0.085$ eV, $\xi_{\mathrm{Ni}} = 0.105$ eV, $\xi_{\mathrm{Cu}} = 0.12$ eV, $\xi_{\mathrm{Pd}} = 0.23$ eV, $\xi_{\mathrm{Ag}} = 0.24$ eV, $\xi_{\mathrm{Pt}} = 0.65$ eV and $\xi_{\mathrm{Au}} = 0.66$ eV are taken from Refs. [95, 128, 129].

With the obtained relations (2.90) and (2.91) for the SO interaction elements in the orbital basis, one immediately finds the final form of the elements of the SO interaction in the Bloch TB basis $|l\boldsymbol{k}\mu\sigma\rangle$,

$$
\begin{aligned}
H^{\sigma\sigma'}_{\mathrm{SO};\,l\mu,l'\nu}(\boldsymbol{k}) &= \sum_j e^{i\boldsymbol{k}\cdot(\boldsymbol{R}_{l'j}-\boldsymbol{R}_{l0})} \langle|l0\mu\sigma|H_{\mathrm{SO}}|l'j\nu\sigma\rangle \\
&= \langle l0\mu\sigma|h^{(l0)}_{\mathrm{SO}}|l0\nu\sigma\rangle\delta_{ll'} \\
&= \xi^{(l)}_{\mathrm{at,L}}\langle\mu\sigma|\boldsymbol{L}\cdot\boldsymbol{S}|\nu\sigma'\rangle\delta_{ll'}
\end{aligned}
\tag{2.92}
$$

which shows that they do not depend on $\boldsymbol{k}$, are diagonal in layer index l and are equal to the matrix elements of the atomic SO coupling. The matrix elements $\langle\mu\sigma|\boldsymbol{L}\cdot\boldsymbol{S}|\nu\sigma'\rangle$ are given by

$$
\langle\mu\uparrow|\boldsymbol{L}\cdot\boldsymbol{S}|\uparrow\nu\rangle = \frac{1}{2}\langle\mu|L^z|\nu\rangle, \tag{2.93a}
$$

$$
\langle\mu\uparrow|\boldsymbol{L}\cdot\boldsymbol{S}|\downarrow\nu\rangle = \frac{1}{2}\langle\mu|L^-|\nu\rangle, \tag{2.93b}
$$

$$
\langle\mu\downarrow|\boldsymbol{L}\cdot\boldsymbol{S}|\uparrow\nu\rangle = \langle\mu\uparrow|\boldsymbol{L}\cdot\boldsymbol{S}|\downarrow\nu\rangle^*, \tag{2.93c}
$$

$$
\langle\mu\downarrow|\boldsymbol{L}\cdot\boldsymbol{S}|\downarrow\nu\rangle = -\langle\mu\uparrow|\boldsymbol{L}\cdot\boldsymbol{S}|\uparrow\nu\rangle \tag{2.93d}
$$

so that they are expressed with the matrix elements of the angular momentum operators L^z and L^-. Below are listed all **nonzero matrix elements** of the two operators,

$$
\begin{aligned}
\langle x|L^-|z\rangle &= -\langle z|L^-|x\rangle = 1\,, \\
\langle y|L^-|z\rangle &= -\langle z|L^-|y\rangle = -i\,, \\
\langle xy|L^-|yz\rangle &= -\langle yz|L^-|xy\rangle = 1\,, \\
\langle xy|L^-|zx\rangle &= -\langle zx|L^-|xy\rangle = -i\,, \\
\langle yz|L^-|x^2-y^2\rangle &= -\langle x^2-y^2|L^-|yz\rangle = -i\,, \\
\langle yz|L^-|3z^2-r^2\rangle &= -\langle 3z^2-r^2|L^-|yz\rangle = -i\sqrt{3}\,, \\
\langle zx|L^-|x^2-y^2\rangle &= -\langle x^2-y^2|L^-|zx\rangle = -1\,, \\
\langle zx|L^-|3z^2-r^2\rangle &= -\langle 3z^2-r^2|L^-|zx\rangle = \sqrt{3}\,, \\
\langle x|L^z|y\rangle &= -\langle y|L^z|x\rangle = -i\,, \\
\langle xy|L^z|x^2-y^2\rangle &= -\langle x^2-y^2|L^z|xy\rangle = 2i\,, \\
\langle yz|L^z|zx\rangle &= -\langle zx|L^z|yz\rangle = i\,.
\end{aligned}
\tag{2.94}
$$

According to the convention applied here spin (S) and orbital (L) angular momentum operators are expressed in units of $\hbar$ so that the Planck constant $\hbar$ is not present in the above matrix elements in Eq. (2.94). The following relations, well-known in quantum mechanics, are applied in calculation of these elements,

$$\langle Y_L^m|L^z|Y_{L'}^{m'}\rangle \quad \sim \quad \delta_{LL'}, \tag{2.95a}$$

$$\langle Y_L^m|L^-|Y_{L'}^{m'}\rangle \quad \sim \quad \delta_{LL'}, \tag{2.95b}$$

$$L^z Y_L^m \quad = \quad m Y_L^m, \tag{2.95c}$$

$$L^\pm Y_L^m \quad = \quad \sqrt{(L \pm m + 1)(L \mp m)} Y_L^{m\pm1}. \tag{2.95d}$$

Additionally, the representation of cubic harmonics in terms of Y_L^m, given by Eqs. (2.60), is used.

The non-relativistic KS equation, which is often used in *ab initio* DFT calculations, leads to electronic states with definite spin, up or down, so that they are fully spin-polarised. Such states form doubly-degenerate energy bands in nonmagnetic systems, whilst spin-up and spin-down energy bands are split due to exchange in ferromagnets.

The inclusion of SO interaction is of importance in band structure calculations for both nonmagnetic and ferromagnetic metals. It modifies the electronic states which become linear combinations of terms with spin-up and spin-down. The electronic energies are modified in the whole BZ though it should be remembered that the Kramers degeneracy due to time reversal symmetry is always preserved. The latter property implies, in particular, that all energy bands in nonmagnetic systems with inversion symmetry, like cubic crystals, are doubly degenerate at general k-points. The SO interaction has a particular large effect on energy bands in heavier elements, like Pt and Au, since the SO coupling constant ξ_M scales as Z^2 with the atomic number Z of the metal M. This interaction can lift the degeneracy (due to spatial symmetry) at high-symmetry points and along high-symmetry lines in the BZ. In ferromagnets, the SO interaction also makes energy bands avoid mutual crossing if two bands determined in the non-relativistic calculation (in the DFT or TB approach) have opposite spins (up and down) and cross each other at some k-points (forming a line in the case of the 2D BZ). Near such k-points (including high-symmetry points) where the degeneracy of energy bands is lifted due to the SO interaction, the involved electronic states can be so strongly spin-mixed that their net spin (along the spin quantisation axis) is very small or even vanishes at the k-points of avoided band crossings where the spin components of the state are equal [130]. If such states with (nearly) zero spin polarisation have energies very close to the Fermi level, the corresponding very restricted regions of k-points on the Fermi surface (FS) are called spin hot spots. This is so because their

44

presence can enhance spin-flip scattering of electrons by several orders of magnitudes. Such effect has been predicted theoretically [131] and later confirmed, e.g., in experiments on fcc Co using magnetic linear dichroism (MLD) measurements [132]. It can be expected that spin hot spots also play a major role in the relaxation of the spin direction in the magnetic systems, i.e., the magnetic damping investigated in the present work. This point will be discussed in Sec. 4.2 below.

2.6 Calculation of Gilbert damping constant

The goal in this section is evaluation of the expression which defines the Gilbert damping constant α in Eq. (2.43) (at $T = 0$) and Eq. (2.44) (at finite T). As seen in Sec. 2.3 the effort to determine the Gilbert damping constant α has given rise to the following trace

$$\mathrm{tr}D = \mathrm{tr}\{A^- \, L(\epsilon - H)A^+ \, L(\epsilon - H)\} \tag{2.96}$$

where $A^- = [S^-, H_{\mathrm{SO}}]$, $A^+ = (A^-)^\dagger = [H_{\mathrm{SO}}, S^+]$ and S^-, S^+ are the spin ladder operators. This trace can be calculated in an arbitrary basis $|i\rangle$

$$\mathrm{tr}D = \sum_i \langle i|A^- \, L(\epsilon - H)A^+ \, L(\epsilon - H)|i\rangle \tag{2.97}$$

but it is done most conveniently using the orthonormalised basis built of the eigenstates $|n\rangle$ of the Hamiltonian. Therefore, by using the unit operator $\sum_{n'} |n'\rangle\langle n'| = 1$ one obtains

$$\mathrm{tr}D = \sum_n \sum_{n'} \langle n|A^-|n'\rangle\langle n'|L(\epsilon - H)A^+ \, L(\epsilon - H)|n\rangle \tag{2.98}$$

that leads to

$$\sum_{n,n'} \langle n|A^-|n'\rangle L(\epsilon - \epsilon_{n'})\langle n'|A^+|n\rangle L(\epsilon - \epsilon_n) = \sum_{n,n'} |\langle n|A^-|n'\rangle|^2 L(\epsilon - \epsilon_n)L(\epsilon - \epsilon_{n'}). \tag{2.99}$$

For bulk metals and layered systems the eigenstates $|n\rangle = |n\boldsymbol{k}\rangle$ and $|n'\rangle = |n'\boldsymbol{k}'\rangle$ of the Hamiltonian are Bloch states labeled with the wave vectors $\boldsymbol{k}, \boldsymbol{k}'$ and the band indices n, n'. The matrix elements

$$\langle n|A^-|n'\rangle = \delta_{\boldsymbol{k}\boldsymbol{k}'}\langle n\boldsymbol{k}|A^-|n'\boldsymbol{k}'\rangle \tag{2.100}$$

are diagonal in $\boldsymbol{k}$ due to the translational symmetry (3D or 2D) of the operator $A^- = A^-(\boldsymbol{r})$. Namely, the relation $A^-(\boldsymbol{r} + \boldsymbol{R}) = A^-(\boldsymbol{r})$ holds for translation by any lattice vector $\boldsymbol{R}$. Thus, the following expression for the Gilbert damping constant is obtained from Eqs. (2.44), (2.99)

and (2.100)

$$\alpha = \frac{\pi}{\mu_{\text{tot}}} \sum_{\boldsymbol{k} \in \text{BZ}} \sum_{n,n'} |A_{nn'}(\boldsymbol{k})|^2 F_{nn'}(\boldsymbol{k}) \tag{2.101}$$

where $A_{nn'}(\boldsymbol{k}) = \langle n\boldsymbol{k}|A^-|n'\boldsymbol{k}\rangle$, and $\mu_{\text{tot}} = 2\langle S_{\text{tot}}^z \rangle$ is the total spin magnetic moment (in units of the Bohr magneton μ_{B}). The summations in Eq. (2.101) are over all $\boldsymbol{k}$-points in the BZ and band indices n, n'. The expression for the SO torque matrix elements $A_{nn'}(\boldsymbol{k})$ obtained within the TB model are presented in the next section. The factor $F_{nn'}(\boldsymbol{k})$ is given by the following integral over energy ϵ,

$$F_{nn'}(\boldsymbol{k}) = \int d\epsilon \, \eta(\epsilon) L(\epsilon - \epsilon_n(\boldsymbol{k})) L(\epsilon - \epsilon_{n'}(\boldsymbol{k})) \tag{2.102}$$

at finite temperature. It reduces to the simpler form $F_{nn'}(\boldsymbol{k}) = L(\epsilon_{\text{F}} - \epsilon_n(\boldsymbol{k})) L(\epsilon_{\text{F}} - \epsilon_{n'}(\boldsymbol{k}))$ at $T = 0$ since in this case $f_{\text{FD}}(\epsilon)$ becomes the Heaviside step function $\theta(\epsilon_{\text{F}} - \epsilon)$ and its negative derivative $\eta(\epsilon)$ is the Dirac δ-function $\delta(\epsilon - \epsilon_{\text{F}})$. Here, $L(\epsilon - \epsilon_n(\boldsymbol{k}))$ and $L(\epsilon - \epsilon_{n'}(\boldsymbol{k}))$ are two Lorentz functions depending on eigenenergies $\epsilon_n(\boldsymbol{k})$, $\epsilon_{n'}(\boldsymbol{k})$, with band indices n, n' and the scattering rate Γ. The calculation of $F_{nn'}(\boldsymbol{k})$ at finite T is discussed in Sec. 2.6.2 and an efficient formula for this factor is derived in Sec. 2.6.3.

In a layered system, the number N_{2D} of $\boldsymbol{k}$-points in the 2D BZ is equal to the number of atoms in a single atomic layer (with periodic boundary conditions imposed). Thus, the total spin magnetic moment in a layered structure with one ferromagnetic layer, N_{FM} monolayers thick, is equal to $\mu_{\text{tot}} = N_{\text{2D}} N_{\text{FM}} \mu_{\text{FM}}$ where μ_{FM} (in units of μ_{B}) is the magnetic moment per atom of the ferromagnetic metal. This gives the following final formula for the damping constant in such systems

$$\alpha = \frac{\pi}{N_{\text{FM}} \mu_{\text{FM}}} \frac{1}{N_{\text{2D}}} \sum_{\boldsymbol{k} \in \text{BZ}} \sum_{n,n'} |A_{nn'}(\boldsymbol{k})|^2 F_{nn'}(\boldsymbol{k}). \tag{2.103}$$

In layered structures with two or more ferromagnetic parts the denominator $N_{\text{FM}} \mu_{\text{tot}}$, which represents the magnetic moment per surface atom, has to be appropriately modified. For bulk metals, the prefactor becomes $\frac{\pi}{\mu_{\text{FM}}} \frac{1}{N_{\text{3D}}}$ where N_{3D} is the number of $\boldsymbol{k}$-points in the 3D BZ.

2.6.1 Matrix elements of spin-orbit torque operator

The next task in evaluation of the trace appearing in the expression for the Gilbert damping constant is to calculate the matrix elements of the operator $A^- = [S^-, H_{\text{SO}}]$. This is done by representing the Hamiltonian eigenstates $|n\boldsymbol{k}\rangle$, $|n'\boldsymbol{k}\rangle$ in the basis of the Bloch states $|\boldsymbol{k}l\mu\sigma\rangle$ (Eq. (2.50)) and the subsequent use of their definition (2.49). Thus, one obtains the following

expression

$$\langle n\boldsymbol{k}|A^-|n'\boldsymbol{k}\rangle = \sum_{l\mu\sigma}\sum_{l'\nu\sigma'} (a^{\sigma}_{nl\mu}(\boldsymbol{k}))^* \, a^{\sigma'}_{n'l'\nu}(\boldsymbol{k})\langle \boldsymbol{k}l\mu\sigma|A^-|\boldsymbol{k}l'\nu\sigma'\rangle$$

$$= \frac{1}{N_{\mathrm{2D}}} \sum_{\mu\sigma,\,\nu\sigma'}\sum_{lj,\,l'j'} (a^{\sigma}_{nl\mu}(\boldsymbol{k}))^* \, a^{\sigma'}_{n'l'\nu}(\boldsymbol{k})\, e^{i\boldsymbol{k}\cdot(\boldsymbol{R}_{l'j'}-\boldsymbol{R}_{lj})}\langle lj\mu\sigma|A^-|l'j'\nu\sigma'\rangle. \quad (2.104)$$

Since the SO coupling given by Eq. (2.89) is a short range interaction, localised around each atom, it is usually assumed that its matrix elements between orbitals centred on different atoms vanish as it is explained in Sec. 2.5. The same argument holds for the SO torque

$$\begin{aligned} A^- = \left[S^-, H_{\mathrm{SO}}\right] &= \sum_{lj} \xi^{(l)}_{\mathrm{at}}(|\boldsymbol{r}-\boldsymbol{R}_{lj}|)\left[S^-, \boldsymbol{L}(\boldsymbol{r}-\boldsymbol{R}_{lj})\cdot\boldsymbol{S}\right] \\ &= \sum_{lj} \xi^{(l)}_{\mathrm{at}}(|\boldsymbol{r}-\boldsymbol{R}_{lj}|)\, A^-_{\mathrm{at}}(\boldsymbol{r}-\boldsymbol{R}_{lj}) \end{aligned} \quad (2.105)$$

where

$$A^-_{\mathrm{at}} = \left[S^-, \boldsymbol{L}\cdot\boldsymbol{S}\right]. \quad (2.106)$$

Indeed, taking into account that $\xi^{(l)}_{\mathrm{at}}(|\boldsymbol{r}-\boldsymbol{R}_{lj}|) \sim |\boldsymbol{r}-\boldsymbol{R}_{lj}|^{-3}$ one finds readily that, to a good approximation, the following relation is satisfied

$$\langle lj\mu\sigma|A^-|l'j'\nu\sigma'\rangle = \langle lj\mu\sigma|A^-|l'j'\nu\sigma'\rangle\delta_{ll'}\delta_{jj'} = \xi_l\langle\mu\sigma|A^-_{\mathrm{at}}|\nu\sigma'\rangle\delta_{ll'}\delta_{jj'} \quad (2.107)$$

where ξ_l denotes the radial average of the $\xi^{(l)}_{\mathrm{at}}(r)$ function, as previously defined for H_{SO} in Sec. 2.5. Thus, from Eqs. (2.104) and (2.107) one can find the final form of the sought matrix elements

$$\begin{aligned} A_{nn'}(\boldsymbol{k}) = \langle n\boldsymbol{k}|A^-|n'\boldsymbol{k}\rangle &= \frac{1}{N_{\mathrm{2D}}} \sum_{lj}\sum_{\mu\sigma}\sum_{\nu\sigma'} a^*_{n\sigma\mu}(\boldsymbol{k})\, a_{n'\sigma'\nu}(\boldsymbol{k})\langle lj\mu\sigma|A^-|lj\nu\sigma'\rangle \\ &= \frac{1}{N_{\mathrm{2D}}} \sum_{l}\sum_{\mu\sigma}\sum_{\nu\sigma'} \xi_l\, a^*_{n\sigma\mu}(\boldsymbol{k})\, a_{n'\sigma'\nu}(\boldsymbol{k})\langle\mu\sigma|A^-_{\mathrm{at}}|\nu\sigma'\rangle \sum_j 1 \\ &= \sum_{l}\sum_{\mu\sigma}\sum_{\nu\sigma'} \xi_l\, a^*_{n\sigma\mu}(\boldsymbol{k})\, a_{n'\sigma'\nu}(\boldsymbol{k})\langle\mu\sigma|A^-_{\mathrm{at}}|\nu\sigma'\rangle. \end{aligned} \quad (2.108)$$

In the last step, the matrix element $\langle\mu\sigma|A^-_{\mathrm{at}}|\nu\sigma'\rangle$ between different s, p and d orbitals $\mu,\nu \in \{xy, yz, zx, x^2-y^2, 3z^2-r^2, s, x, y, z\}$ of both spins $\sigma,\sigma' \in \{\uparrow,\downarrow\}$ are evaluated. The commutator that defines the SO torque A^-_{at} (Eq. (2.106)) coming from a single atom (with the unit SO coupling constant) is given by

$$A^-_{\mathrm{at}} = L_z S^- - L^- S_z. \quad (2.109)$$

so that its matrix elements can be expressed in terms of elements of the orbital angular momentum operators L^- and L_z. However, using the definition (2.106) of A^-_{at} one readily finds that

the elements $\langle \mu\sigma | A_{\mathrm{at}}^- | \nu\sigma' \rangle$ can be represented directly with elements of the SO coupling $\boldsymbol{L} \cdot \boldsymbol{S}$ as follows

$$\langle \mu \uparrow | A_{\mathrm{at}}^- | \nu \uparrow \rangle \;\; = \;\; - \langle \mu \uparrow | \boldsymbol{L} \cdot \boldsymbol{S} | \nu \downarrow \rangle, \tag{2.110a}$$

$$\langle \mu \uparrow | A_{\mathrm{at}}^- | \nu \downarrow \rangle \;\; = \;\; 0, \tag{2.110b}$$

$$\langle \mu \downarrow | A_{\mathrm{at}}^- | \nu \uparrow \rangle \;\; = \;\; 2 \langle \mu \uparrow | \boldsymbol{L} \cdot \boldsymbol{S} | \nu \uparrow \rangle, \tag{2.110c}$$

$$\langle \mu \downarrow | A_{\mathrm{at}}^- | \nu \downarrow \rangle \;\; = \;\; - \langle \mu \uparrow | A_{\mathrm{at}}^- | \nu \uparrow \rangle. \tag{2.110d}$$

These elements vanish for the same spin-orbitals $(\mu\sigma) = (\nu\sigma')$ as well as for orbitals μ and ν with different orbital numbers, regardless of their spins σ, σ', since the corresponding matrix elements of $\boldsymbol{L} \cdot \boldsymbol{S}$ also vanish [133, 134].

Nonzero matrix elements of the atomic SO torque A_{at}^- exist both for $\sigma \neq \sigma'$ and $\sigma = \sigma'$ depending on orbitals μ and ν. Thus, the applied theoretical model predicts that the Gilbert damping is substantially affected by two kinds of electronic excitations: spin-flip and non-spin-flip, in which the electron spin changes or remains unchanged, respectively.

It should also be noted that the damping constant α given by Eq. (2.101) (or Eq. (2.103)) including the matrix elements $A_{nn'}(\boldsymbol{k})$ (Eq. (2.108)) of the total SO torque A^-, contains both intraband ($n = n'$) and intraband ($n \neq n'$) contributions. The former originate from transitions within a single energy band and give the resistivitylike term of damping, whilst the latter correspond to transitions between different energy bands and give the conductivitylike term of damping as it is already discussed in [44, 88] in detail. The contribution of the intraband transitions to the damping constant is proportional the lifetime $\tau = \hbar/\Gamma$ of electronic states whereas the contribution of the interband transitions behaves as $1/\tau \sim \Gamma$. The intraband contribution is connected to the breathing Fermi surface model. Thus, both the intraband (within one band) and interband (between different bands) transitions near the Fermi level due to the SO coupling, combined with the finite lifetime τ of electronic states due to the electron scattering on lattice vibrations and defects, account for underlying microscopic processes of the magnetisation dynamics that lead to transfer of angular momentum from the spin system to the lattice.

2.6.2   Gilbert damping at finite temperature

As seen in the previous section, to calculate the Gilbert damping constant α at finite temperature one needs to perform the integration over energy which appears in the expression (2.103) for α, instead of the mere product of the two Lorentz functions at $T = 0$. This integral formula includes two Lorentzians, which do not depend on temperature, and the negative derivative of

the Fermi-Dirac distribution function. Thus, the latter is the only factor through which the temperature dependence of the Gilbert damping enters the calculations. This derivative can be evaluated as follows

$$
\begin{aligned}
\eta(\epsilon) &= -\frac{\partial f_{\text{FD}}(\epsilon)}{\partial \epsilon} = -\frac{\partial}{\partial \epsilon}\left(\frac{1}{1+e^{\beta(\epsilon-\epsilon_{\text{F}})}}\right) \\
&= \frac{\beta}{2+e^{\beta(\epsilon_{\text{F}}-\epsilon)}+e^{\beta(\epsilon-\epsilon_{\text{F}})}} = \frac{\beta}{2(1+\cosh[\beta(\epsilon-\epsilon_{\text{F}})])}
\end{aligned}
\tag{2.111}
$$

where $\beta = \frac{1}{k_{\text{B}}T}$. To avoid numerical problems (overflow) at energies ϵ lying far from ϵ_{F} the equation (2.111) for $\eta(\epsilon)$ is rewritten in the following form

$$
\eta(\epsilon) = \begin{cases} \frac{\beta e^{x}}{(1+e^{x})^2} & \text{if} \quad \epsilon < \epsilon_{\text{F}} \\ \frac{\beta e^{-x}}{(1+e^{-x})^2} & \text{if} \quad \epsilon > \epsilon_{\text{F}} \end{cases}
\tag{2.112}
$$

where $x = \beta(\epsilon - \epsilon_{\text{F}})$.

Clearly, the integral in Eq. (2.102) is a spectral overlap of three functions and the contributions of different pairs of electron states $|n\boldsymbol{k}\rangle$, $|n'\boldsymbol{k}\rangle$ to the Gilbert damping largely depend on the form of these functions. The presence of the negative derivative $\eta(\epsilon)$ of the Fermi-Dirac distribution function confines the integration over ϵ to the immediate vicinity of the Fermi level ϵ_{F}. Thus, damping is affected solely by states with energies close to ϵ_{F}. The actual range of contributing states also depends strongly on the width Γ of the Lorentzians which represents the electron scattering due to defects and electron-phonon interaction. The numerical calculation of the integral over ϵ defining the factor $F_{nn'}(\boldsymbol{k})$ [Eq. (2.102)] is done by employing the residue theorem and the Matsubara frequencies. This method shall be discussed in detail below.

It is found, in the calculations done for various temperatures from the range $0 \leqslant T \leqslant 600$ K, that the Gilbert damping constant is weakly dependent on temperature. Indeed, the damping constants α calculated for ferromagnetic bulk metals and films at zero and finite T ultimately saturate to very similar values as the number of $\boldsymbol{k}$-points increases. In particular, it is found that in Co(5 ML) and Co(10 ML) films (see Fig. 3.4 in the next chapter) the converged value of α is almost the same at $T = 0$ and $T = 300$ K for $\Gamma \geqslant 0.01$ eV, a significant discrepancy being obtained only for $\Gamma < 0.01$ eV. Thus, using finite temperature is found almost not to affect the actual results for the damping constant except for very small scattering rates Γ. This confirms the previous findings of Gilmore *et al.* [88] in their calculations for bulk ferromagnetic metals. It is convenient to apply the finite temperature formulation since the convergence of the numerical integration over the BZ is much faster than at $T = 0$. Thus, the efficiency of the numerical calculations is improved (see Sec. 3.1 for details).

It should also be mentioned that, to further improve the efficiency different methods of the

integration over $\boldsymbol{k}$ in the BZ (such as the tetrahedron and trilinear interpolation methods) have been tested but they have been found not to improve the convergence of the integration. This failure is attributed to the specific form of the integrated function of $\boldsymbol{k}$, especially the fact that $F_{nn'}(\boldsymbol{k})$ varies rapidly near the $\boldsymbol{k}$-points where energy bands $\epsilon_n(\boldsymbol{k})$, $\epsilon_{n'}(\boldsymbol{k})$ cross ϵ_{F}. For example in the tetrahedron method, that is used for the numerical integration over the 3D BZ, the BZ is divided into many small cubes and each small cube into six tetrahedra, and then the energies $\epsilon_n(\boldsymbol{k}), \epsilon_{n'}(\boldsymbol{k})$ which enter the integrand function are linearised over each tetrahedron (see Ref. [135]). At the crossing points $\boldsymbol{k}$ of two energy bands, the functions $\epsilon_n(\boldsymbol{k}), \epsilon_{n'}(\boldsymbol{k})$ have discontinuous derivatives over $\boldsymbol{k}$ (gradients) since the energies $\epsilon_n(\boldsymbol{k})$ obtained by diagonalisation of the Hamiltonian matrix are numbered with index n, separately at each $\boldsymbol{k}$, only according to the ascending order of the eigenvalues $\epsilon_n(\boldsymbol{k})$. This unwanted property of the numerically determined electron energies severely impairs the linearisation of the band $\epsilon_n(\boldsymbol{k})$ near the crossing points with another band $\epsilon_{n'}(\boldsymbol{k})$.

2.6.3 Integration via residue theorem: Matsubara frequency method

As it has previously been mentioned the efficiency of calculations is remarkably improved by introducing finite temperature into the electronic occupations factors and subsequent summation over the Matsubara frequencies. In the calculation of the Gilbert damping constant at finite temperature one encounters the integral over energy that defines the factor $F_{nn'}(\boldsymbol{k})$ in Eq. (2.102). This integration can be calculated directly but it must be done with suitable care to get accurate results due to the rapid variation of both the two Lorentz functions as well as the negative derivative $\eta(\epsilon)$ of the Fermi-Dirac function.

In this section, by employing the method of contour integration, an analytical expression for the factor $F_{nn'}(\boldsymbol{k})$ is presented. Such expression is derived by replacing the integral of $F(z)$ along the real axis in the complex energy plane with the integral over a finite closed contour in the upper half-plane. Subsequent use of the residue theorem allows one to express the contour integral as the sum

$$\oint F(z)\,dz = 2\pi i \sum_{j=1}^{\infty} a_{-1}^j \tag{2.113}$$

of the residues a_{-1}^j of the integrand function $F(z) = \eta(z)L(z - \epsilon_n)L(z - \epsilon_{n'})$ at all its poles z_j lying in the upper half-plane. These poles include the poles of the Lorentz functions, $L(z - \epsilon_n)$ and $L(z - \epsilon_{n'})$, as well as the poles of $\eta(z)$. Here, the argument $\boldsymbol{k}$ of the electronic energies $\epsilon_n = \epsilon_n(\boldsymbol{k})$, $\epsilon_{n'} = \epsilon_{n'}(\boldsymbol{k})$ is skipped as it is not relevant in the present discussion.

Looking for the poles of the complex function $\eta(z)$, let us first note that the poles of the Fermi-Dirac distribution function $f_{\mathrm{FD}}(z)$ are found from the condition

$$e^{\beta(z-\epsilon_{\mathrm{F}})} = -1 = e^{(2k+1)i\pi} \tag{2.114}$$

($k = 0, \pm 1, \pm 2, \ldots$). That yields

$$z = \omega_k = \epsilon_{\mathrm{F}} + i\pi(2k+1)k_{\mathrm{B}}T \tag{2.115}$$

where $k_{\mathrm{B}}T$ replaces $1/\beta$. The complex poles $z = \omega_k$ are known as the Matsubara frequencies. Thus, in the vicinity of each pole, the FD distribution function can be written in the form

$$
\begin{aligned}
f_{\mathrm{FD}}(z) &= \frac{1}{1 + e^{\beta(z-\epsilon_{\mathrm{F}})}} \\
&= \frac{1}{1 + e^{\beta(z-\omega_k)}e^{\beta(\omega_k-\epsilon_{\mathrm{F}})}} = \frac{1}{1 - e^{\beta(z-\omega_k)}} \\
&= \frac{1}{1 - \left(1 + \beta(z-\omega_k) + \frac{1}{2}\beta^2(z-\omega_k)^2 + \ldots\right)} \\
&= \frac{-1}{\beta}\frac{1}{z-\omega_k}\frac{1}{1 + \frac{1}{2}\beta(z-\omega_k) + \ldots} \\
&= \frac{-1}{\beta}\frac{1}{z-\omega_k}\left(1 - \frac{1}{2}\beta(z-\omega_k) + \ldots\right) \\
&= \frac{-1}{\beta}\frac{1}{z-\omega_k} - \frac{1}{2} + O(z-\omega_k)
\end{aligned}
\tag{2.116}
$$

where the Taylor series for the exponential function $e^x = \sum_{n=0}^{\infty}\frac{x^n}{n!}$ and the formula for the geometric series $\frac{1}{1-x} = 1 + x + x^2 + \ldots$ are used. With this representation one immediately finds that the function $\eta(z)$ can be expressed as

$$\eta(z) = -\frac{df_{\mathrm{FD}}(z)}{dz} = \frac{-1}{\beta}\frac{1}{(z-\omega_k)^2} + O(1) \tag{2.117}$$

around each position ω_k on the complex plane. Thus, the Matsubara frequencies ω_k are the poles of the first order of the Fermi-Dirac function, and the poles of the second order of its first-order derivative, i.e., $\eta(\epsilon)$.

The Lorentz function can be represented as

$$L(z - \epsilon_n) = \frac{\Gamma/2\pi}{(z-\epsilon_n)^2 + (\Gamma/2)^2} = \frac{\Gamma/2\pi}{(z-z_1)(z-z_2)} \tag{2.118}$$

which immediately identifies its two poles

$$
\begin{aligned}
z_1 &= \epsilon_n + i\Gamma/2, \tag{2.119a} \\
z_2 &= \epsilon_n - i\Gamma/2. \tag{2.119b}
\end{aligned}
$$

51

In the same way one finds the poles

$$
\begin{align}
z_1' &= \epsilon_{n'} + i\Gamma/2\,, \tag{2.120a}\\
z_2' &= \epsilon_{n'} - i\Gamma/2 \tag{2.120b}
\end{align}
$$

of the other Lorentz function

$$
L(z - \epsilon_{n'}) = \frac{\Gamma/2\pi}{(z - z_1')(z - z_2')} \tag{2.121}
$$

The poles z_1, z_1' lie in the upper complex half-plane and they contribute to the integral in Eq. (2.102).

To calculate the residues of $F(z)$ at the poles z_1, z_1' and ω_k, the following general formula derived in complex analysis for the residue of a nonanalytic holomorphic function $F(z)$ at its pole z_j of the order m is applied

$$
a_{-1}^{j} = \frac{1}{(m-1)!} \frac{d^{m-1}}{dz^{m-1}} \left(F(z)(z - z_j)^m \right) |_{z=z_j}. \tag{2.122}
$$

For z_1 ($m = 1$) one readily finds the residue using Eqs. (2.116) and (2.121),

$$
\begin{align}
a_{-1}(z_1) &= F(z)(z - z_1)|_{z=z_1} \\
&= \eta(z)L(z - \epsilon_n)L(z - \epsilon_{n'})(z - z_1)|_{z=z_1} \\
&= \eta(z)\frac{\Gamma/2\pi}{z - z_2}L(z - \epsilon_{n'})|_{z=z_1} \\
&= \frac{\Gamma}{2\pi}\frac{\eta(z_1)L(z_1 - \epsilon_{n'})}{z_1 - z_2} \\
&= \frac{\Gamma}{2\pi}\frac{\eta(z_1)}{i\Gamma}\frac{\Gamma/2\pi}{(z_1 - z_1')(z_1 - z_2')} \\
&= -i\frac{\Gamma}{(2\pi)^2}\frac{\eta(z_1)}{(\epsilon_n - \epsilon_{n'})(\epsilon_n - \epsilon_{n'} + i\Gamma)} \tag{2.123}
\end{align}
$$

where the relation $z_1 - z_2 = z_1' - z_2' = i\Gamma$ has been taken into account.

Following the same procedure for z_1' ($m = 1$) leads to

$$
\begin{align}
a_{-1}(z_1') &= F(z)(z - z_1')|_{z=z_1'} = \frac{\Gamma}{2\pi}\frac{\eta(z_1')L(z_1' - \epsilon_n)}{z_1' - z_2'} \\
&= -i\frac{\Gamma}{(2\pi)^2}\frac{\eta(z_1')}{(\epsilon_{n'} - \epsilon_n)(\epsilon_{n'} - \epsilon_n + i\Gamma)}. \tag{2.124}
\end{align}
$$

For the second-order poles ω_k ($m = 2$) the residue of the function $F(x)$ is

$$
a_{-1}(\omega_k) = \frac{d}{dz}[F(z)(z - z_j)^2]|_{z=z_j=\omega_k}
$$

$$
\begin{aligned}
&= \frac{d}{dz}\left[\eta(z)L(z-\epsilon_n)L(z-\epsilon_{n'})(z-\omega_k)^2\right]\big|_{z=\omega_k}\\
&= -\frac{1}{\beta}\frac{d}{dz}\left[L(z-\epsilon_n)L(z-\epsilon_{n'})\right]\big|_{z=\omega_k}\\
&= -\frac{\Gamma^2}{4\beta\pi^2}\left[\frac{-2(z-\epsilon_n)}{\left[(z-\epsilon_n)^2+(\Gamma/2)^2\right]^2}L(z-\epsilon_{n'})+L(z-\epsilon_n)\frac{-2(z-\epsilon_{n'})}{\left[(z-\epsilon_{n'})+(\Gamma/2)^2\right]^2}\right]\big|_{z=\omega_k}\\
&= \frac{\Gamma^2}{2\beta\pi^2}\left[\frac{\omega_k-\epsilon_n}{(\omega_k-z_1)^2(\omega_k-z_2)^2}\frac{1}{(\omega_k-z_1')(\omega_k-z_2')}\right.\\
&\qquad\left.+\frac{\omega_k-\epsilon_{n'}}{(\omega_k-z_1')^2(\omega_k-z_2')^2}\frac{1}{(\omega_k-z_1)(\omega_k-z_2)}\right]
\end{aligned}
\tag{2.125}
$$

where the expansion (2.116) of $\eta(z)$ around $z=\omega_k$ and the equalities

$$
(\omega_k-z_1)(\omega_k-z_2) = (\omega_k-\epsilon_n)^2+(\Gamma/2)^2 \tag{2.126a}
$$

$$
(\omega_k-z_1')(\omega_k-z_2') = (\omega_k-\epsilon_{n'})^2+(\Gamma/2)^2 \tag{2.126b}
$$

have been taken into account. Substituting $\epsilon_n=z_1-i\Gamma/2$ and $\epsilon_{n'}=z_1'-i\Gamma/2$ one obtains

$$
\begin{aligned}
a_{-1}(\omega_k) &= \frac{\Gamma^2}{2\beta\pi^2}\frac{1}{(\omega_k-z_1)(\omega_k-z_2)(\omega_k-z_1')(\omega_k-z_2')}\\
&\quad\times\left(\frac{\omega_k-z_1+i\Gamma/2}{(\omega_k-z_1)(\omega_k-z_2)}+\frac{\omega_k-z_1'+i\Gamma/2}{(\omega_k-z_1')(\omega_k-z_2')}\right)\\
&= \frac{\Gamma^2}{2\beta\pi^2}\frac{1}{(\omega_k-z_1)(\omega_k-z_2)(\omega_k-z_1')(\omega_k-z_2')}\\
&\quad\times\left(\frac{1}{\omega_k-z_2}+\frac{1}{\omega_k-z_2'}+\frac{i\Gamma}{2}\left[\frac{1}{(\omega_k-z_1)(\omega_k-z_2)}+\frac{1}{(\omega_k-z_1')(\omega_k-z_2')}\right]\right).
\end{aligned}
\tag{2.127}
$$

Introducing the notation $C_{ik}=\omega_k-z_i$, $C_{ik}'=\omega_k-z_i'$ and $C_k=C_{1k}C_{2k}C_{1k}'C_{2k}'$ one can simplify the expression (2.127) to

$$
a_{-1}(\omega_k) = \frac{\Gamma^2}{2\beta\pi^2 C_k}\left(\frac{C_{2k}+C_{2k}'}{C_{2k}C_{2k}'}+\frac{i\Gamma}{2C_k}(C_{1k}C_{2k}+C_{1k}'C_{2k}')\right).
\tag{2.128}
$$

Having calculated the residues, the integral (2.113) can be evaluated as follows

$$
\begin{aligned}
\oint F(z)\,dz &= I(z_1)+I(z_1')+\sum_{k=1}^{\infty}I(\omega_k)\\
&= \frac{\Gamma/2\pi}{\epsilon_n-\epsilon_{n'}}\left(\frac{\eta(z_1)}{\epsilon_n-\epsilon_{n'}+i\Gamma}+\frac{\eta(z_1')}{\epsilon_n-\epsilon_{n'}-i\Gamma}\right)+\sum_{k=1}^{\infty}I(\omega_k)\\
&= \frac{\Gamma/2\pi}{\epsilon_n-\epsilon_{n'}}\frac{(\epsilon_n-\epsilon_{n'}-i\Gamma)\eta(z_1)+(\epsilon_n-\epsilon_{n'}+i\Gamma)\eta(z_1')}{(\epsilon_n-\epsilon_{n'})^2+\Gamma^2}+\sum_{k=1}^{\infty}I(\omega_k)\\
&= \frac{\Gamma}{2\pi}\frac{\eta(z_1)+\eta(z_1')}{(\epsilon_n-\epsilon_{n'})^2+\Gamma^2}+\frac{\Gamma/2\pi}{\epsilon_n-\epsilon_{n'}}\frac{i\Gamma(\eta(z_1')-\eta(z_1))}{(\epsilon_n-\epsilon_{n'})^2+\Gamma^2}+\sum_{k=1}^{\infty}I(\omega_k)
\end{aligned}
$$

53

$$= \frac{\Gamma}{2\pi} \frac{\eta(z_1) + \eta(z_1')}{(\epsilon_n - \epsilon_{n'})^2 + \Gamma^2} + \frac{\Gamma/2\pi}{\epsilon_n - \epsilon_{n'}} \frac{i\Gamma(\eta(z_1') - \eta(z_1))}{(\epsilon_n - \epsilon_{n'})^2 + \Gamma^2} + \sum_{k=1}^{\infty} I(\omega_k)$$

$$= \frac{\Gamma}{2\pi} \frac{\eta(z_1) + \eta(z_1')}{(\epsilon_n - \epsilon_{n'})^2 + \Gamma^2} - i\frac{\Gamma^2}{2\pi} \frac{1}{(\epsilon_n - \epsilon_{n'})^2 + \Gamma^2} \frac{\eta(z_1') - \eta(z_1)}{z_1' - z_1} + \sum_{k=1}^{\infty} I(\omega_k) \qquad (2.129)$$

where $I(z_1) = 2\pi i\, a_{-1}(z_1)$, $I(z_1') = 2\pi i\, a_{-1}(z_1')$ and $I(\omega_k) = 2\pi i\, a_{-1}(\omega_k)$ are contributions to the integral from the poles z_1, z_1' and ω_k, respectively. The relation $\epsilon_n - \epsilon_{n'} = z_1 - z_1'$ has also been used in the last step. Then, substituting the expression (2.128) obtained for $a_{-1}(\omega_k)$ one is finally left with the following analytical formula

$$F_{nn'}(\boldsymbol{k}) = \oint F(z)\, dz = J_1 + iJ_2 \qquad (2.130)$$

where J_1 and J_2 are given by

$$J_1 = \frac{\Gamma}{2\pi} \frac{\eta(z_1) + \eta(z_1')}{(\epsilon_n - \epsilon_{n'})^2 + \Gamma^2} - \frac{\Gamma^3}{2\pi\beta} \sum_{k=0}^{\infty} \frac{C_{1k}C_{2k} + C_{1k}'C_{2k}'}{C_k^2}, \qquad (2.131\text{a})$$

$$J_2 = -\frac{\Gamma^2}{2\pi} \frac{1}{(\epsilon_n - \epsilon_{n'})^2 + \Gamma^2} \frac{\eta(z_1') - \eta(z_1)}{z_1' - z_1} + \frac{\Gamma^2}{\pi\beta} \sum_{k=0}^{\infty} \frac{C_{2k} + C_{2k}'}{C_k C_{2k} C_{2k}'}. \qquad (2.131\text{b})$$

Let us note that both J_1 and J_2 are complex numbers.

The ratio

$$R = \frac{\eta(z_1') - \eta(z_1)}{z_1' - z_1} \qquad (2.132)$$

present in Eq. (2.131b) becomes ill-defined numerically if the energies $\epsilon_n, \epsilon_{n'}$ are equal or very close to each other, in particular, for $n = n'$. To avoid numerical problems in such cases one can expand the function $\eta(z_1')$ in the Taylor series around $z = z_1$,

$$\eta(z_1') = \eta(z_1) + \sum_{m=1}^{\infty} \frac{1}{m!} \frac{d^m \eta(z)}{dz^m}\Big|_{z=z_1} (z_1' - z_1)^m. \qquad (2.133)$$

This leads to the following expansion

$$R = \sum_{m=1}^{\infty} \frac{1}{m!} \frac{d^m \eta(z)}{dz^m}\Big|_{z=z_1} (z_1' - z_1)^{m-1} = \sum_{m=1}^{\infty} \frac{1}{m!} \frac{d^m \eta(z)}{dz^m}\Big|_{z=z_1} (\epsilon_n' - \epsilon_n)^{m-1} \qquad (2.134)$$

which converges quickly if $\beta|\epsilon_{n'} - \epsilon_n| \ll 1$. It is found that including its terms up to $m = 6$ (and neglecting the ones with $m \geqslant 7$) is sufficient, if $\beta|\epsilon_{n'} - \epsilon_n| < 0.01$, to get full convergence of R in the numerical calculations, using the double-precision representation of the floating point variables. For $\beta|\epsilon_{n'} - \epsilon_n| \geqslant 0.01$, accurate values of R are obtained from the formula (2.132) that defines the ratio R.

To evaluate the ratio R with the expansion (2.134) one needs to calculate its coefficients first. They are given by the derivatives $\eta^{(m)}(z) = d^m \eta(z)/dz^m$ which can be found from the following relation

$$\eta = \beta f(1 - f). \tag{2.135}$$

where $f = f_{\text{FD}}(z)$. Its application leads to a recursion expression for $\eta^{(m)}$ in terms of $f, \eta, ..., \eta^{(m-1)}$ as follows

$$
\begin{aligned}
\eta^{(m)} &= -\beta \sum_{k=0}^{m} \binom{m}{k} f^{(k)} f^{(m-k)} + \beta f^{(m)} \\
&= -\beta \sum_{k=1}^{m-1} \binom{m}{k} \eta^{(k-1)} \eta^{(m-k-1)} - \beta(1 - 2f)\, \eta^{(m-1)}
\end{aligned}
\tag{2.136}
$$

where $f^{(k)}$ has been replaced by $-\eta^{(k-1)}$ for $k \geqslant 1$. In particular, from the above recursive formula one obtains

$$\eta' = -\beta(1 - 2f)\eta\,, \tag{2.137a}$$

$$\eta'' = -2\beta\eta\eta - \beta(1 - 2f)\eta'\,, \tag{2.137b}$$

$$\eta''' = -6\beta\eta\eta' - \beta(1 - 2f)\eta''. \tag{2.137c}$$

Other derivatives $\eta^{(m)}$, up to $m = 10$, calculated with the formula (2.136) can be found in the appendix A. In this way, one can evaluate the integral defining the factor $F_{nn'}(\boldsymbol{k})$ in Eq. (2.102) analytically by employing the Matsubara frequency method and perform the numerical calculation of the Gilbert damping constant α at finite temperature in an effective way. It has been found that, for the applied temperature $T = 300$ K, the infinite series in Eqs. (2.131a) and (2.131b) can be truncated to the finite sum of the first 40 terms ($k = 1, 2, ..., 40$) without losing numerical accuracy of α.

2.7 Green function approach to Gilbert damping

Calculation of the Gilbert damping constant is usually done within the well-known Kamberský formula which depends explicitly on electron states and their energies (Eqs. (2.101), (2.103)). However, in the case of systems for which diagonalisation of Hamiltonian cannot be easily performed or is not feasible at all (due to their largely reduced symmetry) an alternative expression for the damping constant is of great interest. In this context, the use of Green functions, as a

powerful mathematical technique, has often proved to be very efficient in theoretical determin-
ation of physical quantities. One of numerous examples of such approach is the calculation of
MCA originating from a monoatomic step on Co surface [136]. This section is devoted to finding
an explicit expression for the damping constant α in terms of the Green function.

Determination of the damping constant α for a magnetic system described with the Hamilto-
nian H involves the calculation of the trace

$$\mathrm{tr}D(\epsilon) = \sum_a \langle a|A^- L(\epsilon - H)A^+ L(\epsilon - H)|a\rangle. \tag{2.138}$$

This trace can be evaluated in any complete basis $|a\rangle$ due to the property of trace invariance
under the choice of basis. Previously, in Sec. 2.6, the basis states $|a\rangle$ have be chosen to be
the eigenstates $|n\rangle$ of the Hamiltonian, namely $|n\rangle = |n\boldsymbol{k}\rangle$ for the investigated layered systems.
With this choice of basis the expression (2.101) for α is obtained. For a general magnetic system,
such direct method requires the diagonalisation of the Hamiltonian which in the TB model is
represented by a matrix whose dimension depends on the size of the system. For a layered system
with N atomic layers this matrix is reduced to an $18N \times 18N$ array. However, for a system
without translational symmetry, like films on vicinal (i.e., stepped) surfaces or nanoclusters, the
dimension of the Hamiltonian matrix becomes very large, ultimately equal to $(18N_{\mathrm{at}}) \times (18N_{\mathrm{at}})$,
where N_{at} is the total of atoms in the system. In such cases, the numerical diagonalisation
of the Hamiltonian is not possible. However, calculation of the investigated property, i.e., the
damping constant α can be still effectively performed if the formula for α is expressed in terms
of the Green function $G(z) = G(z - H)^{-1}$ since the latter can be found without resorting to the
inversion of the very large matrix of $(z - H)$. It can be done, e.g., with the recursion method
[137].

The expression for α in terms of the Green function can be formulated in any basis $|a\rangle$, in
particular, in the TB basis of orbitals $|j\mu\rangle$ localised on different atoms j or the Bloch basis states
$|\boldsymbol{k}l\mu\sigma\rangle$ in the case of layered systems. For any basis $|a\rangle$ the trace in Eq. (2.138) can be rewritten
as

$$\begin{aligned}
\mathrm{tr}D(\epsilon) &= \sum_{a,a'} \langle a|A^- L(\epsilon - H)|a'\rangle\langle a'|A^+ L(\epsilon - H)|a\rangle \\
&= \sum_{a,a'} \langle a|A^- L(\epsilon - H)|a'\rangle\langle a|L(\epsilon - H)A^-|a'\rangle^*
\end{aligned} \tag{2.139}$$

where the identity operator $\sum_{a'} |a'\rangle\langle a'| = 1$ has been introduced.

The Lorentz function $L(\epsilon - H) = \frac{\Gamma}{2\pi} \left[(\epsilon - H)^2 + (\Gamma/2)^2\right]^{-1}$ is the operator (in the Hilbert

space of quantum states) defined as the function of Hamiltonian operator H. This operator function can be transformed as follows

$$
\begin{aligned}
L(\epsilon - H) &= \frac{\Gamma}{2\pi} \left[(\epsilon - H - i\frac{\Gamma}{2})(\epsilon - H + i\frac{\Gamma}{2}) \right]^{-1} \\
&= \frac{\Gamma}{2\pi} \left[(z^* - H)(z - H) \right]^{-1} = \frac{\Gamma}{2\pi} (z - H)^{-1}(z^* - H)^{-1} \\
&= \frac{\Gamma}{2\pi} G(z)G(z^*).
\end{aligned}
\tag{2.140}
$$

Thus, it is expressed in terms of the Green function operators

$$
G(z) = (z - H)^{-1} \tag{2.141a}
$$

$$
G(z^*) = (z^* - H)^{-1} \tag{2.141b}
$$

where $z = \epsilon + i\frac{\Gamma}{2}$ is the complex energy with the imaginary part equal to half of the scattering rate Γ. The expression (2.140) for $L(z - H)$ can be further simplified to

$$
L(\epsilon - H) = \frac{i}{2\pi} \left[G(z) - G(z^*) \right] \tag{2.142}
$$

by noting but

$$
\begin{aligned}
G(z) - G(z^*) &= (z - H)^{-1} - (z^* - H)^{-1} \\
&= (z - H)^{-1}(z^* - H)^{-1} \left[(z^* - H) - (z - H) \right] \\
&= (-i\Gamma)G(z)G(z^*).
\end{aligned}
\tag{2.143}
$$

The obtained relation between the operators $L(z - H)$ and $G(z), G(z^*)$ can also be derived without resorting to the operator algebra presented above. Indeed, one can prove the relation (2.140) and (2.142) by showing that they hold in the basis of the eigenstates $|n\rangle$ of H. Indeed, one finds readily that

$$
\begin{aligned}
\langle n'|L(\epsilon - H)|n\rangle &= \frac{\Gamma/2\pi}{(\epsilon - \epsilon_n)^2 + (\Gamma/2)^2} \delta_{nn'} = \frac{-1}{\pi} \mathrm{Im} \left(\frac{1}{z - \epsilon_n} \right) \delta_{nn'} \\
&= \frac{-1}{\pi} \mathrm{Im}\, G_{nn}(z)\, \delta_{nn'} = \frac{i}{2\pi} \left(G_{nn}(z) - G_{nn}(z^*) \right) \delta_{nn'} \\
&= \frac{i}{2\pi} \left(G_{nn'}(z) - G_{nn'}(z^*) \right)
\end{aligned}
\tag{2.144}
$$

where

$$
G_{nn'}(z) = \langle n'|G(z)|n\rangle = \frac{1}{z - \epsilon_n} \delta_{nn'} = G_{nn}(z)\, \delta_{nn'}. \tag{2.145}
$$

57

In this way using the relations (2.138) and (2.142) we finally arrive at the expression

$$\mathrm{tr}D(\epsilon) = \frac{1}{4\pi^2} \sum_{aa'} P_{aa'} Q_{aa'}^* \tag{2.146}$$

where

$$P = A^- \left[G(z) - G(z^*) \right], \tag{2.147a}$$

$$Q = \left[G(z) - G(z^*) \right] A^-. \tag{2.147b}$$

An alternative formula for $\mathrm{tr}D(\epsilon)$ is found with the relations (2.138) and (2.140),

$$\mathrm{tr}D(\epsilon) = \frac{\Gamma^2}{4\pi^2} \sum_{aa'} \widetilde{P}_{aa'} \widetilde{Q}_{aa'}^* \tag{2.148}$$

where

$$\widetilde{P} = A^- G(z) G(z^*), \tag{2.149a}$$

$$\widetilde{Q} = G(z) G(z^*) A^-. \tag{2.149b}$$

The matrix elements $P_{aa'}$ and $Q_{aa'}$ are directly expressed in terms of the elements of the Green function and the matrix elements of the SO torque A^-

$$P_{aa'} = \sum_b A_{ab}^- \left[G_{ba'}(z) - G_{ba'}(z^*) \right], \tag{2.150a}$$

$$Q_{aa'} = \sum_b \left[G_{ab}(z) - G_{ab}(z^*) \right] A_{ba'}^- \tag{2.150b}$$

where

$$G_{ab} = \langle a|G(z)|b \rangle, \tag{2.151a}$$

$$A_{ab}^- = \langle a|A^-|b \rangle. \tag{2.151b}$$

Similar expressions for $\widetilde{P}_{aa'}$ and $\widetilde{Q}_{aa'}$

$$\widetilde{P}_{aa'} = \sum_{b,b'} A_{ab}^- G_{bb'}(z) G_{b'a'}(z^*), \tag{2.152a}$$

$$\widetilde{Q}_{aa'} = \sum_{b,b'} G_{ab}(z) G_{bb'}(z^*) A_{b'a'}^- \tag{2.152b}$$

involve additional summation over the chosen basis states b', in comparison with $P_{aa'}, Q_{aa'}$, thus

making the numerical calculation of the trace $trD(\epsilon)$ longer. On the other hand, the formula (2.148) could be more favourable numerically for very small values of Γ since it avoids possible inaccuracies in the matrix elements of the difference $G(z) - G(z^*) = G(\epsilon + i\frac{\Gamma}{2}) - G(\epsilon - i\frac{\Gamma}{2})$.

Therefore, having found the expressions (2.146) and (2.148) for the trace appearing in the expression for the Gilbert damping constant finally, one can rewrite the general expression (2.144) for Gilbert damping constant in terms of Green function in the following two alternative forms

$$
\begin{aligned}
\alpha &= \frac{\pi}{\mu_{\text{tot}}} \int_{-\infty}^{\infty} d\epsilon \, \eta(\epsilon) \, \text{trD}(\epsilon) \\
&= \frac{\pi}{\mu_{\text{tot}}} \frac{1}{4\pi^2} \sum_{a,c} \int_{-\infty}^{\infty} d\epsilon \, \eta(\epsilon) P_{ac}(z) Q_{ac}^*(z) \\
&= \frac{\pi}{\mu_{\text{tot}}} \frac{\Gamma^2}{4\pi^2} \sum_{a,c} \int_{-\infty}^{\infty} d\epsilon \, \eta(\epsilon) \widetilde{P}_{ac}(z) \widetilde{Q}_{ac}^*(z)
\end{aligned}
\tag{2.153}
$$

where $\mu_{\text{tot}} = 2\langle S_{\text{tot}}^z \rangle$ is the total spin magnetic moment (in units of μ_{B}). The expressions (2.153) can be directly used for evaluation of the Gilbert damping constant α at finite temperature, whilst at $T = 0$ the two integrals over energy present in Eq. (2.153) reduce to $P_{ac}(\epsilon_{\text{F}} + i\frac{\Gamma}{2}) Q_{ac}^*(\epsilon_{\text{F}} + i\frac{\Gamma}{2})$ and $\widetilde{P}_{ac}(\epsilon_{\text{F}} + i\frac{\Gamma}{2}) \widetilde{Q}_{ac}^*(\epsilon_{\text{F}} + i\frac{\Gamma}{2})$, respectively, since $\eta(\epsilon) = \delta(\epsilon - \epsilon_{\text{F}})$ for $T = 0$. It has been checked, for bulk ferromagnets, that the expression (2.153) leads to the same results as the previously obtained expression for α in terms of the Hamiltonian eigenstates. The latter formula, in the form of Eq. (2.101) is, however, more convenient for systems with translational symmetry and, thus, it is used in the calculation of the damping constant α throughout the thesis.

Chapter 3

Gilbert damping in magnetic nanostructures

This chapter presents the results obtained for the Gilbert damping constant α in bulk ferromagnets and various magnetic nanostructures such as pure ferromagnetic films, FM/NM bilayers, NM/Co/NM and Co/NM1/NM2 trilayers as well as binary superlattices. The calculations reported in this thesis are performed within a realistic nine-band tight-binding formalism and using the general formula (2.103) for the Gilbert damping constant obtained in Sec. 2.3, based on Kamberský's torque-correlation model. After discussion on the convergence and efficiency of numerical calculations, the Gilbert damping in bulk ferromagnets is investigated and the obtained results are compared with previously reported results of DFT calculations. Then, the damping constant α in ultrathin ferromagnetic films is studied. New results for pure Fe, Co and Ni films are presented and compared with experiment. The Gilbert damping is also investigated in various magnetic layered structures (bilayers, trilayers and multilayers) composed of Co films in contact with nonmagnetic metals. The effect of nonmagnetic metals on the Gilbert damping and its enhancement due to change of the electronic structure and the SO coupling will be discussed. The FM/NM layered systems are of particular interest since the presence of nonmagnetic layers leads to the GMR effect, the interlayer exchange coupling and the STT which are the key phenomena in spintronics devices. Finally, in the last section, the calculation of α, previously done for the (001) direction corresponding to out-of-plane magnetisation in the considered films, is generalised to an arbitrary direction of magnetisation and thus the angular dependence of α in bulk ferromagnets and ferromagnetic films is studied.

3.1   Numerical efficiency and convergence

The expression for the Gilbert damping constant α [Eq. (2.103)] includes the factor $F_{nn'}(\boldsymbol{k})$ which depends on two energies, $\epsilon_n(\boldsymbol{k})$ and $\epsilon_{n'}(\boldsymbol{k})$. This factor can be calculated directly as an integral over energy according to its definition given in Eq. (2.102). Such direct integration was presumably used in the DFT calculations of α in bulk ferromagnetic metals in Ref. [88] where the same formula for $F_{nn'}(\boldsymbol{k})$ is used. This energy integral includes two Lorentzians, depending on $\epsilon - \epsilon_n(\boldsymbol{k})$ and $\epsilon - \epsilon_{n'}(\boldsymbol{k})$, respectively, as well as the negative derivative $\eta(\epsilon)$ of the Fermi-Dirac function which depends on temperature. Each of these factors varies rapidly with the energy ϵ. Hence, the integration must be performed with suitable care to get accurate results. One way to compute such integral more efficiently is taking the advantage of the residue theorem instead of using numerical integration. The factor $F_{nn'}(\boldsymbol{k})$ is then determined by replacing the integral by the sum of the residues of the integrand function. Simultaneously, easy control of the numerical accuracy is achieved by including in this sum a sufficient number of the Matsubara frequencies (about 40 of them have been found to be sufficient for $T = 300$ K). Thus, the efficiency of calculations is remarkably improved by the finite temperature ansatz as well as subsequent summation over Matsubara frequencies. Other details of the evaluation of α at finite temperature are similar to $T = 0$, regardless of the method used to compute the energy integral that defines the factor $F_{nn'}(\boldsymbol{k})$. The detailed analytical expression for $F_{nn'}(\boldsymbol{k})$ is derived in Sec. 2.6.3.

Figures 3.1-3.3 present the convergence of α with the number of $\boldsymbol{k}$-points in the BZ for bulk bcc Fe, fcc Co and fcc Ni as well as for (001) bcc Fe, (001) fcc Co and (001) fcc Ni films of various thicknesses with different values of the scattering rate Γ. One may notice the faster convergence of α with number of $\boldsymbol{k}$-points at $T = 300$ K than at $T = 0$ in both the bulk and film structures.

Indeed, for bulk ferromagnets (Fig. 3.1) the convergence of α calculated with $T = 300$ K is reached with as few as $(100)^3$ $\boldsymbol{k}$-points for $\Gamma \geqslant 0.001$ eV whilst as many as $(300)^3$ and $(600)^3$ $\boldsymbol{k}$-points are needed to attain convergence for $\Gamma = 0.01$ eV and $\Gamma = 0.001$ eV, respectively, at $T = 0$. A similar number of $\boldsymbol{k}$-points, $(100)^3$ or slightly more, has been used in the previously reported *ab initio* (DFT) calculations for bulk systems where the same general expression for α given by Eqs. (2.101), (2.102) and including finite temperature, has been applied [88, 92].

As for the layered systems with $\Gamma \geqslant 0.01$ eV, the convergence is obtained with $(80)^2$ $\boldsymbol{k}$-points for Fe, $(100)^2$ $\boldsymbol{k}$-points for Co and $(60)^2$ $\boldsymbol{k}$-points for Ni films at $T = 300$ K whilst one may need more than $(400)^2$ $\boldsymbol{k}$-points for some film thicknesses at $T = 0$. A more intensive calculation is required to achieve convergence for smaller Γ. For the smallest considered scattering
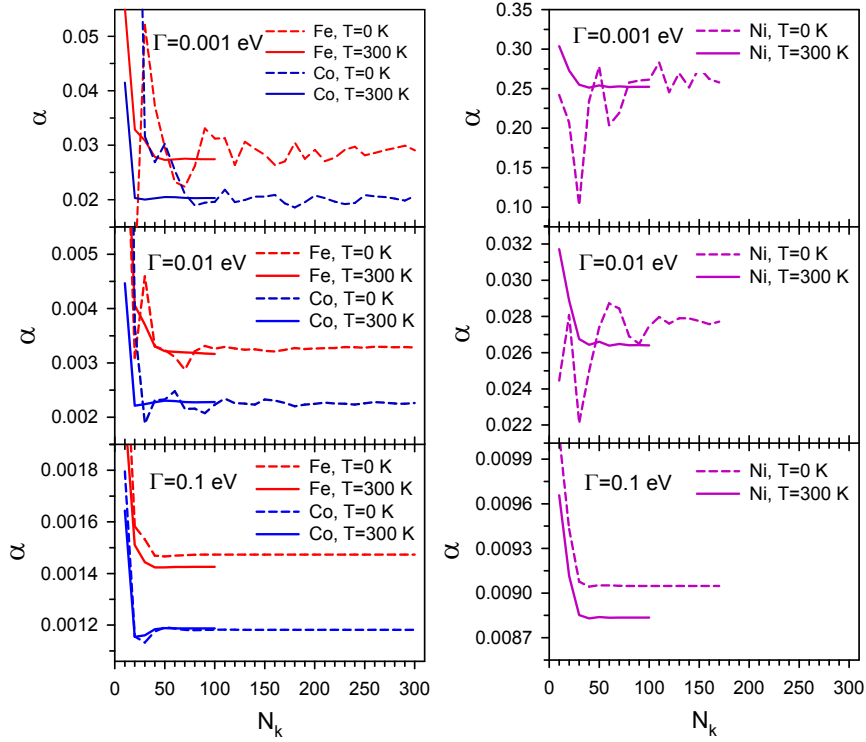
Figure 3.1: Convergence of the Gilbert damping constant α with N_k at $T = 0$ and $T = 300$ K, for different scattering rate Γ in *left*: bulk bcc Fe (red lines) and bulk fcc Co (blue lines), *right*: bulk fcc Ni. The parameter N_k defines the number $(2N_k + 1)^3$ of $\boldsymbol{k}$-points in the 3D BZ.

rate $\Gamma = 0.001$ eV, about $(1000)^2$ $\boldsymbol{k}$-points are needed to give a satisfactory convergence of α calculated with $T = 300$ K whilst even four times this value does not lead to a convergent result for $T = 0$.

The temperature dependence of the Gilbert damping constant α has also been investigated. Calculations were done for various temperatures $0 \leqslant T \leqslant 600$ K. It is found that α is weakly dependent on temperature. This confirms the previous findings of Gilmore *et al.* [88] in their *ab initio* calculations for bulk ferromagnetic metals. Indeed, the damping constants α calculated for ferromagnetic bulk metals and films at zero and finite T ultimately saturate to very similar values as the number of $\boldsymbol{k}$-points increases. In particular, in the case of Co(5 ML) and Co(10 ML) films (Fig. 3.4) α converges almost to the same value at $T = 0$ and $T = 300$ K for $\Gamma \geqslant 0.01$ eV. An intensive calculation for the two Co films at $T = 0$ has shown that a significant difference between the values of α for zero and finite T is found only for $\Gamma < 0.01$ eV. Thus it is concluded that using finite temperature, whilst improving efficiency of the calculations, almost does not affect the actual results for the Gilbert damping except for very small scattering rates Γ. All calculations of α presented below are performed with $T = 300$ K.

Apart from employing finite temperature, one can also improve efficiency of the calculations by using the system's symmetry. In the considered case of layered systems with the cubic sym-
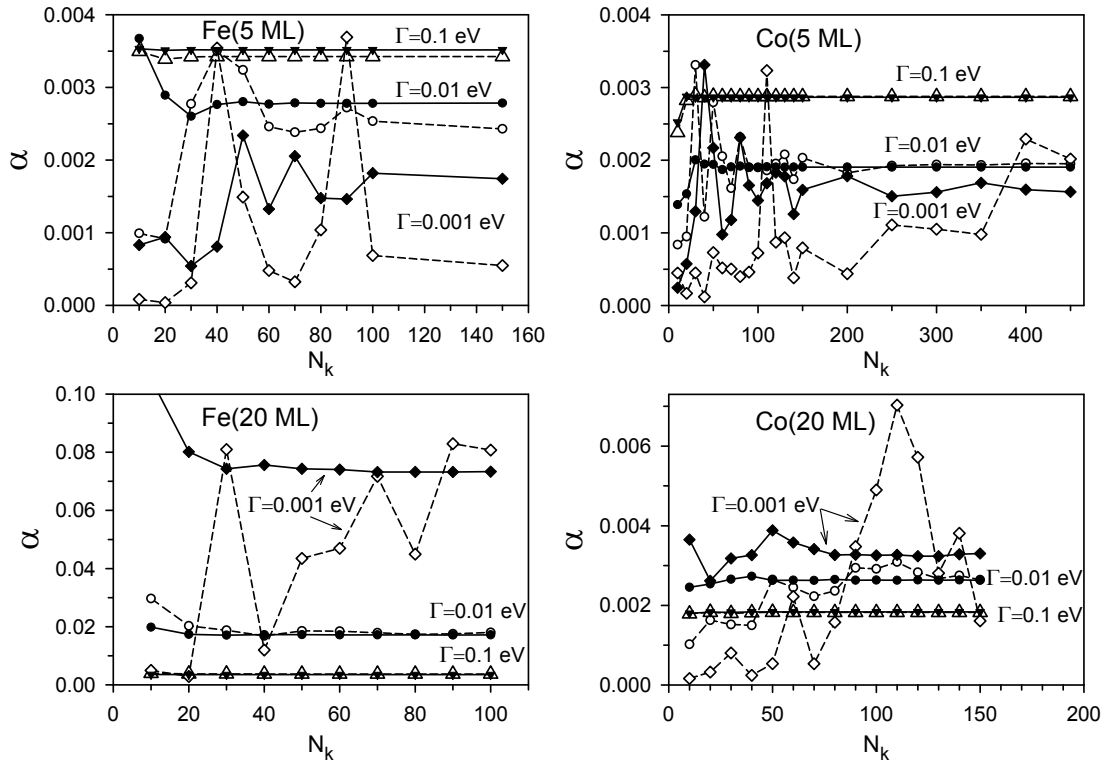
Figure 3.2: Convergence of the Gilbert damping constant α with the number $(2N_k+1)^2$ **k**-points in the 2D BZ for FM(5 ML) and FM(20 ML) films (FM=Fe, Co) at $T = 0$ (open symbols, dashed lines) and $T = 300$ K (solid symbols and lines), for different scattering rates: $\Gamma = 0.001$ eV (diamonds), $\Gamma = 0.01$ eV (circles) and $\Gamma = 0.1$ eV (triangles).
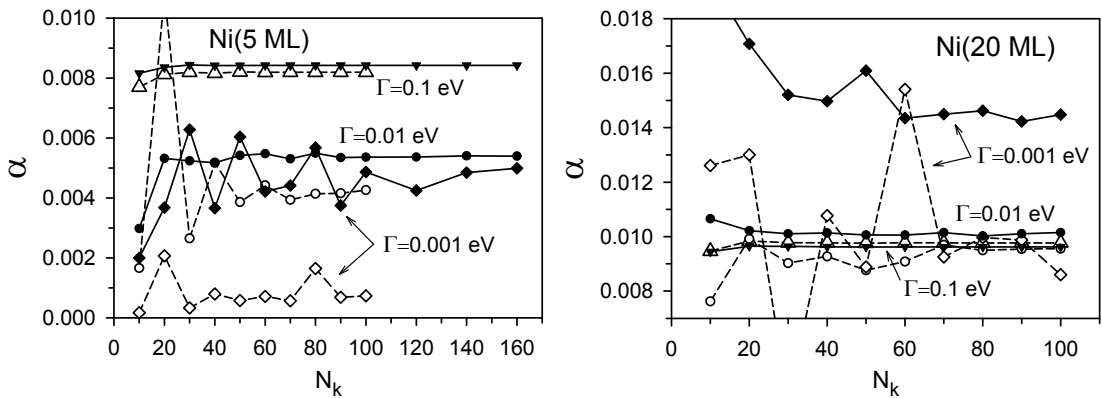
Figure 3.3: Convergence of the Gilbert damping constant α with the number $(2N_k+1)^2$ **k**-points in the 2D BZ for Ni(5 ML) and Ni(20 ML) films at $T = 0$ (open symbols, dashed lines) and $T = 300$ K (solid symbols and lines), for different scattering rates: $\Gamma = 0.001$ eV (diamonds), $\Gamma = 0.01$ eV (circles) and $\Gamma = 0.1$ eV (triangles).
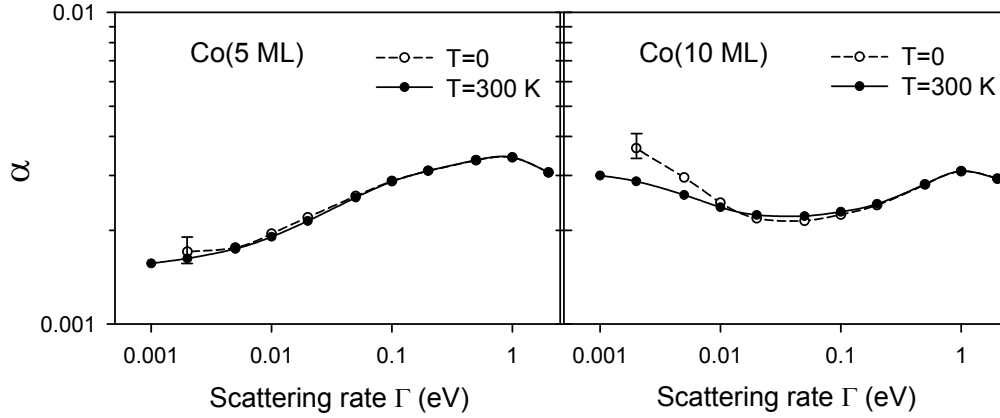
Figure 3.4: Gilbert damping constant α versus the scattering rate Γ in Co(5 ML) and Co(10 ML) films at $T = 0$ and $T = 300$ K. Open symbols show damping at $T = 0$ and the solid ones stand for $T = 300$ K. The error bars shown for $\Gamma = 0.002$ eV at $T = 0$ reflect the not fully converged summation over the BZ with $N_{\rm k} = 1000$ for Co(5 ML) and $N_{\rm k} = 700$ for Co(10 ML).

metry the numerical efficiency of the Gilbert damping calculations can be improved by limiting the integration over $\boldsymbol{k}$ in Eq. (2.103) to the irreducible BZ, which is the 1/8 BZ. Numerical tests for each investigated system have shown that the identical values of α are obtained with both of the integrations, over the 1/8 BZ and the full BZ. This equality is attributed to the invariance of the Hamiltonian including the SO interaction under the spatial and time reversal symmetry operations.

3.2 Bulk ferromagnets

The (intrinsic) Gilbert damping constant α in bulk ferromagnetic transition metals bcc Fe, fcc Co and fcc Ni is calculated within the TB model as a function of the electron scattering rate Γ and it is shown in Fig. 3.5 for two different cases: with and without the SO interaction in the calculation of electronic band structure. This figure also includes the plots of intraband (diagonal) and interband (off-diagonal) contributions to the damping constant α for the case of nonzero SO interaction. These contributions correspond to transitions within the one band ($n = n'$) and between different bands ($n \neq n'$), respectively. A few points concerning the results presented in Fig. 3.5 should be clarified.

First, as shown, the inclusion of the SO coupling term in the Hamiltonian is found to be essential for the intraband terms ($n = n'$) which gives no contribution if this term is absent. Note that, this distinction (including or not the SO interaction) solely affects states $|n\boldsymbol{k}\rangle$ and energies $\epsilon_n(\boldsymbol{k})$, i.e., the band structure, and in both cases (with and without the SO interaction) the same full SO coupling is kept in the SO torque A^-. Thus, it is emerging that including the
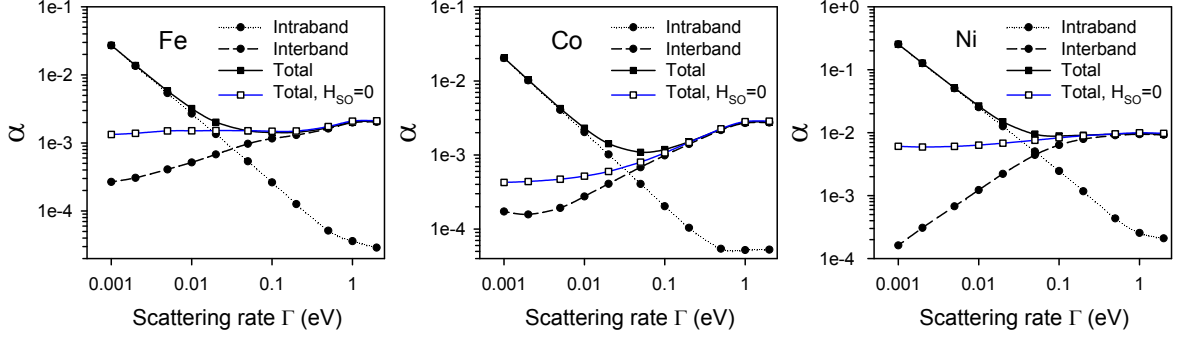
Figure 3.5: Calculated Gilbert damping constant α vs scattering rate Γ for bulk Fe, Co and Ni. Solid, dotted and dashed curves show the total damping constant as well as intraband and interband contributions, respectively. Open squares mark results obtained with electronic states found for $H_{SO} = 0$. The corresponding interband term coincides with the total α as the intraband term vanishes.

SO interaction H_{SO} in the Hamiltonian gives a significant contribution to the damping constant α and it is crucial for reproducing correct trends in the dependence of α on the scattering rate Γ, especially in the range of small $\Gamma \leqslant 0.2$ eV for which the intraband term dominates (see Fig. 3.5). A similar result has been previously reported for bulk Fe (cf. Ref. [138]). These results can be accounted for as follows.

The intraband terms of the factor $A_{nn'}(\boldsymbol{k})$ in Eq. (2.103), with $n = n'$, vanish if the SO coupling is neglected in the calculation electronic structure for cubic ferromagnets as well as for layered systems with the inversion symmetry. Indeed, if the H_{SO} is disregarded the states $|n\boldsymbol{k}\rangle$ convert to the eigenstates $|n_0\sigma\boldsymbol{k}\rangle$ of S_z so that the resultant matrix elements

$$
\begin{aligned}
A_{nn}(\boldsymbol{k}) &= \sum_{lj} \xi_l \langle n_0\sigma\boldsymbol{k}|A_{\mathrm{at}}^-(\boldsymbol{r} - \boldsymbol{R}_{lj})|n_0\sigma\boldsymbol{k}\rangle \\
&= -\frac{1}{2}s_\sigma \sum_{lj} \xi_l \langle n_0\sigma\boldsymbol{k}|L^-(\boldsymbol{r} - \boldsymbol{R}_{lj})|n_0\sigma\boldsymbol{k}\rangle \\
&= -\frac{1}{2}s_\sigma \langle n_0\sigma\boldsymbol{k}|O^-(\boldsymbol{r})|n_0\sigma\boldsymbol{k}\rangle
\end{aligned}
\tag{3.1}
$$

(where $s_\uparrow = 1, s_\downarrow = -1$ and $O^- = O_x + iO_y$) found with A_{at}^- given by Eq. (2.109) vanish for any non-degenerate state $|n_0\sigma\boldsymbol{k}\rangle$ due to quenching of the orbital angular momentum. This can be shown by noting that the operator $O_\zeta(\boldsymbol{r}) = \sum_{lj} \xi_l L_\zeta(\boldsymbol{r} - \boldsymbol{R}_{lj})$ ($\zeta = x, y, z$) becomes $[O_\zeta(-\boldsymbol{r})]^* = -O_\zeta(\boldsymbol{r})$ under the combined action of the complex conjugation and the inversion operator $\boldsymbol{r} \to -\boldsymbol{r}$ whilst the non-degenerate states $|n_0\sigma\boldsymbol{k}\rangle$ remain unchanged up to a constant phase factor $e^{i\varphi}$ (see appendix A of Ref. [129]). The contribution of degenerate states is negligible since they correspond to a set of $\boldsymbol{k}$-points with zero measure.

It is worth mentioning that the perturbation theory for non-degenerate states seemingly fails

to reproduce the correct ξ^3 dependence of the intraband term α_{intra} on the SO coupling constant ξ in bulk ferromagnets (see Ref. [139]). Indeed, the first-order expansion $|n\boldsymbol{k}\rangle = |n_0\sigma\boldsymbol{k}\rangle + |n\boldsymbol{k}\rangle^{(1)}$ with $|n\boldsymbol{k}\rangle^{(1)} \sim \xi$ leads to the relation $A_{nn}(\boldsymbol{k}) \sim \xi^2$ and consequently to $\alpha_{\text{intra}} \sim \xi^4$ (since α_{intra} depends on $|A_{nn}(\boldsymbol{k})|^2$). However, the perturbation theory for nearly degenerate states guarantees the ξ^3 dependence of α_{intra}, i.e., a non-vanishing ξ^3 term in its expansion, as it has already been shown for bulk metals in the original work by Kamberský [44]. Therein, the contribution to α_{intra} proportional to ξ^3 is shown to come from a finite area of the Fermi surface (or rather, for $T > 0$, a finite slice of the BZ including this part of the Fermi surface). The $\boldsymbol{k}$-points in this area form a strip-like region on the Fermi surface around the line where two different energy bands cross each other at the Fermi surface in the absence of H_{SO}. The states from the two bands can be considered as nearly degenerate as long as their energy separation is of the order of ξ, so that the strip width is proportional to ξ. Then, one can approximate the perturbed states by combinations of the two unperturbed states only, so that the corresponding matrix elements $A_{nn}(\boldsymbol{k})$ do not vanish for the perturbed states. Since $A_{nn}(\boldsymbol{k})$ are proportional to ξ the contribution to α_{intra} coming from the strip-like region in the BZ is proportional to $\xi^2 \cdot \xi = \xi^3$. Note also that the interband term of the damping constant depends quadratically on the SO coupling constant. Such quadratical dependence of the interband term of the damping constant α on the SO coupling constant ξ has already been addressed in Ref. [139].

The second point one can notice in Fig. 3.5 is that for small Γ the dominant contribution to α comes from the intraband transitions since it is inversely related to Γ, i.e., related to lifetime $\tau = \hbar/\Gamma$ of electron states. For large Γ, the interband contribution, proportional to $\Gamma \sim 1/\tau$, is dominant [139]. The combination of these two contributions results in a minimum in the total damping on the scattering rate although it is hardly visible in the case of bulk Ni in Fig. 3.5. Similar minima of the damping constant as a function of temperature have been found experimentally for bulk Fe, Co and Ni [140]. Thus, inclusion of interband transitions in the torque-correlation model, in addition to intraband transitions accounted for by the breathing Fermi surface model, is important for correct theoretical description of the Gilbert damping.

The presently reported dependence of α on the scattering rate Γ is very similar to that obtained for the three bulk ferromagnets in the *ab initio* calculations by Gilmore *et al.* [88]. In particular, the characteristic minimum of α occurs at Γ close to 0.1 eV due to the dominance of intraband and interband contributions to α at small and large Γ, respectively. In Fig. 3.6 the calculated damping constant α against the scattering rate Γ for bulk Fe, Co and Ni is shown, for comparison, in one panel. As shown, the largest damping constant α is obtained for bulk Ni, which can be partly attributed to the large SO coupling in Ni (although this is not the only
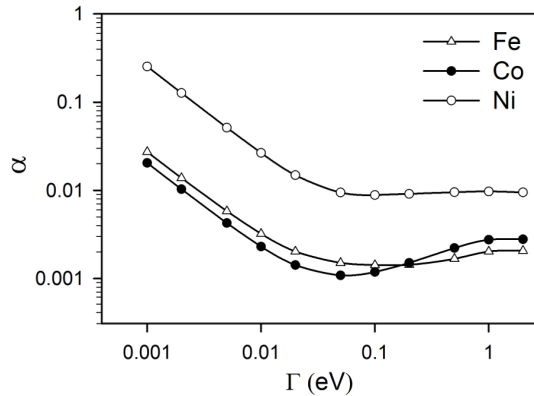
66

Figure 3.6: Calculated Gilbert damping constant α vs scattering rate Γ for bulk Fe, Co and Ni.

factor) whereas the damping constants of bulk Fe and Co are close to each other, although α for Fe is slightly larger ($\sim 30 - 40\%$) than for Co within the range of $\Gamma < 0.1$ eV. They both have the same value at $\Gamma = 0.2$ eV and α of Co exceeds that of Fe for $\Gamma > 0.5$ eV. The results obtained for both metals show that α depends strongly on the scattering rate Γ, but as it will be discussed in the following (cf. Sec. 3.4) the Gilbert damping can also be strongly affected by two other main factors: the SO coupling and the density of states (DOS) close to the Fermi level ϵ_F.

3.3 Ferromagnetic films

Extrinsic magnetic damping can occur when the system's symmetry is reduced like in ultrathin films. As mentioned in previous sections, there have been many experimental works on damping in magnetic structures [37, 39, 55, 57, 58, 74, 78, 81, 141]. However, there have been hardly any theoretical calculations of the Gilbert damping in layered structures [85, 91]. Hence, providing a quantum-mechanical description of the Gilbert damping in layered magnetic structures is highly desirable. It is the main objective of this thesis whilst part of the obtained results is also reported in the papers co-authored by the present author [62, 94, 142]. In this section the Gilbert damping in free-standing films of metallic ferromagnets, which has not been addressed theoretically before, is investigated. In particular, the film thickness dependence of the Gilbert damping as well as its dependence on the electron scattering rate in Fe, Co and Ni films with the (001) surface are discussed in detail. The direction of magnetisation is assumed to be perpendicular to the film surface, in the z direction. In this context, it is worth noting that the threshold current in current-induced DW systems with out-of-plane magnetisation is predicted to be smaller than in those with the in-plane orientation of magnetisation [143].
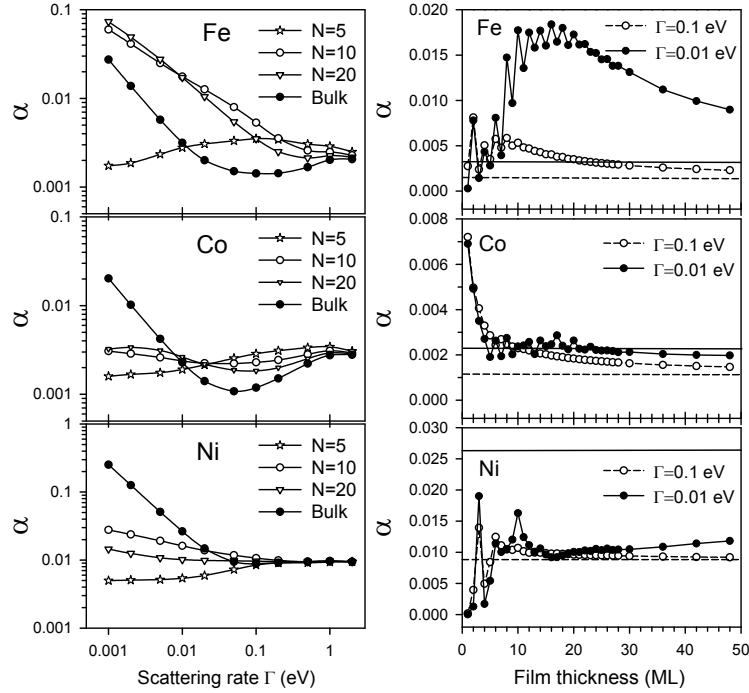
Figure 3.7: Gilbert damping constant α *left*: vs scattering rate Γ in bulk ferromagnets (bcc Fe, fcc Co, fcc Ni) and (001) ferromagnetic films with different thicknesses N, *right*: vs film thickness in (001) bcc Fe, fcc Co and fcc Ni films, calculated with scattering rates $\Gamma = 0.01$ eV and $\Gamma = 0.1$ eV; The horizontal lines mark the bulk values of α for $\Gamma = 0.1$ eV (dashed line) and $\Gamma = 0.01$ eV (solid line).

It has turned out that the Gilbert damping constant α calculated for (001) bcc Fe, fcc Co and fcc Ni ferromagnetic films is considerably modified (enhanced or reduced) in comparison with the corresponding bulk ferromagnets [62]. An enhanced Gilbert damping in ultrathin films in comparison with their bulk counterparts is also usually reported in experimental papers [58, 73, 79, 80]. Such enhancement originates from the presence of the substrate on which the film deposited on and/or the cap that covers it. Thus, the results presented for free-standing ferromagnetic films in this section cannot be compared directly with the experimental data. As it will be shown here the damping enhancement is not theoretically predicted for all ranges of scattering rate and film thicknesses. The modifications of α are strongly affected by the scattering rate and the film thickness. Figure 3.7 (left panel) presents α versus scattering rate Γ for both bulk and ferromagnetic films in one graph. The most remarkable changes of the Gilbert damping occur for films of a few monolayer thickness and a range of the scattering rates Γ that depends on the system (this range changes with the thickness of Fe films, includes $\Gamma \neq 0.01$ eV for Co films, corresponds to $\Gamma \leqslant 0.01$ eV for Ni films). The reduction of α at $\Gamma = 0.001$ eV is over tenfold for 5 ML films of Fe, Co, and over 50-fold for 5 ML films of Ni.

The Gilbert damping in Fe films of a few monolayer thickness with even and odd number

68

of atomic layers behaves differently, particularly for smaller Γ at which the reduction occurs, causing the Gilbert damping to be more reduced for films with odd numbers of layers. The Gilbert damping α is enhanced for Fe films thicker than 9 ML in the entire investigated range of Γ, especially, for $\Gamma \leqslant 0.5$ eV. For ultrathin Fe films of a few ML thickness, the enhancement of α is limited to some intermediate ranges of investigated scattering rate, e.g., 0.02 eV $\leqslant \Gamma \leqslant 1$ eV for $N = 5$ whilst the aforementioned reduction of α is found for smaller Γ (the thicker Fe, the smaller Γ at which the reduction starts).

The Gilbert damping constant α in Co films is enhanced for 0.01 eV $\leqslant \Gamma \leqslant 1$ eV and it is reduced for $\Gamma \leqslant 0.01$ eV. For Co films with $\Gamma = 0.01$ eV (except for those of 1, 2 and 3 ML thicknesses) the damping constant α, surprisingly, has nearly the same value as in bulk Co. In the case of Ni films the calculated α with $\Gamma \leqslant 0.02$ eV is largely reduced in comparison with bulk Ni. The damping constant of the considered (001) fcc Ni films is slightly larger than that of bulk Ni only for the scattering rates Γ close to 0.1 eV.

For large scattering rates ($\Gamma \geqslant 1$ eV for Fe and Co, and $\Gamma > 0.1$ eV for Ni) the damping constant α for thin films is close to the bulk value. As a general trend, it is found that the values of α calculated for ferromagnetic films tend to the corresponding bulk values with increasing film thickness for the majority of the assumed scattering rates 0.001 eV $\leqslant \Gamma \leqslant 2$ eV. However, the convergence to the bulk value is slow in most cases, e.g., for $\Gamma = 0.01$ eV in the case of Ni films, as seen in Fig. 3.7 (right panel).

The damping constant α is plotted as a function of the film thickness for ferromagnetic bcc Fe, fcc Co and fcc Ni films with two different scattering rates in Fig. 3.7 (right panel). The characteristic oscillations of the magnetic damping with the film thickness are obtained for all three metals and they are attributed to quantum well (QW) states with energies close to the Fermi level ϵ_F (e.g., the clear oscillation period of 2 ML is found for Fe films). This interpretation is supported by the fact that the obtained oscillations have a smaller amplitude if Γ increases since it results in larger smearing of the electronic energy levels (and the energies of QW states, in particular) described by the Lorentz function. The occurrence of QW states in metallic films is a well-known phenomenon which also leads to oscillations of interlayer exchange coupling and magnetic anisotropy with varying thicknesses of ferromagnetic films and/or nonmagnetic layers [144, 145, 146, 147]. Further discussion on the oscillations of the Gilbert damping is given below in this section.

For bcc Fe films, the damping constant α has a broad maximum at a thickness of several ML. This maximum occurs at lower film thicknesses for larger scattering rates (at 16 ML for $\Gamma = 0.01$ eV, and at 7 ML for $\Gamma = 0.1$ eV). Then, α begins to decline showing a slow monotonic decay

as the film thickness increases towards the Fe bulk value for larger thicknesses. However, the damping constant α for both considered scattering rates is still far from the corresponding bulk values even for the thickest investigated film thickness of $N = 48$ ML, especially for $\Gamma = 0.01$ eV.

For fcc Co films, the damping constant α decreases, steeply from 1 ML to 5ML, upon increasing the film thickness; small oscillations coming from QW states are superimposed on this monotonic dependence. If these small oscillations are neglected, α declines gradually with increasing film thickness and saturates eventually at the bulk value of 0.0023 for $\Gamma = 0.01$ eV, already at $N = 10$, and approaches closely the bulk value of 0.0012 for $\Gamma = 0.1$ eV at Co thicknesses of $N \approx 40$.

In the case of fcc Ni films, the damping constant α increases steeply when the film thickness changes from a monolayer up to 3 ML at which thickness it reaches its first peak, as it is clear from Fig. 3.7 (right panel). This is followed by a sharp fall of α at the Ni film thickness of 4 ML and a subsequent increase to its second peak at 6 ML and third peak at 10 ML (the latter peak is only weakly pronounced for $\Gamma = 0.1$ eV). Although α oscillates with Ni film thickness, in general, it shows an overall upward trend upon increasing the film thickness. The obtained large oscillations of α owing to QW states in Ni films disturb this trend more strongly, especially for $N \leqslant 12$ ML, than oscillations due to QW states in Fe and Co films. The Gilbert damping constant for Ni films with $\Gamma = 0.1$ eV saturates at the bulk value for $N \approx 20$ ML. For smaller scattering rate of $\Gamma = 0.01$ eV, α seemingly starts to saturate at $N \approx 17$ ML. However, this trend is deceptive since α is only a third of its calculated bulk value (0.026) at $N = 17$ ML and for the Ni thickness larger than 30 ML the damping constant increases monotonically up to the largest investigated thickness of $N = 48$ ML. Thus, it is expected that for $\Gamma = 0.01$ eV the actual convergence of α to the bulk Ni value will take place at much larger film thicknesses, presumably around 300 ML as it can be roughly estimated by extrapolating the monotonic dependence seen for $N \gtrsim 30$ ML in Fig. 3.7 (right panel).

It is inferred from the results obtained for ferromagnetic films that the Gilbert damping can be enhanced several times in comparison to bulk metals. The maximum enhancement for $\Gamma = 0.01$ eV is found for the 16 ML Fe film (5.5 times) and the Co monolayer (over threefold). In the case of Ni films a significant enhancement (nearly 67% for Ni(3 ML) with $\Gamma = 0.05$ eV) occurs merely for larger scattering rates ($0.02\,\mathrm{eV} \leqslant \Gamma \leqslant 0.2\,\mathrm{eV}$). Simultaneously, a large reduction of α (over tenfold) is obtained for Fe and Ni films of a few ML thickness, in particular for $N = 1, 3$ ML for Fe with $\Gamma \leqslant 0.02$ eV and $N = 1, 2, 4$ ML for Ni in the whole range of considered Γ. The obtained enhancement of α oscillates with the film thicknesses and it decays

for thicker films as the damping constant approaches the bulk limit. The enhancement of the Gilbert damping (or, more generally, its modification) in free-standing ultrathin ferromagnetic films, in comparison to bulk metals, is related to change of the electronic structure due to the loss of 3D translational symmetry. In particular, this change gives rise to quantisation of the wave vector in the direction perpendicular to the film surface and the subsequent occurrence of the QW states which in turn leads to oscillations of the damping constant with increasing film thickness.

The oscillations appearing in the film thickness dependence of the damping constant have a different character for different metals. A clear period of 2 ML is present for Fe films whilst the identification of similar periods for Co and Ni films is not straightforward, with two different periods being possible (e.g., ~ 3.5 ML and ~ 7 ML for Ni); cf. Fig. 3.7 (right panel). The oscillation periods associated with QW states are related to the extremal radii of Fermi surface sheets of the corresponding bulk metals. However, further investigations are required to determine which points or regions in the 2D BZ are responsible for the occurrence of the QW states contributing to the Gilbert damping oscillations. Such identification of relevant $\boldsymbol{k}$-points has been successfully done for the MCA part of the magnetic anisotropy energy (also related to the SO coupling) of (001) fcc Co films which oscillates with one clear period close to 2 ML, as predicted theoretically [148, 149] and recently confirmed experimentally [150, 151]. It has been found that these oscillations come from the centre of the 2D BZ where there are pairs of QW states degenerate at the $\overline{\Gamma}$ point [149].

The oscillations of the Gilbert damping constant with film thicknesses are found to have origin mainly in the interband term, so that the obtained oscillations stem from pairs of QW states with energies close to each other as well as to the Fermi level ϵ_{F}. Thus, it is deduced that the oscillations of the Gilbert damping arise due to a similar mechanism as oscillations of the MCA energy which have been shown to come from pairs of QW states, one state lying below ϵ_{F} and the other above ϵ_{F} [146, 149, 152]. However, the important difference is that the states significantly contributing to the Gilbert damping lie within a few Γ off the Fermi level ϵ_{F}, due to the presence of the product $L(\epsilon - \epsilon_n(\boldsymbol{k}))L(\epsilon - \epsilon_{n'}(\boldsymbol{k}))$ in Eq. (2.102). In the case of MCA the energy range of the contributing states is much wider as the suppressing factor $1/(\epsilon_n(\boldsymbol{k}) - \epsilon_{n'}(\boldsymbol{k}))$ present in the second-order perturbation theory expression for the MCA energy does not decay so rapidly when the energies, $\epsilon_n(\boldsymbol{k})$ and/or $\epsilon_{n'}(\boldsymbol{k})$, move away from ϵ_{F}. Accordingly, the regions in the $\boldsymbol{k}$-space that give dominating contributions to the magnetic damping are much more restricted than for the MCA. This conclusion should also hold for the contributions to α from QW states.
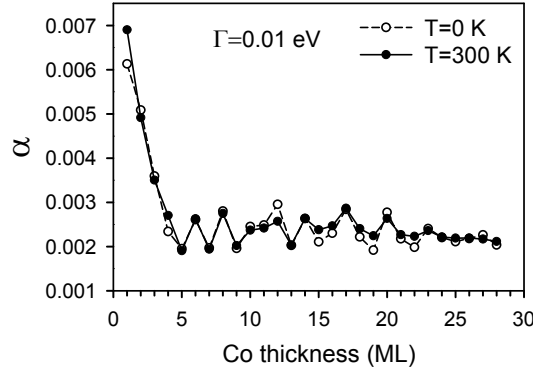
Figure 3.8: Gilbert damping constant α vs film thickness at $T = 0$ and $T = 300$ K in (001) fcc Co films; $\Gamma = 0.01$ eV.

The calculations of the Gilbert damping constant α and the MCA energy also differ significantly since operators applied in the expressions for the two quantities are different. These operators are the SO torque A^- in the former case, and the SO interaction H_{SO} (for two separate orientations of magnetisation) in the latter. Therefore, a particular pair of QW states can contribute to the Gilbert damping and the MCA energy in a significantly different way, or even not contribute at all for one of them, due to specific spin and spatial symmetry of the corresponding operators. A further investigation is required to explain the actual role of QW states in the Gilbert damping oscillations to clarify the associated oscillation periods.

Temperature dependence of the Gilbert damping is also investigated. Figure 3.8 presents the damping constant α versus film thickness at two different temperatures ($T = 0$ and $T = 300$ K) in Co films. As shown, α changes only slightly upon the change of temperature and for most thicknesses it is almost the same at both $T = 0$ and $T = 300$ K, although the oscillations of α with changing Co film thickness have a larger amplitude at $T = 0$ due to the lack of the direct thermal contribution (via $f_{FD}(\epsilon)$) to smearing of energy levels. A similar conclusion was previously found to hold for the MCA energy and its oscillations in Co films [129].

3.4 Ferromagnet/nonmagnet bilayers

In magnetic layered systems nonzero magnetisation is confined almost entirely within its ferromagnetic parts. However, the presence of nonmagnetic metal in contact with ferromagnetic metals can alter profoundly the magnetic properties of the latter. A well-known example is magnetic anisotropy of ultrathin ferromagnetic films. The anisotropy energy can change sign due to the presence of a nonmagnetic cap (which affects the MCA energy term), thus leading to reorientation of the film magnetisation [32, 33, 34, 35, 36]. The presence of a nonmagnetic layer

can also strongly affect magnetisation dynamics of ferromagnetic films. The Gilbert damping has been investigated experimentally in various magnetic metallic structures which include FM/NM bilayers [39, 55, 79, 80, 82] and the damping constant is found to be enhanced if compared to the bulk ferromagnets. Such bilayers occur, in particular, as building blocks in [FM/NM]$_N$ multilayers which are of great interest in spintronics. In particular, in Ref. [78] the Gilbert damping in Fe/Au bilayers has been investigated by FMR and an additional FMR linewidth, corresponding to an extra Gilbert damping, due to the Au capping layer has been found. The peak-to-peak FMR linewidth for FM/NM bilayers with different FM and NM layers has been analysed in Ref. [37]. Therein, the corresponding Gilbert damping for magnetic field applied in different directions has been found.

Magnetisation dynamics in ferromagnetic films in contact with NM layers has been first theoretically investigated, separately, by Berger [45] and Slonczewski in 1996 [153]. Several years later the theory based on spin pumping has been proposed [6, 7] to account for the enhanced magnetic damping in systems including FM and NM layers. The latter theory is recalled in several parts of this thesis to compare the obtained results with its predictions.

The spin pumping theory is currently the common approach to semi-phenomenological description of spin relaxation in magnetic layered systems. Based on this theory the Gilbert damping is enhanced in a ferromagnetic metal in contact with a nonmagnetic metal due to the transfer of angular momentum from the ferromagnet to the nonmagnet through their interface. The physical parameter that represents the effect of interface in this theory is the spin mixing conductance $G_{\uparrow\downarrow}$. Another key factor in transfer of angular momentum in magnetic layered systems is the spin-flip rate τ_{sf}^{-1} which is related to the SO coupling in metals and thus to the atomic number Z; the heavier atom, the larger τ_{sf}^{-1}. It is noteworthy mentioning that, the expression for the enhancement due to the spin pumping is valid merely for precession frequency smaller than τ_{sf}^{-1} [39]. This condition also holds in the SO torque correlation model applied in the present calculations of the Gilbert damping since arbitrarily small magnetic field corresponding to very small precession frequency ω_0 is considered to extract the expression (2.103) for the damping constant α. The enhanced magnetic damping in FM/NM layered systems can be explained within the spin pumping theory as follows.

The enhanced damping in FM/NM layered systems observed in experiment is usually accounted for by relating it to the atomic number of the NM [39]. According to the spin pumping theory, in the case of light nonmagnetic metals like Cu the small spin-flip rate ($\tau_{\mathrm{sf, Cu}}^{-1} \approx 10^{11}$ s^{-1} [39]) leads to a nonzero backflow of the transferred angular momentum, from the NM back to the FM, which results in no appreciable enhancement in the Gilbert damping of ferromagnetic

metals. For heavier nonmagnetic metals (NM=Pd, Pt and Au herein, all with similar $G_{\uparrow\downarrow}$ [59]) the spin pumping theory predicts that the large spin-flip rate causes a negligible backflow of transferred angular momentum. This leads to a significant enhancement in the Gilbert damping of the FM. However, according to the results of the present calculations reported in this section it is rather the DOS at the Fermi level in the adjacent nonmagnetic metal, combined with the large spin-flip rate in the NM due to its SO coupling, that is responsible for the enhanced Gilbert damping.

Furthermore, within the spin pumping theory the enhancement of the damping constant α is related to the spin-diffusion length λ_{sd} of the NM and it is inversely proportional to the FM thickness. For $N_{NM} \ll \lambda_{sd}$ the net transmitted spin angular momentum through the FM/NM interface is zero (flow=backflow) and no enhancement is predicted. This has particularly been found in Ni/V(5 nm) bilayers where no extra damping has been observed due to adding the adjacent V layer next to Ni [81]. For the NM layer thicknesses N_{NM} comparable to λ_{sd} a nonzero enhancement of the magnetic damping is obtained due to the reduced backflow. This enhancement reaches its maximum in the regime of $N_{NM} \gg \lambda_{sd}$ that is referred to as perfect spin sink limit (see Ref. [39] for details). In this case the transmitted spin moment is totally absorbed within the nonmagnetic metal.

In this section the Gilbert damping constant α in perpendicularly magnetised ultrathin ($\leqslant 10$ nm) (001) fcc FM/NM bilayers with Co as a ferromagnetic substrate and various nonmagnetic caps NM=Cu, Pd, Ag, Pt and Au will be discussed. The dependence of α on both the Co and NM thicknesses, $N_{FM} = N_{Co} \leqslant 28$ ML and $N_{NM} \leqslant 22$ ML, as well as on the electron scattering rate Γ is investigated. The results obtained for bilayers are compared with those obtained for pure ferromagnetic films, presented in the previous section, and with experimental observations. Particularly, the effect of NM caps on the magnetic damping enhancement in Co/NM bilayers will be discussed, by investigating its relation to the strength of the SO coupling in the nonmagnetic metals and the systems' electronic structure near the Fermi level.

The Gilbert damping in FM/NM bilayers is calculated using the formula (2.103) derived for layered systems within the TB model. This formula depends on the eigenstates (both their energies and probability amplitudes) of the TB Hamiltonian which includes the SO interaction and is constructed in the way described in Sec. 2.4. The dimension ($18N \times 18N$) of the TB Hamiltonian matrix for layered systems grows quickly as the number N of atomic layers increases, which makes the calculations difficult numerically when the bilayer thickness becomes large. It should also be noted that the SO coupling is not uniform throughout the system since it is different in the Co and NM parts.

74

The Gilbert damping is found to be remarkably enhanced in the investigated Co/NM(6 ML) bilayers, particularly strongly for very small Co thickness (cf. Fig. 3.9). This result also holds for Co/NM bilayers with the NM cap of other thicknesses, even as thin as 2 ML (Fig. 3.11). In the presence of the NM caps the damping constant α is about an order of magnitude larger than in pure Co films, and even a few times more in the case of the Pt cap. The dependence of α on the Co thickness N_{Co} shows a monotonic decrease with increasing N_{Co} so that the enhancement of α in Co/NM bilayers becomes weaker for thicker Co films. The damping constant of Co/NM(6 ML) bilayers decreases by more than an order of magnitude (about 27 times for Cu, 22 times for Ag, 42 times for Pd, 45 times for Pt and 47 times for Au caps) as the Co thickness increases from 1 ML to 28 ML.

The results obtained for Co/NM bilayers satisfy the following approximate linear dependence on $1/N_{\mathrm{FM}}$ ($= 1/N_{\mathrm{Co}}$ herein)

$$\alpha \approx \alpha_{\mathrm{b}} + \alpha_{\mathrm{s}}/N_{\mathrm{FM}} \tag{3.2}$$

which is demonstrated in Fig. 3.9 where the additional damping (enhancement) $\alpha - \alpha_{\mathrm{b}}$ due to adding the NM caps is shown. It can be inferred from Eq. (3.2) that the total damping constant α in Co/NM bilayers, redefined as the extensive quantity $\tilde{\alpha} = N_{\mathrm{FM}}\alpha$, consists of two terms: the bulk-like contribution $N_{\mathrm{FM}}\alpha_{\mathrm{b}}$ from the ferromagnet and the additional term α_{s} responsible for the enhancement. The latter term is the combined contributions coming from the FM/vacuum and FM/NM interfaces present in the system. In the case of NM=Pd and Pt, as will be shown in chapter 4, the term α_{s} originates mainly from several atomic layers inside the NM cap close to the FM/NM interface (see Sec. 4.1). It turns out that the approximate relation (3.2) also holds for pure ferromagnetic films. This equation, therefore, presents a direct connection between the film and bulk regime.

This result agrees with the general prediction of the spin pumping theory [6, 7, 58, 59] which assumes that the damping enhancement $\alpha - \alpha_{\mathrm{b}}$ is inversely proportional to the FM thickness, whilst the proportionality coefficient (α_{s} herein) depends on the type of FM/NM interface (through its mixed spin conductance), and properties of the NM cap (in particular, on whether it is a good or poor spin sink). However, it has to be emphasised again that the spin pumping theory predicts a significant enhancement of damping only for $N_{\mathrm{NM}} \gtrsim \lambda_{\mathrm{sd}}$, contrary to the presently obtained substantial enhancement due to modification of electronic structure in the Co/NM bilayers. This can be clearly seen in Fig. 3.10 in which α is enhanced regardless of the thickness of the NM cap even for poor spin sinks, i.e. Cu and Ag with λ_{sd} of the order of 10^3 ML.
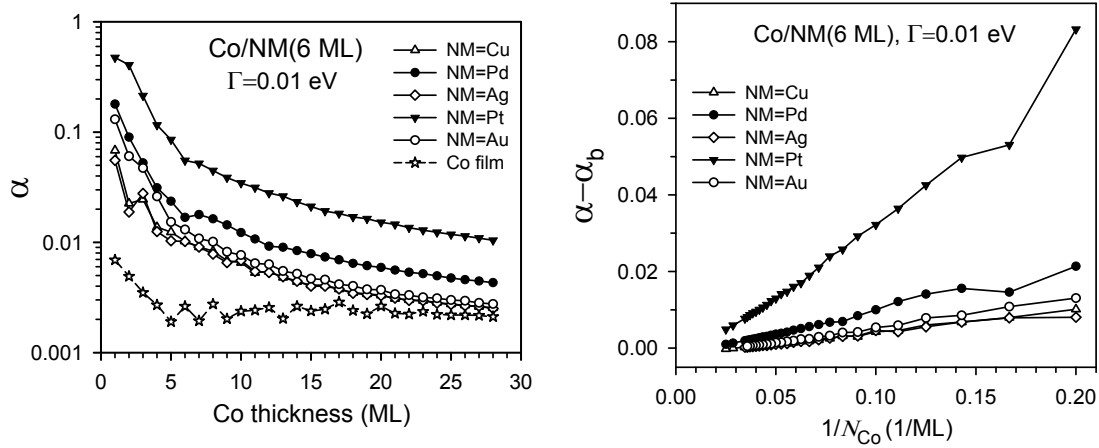
Figure 3.9: *Left*: Gilbert damping constant vs Co thickness in (001) fcc Co/NM(6 ML) bilayers, *right*: Inverse Co thickness dependence of the additional damping, with respect to the bulk value of Co, in Co/NM(6 ML) bilayers; $\Gamma = 0.01$ eV.

A monotonic dependence on $1/N_{FM}$, similar to the relation (3.2) though following a sublinear power law, is also found in Ref. [86] for the ratio $\Delta\omega/\omega_0$ of the linewidth $\Delta\omega$ and the frequency ω_0 of a long-wavelength spin wave in an (001) Co/Pd bilayer. Assuming the usual definition of $\Delta\omega$ as the full width at half maximum (though not stated explicitly in Refs. [85, 86]) the linewidth $\Delta\omega$ is twice the imaginary part ω_1 of the complex spin-wave frequency $\omega = \omega_0 - i\omega_1$. Then, the damping constant α obtained for Co/Pd bilayer (Fig. 3.9) is about 2 or 3 times larger than the values of $\alpha = \omega_1/\omega_0 = 0.5\Delta\omega/\omega_0$ reported in Ref. [86]. However, it should be emphasised that the two methods of calculating α are significantly different since the cited calculations of the spin-wave spectrum do not account for the lifetime $\tau = 1/\Gamma$ of electron states due to electron-phonon scattering.

The $1/N_{FM}$ proportionality of the enhancement of the Gilbert damping has also been observed in experiment by determining the FMR linewidth and its term proportional to α. A linear dependence of α on $1/N_{Co}$ has recently been found experimentally in Pt/Co/Pt trilayers [57]. A similar linear dependence of the magnetic damping constant on the inverse of the ferromagnetic film thickness in Eq. (3.2) has also been observed in experiments on ultrathin bcc Fe(001) films grown on Ag(001) [73], Fe/Au films [78], Ni-based bilayers [81] as well as CoFeB [82].

In Fig. 3.10 the damping constant α is presented as a function of the NM cap thickness in Co(6 ML)/NM bilayers. For comparison, the value of α for the Co(6 ML) film ($\alpha = 0.0026$ for $\Gamma = 0.01$ eV) is also marked in the plot. As already mentioned the enhancement of the Gilbert damping is obtained even for the thinnest NM overlayers, 1 ML or 2 ML thick. For NM=Pd and Pt caps a large initial increase makes an upward trend of α for the cap thicknesses extending up to 4 ML where the damping constant reaches its maximum value, whilst for thicker caps
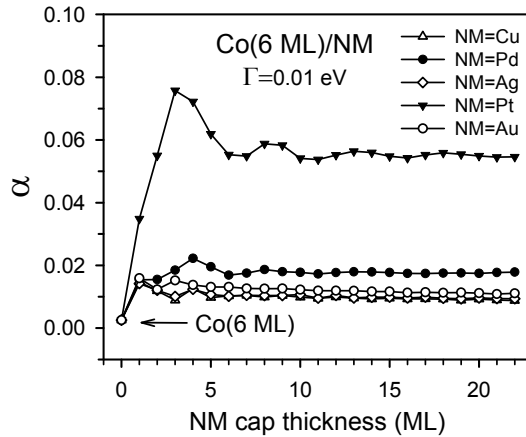
Figure 3.10: Gilbert damping constant vs NM cap thickness in (001) fcc Co(6 ML)/NM bilayers; $\Gamma = 0.01$ eV.

it oscillates with the cap thicknesses. The enlarged view of plots reveals that such oscillatory dependence on the NM cap thickness is present for all investigated bilayers though the oscillations depend on the type of NM metals; they are not well visible for NM=Cu, Ag and Au in Fig. 3.10 due to the figure's scale.

The damping constant oscillations, whose amplitude decreases with the increase of the cap thickness, are attributed to the QW states present in the NM metal. The oscillation periods can be related to extremal radii of the FS of the bulk nonmagnets. For bulk Pd and Pt, the sheet of the FS coming from the bulk d band of the Δ_5 symmetry yields the same period of 5.7 ML [154]. This oscillation period has previously been found for the MCA energy in Co/Pd systems [146, 152]. Similar, though slightly shorter, period of about 5 ML is presently found in the dependence of the Gilbert damping constant on the Pd and Pt cap thicknesses (see Fig. 3.10).

In Fig. 3.11 the additional damping $\alpha - \alpha_{Co}$ due to adding the NM caps only, accompanying the damping α_{Co} of the free-standing Co film, is presented as a function of Co thickness (in this discussion α is compared with α_{Co} rather than with the bulk damping α_b as in Fig. 3.9 above). The additional damping obeys the same trend (decreasing with increasing Co thickness) as the total damping constant α in NM-capped Co films since the NM contribution to the total damping is dominant. The additional damping is positive (which corresponds to damping enhancement) for Co films with all considered NM caps. For Co films with NM=Cu, Ag and Au caps and thicker than 13 ML the additional damping is smaller than the damping α_{Co} of pure Co films but for the Pt cap the additional damping is still far above α_{Co} for Co thicknesses up to 17 ML.

The obtained additional damping in Co/NM(2 ML) bilayers due to adding the NM caps
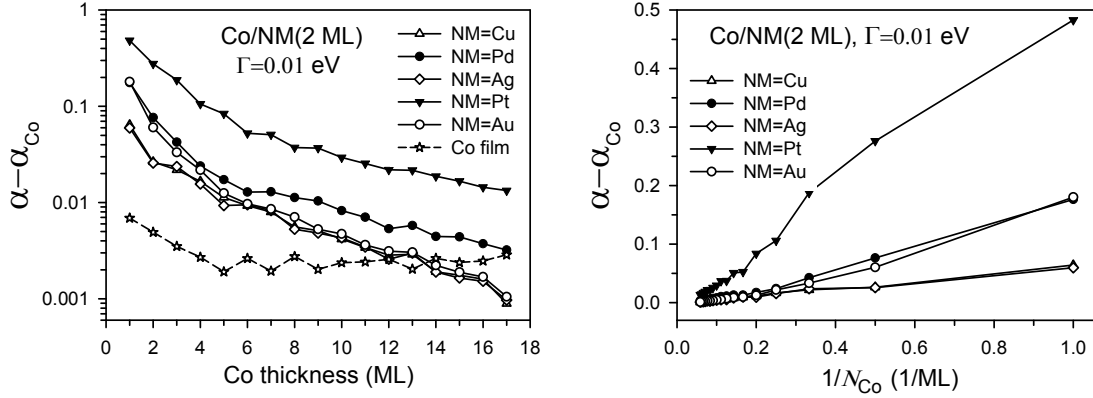
Figure 3.11: *Left*: Additional Gilbert damping due to the presence of NM caps in (001) fcc Co/NM(2 ML) bilayers vs Co thickness; the damping of the Co films has also been shown for comparison, *right*: Inverse Co thickness dependence of the additional damping in Co/NM(2 ML) bilayers; $\Gamma = 0.01$ eV.

follows a linear dependence on the inverse Co thickness (as it is shown in Fig. 3.11). Again, this can be explained by nonlocal spin relaxation processes which take place in the NM layer and dominate damping in the bilayer so that α calculated with the formula (2.103) will be proportional to $1/N_{\mathrm{FM}}$ with a good approximation.

Within the applied SO torque correlation model the obtained enhancement of the Gilbert damping in Co/NM bilayers results from two main factors:

(i) strong SO coupling in nonmagnetic elements heavier than Co,

(ii) change of electronic structure due to hybridisation at the Co/NM interface.

The former explicitly appears in the expression for α, namely in Eq. (2.108) for the SO torque elements $A_{nn'}(\boldsymbol{k})$, whilst both factors affect damping through the modification of the electronic states and their energies which enter Eqs. (2.108) and (2.102), respectively. To clarify the role of the two factors and their possible interplay the damping constant is calculated for Co/NM bilayers with zero and full SO coupling strength ξ_{NM} in the NM cap (see Fig. 3.12). To do this, the calculations are repeated with the SO coupling switched off in the nonmagnetic caps. It is found that, the Gilbert damping in Co/NM bilayers falls dramatically for NM=Pd and Pt whereas the change is not significant for NM=Cu, Ag and Au. Although the two nonmagnetic metals, Pt and Au, have very similar SO coupling constants, around 8.5 times larger than Co, switching off this coupling has a diametrically different effect on α in the two bilayer systems. The results for the Co/Au bilayer obtained with $\xi_{\mathrm{Au}} = 0$ and $\xi_{\mathrm{Au}} = 0.66$ eV differ by less than 15%, whereas the damping constant for the Co/NM bilayers falls by over twofold and fivefold for NM=Pd and Pt, respectively, if the SO coupling of the NM is switched off. In the case of the Co/Cu and Co/Ag bilayers α increases slightly, about 7%, if $\xi_{\mathrm{Cu}} = \xi_{\mathrm{Au}} = 0$ is used instead

78
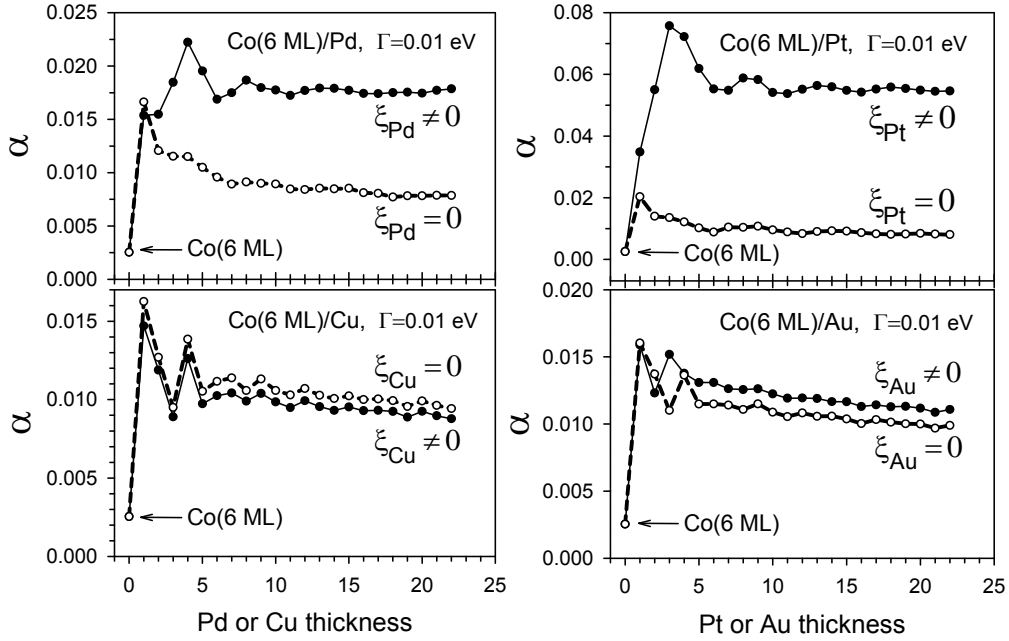
Figure 3.12: Gilbert damping constant vs NM thickness in (001) fcc Co(6 ML)/NM bilayer (NM=Cu, Pd, Pt and Au), in the presence (solid circles) and the absence (open circles) of the SO coupling in NM; $\Gamma = 0.01$ eV.

of $\xi_{Cu} = 0.12$ eV and $\xi_{Ag} = 0.24$ eV. This is caused presumably by the change of the electronic structure after switching off the SO coupling constants of Cu and Ag.

Thus, it is found that the Gilbert damping depends strongly on the SO coupling of the NM=Pd and Pt caps but only slightly on the SO coupling of the NM=Cu, Ag and Au caps. This remarkably different dependence of α on ξ_{NM} is due to the presence of d states at the Fermi level ϵ_F in NM=Pd and Pt, and the lack of such states in NM=Cu, Ag and Au. This conclusion can particularly well justified by the case of Au. Although Au has the SO coupling much larger than Pd and similar to Pt, its d-band is well below the Fermi level which makes its magnetic damping smaller than that of Co/Pd or Co/Pt bilayers. This can be illustrated by analysis of the band structure in the constituent metals of the bilayers presented below in this section. To explain this relationship one has to take a closer look at the underlying physics of the magnetic damping and the parameters entering the expression (2.103) for the Gilbert damping constant α. The expression for α is strongly affected by quantum states with energies in the immediate vicinity of ϵ_F (due to the form of the integrand in Eq. (2.102)). Different positions of the narrow d band in Pt and Au on the energy scale cause the DOS at ϵ_F to be high in Pt and low in Au. As a result a relatively small number of states (with the dominant sp symmetry) present at ϵ_F in Au contribute only weakly to α, despite large ξ_{Au}, whilst d states present at ϵ_F in Pt give a large contribution. For the same reason the SO coupling of the NM metal has a strong effect on the magnetic damping also for the Pd cap, whilst this effect is very weak for NM=Cu and Ag
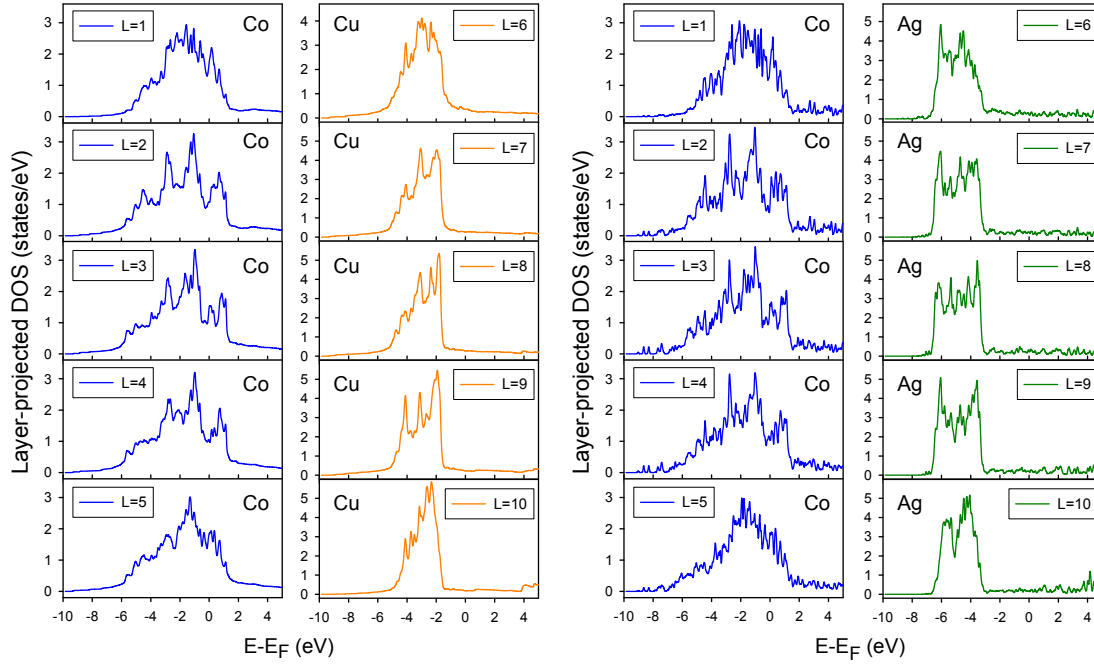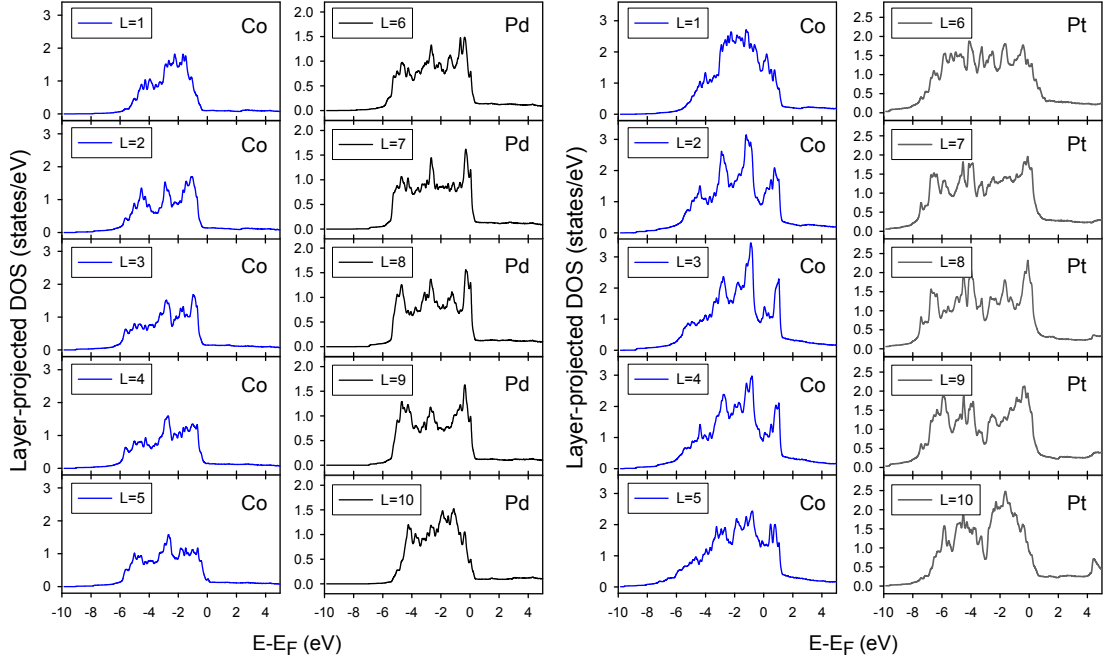
Figure 3.13: Layer-projected DOS in different atomic layers L in *left*: Co(5 ML)/Cu(5 ML), *right*: Co(5 ML)/Ag(5 ML) bilayers.

(Fig. 3.12). A strong dependence of the damping constant on the SO coupling strength (with α proportional to ξ_{SO}^2) has been shown recently, theoretically and experimentally [77].

Another probable scenario accounting for the large enhancement of the Gilbert damping could be d(Co)-s, p(NM) hybridisation at Co/NM interface which has been turned out to play a minor role in increasing magnetic damping in Co/Pd and Co/Pt systems. Although it is commonly assumed that the SO coupling plays the major role in magnetic damping in Co/Pd and Co/Pt bilayers, the performed test calculations with $\xi_{NM} = 0$ show that there is still a significant contribution to the enhancement of α due to the change of electronic structure in Co, invoked by the hybridisation of quantum states at the Co/NM interface (see Fig. 3.12). This enhancement factor dominates for Co/NM bilayers with NM=Cu, Ag and Au in which the d band lies below ϵ_F; for such bilayers α shows a very similar dependence on the NM cap thickness (Fig. 3.10). Similar assumption has previously been considered in the experimental report [57].

To illustrate the effect of the DOS at the Fermi level on the Gilbert damping, the DOS for ferromagnetic films and the considered Co/NM bilayers is calculated in the following. The DOS is defined with the energies $\epsilon_n(\boldsymbol{k})$ of electronic states as

$$\rho(\epsilon) = \frac{1}{N_{2D}} \sum_{n\boldsymbol{k}} \delta(\epsilon - \epsilon_n(\boldsymbol{k})). \tag{3.3}$$

and the prefactor $\frac{1}{N_{2D}}$ (where the parameter N_{2D} denotes the number of $\boldsymbol{k}$-points in the BZ, cf.

Figure 3.14: Layer-projected DOS in different atomic layers L in *left*: Co(5 ML)/Pd(5 ML), *right*: Co(5 ML)/Pt(5 ML) bilayers.

Sec. 4.2) is introduced to obtain the value of DOS per surface atom. The function $\rho(\epsilon)$ can also be found as the derivative $\frac{\partial N_{\mathrm{occ}}}{\partial \epsilon}$ where $N_{\mathrm{occ}} = N_{\mathrm{2D}}^{-1} \sum_{n\boldsymbol{k}} \theta(\epsilon - \epsilon_n(\boldsymbol{k}))$ is the number of electrons (per surface atom) with energies up to ϵ at zero temperature. To speed up the convergence of the numerical integration in the BZ (the sum over $\boldsymbol{k}$), it is convenient to replace, in $N_{\mathrm{occ}}(\epsilon)$, the step function $\theta(x)$ with the Fermi-Dirac distribution function $f_{\mathrm{FD}}(x) = 1/(1 + e^{\beta x})$ where $x = \epsilon - \epsilon_n(\boldsymbol{k})$ and $\beta = 1/k_{\mathrm{B}}T$ corresponds to finite temperature T (note that ϵ replaces here the usual ϵ_{F} in this generalisation of f_{FD}). Thus the following formula

$$\rho(\epsilon) = \frac{1}{N_{\mathrm{2D}}} \sum_{n\boldsymbol{k}} \frac{\partial f_{\mathrm{FD}}(\epsilon - \epsilon_n(\boldsymbol{k}))}{\partial \epsilon} \tag{3.4}$$

is used for the total DOS (per surface atom). To get better insight into the system's electronic structure the layer-projected DOS (per atom in atomic layer) is defined in the usual way as

$$\rho_l(\epsilon) = \frac{1}{N_{\mathrm{2D}}} \sum_{n\boldsymbol{k}} P_{n\boldsymbol{k}}^l \frac{\partial f_{\mathrm{FD}}(\epsilon - \epsilon_n(\boldsymbol{k}))}{\partial \epsilon}. \tag{3.5}$$

The factor $P_{n\boldsymbol{k}}^l = \sum_{\mu\sigma} |a_{nl\mu}^\sigma(\boldsymbol{k})|^2$ is obtained by the projection of a quantum state $|n\boldsymbol{k}\rangle$ onto the spin-orbital Bloch basis states $|\boldsymbol{k}l\mu\sigma\rangle$ in layer l and it represents the probability of finding an electron occupying state $|n\boldsymbol{k}\rangle$ in layer l.

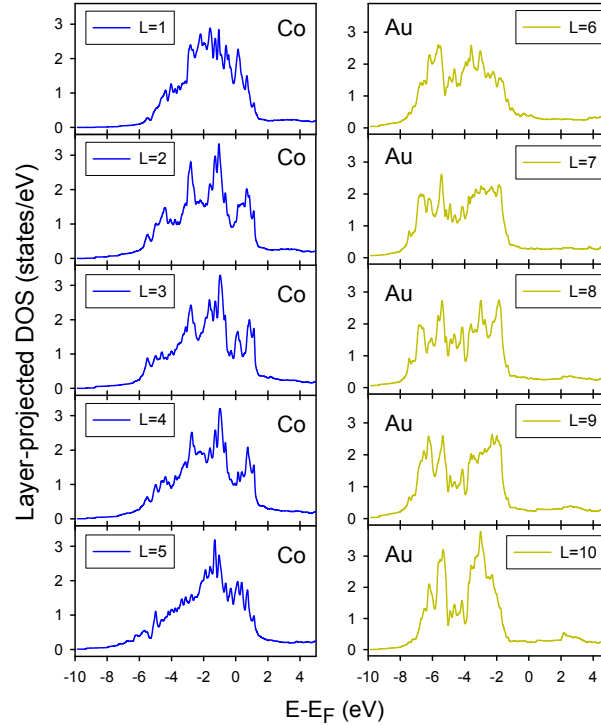The calculated layer-projected DOS for an Co(5 ML)/NM(5 ML) bilayer is shown in Figs.

81

Figure 3.15: Layer-projected DOS in an Co(5 ML)/Au(5 ML) bilayer for different atomic layer *L*. *left panel*: Co substrate (L=1-5), *right panel*: Au cap (L=6-10).

3.13-3.15. As it is obvious from the plots, in the Co part (substrate) there are d states close to the Fermi energy ϵ_F (where DOS has high values) that give contributions to the damping from ferromagnetic Co. The extra damping due to the NM caps is related to the number of states close to the Fermi energy. For NM=Pd and Pt caps, the DOS in the NM layers is large in the vicinity of ϵ_F in the NM caps. This means that there are d states in the nonmagnetic part which give contributions to the Gilbert damping from this part (Fig. 3.14). In the Cu, Ag and Au caps, large values (peaks) of the DOS occur at energies well below the Fermi level ϵ_F so that the top of the d band is well below ϵ_F in the NM. Thus, there are few states in the vicinity of ϵ_F in the nonmagnetic part and their contributions to the damping are marginal (see Figs. 3.13 and 3.15). Similar argument can be found in Ref. [38] where the DOS is used to explain low magnetic damping constant in manganese alloys films with large perpendicular magnetic anisotropy.

As the last point in this section, the dependence of the damping constant α on the scattering rate Γ in Co(6 ML)/NM(2 ML) bilayers is obtained. It can be seen in Fig. 3.16 that for all considered NM metals α decreases to its minimum value at Γ close to 0.1 eV, similar to the bulk ferromagnets (Fig. 3.5), as Γ increases from its lowest considered value ($\Gamma = 0.001$ eV). For $\Gamma \geqslant 0.1$ eV, the damping constant α slightly increases with increasing Γ. One may also notice the pronounced shift of α for Pt, in the whole considered range of Γ, in comparison with other
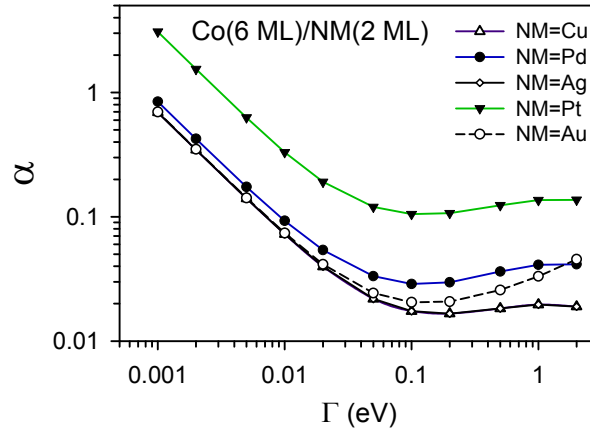
82

Figure 3.16: Gilbert damping constant α vs electron scattering rate Γ in Co(6 ML)/NM(2 ML) bilayers.

considered NM caps. Similar Γ dependence of α is also found in the calculations for $[\text{Co/NM}]_N$ multilayers (see Sec. 3.6).

3.5 Magnetic trilayers

In previous sections the Gilbert damping in bulk ferromagnets, ferromagnetic films and FM/NM bilayers was addressed. This section is devoted to the discussion of Gilbert damping in trilayer systems and presentation of the results obtained for the investigated magnetic trilayers. Much attention in this section will be paid to nonlocal magnetic damping in Co/NM1/NM2 trilayers.

Magnetic metallic trilayers are commonly used to investigate the magnetisation dynamics in view of potential spintronic applications. Magnetic damping has also been investigated experimentally in similar layered systems [10, 55, 57, 155, 156]. In particular, the Gilbert damping in Cu/Co/Cu trilayers and the effect of adjacent Pt layers has been investigated in Ref. [51] (see also [141]). Therein, it has been shown that the Gilbert damping is significantly enhanced by adding Pt caps to one or both sides of the Cu/Co/Cu system, particularly for very thin ($\leqslant$ 4 nm) Co films. Such an experimental evidence clearly shows that there is a highly nonlocal mechanism of the Gilbert damping enhancement in magnetic layered systems. Additionally, it has been shown, experimentally, for a system of Cu/Co/Cu sandwiched between Pt layers, in Refs. [51], that the two-magnon scattering cannot explain the thickness dependence of the FMR linewidth so that it is governed mainly by the Gilbert damping (see Eq. (1.1)).

The enhanced Gilbert damping in NM/FM/NM trilayers is explained in a general way in Ref. [6] by spin pumping from ferromagnet into the adjacent nonmagnetic (normal metal) layer. The spin pumping theory also predicts enhancement of the damping in FM/NM1/NM2 struc-
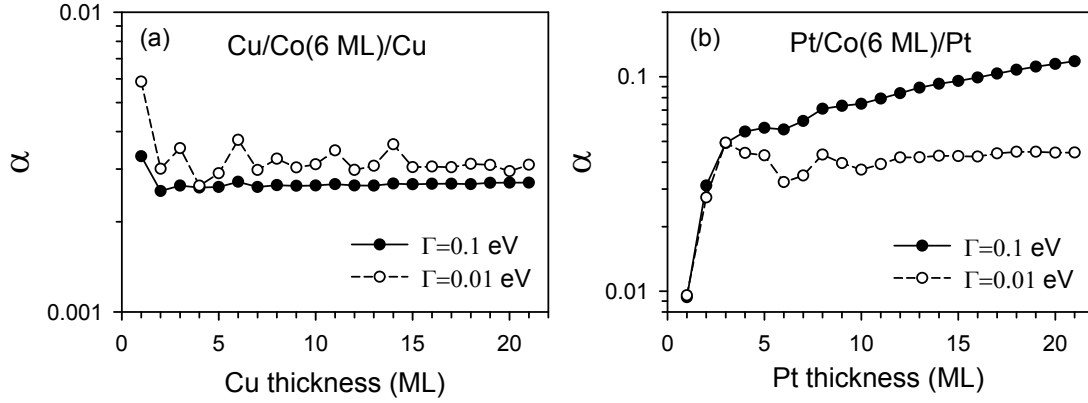
Figure 3.17: Gilbert damping constant α, (a): in Cu/Co(6 ML)/Cu trilayers vs Cu thickness, (b): in Pt/Co(6 ML)/Pt trilayers vs Pt thickness, with scattering rates $\Gamma = 0.1, 0.01$ eV.

tures due to highly nonlocal extrinsic damping in the second nonmagnetic cap (NM2) which is considered to be a good spin sink. Simultaneously, the damping enhancement is predicted to depend on the thickness of the first nonmagnetic layer (the spacer NM1) and its spin-diffusion length. Although spin pumping theory gives a plausible general explanation of spin relaxation in magnetic mutilayer systems, it does not provide a fully quantum-mechanical description of this phenomenon. Such a description is given by Kamberský's torque-correlation model on which the present calculations are based.

The applied TB model can be immediately implemented for calculation of the Gilbert damping constant, with the formula (2.103), in all investigated trilayer structures. In this section, the obtained results of such quantum-mechanical calculations are presented and they are shown to be in agreement with previous experimental observations in magnetic trilayers [10, 55, 57, 155, 156]. In particular, the applied quantum mechanical model predicts nonlocal enhanced damping in magnetic trilayer systems, in accordance with the spin pumping theory. Within the present model one is able to investigate the film thickness dependence of magnetic damping, the weak point of the two-magnon scattering approach. The dependence of α on Co and nonmagnetic caps thicknesses, for various scattering rates, is investigated and compared with recent experiments. Calculations are reported for NM/Co/NM with NM=Cu, Pt as well as for Co/NM/Pt trilayers with NM=Cu, Ag as spacer. It has been checked that, also for considered trilayer configurations one can take the advantage of integration over the 1/8 2D BZ to speed up the calculations. Thanks to this simplification, the calculation of α has been efficiently done for trilayers up to 48 ML thick with the available computer facilities (a Linux workstation).

Figure 3.17 shows α for NM/Co(6 ML)/NM trilayers (NM=Cu and Pt) as a function of the NM thickness. The obtained value of α in the Cu/Co(6 ML)/Cu system is almost independent

of the Cu thickness and it is close to the Co bulk value. This is in accord with the experimental results for Cu/Py/Cu [141]. For the Pt/Co(6 ML)/Pt system the Gilbert damping increases significantly due to adding a few monolayers of Pt to the both sides of the Co film. With further increase of the Pt substrate and cap thickness N_{Pt} the damping constant α oscillates with quickly decaying amplitude (larger for smaller Γ), in a similar way as for the Co/Pt bilayers (see Fig. 3.10). The damping saturates at $N_{\text{Pt}} \approx 15$ ML for $\Gamma = 0.01$ eV whilst α is found to steadily grow at least up to the largest considered Pt thickness (21 ML) for $\Gamma = 0.1$ eV. It is expected that α eventually saturates also in this case as the Pt substrate and capping layers get thicker. Such significantly different dependence of α on the Pt thickness for different Γ does not have an immediate explanation and requires further investigation. The obtained value of $\alpha = 0.23$ for Pt/Co/Pt with $N_{\text{Co}} = 3$ ML and $\Gamma = 0.005$ eV is very close to the experimental value $\alpha \simeq 0.3$ for the same system reported in Ref. [157].

Similar investigation has been recently performed experimentally for multilayers of Ta(3 nm)/NM/Co$_{90}$Fe$_{10}$(2 nm)/NM/Ta(3 nm) with NM=Cu, Pd and the results have been fitted to the general formula found with the spin pumping theory [58]. There are two main differences between systems investigated in the experiment and the one in the present calculations. Firstly, the experimental NM/Co$_{90}$Fe$_{10}$/NM trilayer was sandwiched between Ta capping layers (with large SO coupling constant $\xi_{\text{Ta}} \simeq 0.57$ eV) and secondly, the ferromagnetic film (Co$_{90}$Fe$_{10}$) is different from the one considered here (Co). Although both these factors affect the Gilbert damping and can make it differ significantly from the present results, the obtained theoretical damping constants are of the same order of magnitude ($\alpha \sim 0.01 - 0.04$) as the ones found in experiment. Furthermore, the obtained dependence of α on Cu thickness N_{Cu} is in qualitative agreement with experiment, particularly for very thin Cu films ($N_{\text{Cu}} < 5$ ML) where the theoretical fit given in Ref. [58] breaks down.

The damping constant α has also been calculated for systems of Co film sandwiched between NM layers (NM=Cu or Pt) of the same fixed thicknesses [i.e., NM(6 ML)/Co/NM(6 ML) trilayers] with and various Co film thicknesses. The results obtained for such trilayer systems are also in accordance with the predictions of the spin pumping theory [6, 7] and previous experimental reports [79]. As it is seen in Fig. 3.18, the change of α due to adding the Cu(6 ML) layer to the both sides of the Co film is not significant whereas it is quite large (more than 25-fold for 1-ML Co) for the Pt layers and it declines as the Co thickness increases.

A possible reason for no extra damping in the trilayer systems with the Cu cap and underlayer is the relatively small SO coupling of Cu (in comparison with Pt) and low of density of quantum states with energies at ϵ_{F} in Cu which contribute to the Gilbert damping constant according
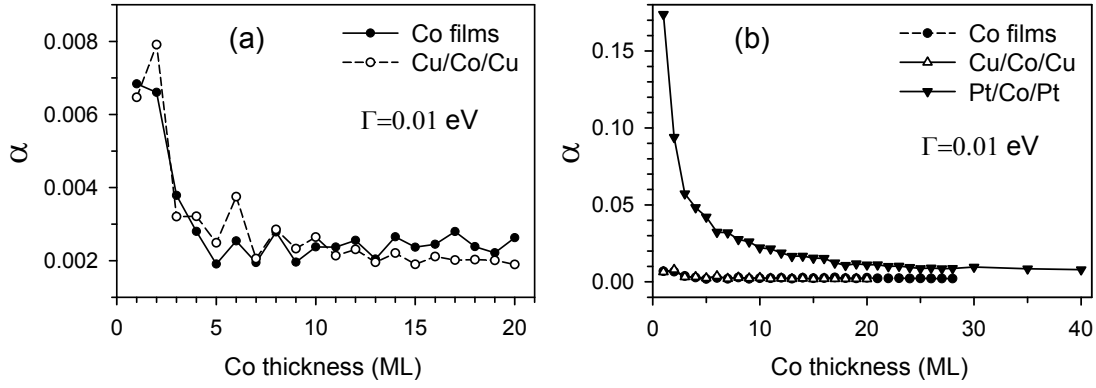
Figure 3.18: Gilbert damping constant α, (a): in Co films and Cu(6 ML)/Co/Cu(6 ML) trilayers, (b): in Co films and NM(6 ML)/Co/NM(6 ML) trilayers (NM=Cu, Pt) vs Co thickness, with scattering rate $\Gamma = 0.01$ eV.

to the formula (2.103). The lack of magnetic damping enhancement might also be attributed to the fact that the induced spin moment in the Cu part, parallel to the Co moment, is negligible (about 100 times smaller than that in Co) [158]. The latter property is related to Cu d-bands lying below the Fermi level ϵ_F and the resulting low DOS at ϵ_F. However, establishing a direct connection between very small induced spin magnetic moment in Cu and no significant magnetic damping enhancement in Cu/Co/Cu trilayers needs further investigation whilst, at present, the two properties seem to be different consequences of the low DOS at ϵ_F in Cu. Finally, it is evident that the change of electronic structure in such trilayers in comparison to Co/Cu bilayers does not lead to enhanced damping unlike in Co/Cu bilayers (Sec. 3.4).

On the other hand, based on the spin pumping theory Cu is a poor spin sink so that adding ultrathin Cu layers next to a ferromagnetic film leads to no significant change in its Gilbert damping. It has been previously observed, in the case of Py/Cu bilayers [39] and Cu/FM/Cu trilayers [58], that one requires a Cu layer as thick as its spin-diffusion length λ_{sd}^{Cu} (200 ± 50 nm [10, 58]) to obtain an enhanced damping. Similar results have been found in experiment on an Cu/Py/Cu trilayer [79] and confirmed within a semiclassical theory based on the LLG equation in the ferromagnetic part and the spin diffusion equation in the nonmagnetic parts [159]. These reports are in accord with the present theoretical results for Cu/Co(6 ML)/Cu since the ultrathin Cu films ($N_{Cu} \leqslant 11$ ML) considered here are much thinner than λ_{sd}^{Cu} and thus no enhancement in Cu/Co/Cu trilayers is obtained. Similar trend, almost no change for NM=Cu and a decrease with increasing Co thickness for NM=Pd and Pt, has been observed in experiment for α in NM/Py/NM (NM=Cu, Ta, Pd, Pt) trilayers [160]. The calculated values of α are also of the same order as previously reported in experiment [141].

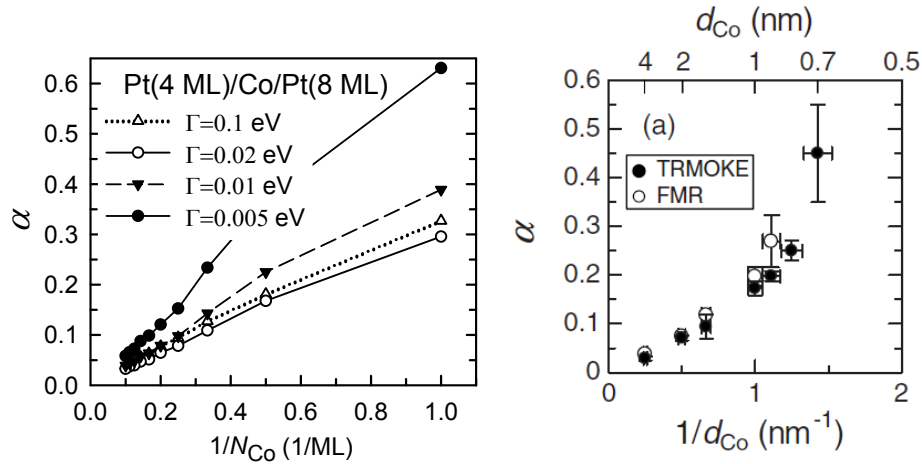Figure 3.19 (left panel) presents α for an Pt(4 ML)/Co/Pt(8 ML) trilayer as a function of

Figure 3.19: Inverse thickness $1/N_{Co}$ dependence of Gilbert damping constant α in Pt/Co(N_{Co})/Pt trilayers; *left*: calculated α, *right*: experiment (Ref. [57]), reproduced with permission from [S. Mizukami, E. P. Sajitha, D. Watanabe, F. Wu, T. Miyazaki, H. Naganuma, M. Oogane, and Y. Ando, Appl. Phys. Lett. **96**, 152502 (2010)]. Copyright [2010], AIP Publishing LLC.

the inverse Co thickness $1/N_{Co}$ for different scattering rates Γ. As seen, the damping constant α increases linearly with $1/N_{Co}$ as the Co thickness N_{Co} decreases. It is revealed that α in Pt(4 ML)/Co/Pt(8 ML) trilayers has a minimum at $\Gamma \simeq 0.03$ eV, but further investigations have shown that the position of this minimum moves or no minimum is present for other thicknesses of Co and Pt layers. For example, it is found that in symmetric Pt/Co/Pt trilayers, i.e., with Pt layers of the same thicknesses, α grows monotonically upon increasing Γ for odd N_{Co} whilst for even N_{Co} a shallow minimum of α occurs at Γ close to 0.01 eV. The linear dependence of α on $1/N_{Co}$ in Pt/Co/Pt trilayers has been observed in experiment with TRMOKE by Mizukami *et al.* [57] (right panel in Fig. 3.19). In this plot the linear dependence of α on $1/d_{Co}$ can clearly be seen for Co thicknesses d_{Co} down to 1.4 nm (0.25 nm^{-1} $\leqslant 1/d_{Co} \leqslant 0.7$ nm^{-1}). One can see the excellent agreement between α calculated with $\Gamma = 0.005$ eV and the experimental values, taking into account the relation $1/d_{Co} = 5.6/N_{Co}$ [nm^{-1}]. A similar inverse proportionality to the FM thickness N_{FM} was previously observed in Fe/Au films for the additional FMR linewidth $\triangle H_{Gil} = \alpha \frac{\omega}{\gamma}$ which is governed by α [78]. A linear trend in the dependence of α on $1/N_{FM}$ has also been reported for CoFeB films [82].

The obtained dependence of α on the Co thickness is similar to that found for the investigated Co/Pt bilayers discussed in the previous section (cf. Fig. 3.9). For a Pt/Co/Pt trilayer as compared to the corresponding Co/Pt bilayer (with the same Co thickness) one can expect an extra damping due to additional Pt layer. This extra damping actually occurs, but only at sufficiently large Co layer thicknesses depending on scattering rate Γ: for Co layer thicker than 30 ML with $\Gamma = 0.01$ eV and for any Co thickness with $\Gamma > 0.1$ eV. The smaller Γ, the thicker
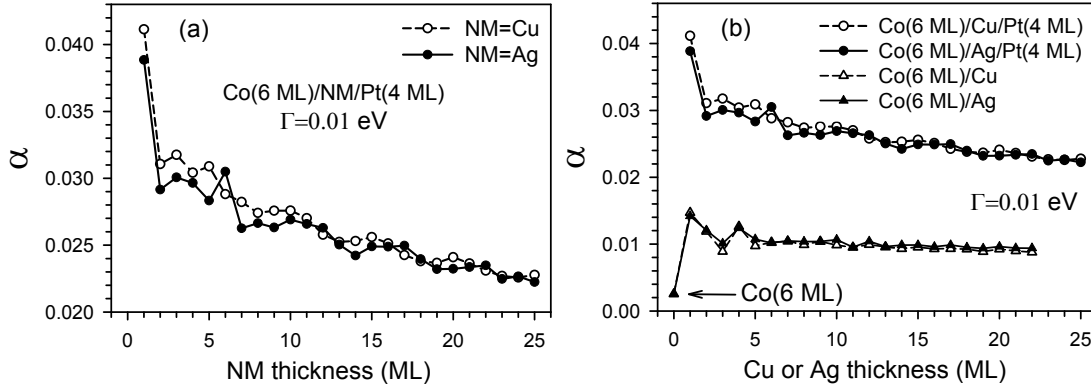
Figure 3.20: (a): Gilbert damping constant α in Co(6 ML)/NM/Pt(4 ML) trilayers, (b): Comparison of α in an Co(6 ML) film, Co(6 ML)/NM bilayers and Co(6 ML)/NM/Pt(4 ML) trilayers vs NM=Cu, Ag thickness; $\Gamma = 0.01$ eV.

Co thickness at which the damping constant α in Pt/Co/Pt trilayers starts to exceed α in Co/Pt bilayers. Similar conclusions can be drawn for Cu/Co/Cu trilayers in which the damping constant is much smaller than Co/Cu bilayers. This relation is presumably reversed if the Co film thickness becomes larger than 100 or 200 ML as it can be roughly estimated by an extrapolation of the plots in Fig. 3.12 and 3.18 to so large Co thicknesses.

Calculations have also been performed for Co/NM1/NM2 trilayers. The considered NM1 spacers of Cu and Ag are poor spin sinks possessing relatively long spin-diffusion lengths λ_{sd}^{NM} ($\lambda_{sd}^{Cu} = 200 \pm 50$ nm [10, 58] and $\lambda_{sd}^{Ag} = 132 - 195$ nm [161]) and NM2 is Pt with short λ_{sd} ($\lambda_{sd}^{Pt} = 0.5 \pm 0.3$ nm [58]) acting as perfect (ideal) spin sink, in the language of the spin pumping theory. Figure 3.20 depicts the damping constant α against the spacer thickness in Co(6 ML)/NM1/Pt(4 ML) trilayers (NM1=Cu and Ag) for the scattering rate $\Gamma = 0.01$ eV. One can clearly see that α declines monotonically, although it also oscillates, as the thickness of the NM1 spacer layer increases. The oscillation periods are 5 ML for Cu and 5-7 ML for Ag, although the value of the period is much more clear in the case of Cu. Comparison with the Gilbert damping in Co/NM1 bilayers shows that the total damping α in Co/NM1/NM2 trilayers, which refers to the relaxation of the precessing magnetisation in the Co part, has a large contribution from the NM2 part (which is also clearly visualised by the spatial distribution of α discussed in chapter 4). The obtained decline of α with the NM1 thickness implies that the thicker spacer becomes, the smaller contribution from the Pt cap is. This result of quantum-mechanical calculation supports the prediction of the spin pumping theory according to which as the thickness of the NM1 spacer increases, less spin angular momentum can be transferred to the Pt part and such spin transfer becomes ineffective if the spacer thickness is much larger than its λ_{sd}.

As seen in Fig. 3.20, the damping constant α obtained for the Co/Cu/Pt trilayer is 2-3 times larger than that of Co/Cu bilayer. The reported experimental enhancement for the same system is about two times and dies out as Cu thickness approaches its spin-diffusion length [141]. Such damping enhancement, due to adding the second nonmagnetic layer, has also been experimentally observed by Ghosh and co-workers in FM/Cu/Pt/Al hererostructures [155, 156] (see also [10]) where the added Pt layer leads to the enhancement, which they call nonlocal Gilbert relaxation. Therein, it is also demonstrated that $\triangle\alpha$, which is the additional damping introduced by the Pt cap alone, is inversely proportional to the FM thickness. This is in agreement with the $1/N_{\mathrm{Co}}$ dependence presented here. It has been experimentally shown in Py/Cu/Ta trilayers [39] and an Cu/Py/Cu/Pt system [10] that the contribution from the second nonmagnetic layer (i.e., NM2=Ta and Pt, respectively) diminishes for the spacer layer thicker than its spin-diffusion length. Thus, one expects the contribution from Pt in the investigated Co/NM1/Pt trilayers to vanish for Cu or Ag spacer layers as thick as their spin-diffusion lengths ($\lambda_{\mathrm{sd}}^{\mathrm{Cu}} = 200 \pm 50$ nm [10, 58] and $\lambda_{\mathrm{sd}}^{\mathrm{Ag}} = 132 - 195$ nm [161]). However, such spacers are too thick to be considered in the calculation of the damping constant within the present model.

The dependence of Gilbert damping on the spacer layer thickness is addressed in the spin pumping theory by relating it to the electron mean free path, spin-flip relaxation rate and spin-diffusion length in the nonmagnetic parts of trilayers as well as the spin mixing conductance of FM/NM1 interface [53, 57, 58, 7]. This theory predicts the damping enhancement due to spin relaxation in the second nonmagnetic layer (NM2) decays with increasing NM1 spacer thickness. This enhancement vanishes completely for infinite spacer thickness. For the spacer thickness N_{NM1} much smaller than the spin-diffusion length λ_{sd} the dependence of α on N_{NM1} has the general form

$$\alpha = A + \frac{B}{1 + C N_{\mathrm{NM1}}} \tag{3.6}$$

where A, B and C are some functions of the nonmagnetic materials' properties such as spin-flip rate τ_{sf}^{-1} and λ_{sd} which are constants for each metal. The relation (3.6) can be obtained by replacing $\tanh(N_{\mathrm{NM1}}/\lambda_{\mathrm{sd}})$ with $N_{\mathrm{NM1}}/\lambda_{\mathrm{sd}}$ in the formula for α derived within the spin pumping theory in Refs. [7, 58]. The present results for Co(6 ML)/NM1/Pt(4 ML) trilayers, plotted in Fig. 3.20, can be easily fitted (if the small oscillations of α are neglected) to the above general formula but the range of the NM spacer thickness (up to 25 ML, i.e, 4.5 nm) is too small in comparison with λ_{sd} to verify such thickness dependence, predicted by the spin pumping theory, within the present quantum-mechanical model.

In the spin pumping theory there are two contributions to the Gilbert damping in such

trilayer structures. One coming from the spin current transmitting to the second NM through the spacer and the other from the spin current reflected back into the FM through the FM/NM1 interface. Thus, both the FM/NM1 and NM1/NM2 interfaces affect the damping process through their spin mixing conductances. In the present model, however, the obtained results can be justified as follows. The NM1=Cu and Ag spacer layers have small SO coupling and the d band below the Fermi level ϵ_F, which results in their small contributions to the total Gilbert damping of the system. On the other hand, the Pt cap with the strong SO coupling and d states at the ϵ_F leads to a remarkable enhancement in the damping constant as it couples to the Co layer through the NM spacer layer. Such coupling can be explained on the grounds of quantum mechanics as follows. The d states at the ϵ_F in Co hybridise with s,p states in the NM1, which, in turn, hybridise with d states in Pt. The resulting quantum states with large probability amplitude in Co have tails in the NM1 and Pt parts and their amplitude in Pt decreases when the NM1 spacer thickness increases. Thus as the spacer gets thicker, contribution from the Pt cap to the total damping becomes weaker since it depends on the probability amplitude of these states in Pt, according to the general formula (2.103).

3.6 Binary superlattices

A periodic configuration of alternating layers of two or more different materials is called a super-lattice. Superlattices are utilised in nanodevice structures since they possess new properties that the constituents do not (e.g., high resistivity against shearing, shear strength or large perpendicular magnetic anisotropy). The two important parameters in binary superlattices, or rather multilayers with superlattice structure, are the thicknesses of the two constituent layers and the stacking number (the number of repetitions). Such magnetic multilayers have been widely investigated in experiments since they allow for engineering magnetic damping in spintronic devices [52, 76, 162, 163, 164]. The presence of FM/NM interfaces in binary superlattices results in larger damping in such systems in comparison with pure FM films and FM/NM bilayers. This makes them promising for application in those spintronic devices where large magnetic damping is desirable (e.g., in magnetic sensors rather than in STT-MRAM devices with the demand for low damping).

In this section, Co-based superlattices with fcc structure made of repeated bilayers of Co and NM where NM=Cu, Ag, Pd, Pt and Au are considered. The Gilbert damping constant α is calculated for two different cases:

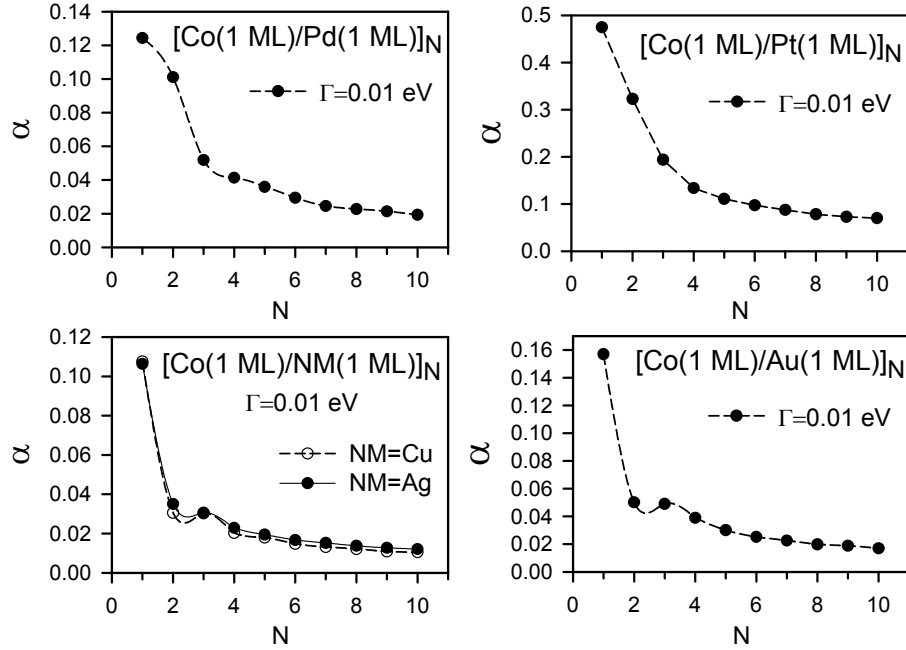(i) the so-called $L1_0$ superlattices that are composed of alternating Co and NM monolayers:

Figure 3.21: Gilbert damping constant in $[\text{Co}(1\ \text{ML})/\text{NM}(1\ \text{ML})]_N$ $\text{L}1_0$ superlattices with scattering rate $\Gamma = 0.01$ eV.

$[\text{Co}(1\ \text{ML})/\text{NM}(1\ \text{ML})]_N$ and are considered to be a type of ordered alloys,

(ii) binary superlattices with arbitrary Co and NM thicknesses that include $N \cdot N_{\text{Co}}$ monolayers of Co and $N \cdot N_{\text{NM}}$ monolayers of NM: $[\text{Co}(N_{\text{Co}}\ \text{ML})/\text{NM}(N_{\text{NM}}\ \text{ML})]_N$.

Figure 3.21 shows the damping constant α against the stacking number N in $[\text{Co}(1\ \text{ML})/\text{NM}(1$ $\text{ML})]_N$ $\text{L}1_0$ superlattices with scattering rate $\Gamma = 0.01$ eV. The damping constant α declines in all investigated $\text{L}1_0$ superlattices as the thicknesses of films ($2N$ ML) increase and it saturates for $N > 10$ ML. The decrease of α in the considered $\text{L}1_0$ superlattices upon increasing N from 1 to 10 is about 10 times for Cu, 6 times for Pd, 7 times for Pt, and 9 times for Ag and Au. Such dependence seems to be in agreement with the results obtained for the Gilbert damping in Co/NM bilayers (Sec. 3.4), where α found to be a decreasing function of the Co thickness (whilst it is not very sensitive to the change of NM thickness after first two NM monolayers are added). However, the correspondence between the bilayers and the $\text{L}1_0$ superlattices cannot be exact because although increasing the stacking number N leads to increasing the total thickness of Co layers, it also results in occurrence of more Co/NM interfaces. The Gilbert damping is also found to increase with the decreasing scattering rate Γ for all investigated $\text{L}1_0$ superlattices. As seen, there is a noticeable difference between the dependences of the Gilbert damping constant α on the stacking number N obtained for the binary superlattices with NM=Cu, Ag and Au and those with NM=Pd and Pt. In particular, a sharp fall of damping occurs on going from $N = 1$ to $N = 2$ in systems with NM=Cu, Ag and Au, whilst the decline of α is smoother for
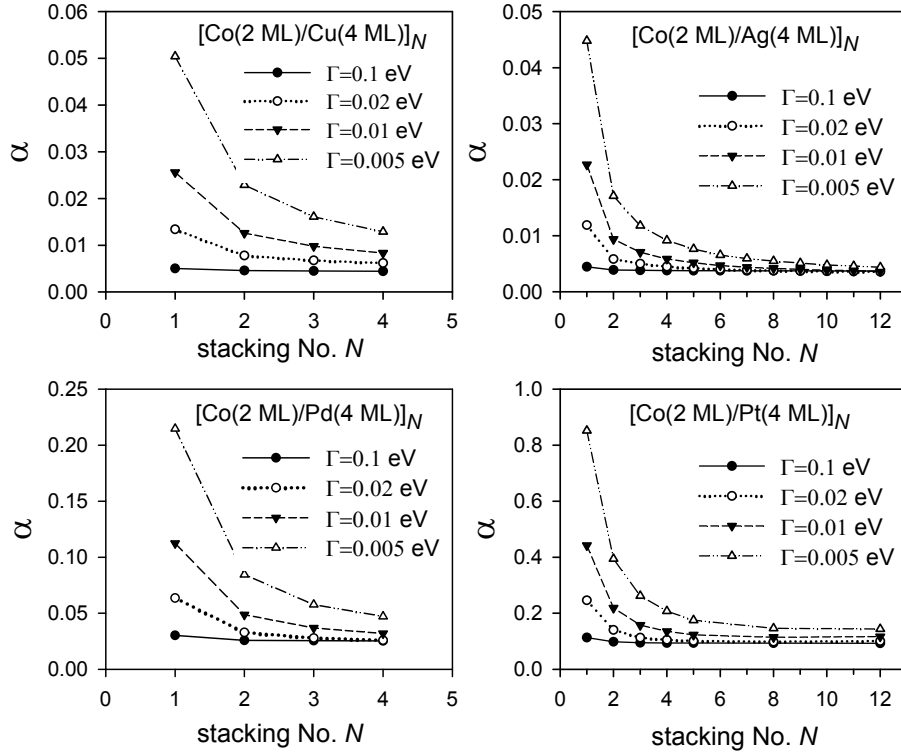
Figure 3.22: Gilbert damping constant in $[Co(2\ ML)/NM(4\ ML)]_N$ multilayers as a function of stacking number N, obtained with different scattering rates Γ.

NM=Pd and Pt. A possible way to account for this difference is to attribute it to the different DOS of NM metals at Fermi level (see the related discussion in Sec. 3.4).

As previously found in the case of magnetic bilayers and trilayers, also for the L1$_0$ superlattices one can see the strong effect of the large SO coupling of Pt, in comparison with the other NM metals, in raising the Gilbert damping. Comparing the damping constant of Co(N ML)/NM(N ML) bilayers with their $[Co(1\ ML)/NM(1\ ML)]_N$ superlattice counterparts (Fig. 3.21), at the same Co and NM total thicknesses, leads us to the conclusion that α is enhanced (up to two times for Pt(6 ML)) in the L1$_0$ superlattices. One probable reason for this enhancement is the number of Co/NM interfaces which is larger in a $[Co(1\ ML)/NM(1\ ML)]_N$ superlattice than a Co/NM bilayer ($2N-1$ interfaces in superlattices compared to only one in Co/NM bilayers). This is a valuable result for engineering spintronic devices in which a large damping is desirable.

The calculations of the damping constant α are also extended to binary superlattices with constituent metals thicker than a monolayer (magnetic multilayers). In Fig. 3.22, α is plotted against the stacking number N for $[Co(2\ ML)/Pd(4\ ML)]_N$ multilayers with different scattering rates Γ. The Gilbert damping appreciably declines, especially for $\Gamma \leqslant 0.01$ eV, with increasing the stacking number N for a fixed Γ. The obtained approximate $1/N$ dependence of α is in agreement with experimental results for similar system. For instance, such $1/N$ dependence of α
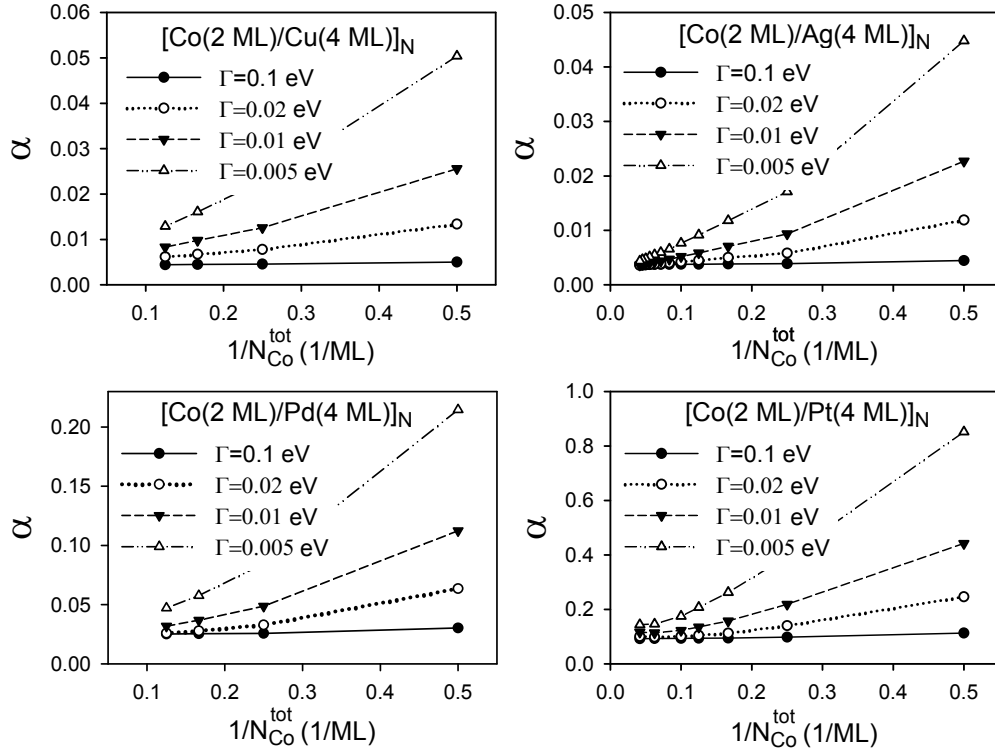
Figure 3.23: Gilbert damping constant in $[\text{Co}(2~\text{ML})/\text{NM}(4~\text{ML})]_N$ multilayers with different stacking numbers N and scattering rates Γ versus inverse of the Co total thickness $N_{\text{Co}}^{\text{tot}} = 2N$.

has been reported for $[\text{Ni}/\text{Co}]_N$ multilayers with $N \leqslant 10$ in Ref. [165], although α is found to be almost independent of the stacking number for $N \geqslant 10$. In Ref. [164] a system of perpendicularly magnetised $[\text{Ni}/\text{Co}]_N$, sandwiched between Pt layers, has also been investigated and the monotonically decreasing dependence of α on the stacking number N has been observed. However, the present results obtained for $[\text{Co}(2~\text{ML})/\text{Pt}(4~\text{ML})]_N$ do not fully agree with experimental data reported for the same system [76] since experimentally observed α increases slowly with increasing N. Nevertheless, it has to be noted that the calculated and measured values of α are close to each other. Although the thickness of Co individual layers is fixed (at 2 ML), varying the stacking number N leads to different total Co thicknesses $N_{\text{Co}}^{\text{tot}} = 2N$ ML in the considered system which can explain the N dependence of α.

Figure 3.23 presents the dependence of α for $[\text{Co}(2~\text{ML})/\text{NM}(4~\text{ML})]_N$ multilayers, with different Γ, against the inverse of the total Co thickness $N_{\text{Co}}^{\text{tot}} = 2N$. The stacking numbers $N = 1, 2, ..., 12$ for Cu and Ag, $N = 1, 2, 3, 4$ for Pd and $N = 1, 2, ..., 5, 8, 12$ for Pt have been considered. As seen, the damping constant α decreases in all these superlattice structures as the total Co thickness (or equivalently the total film thickness $6N$ ML) increases. The slope of the α versus $1/N_{\text{Co}}^{\text{tot}}$ dependence for $[\text{Co}(2~\text{ML})/\text{NM}(4~\text{ML})]_N$ multilayers is larger than that for Co/NM bilayers, implying that the obtained enhancement of α in the multilayers has origin in
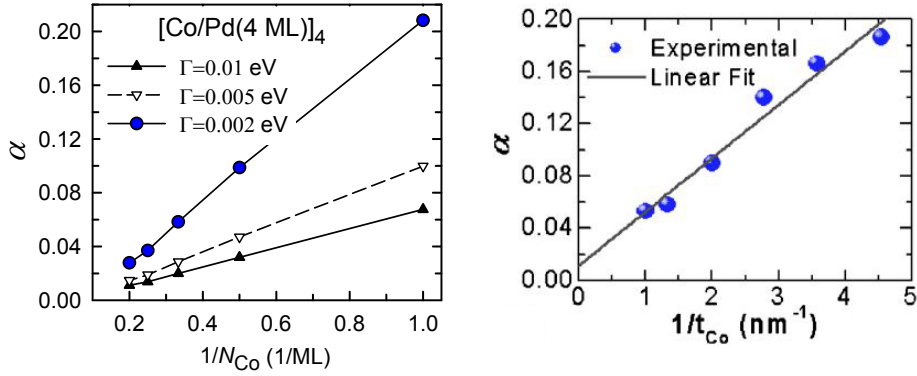
93

Figure 3.24: Inverse thickness $1/N_{Co}$ dependence of Gilbert damping constant α in [Co/Pd(4 ML)]$_N$ multilayers; *left*: calculated α for $N = 4$, *right*: experiment for $N = 8$ (Ref. [163]), reproduced with permission from [S. Pal, B. Rana, O. Hellwig, T. Thomson, and A. Barman, Appl. Phys. Lett. **98**, 082501 (2011)]. Copyright [2011], AIP Publishing LLC. Note that, 1/ML corresponds to 5.6 nm^{-1}.

the Co/NM interfaces.

Figure 3.24 compares the calculated damping constant α for [Co(N_{Co} ML)/Pd(4 ML)]$_4$ multilayers with various Co layer thicknesses to the results of a recent experiment on [Co(t_{Co} nm)/Pd(0.9 nm)]$_8$ multilayers [163]. As shown, α increases linearly with $1/N_{Co}$, whilst increasing with decreasing the scattering rate Γ. In the case of considered [Co/Pd]$_N$ multilayers assuming the scattering rate $\Gamma \simeq 0.002$ eV leads to an excellent agreement of the calculated α with experiment. Choosing the stacking number $N = 4$ here was due to the fact that α in [Co(N$_{Co}$)/Pd(4 ML)]$_4$ multilayers with $\Gamma \leqslant 0.01$ eV almost saturates at $N = 4$ (cf. Fig. 3.22) and then one can compare these results (obtained with less numerical effort than for $N = 8$) with those investigated for $N = 8$ in the mentioned experiment. In this experiment, the damping constant $\alpha = 0.011$ has also been found for bulk Co which corresponds to the value of α obtained with $\Gamma \simeq 0.002$ eV in the present calculations for bulk Co (cf. Fig. 3.6 or Ref. [62]). Thus, the agreement of the theoretical and experimental values of α is achieved for the same value of Γ. The presently obtained linear dependence of α on $1/N_{Co}$ also agrees with the results of recent experiments on Co/Pd multilayers [166] where the damping constant α measured in [Co(t_{Co} nm)/Pd(t_{Pd} nm)]$_6$ multilayers with various Co thickness t_{Co} and three different Pd thicknesses t_{Pd} (0.8, 1.0, 1.5 nm) was found to depend linearly on the ratio $x = t_{Co}/t_{Pd}$ (in the range $0.9 \leqslant x \leqslant 2.2$). Furthermore, the calculated value of $\alpha = 0.037$ for $N_{Co} = N_{Pd} = 4$ ML with $\Gamma = 0.002$ eV (Fig. 3.24) is close to the experimental value $\alpha = 0.045$ reported for $x = 1.0$ in Ref. [166].

In Fig. 3.25 the damping constant α is plotted for [Co(2 ML)/NM(4 ML)]$_N$ multilayers with different nonmagnetic metals and stacking numbers N against the scattering rate Γ. One may

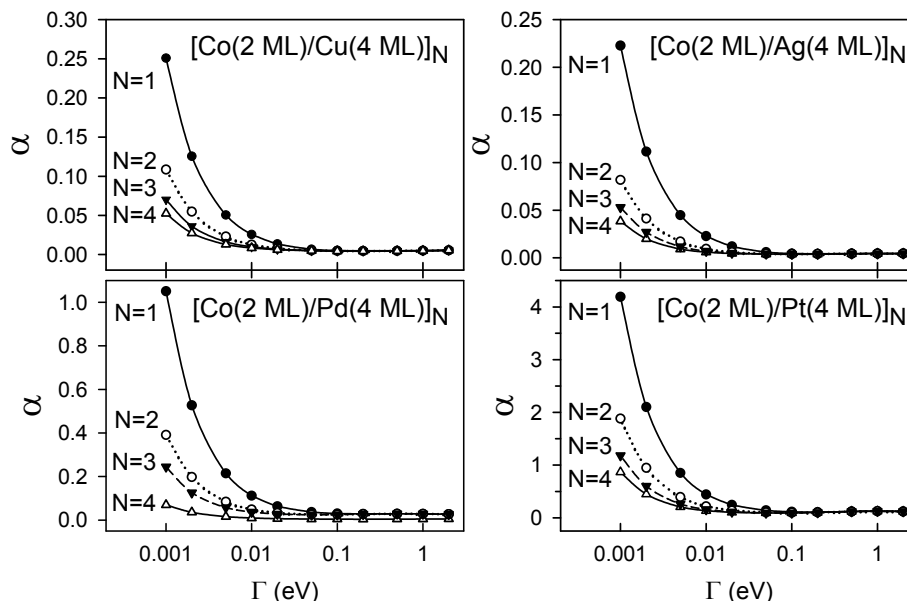Figure 3.25: Gilbert damping constant vs scattering rate Γ in $[\text{Co(2 ML)}/\text{NM(4 ML)}]_N$ multilayers for different stacking numbers N.

notice that the Γ dependence of α resembles the one for the bulk Co (Fig. 3.6 in Sec. 3.2) as the thickness of the multilayer increases, regardless of the fact that the damping is enhanced in multilayers due to the presence of the NM. In particular, the shallow minima of damping with respect to the scattering rate occur at Γ close to 0.1 eV (at $\Gamma = 0.2$ eV for Cu, at $\Gamma = 0.1$ eV for Ag and at $\Gamma = 0.05$ eV for Pd and Pt). Furthermore, the increasing trend Ag$\rightarrow$Cu$\rightarrow$Pd$\rightarrow$Pt in the Gilbert damping constants of $[\text{Co}/\text{NM}]_N$ multilayers is also clearly noticeable.

3.7 Angular dependence of Gilbert damping

What have been strived to calculate so far was the Gilbert damping constant α for bulk cubic ferromagnets with magnetisation along [001] axis (or an equivalent direction) as well as for ferromagnetic films and fcc Co-based magnetic layered systems with (001) surface and out-of-plane magnetisation, i.e., oriented along the (001) axis which is perpendicular to the film surface and chosen to be the z direction [62]. As mentioned before, in Sec. 3.2, the damping constants α obtained for bulk ferromagnets in the present TB calculations agree with previous findings obtained with the *ab initio* DFT method [62, 88]. The damping constant has also been found to be considerably enhanced in purely ferromagnetic films of a few ML thickness. Further remarkable enhancement has been obtained as a result of covering Co films with a nonmagnetic cap in Co/NM bilayers.

The energy of a magnetic system depends on the orientation of the magnetisation. This

dependence, known as the magnetic anisotropy, arises due to the long-range dipole-dipole interaction leading to the shape anisotropy as well as the local SO coupling which is the source of the MCA. Since the Gilbert damping also originates from the SO interaction it is expected to depend on the magnetisation orientation. Such dependence has indeed been observed experimentally [37].

The angular dependence of the Gilbert damping constant is of importance in magnetic layered structures. Changing the magnetisation orientation affects the magnetic damping, and consequently, it affects the process of spin transport in the system. The purpose of this section is to explore the Gilbert damping for an arbitrary magnetisation direction in ferromagnetic metallic systems. The dependence of the Gilbert damping on magnetisation orientation is investigated for bulk Fe, Co and Ni as well as (001) bcc Fe, (001) fcc Co and (001) fcc Ni films.

The Kamberský's torque correlation formula (2.103) [44] for the Gilbert damping constant has been derived with the usual assumption that the z axis is along the direction of the (equilibrium) magnetisation $\boldsymbol{M}$, which has been chosen to be along the [001] axis in the calculations presented in other sections of this thesis. Then, the damping constant is expressed in terms of the electronic states $|n\boldsymbol{k}\rangle$ obtained with the Hamiltonian including the SO interaction H_{SO} and the matrix elements $A_{nn'}(\boldsymbol{k})$ of the SO torque operator $A^- = [S^-, H_{\mathrm{SO}}]$ (Eq. (2.108)). The SO interaction H_{SO} is the sum (2.89) of atomic SO couplings which can be represented as

$$\boldsymbol{L} \cdot \boldsymbol{S} = L_z S_z + \frac{1}{2}(L^+ S^- + L^- S^+) \tag{3.7}$$

with the orbital and spin angular momenta operators (L_z, $L^\pm = L_x \pm iL_y$ and S_z, $S^\pm = S_x \pm iS_y$). These operators are defined with the fixed x, y, z axes chosen along the [100], [010] and [001] crystallographic axes, respectively. The matrix elements of the atomic SO interaction $\boldsymbol{L} \cdot \boldsymbol{S}$ in the spin basis $|\uparrow\rangle$, $|\downarrow\rangle$, corresponding to the spin quantisation along the z axis, are then given by Eq. (2.93). However, the expression (2.103) for the damping constant α is valid for any direction of magnetisation $\boldsymbol{M}$ provided that the SO torque $A^- = [S^-, H_{\mathrm{SO}}]$ is replaced by $A_r^- = [S_r^-, H_{\mathrm{SO}}]$ where the spin operator $S_r^- = S_{x'} - iS_{y'}$ is defined in the rotated frame of reference with the z' axis parallel to $\boldsymbol{M}$. In calculation of A_r^- the SO interaction operator H_{SO} can be represented as in Eq. (3.7) or using a similar expression for $\boldsymbol{L} \cdot \boldsymbol{S} = \boldsymbol{L}' \cdot \boldsymbol{S}'$ with $L_{z'}$, $L_r^\pm = L_{x'} \pm iL_{y'}$, $S_{z'}$, S_r^- and $S_r^+ = S_{x'} + iS_{y'}$, whichever method is more convenient.

The dependence of the damping constant on the magnetisation direction also arises through electronic states and, in particular, through their spin parts. For arbitrary direction of magnetisation $\boldsymbol{M} = \boldsymbol{M}(\theta, \phi)$, described with the polar and azimuthal angles θ, ϕ, the exchange part

of the Hamiltonian is diagonal in the spin basis $|\uparrow_r\rangle$, $|\downarrow_r\rangle$ which are eigenstates of the spin operator $S_{z'}$ corresponding to spin quantisation axis z' aligned along $\boldsymbol{M}$. Thus, in the absence of the SO interaction H_{SO} the total Hamiltonian is also diagonal in this rotated spin basis so that its eigenstates $|n_0\boldsymbol{k}\,\sigma_r\rangle$ have definite spin σ_r ($\uparrow_r$ or $\downarrow_r$) along the z' axis and they are labeled with the energy band index n_0 separately for each spin σ_r. Upon the inclusion of H_{SO}, the electronic states $|n\boldsymbol{k}\rangle$ become superpositions of components with spin $\uparrow_r$ and spin $\downarrow_r$ in a similar way as it is discussed in Sec. 2.5 within the spin basis $|\uparrow\rangle$, $|\downarrow\rangle$. The construction of the TB Hamiltonian and its eigenstates $|n\boldsymbol{k}\rangle$ is then performed using the rotated spin basis which is simply achieved by replacing the spin indices σ, σ' with σ_r, σ_r' in all relevant formulas in Sec. 2.4.1-2.4.3. It should be noted here that the TB on-site energies and the hopping integrals or two-centre Slator-Koster parameters do not change under the rotation of the spin basis since the atomic orbitals $\phi_\mu(\boldsymbol{r})$ are chosen to be still defined with respect to the fixed frame $Oxyz$. The only difference is that these TB parameters, which in ferromagnets are different for majority spin and minority spin, now refer to spin states $|\uparrow_r\rangle$ and $|\downarrow_r\rangle$, respectively, quantised along the z' axis. On the other hand, although the operator H_{SO} of the SO interaction does *not* depend on the direction of $\boldsymbol{M}$, defined with the angles θ and ϕ, the matrix elements of H_{SO} in the rotated spin basis clearly depend on θ and ϕ. Thus, to determine the Gilbert damping constant for arbitrary θ, ϕ the matrices of all the spin dependent operators, i.e., the SO interaction H_{SO} and the SO torque $A_r^- = [S_r^-, H_{\mathrm{SO}}]$, need to be found in the rotated spin basis.

The rotated spin basis states are expressed as follows

$$
\begin{aligned}
|\uparrow\rangle_r &= \left(e^{-i\phi/2}\cos(\theta/2)\right)|\uparrow\rangle + \left(e^{i\phi/2}\sin(\theta/2)\right)|\downarrow\rangle, & \text{(3.8a)}\\
|\downarrow\rangle_r &= \left(-e^{-i\phi/2}\sin(\theta/2)\right)|\uparrow\rangle + \left(e^{i\phi/2}\cos(\theta/2)\right)|\downarrow\rangle & \text{(3.8b)}
\end{aligned}
$$

with $|\uparrow\rangle$ and $|\downarrow\rangle$ which are the eigenstates of the component S_z of the spin angular momentum along the fixed z axis. In this way, one can find the matrix elements of the unit atomic SO operator $\boldsymbol{L}\cdot\boldsymbol{S}$ in the rotated spin basis straightforwardly as

$$
\begin{aligned}
\langle\mu\uparrow_r|\boldsymbol{L}\cdot\boldsymbol{S}|\nu\uparrow_r\rangle &= \frac{1}{2}\cos\theta\, L_{\mu\nu}^z + \frac{1}{4}\sin\theta\left(e^{i\phi}\,L_{\mu\nu}^- + e^{-i\phi}\,L_{\mu\nu}^+\right), & \text{(3.9a)}\\
\langle\mu\uparrow_r|\boldsymbol{L}\cdot\boldsymbol{S}|\nu\downarrow_r\rangle &= \frac{-1}{2}\sin\theta\, L_{\mu\nu}^z + \frac{1}{2}\left(e^{i\phi}\cos^2(\theta/2)\,L_{\mu\nu}^- - e^{-i\phi}\sin^2(\theta/2)\,L_{\mu\nu}^+\right), & \text{(3.9b)}\\
\langle\mu\downarrow_r|\boldsymbol{L}\cdot\boldsymbol{S}|\nu\uparrow_r\rangle &= \left(\langle\nu\uparrow_r|\boldsymbol{L}\cdot\boldsymbol{S}|\mu\downarrow_r\rangle\right)^*, & \text{(3.9c)}\\
\langle\mu\downarrow_r|\boldsymbol{L}\cdot\boldsymbol{S}|\nu\downarrow_r\rangle &= -\langle\mu\uparrow_r|\boldsymbol{L}\cdot\boldsymbol{S}|\nu\uparrow_r\rangle & \text{(3.9d)}
\end{aligned}
$$

where the matrix elements $L_{\mu\nu}^z = \langle\mu|L_z|\nu\rangle$ and $L_{\mu\nu}^\pm = \langle\mu|L^\pm|\nu\rangle$ are found with orbital angular

momentum operators L_z and $L^\pm$ and orbitals $\phi_\mu(\boldsymbol{r})$, $\phi_\nu(\boldsymbol{r})$ all defined in the fixed frame of reference $Oxyz$. Similar derivation of the angular dependence of the H_{SO} matrix can be found in [134].

The SO torque $A_r^- = [S_r^-, H_{\mathrm{SO}}]$ is the sum of the atomic SO torques $A_{\mathrm{at},r}^- = [S_r^-, \boldsymbol{L} \cdot \boldsymbol{S}]$ multiplied by the SO coupling constant ξ_{at} on different atoms. The matrix elements of $A_{\mathrm{at},r}^-$ in the rotated spin basis have the same form (Eq. (2.110)) as the elements of the atomic SO torque $A_{\mathrm{at}}^- = [S^-, \boldsymbol{L} \cdot \boldsymbol{S}]$ in the unrotated (fixed) spin basis,

$$\langle \mu\uparrow_r | A_{\mathrm{at},r}^- | \nu\uparrow_r \rangle = -\langle \mu\uparrow_r | \boldsymbol{L} \cdot \boldsymbol{S} | \nu\downarrow_r \rangle, \tag{3.10a}$$

$$\langle \mu\uparrow_r | A_{\mathrm{at},r}^- | \nu\downarrow_r \rangle = 0, \tag{3.10b}$$

$$\langle \mu\downarrow_r | A_{\mathrm{at},r}^- | \nu\uparrow_r \rangle = 2\langle \mu\uparrow_r | \boldsymbol{L} \cdot \boldsymbol{S} | \nu\uparrow_r \rangle, \tag{3.10c}$$

$$\langle \mu\downarrow_r | A_{\mathrm{at},r}^- | \nu\downarrow_r \rangle = \langle \mu\uparrow_r | \boldsymbol{L} \cdot \boldsymbol{S} | \nu\downarrow_r \rangle \tag{3.10d}$$

so they are expressed with the elements of the atomic SO interaction. Both types of the matrix elements depend on the angles θ and ϕ. Thus having found the angle-dependent matrix elements of these two relevant operators ($\boldsymbol{L} \cdot \boldsymbol{S}$ and A_r^-) in the rotated spin basis, one can readily calculate the Gilbert damping constant for arbitrary direction of magnetisation $\boldsymbol{M}(\theta, \phi)$.

The calculated damping constant α for bulk cubic ferromagnets is the same for $\boldsymbol{M}$ lying along different principal axes. Figure 3.26 shows α as a function of the polar angle θ, in the xz plane ($\phi = 0$), for bulk bcc Fe, fcc Co and fcc Ni. The plot of $\alpha(\theta)$ is symmetric with respect to $\theta = 45°$, as expected. At $\theta = 45°$ a maximum damping for Fe and minimum damping for Co are found. For bulk Ni such minimum is present for scattering rates $\Gamma \leqslant 0.05$ eV and it is replaced by a weakly pronounced maximum for larger Γ. In general, the change of α with changing the magnetisation direction is relatively small, not exceeding 13% , 3% and 18% for Fe, Co and Ni, respectively, with $\Gamma = 0.01$ eV. The Gilbert damping is found to be less sensitive to the magnetisation direction for larger Γ whilst it depends strongly on this direction for smaller Γ.

The dependence of the Gilbert damping on the direction of magnetisation is much stronger in thin films than in bulk metals. Figure 3.27 presents the damping constant α of (001) bcc Fe(10 ML), fcc Co(10 ML) and fcc Ni(10 ML) films as a function of polar angle θ for the scattering rate $\Gamma = 0.01$ eV.

For 10 ML Fe film, α has its maximum at around $\theta = 30°$ where its value increases, by nearly 30% and 56%, in comparison with out-of-plane ($\theta = 0$) and in-plane ($\theta = 90°$) orientations, respectively. The location of the maximum oscillates, around $\theta = 40°$, with the Fe thickness for $\Gamma = 0.01$ eV. Such maximum disappears for $\Gamma \geqslant 0.05$ eV, moving to one of the ends of the polar
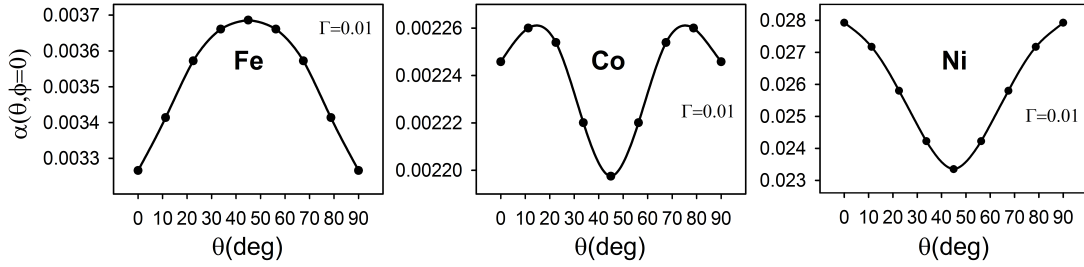
Figure 3.26: Gilbert damping constant for bulk bcc Fe, fcc Co, fcc Ni vs the magnetisation direction defined by polar angle θ within the xz plane ($\phi = 0$), obtained with the scattering rate $\Gamma = 0.01$ eV.
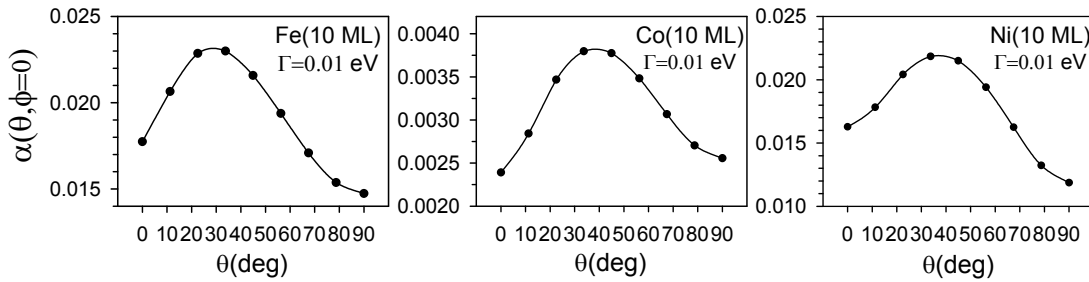

Figure 3.27: Angular dependent Gilbert damping constant: α versus θ ($\phi = 0$) for ferromagnetic Fe, Co and Ni films; $\Gamma = 0.01$ eV.

angle interval, $\theta = 0$ or $\theta = 90°$, depending on the value of Γ.

For 10 ML Co film with $\Gamma = 0.01$ eV, the damping constant has its maximum at around $\theta = 40°$ where its value increases, by nearly 60%, in comparison with in-plane and out-of-plane orientations. The position of the maximum oscillates, around $\theta = 45°$, with the Co thickness for $\Gamma = 0.01$ eV whilst no such maximum is present for $\Gamma \geqslant 0.1$ eV.

For 10 ML Ni film, the damping constant for $\Gamma = 0.01$ eV has its maximum at around $\theta = 40°$ where its value increases, by nearly 34% and 84%, in comparison with out-of-plane and in-plane orientations, respectively. The position of the maximum oscillates, around $\theta = 40°$, with the Ni thickness for $\Gamma = 0.01$ eV whilst the maximum disappears for $\Gamma \geqslant 0.05$ eV.

In Fig. 3.28 (right panel) the Gilbert damping constant α is plotted for (001) bcc Fe, fcc Co and fcc Ni films as a function of film thickness for two different directions of magnetisation (in-plane and out-of-plane) and the scattering rate $\Gamma = 0.01$ eV. The change of α upon changing magnetisation direction from out-of-plane to in-plane varies with film thickness in all three considered metals. The dependence of α on the FM film thickness, has the same general trend [increasing for Fe (up to about 12-16 ML, depending on the value of Γ) and Ni but decreasing for Co] for in-plane and out-of-plane magnetisations. Similar oscillations (though not identical) of α versus film thickness are obtained for both magnetisation orientations in Fe and Ni films, whilst oscillations of α are much less pronounced in Co films with in-plane orientation of magnetisation.
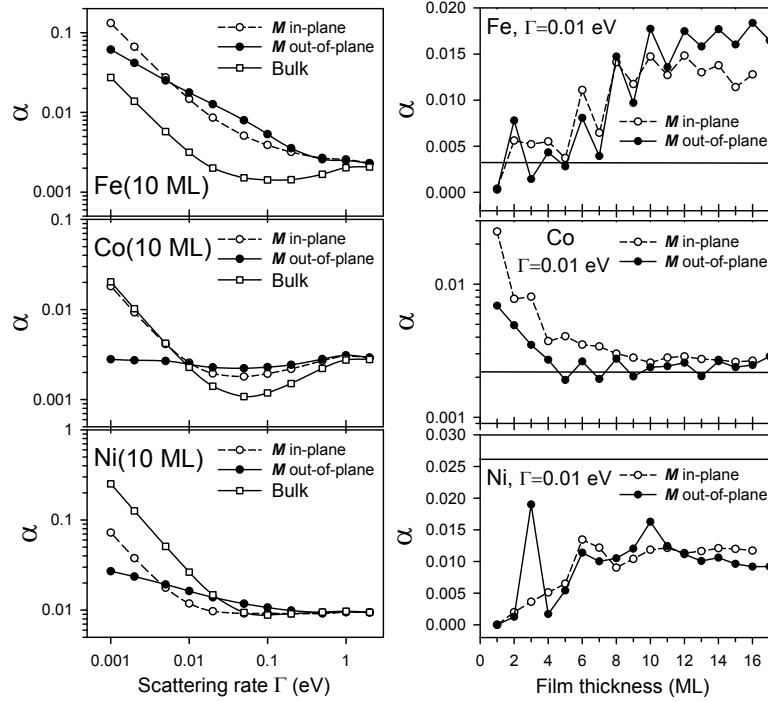
Figure 3.28: Gilbert damping constant α in *left*: bulk and FM(10 ML) films (FM=Fe, Co and Ni) with in-plane and out-of-plane magnetisation $\boldsymbol{M}$ vs scattering rate Γ, *right*: Fe, Co and Ni films with in-plane and out-of-plane magnetisation vs film thickness for $\Gamma = 0.01$ eV; The horizontal lines mark the bulk values for $\Gamma = 0.01$ eV.

The values of $\alpha = \alpha_\parallel$ for in-plane $\boldsymbol{M}$ are larger or smaller than $\alpha = \alpha_\perp$ for out-of-plane $\boldsymbol{M}$, depending on the film thickness and the type of metal. The difference $\alpha_\perp - \alpha_\parallel$ of the damping constants obtained for the two orientations can be particularly large in some cases [e.g., for Fe(16 ML), Co(1 ML) and Ni(3 ML)] but it is expected to diminish for larger film thicknesses (approaching bulk limit) as α has the same value for $\theta = 0$ and $\theta = 90°$ in bulk cubic metals (cf. Fig. 3.26).

In the case of a Fe monolayer, the damping constant α is almost the same for the two magnetisation orientations. Except for the thickness 2 ML Fe, at which the $\alpha_\perp$ is slightly above $\alpha_\parallel$, the damping constant $\alpha_\parallel$ of Fe films with the in-plane magnetisation is larger than $\alpha_\perp$ for thicknesses up to 9 ML; from 10 ML the out-of-plane damping constant $\alpha_\perp$ starts to exceed $\alpha_\parallel$ and the biggest difference $\alpha_\perp - \alpha_\parallel$ (about 56%) is achieved at 16 ML (the thickest film considered for both orientations).

For the Co monolayer, the change of α upon the change of the magnetisation orientation from out-of-plane to in-plane is more than threefold. As already mentioned, the obtained oscillatory dependence of α on film thickness for Co films with out-of-plane magnetisation almost disappears in the case of Co films with in-plane magnetisation. In general, for the investigated Co films (with thicknesses up to 16 ML) the Gilbert damping is enhanced when the magnetisation turns from

out-of-plane to in-plane.

In the case of Ni films, clearly the most distinctive feature of the calculated Gilbert damping constant $\alpha_\parallel$ for the in-plane magnetisation in comparison with the constant $\alpha_\perp$ obtained for the out-of-plane orientation is the disappearance of the maximum at film thickness 3 ML, whilst the maximum at 10 ML becomes much less pronounced and its position is shifted to 11 ML. The change of α upon the change of the magnetisation orientation from in-plane to out-of-plane is more than fivefold for the 3 ML Ni films and 44% for 10 ML Ni films. For Ni films thicker than 12 ML the in-plane damping $\alpha_\parallel$ starts to exceed the $\alpha_\perp$.

Figure 3.28 (left panel) shows the Gilbert damping constants for Fe, Co and Ni films, all of thickness 10 ML, as functions of the scattering rate Γ for in-plane and out-of-plane magnetisation as well as the damping constants of their bulk cubic counterparts. For the Fe film the damping constant decreases with increasing scattering rate Γ for both in-plane and out-of-plane orientations of magnetisation. The damping constant is larger for the out-of-plane direction of magnetisation than for its in-plane orientation for the range of the scattering rates $0.005\,\mathrm{eV} \leqslant \Gamma \leqslant 0.2$ eV. For both directions, the damping constants of the Fe films lie above that of bulk Fe.

For the Co films with very large scattering rate $\Gamma \geqslant 1$ eV, the damping constants obtained for in-plane and out-of-plane magnetisation match each other whilst they both have their minima at $\Gamma = 0.05$ eV, similar to the bulk Co. The in-plane damping constant $\alpha_\parallel$ is slightly lower than $\alpha_\perp$ for $0.01\,\mathrm{eV} \leqslant \Gamma \leqslant 1$ eV. At $\Gamma = 0.01$ eV the two constants reach almost the same value again (this can also be seen in the right panel of Fig. 3.28). For $\Gamma < 0.01$ eV the in-plane damping constant exceeds the out-of-plane one and approaches the bulk value.

In the Ni films the Gilbert damping decreases with increasing Γ and in a similar way as in the Co films. The in-plane and out-of-plane damping constants are nearly equal for $\Gamma \geqslant 0.2$ eV. The in-plane damping constant $\alpha_\parallel$ coincides with the bulk Ni value for $\Gamma \geqslant 0.05$ eV, whilst $\alpha_\perp$ matches this value for $\Gamma \geqslant 0.5$ eV.

Thus, one can see that the in-plane damping constants of all three considered ferromagnetic films have similar combined dependence on the scattering rate and the magnetisation orientation; $\alpha_\parallel$ is much larger than $\alpha_\perp$ in a range of small Γ (smaller than 0.01 eV or less, depending on metal) whilst $\alpha_\parallel$ is slightly lower than $\alpha_\perp$ for the remaining range of larger Γ.

To conclude this section, the Gilbert damping constant is found to depend on the magnetisation orientation, weakly for bulk ferromagnets but much strongly for ultrathin ferromagnetic films. The damping is particularly strongly enhanced, depending on the electron scattering rate, in ferromgnetic films with magnetisation orientation intermediate between in-plane and out-of-plane directions. For all ferromagnetic films as well as, to lesser extent, for bulk Fe and Ni

significant variation of α with the polar angle θ is obtained. The Gilbert damping constant is found to have maxima at an angle θ in the interval $30° \leqslant \theta \leqslant 45°$ almost for all considered films which does *not* correspond to any symmetry axis. A brief report on the above results for Gilbert damping with arbitrary direction of $\boldsymbol{M}$ can be found in [142].

According to the present model based on Kamberský's approach, spin relaxation processes in magnetic materials are governed by the electron transitions between quantum states close to the Fermi level. The dependence of the Gilbert damping constant on the magnetisation orientation is related to the fact that the changes of electronic states and their energies due to the SO interaction depend on the direction of $\boldsymbol{M}$. In particular, they result in the slight changes of the Fermi surface which are dependent on the orientation of magnetisation. This leads to the orientation dependence of the intraband contributions to intrinsic Gilbert damping which are associated with the "breathing" of Fermi surface [83], i.e., the periodic distortion of this surface when the magnetisation precesses around its equilibrium direction.

Chapter 4

Analysis of Gilbert damping in real space and momentum space

4.1 Layer contributions to damping constant

In the previous sections, the Gilbert damping constant α was found for various magnetic nano-structures including ferromagnetic and nonmagnetic layers. The film thickness dependence of α in free-standing ferromagnetic films, Co/NM bilayers, trilayers and multilayers was analysed. However, it is worth understanding where magnetic damping actually takes place and, in particular, realising which part of the system plays a dominant role in the damping process. Such analysis is helpful for understanding the fundamental physics behind the damping phenomenon in a theoretical way and provides a deeper insight into the mechanism of magnetic damping in layered systems. It is the purpose of this section to explore this issue in the considered layered systems in detail.

In the spin pumping theory, the effective magnetic damping in magnetic multilayers can be considered as sum of the intrinsic damping (of a ferromagnetic metal in bulk) plus damping due to the spin pumping into nonmagnetic layers ($\alpha = \alpha_{\mathrm{b}} + \alpha_{\mathrm{pump}}$) [6, 7, 55]. This assumption is similar to the formula (3.2) in which the second term has been considered to be due to the nonmagnetic layers and interfaces present in the layered system. The spin pumping theory includes the sample parameters connected to the geometry of the system. Apart from thicknesses of constituent metallic layers, one of the main quantities entering the formalism of this theory and strongly affecting the spin pumping process is the spin-diffusion length λ_{sd}, as discussed earlier. For example the pumped spin current in a FM/NM bilayer system is inversely proportional to the spin-diffusion length of the NM spacer layer if $d_{\mathrm{NM}} \gg \lambda_{\mathrm{sd}}$ [54]. Moreover, to achieve an efficient

spin pumping in FM/NM bilayers the thickness of the NM layer d_{NM} needs to be comparable to or larger than its spin-diffusion length [39]. However, to gain a remarkable additional damping from the second nonmagnetic cap (NM2) in FM/NM1/NM2 trilayers the thickness of spacer layer (NM1) with low spin-flip rate has to be less than its λ_{sd} (see Sec. 3.5) to avoid backflow of spin current into the FM. In other words, λ_{sd} is one of the key factors in transfer of spin angular momentum into adjacent nonmagnetic layers.

Despite such knowledge about the magnetic damping due to the spin pumping process there are no theoretical studies, except for a very recent report on (001) fcc Co semi-infinite crystal [91], on spatial distribution of the magnetic damping in layered systems. In this section a novel strategy is introduced in order to explore and analyse the magnetic damping in real space. As a result, it is found from which layers significant portions of the Gilbert damping come from. For this purpose, the Gilbert damping constant α is broken down into contributions to α coming from individual atomic layers. These atomic layer contributions are found as follows.

According to the general formulas (2.43) and (2.44), the Gilbert damping constant α is proportional to the trace of the operator $D(\epsilon) = A^- L(\epsilon - H) A^+ L(\epsilon - H)$ at $\epsilon = \epsilon_F$ for $T = 0$ or rather to the integral $\int_{-\infty}^{\infty} \eta(\epsilon) \, \mathrm{tr} D(\epsilon) \, d\epsilon$ if the calculations are done at finite temperature T. By introducing into $\mathrm{tr} D(\epsilon)$ two unit operators $\sum_{n\boldsymbol{k}} |n\boldsymbol{k}\rangle\langle n\boldsymbol{k}| = 1$ built of the eigenstates $|n\boldsymbol{k}\rangle$ of the Hamiltonian, one finds, for any basis $|i\rangle$, that

$$\mathrm{tr} D(\epsilon) \;=\; \sum_i \sum_{\boldsymbol{k}} \sum_{n,n'} A^-_{i,n'\boldsymbol{k}} \, L(\epsilon - \epsilon_{n'}(\boldsymbol{k})) A^+_{n'\boldsymbol{k},n\boldsymbol{k}} \, L(\epsilon - \epsilon_n(\boldsymbol{k})) \langle n\boldsymbol{k}|i\rangle \tag{4.1}$$

where $A^-_{i,n'\boldsymbol{k}} = \langle i|A^-|n'\boldsymbol{k}\rangle$ and $A^+_{n'\boldsymbol{k},n\boldsymbol{k}} = \langle n\boldsymbol{k}|A^-|n'\boldsymbol{k}\rangle^* = (A_{nn'}(\boldsymbol{k}))^*$. The expression (2.103) for the total damping constant α has been obtained with the basis $|i\rangle = |n\boldsymbol{k}\rangle$. However, taking the advantage of the trace invariance under the choice of basis, the trace $\mathrm{tr} D(\epsilon)$ can also be calculated by choosing the TB basis states $|i\rangle = |\boldsymbol{k}l\mu\sigma\rangle$, each of which is obtained by a combination of orbitals located on different atoms in the same layer l. In this way one obtains

$$\mathrm{tr} D(\epsilon) \;=\; \sum_{\boldsymbol{k}\, l\mu\sigma} \sum_{n,n'} A^-_{\boldsymbol{k}l\mu\sigma,n'\boldsymbol{k}} (A_{nn'}(\boldsymbol{k}))^* \, (a^\sigma_{nl\mu}(\boldsymbol{k}))^* \, L(\epsilon - \epsilon_n(\boldsymbol{k})) L(\epsilon - \epsilon_{n'}(\boldsymbol{k})) \tag{4.2}$$

where $a^\sigma_{nl\mu}(\boldsymbol{k}) = \langle \boldsymbol{k}l\mu\sigma|n\boldsymbol{k}\rangle$.

Apart from the product of the two Lorentz functions, the same as in the calculation of the Gilbert damping constant with Eq. (2.103), and the matrix elements $A_{nn'}(\boldsymbol{k})$, given by Eq.

(2.108), the right-hand side of Eq. (4.2) also includes

$$A^-_{\boldsymbol{k}l\mu\sigma,n'\boldsymbol{k}} = \sum_{l'\mu'\sigma'} a^{\sigma'}_{n'l'\mu'}(\boldsymbol{k})\langle\boldsymbol{k}l\mu\sigma|A^-|\boldsymbol{k}l'\mu'\sigma'\rangle = \xi_l\sum_{\mu'\sigma'}a^{\sigma'}_{n'l\mu'}(\boldsymbol{k})\langle\mu\sigma|A^-_{\mathrm{at}}|\mu'\sigma'\rangle. \qquad (4.3)$$

Substituting Eq. (4.3) into Eq. (4.2) one can write down the expression for the damping constant $\alpha \sim \int \eta(\epsilon)\mathrm{tr}D(\epsilon)d\epsilon$ as a sum of layer contributions α_l. Thus, the following breakdown of the Gilbert damping constant is achieved

$$\alpha = \frac{1}{N_{\mathrm{FM}}}\sum_l \alpha_l \qquad (4.4)$$

where each layer contribution α_l is given explicitly as

$$\alpha_l = \frac{\pi\xi_l}{\mu_{\mathrm{FM}}}\frac{1}{N_{2D}}\sum_{\boldsymbol{k}}\sum_{n,n'}Q_{nn'l}(\boldsymbol{k})(A_{nn'}(\boldsymbol{k}))^*F_{nn'}(\boldsymbol{k}) \qquad (4.5)$$

where

$$Q_{nn'l}(\boldsymbol{k}) = \sum_{\mu\sigma}\sum_{\mu'\sigma'}(a^\sigma_{nl\mu}(\boldsymbol{k}))^*\,a^{\sigma'}_{n'l\mu'}(\boldsymbol{k})\langle\mu\sigma|A^-_{\mathrm{at}}|\mu'\sigma'\rangle. \qquad (4.6)$$

and $F_{nn'}(\boldsymbol{k})$ is defined in Eq. (2.102). The factor $A_{nn'}(\boldsymbol{k})$, defined in Eq. (2.108), can also be calculated as

$$A_{nn'}(\boldsymbol{k}) = \sum_{l'}\xi_{l'}Q_{nn'l'}(\boldsymbol{k}). \qquad (4.7)$$

This relation immediately proves that the sum (4.4) of the layer contributions (4.5) yields the total damping constant α given by Eq. (2.103). All terms appearing in (4.4) have already been evaluated during calculation of the total α. Thus, having found the expressions (4.4)-(4.7) for α_l one can readily calculate contributions from different atomic layers to the Gilbert damping constant in a wide variety of layered systems (though a modification of N_{FM} and μ_{FM} in Eqs. (4.4) and (4.5) is needed if more than one ferromagnet is present).

The time-consuming evaluation of (4.5) and the mirror symmetries in the calculated contributions to α_l in the $\boldsymbol{k}$-space, prompt one to speed up the numerical calculations of α_l. This is done by limiting the region of the integration over $\boldsymbol{k}$ in Eq. (4.5) to the 1/8 BZ instead of the whole BZ, which has been found not to alter the results for the investigated layered structures (monometallic films, bilayers and trilayers) and can be justified in a similar way as in the calculation of the total α (see Sec. 3.1).

The layer contributions to the Gilbert damping in (001) bcc Fe, fcc Co and fcc Ni films with
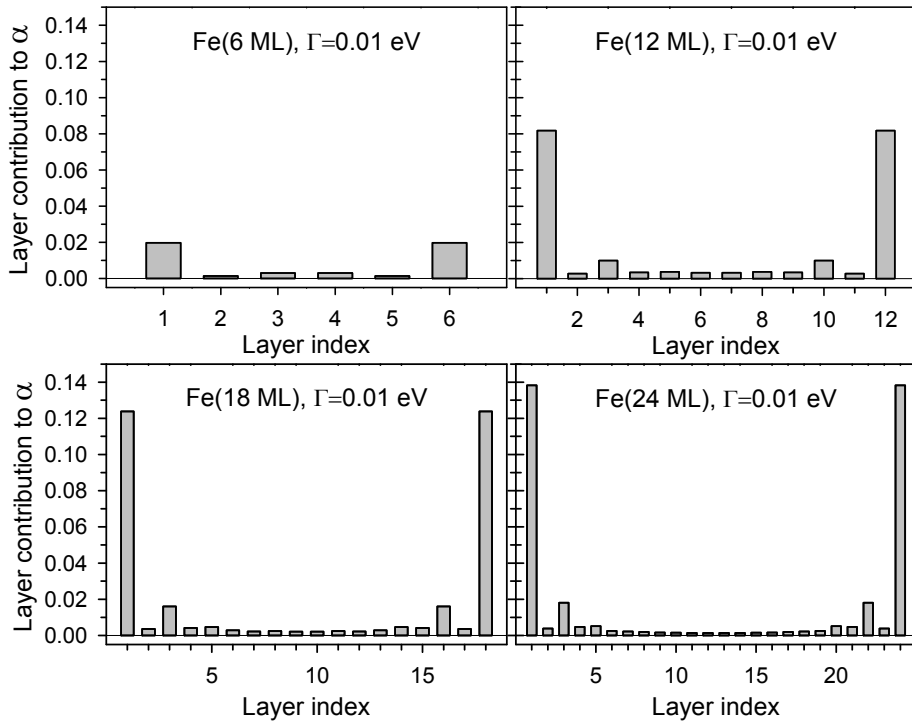
105

Figure 4.1: Layer contributions to the Gilbert damping constant in Fe(N ML) films ($N = 6, 12, 18, 24$); $\Gamma = 0.01$ eV.
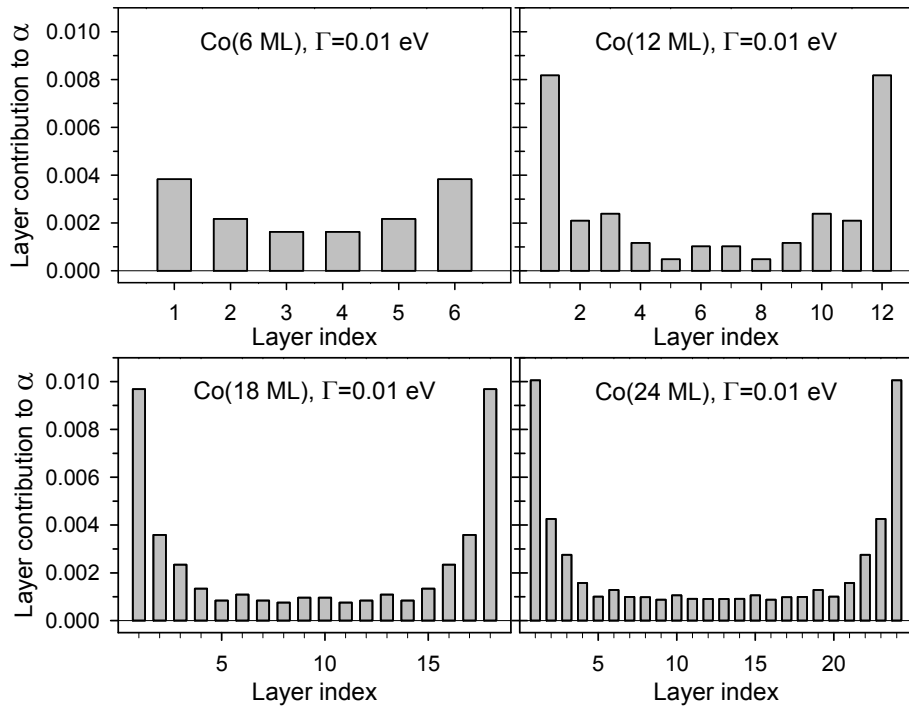

Figure 4.2: Layer contributions to the Gilbert damping constant in Co(N ML) films ($N = 6, 12, 18, 24$); $\Gamma = 0.01$ eV.
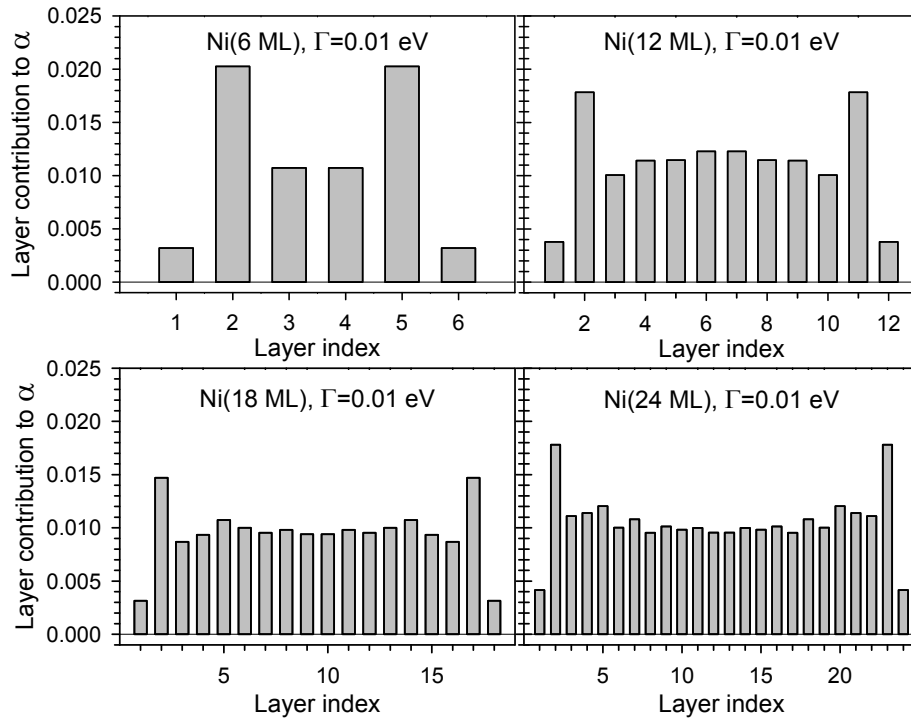
Figure 4.3: Layer contributions to the Gilbert damping constant in Ni(N ML) films ($N = 6, 12, 18, 24$); $\Gamma = 0.01$ eV.

different thicknesses are shown in Figs. 4.1, 4.2 and 4.3, respectively. For purely ferromagnetic Fe, Co and Ni films the distribution of the layer contributions is symmetric with respect to the central symmetry plane of the film.

For Fe and Co films the largest contributions come from the surface layers and for Co films they decline steadily to a minimum value when approaching the central layer(s). A similar increase of the layer contribution α_l is found at the (001) surface of the fcc Co semi-infinite crystal in Ref. [91] using a generalised formula for the Gilbert damping tensor and a different TB parametrisation. In the case of Ni films the surface layers have the smallest contributions to the damping and the largest contributions come from the first subsurface layers ($l = 2$ and $N - 1$).

The layer contributions to the Gilbert damping in Co/NM bilayers (NM=Cu, Pd, Ag, Pt and Au) are shown in Figs. 4.4 and 4.5 respectively. As seen in these figures, adding a NM cap to the Co film not only alters the symmetric distribution of the damping in the pure Co film but it also increases the overall contribution stemming from the Co part of the film. This is caused by change of the electronic structure in Co due to adding the NM cap. The asymmetric distribution of the layer damping contributions in the Co film is very similar in all investigated Co/NM bilayers (with the exception of the interface Co layer) and it is very weakly affected by the thickness of the NM cap. Let us also note that small negative contributions α_l are obtained
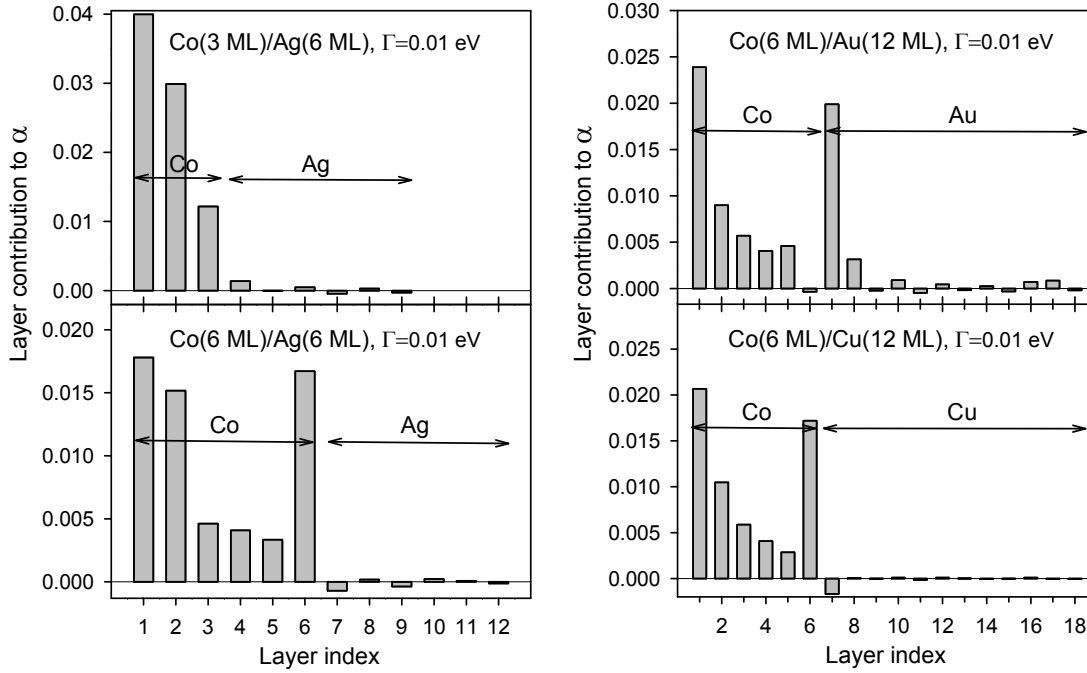
Figure 4.4: Layer contributions to the Gilbert damping constant α *left*: in Co(3 ML)/Ag(6 ML) and Co(6 ML)/Ag(6 ML) bilayers, *right*: in Co(6 ML)/NM(12 ML) bilayers (NM=Cu, Au); $\Gamma = 0.01$ eV.

for some l in the bilayer systems since the applied method of the layer-resolved breakdown of the damping constant α does not guarantee the positive sign of all α_l though the total α is positive according to Eq. (2.103).

The layer contributions α_l inside the NM caps of metals with the top of the d band below ϵ_F are much smaller than in the Pd or Pt caps. They are marginal in the Cu and Ag caps so that the Gilbert damping in the Co/Cu and Co/Ag bilayers comes almost entirely from the Co film. This result holds with changing the thickness of Co (for fixed Cu or Ag thickness cap) although the asymmetric distribution in the Co film is modified when the Co thickness increases, as can be noticed in Fig. 4.4. In the case of the Au cap the very interface Au atomic layer contributes to the damping significantly, as strongly as the surface Co layer (see Fig 4.4). This is a result of the large SO coupling of Au and, presumably, an increase of the local DOS in the Au interface layer due to the hybridisation of s, p states in Au with d states in Co across the Co/Au interface.

For Co/NM bilayers with nonmagnetic metals like Pd and Pt, whose d band crosses the ϵ_F, the dominant contributions to the damping come from the NM caps. In such bilayers the majority of damping originates from a few atomic layers of the NM cap that are closest to the Co/NM interface (the first three layers of NM=Pd or Pt). This can explain a remarkable increase of the damping after covering a Co film with 3 ML of NM=Pd or Pt, whilst further increasing the NM thickness does not affect α strongly because the contributions from interior
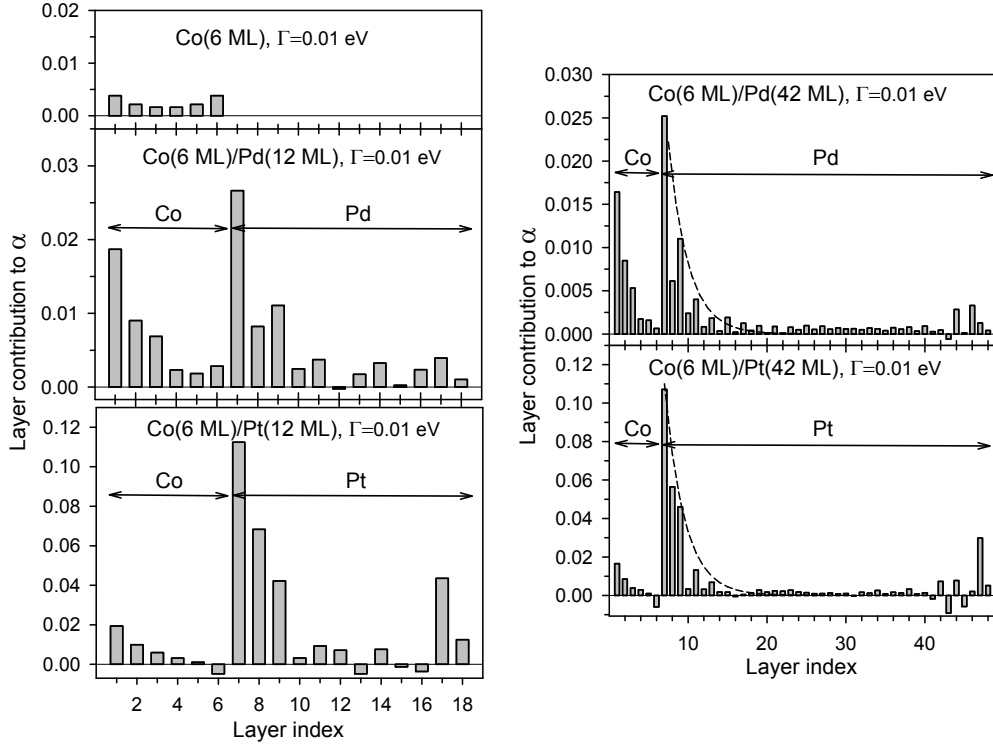
Figure 4.5: Layer contributions to the Gilbert damping constant α *left*: in Co(6 ML) film and Co(6 ML)/NM(12 ML) bilayers (NM=Pd, Pt), *right*: in Co(6 ML)/NM(42 ML) bilayers; $\Gamma = 0.01$ eV.

NM layers are much smaller than the ones near the Co/NM interface. Surprisingly, significant contributions also come from few most external layers of the NM cap. One may also notice that the Co/NM bilayers with nonmagnetic metals which belong to the same group of periodic table like NM=Pd, Pt or NM=Cu, Ag, Au have quite similar distribution of layer contributions to the damping, although with different amplitudes, depending on the strength of the SO coupling in the NM.

The damping contribution in the Pd and Pt caps is largest at the Co/NM interface (NM=Pd or Pt) atomic layer $l = l_1^{NM}$ and it decays with the increasing distance $z = (l - l_1^{NM})a/2$ from the interface (Fig. 4.5, right panel). The obtained decay of α, though not strictly monotonic, can be roughly approximated with an exponential function $\alpha = \alpha(z = 0)e^{-z/\lambda}$. This can be related to a similar dependence obtained in the spin pumping theory for the magnetisation density $\mu(z)$ induced in the NM cap by the precessing magnetisation in the ferromagnet in the presence of a spin-flip mechanism in the NM. In the spin pumping approach, the exponential decay of $\mu(z) \sim e^{-z/\lambda_{sd}}$ holds if the spin-diffusion length λ_{sd} in the NM is much smaller than the NM cap thickness $d_{NM} = N_{NM}a/2$. Although the direct identification of λ with λ_{sd} is not certain at present, the obtained approximate value of $\lambda = 0.45$ nm for both Pd and Pt is in quite good agreement with the recently measured values of $\lambda_{sd}^{Pt} = 0.5 \pm 0.3$ nm for Pt [58] but it
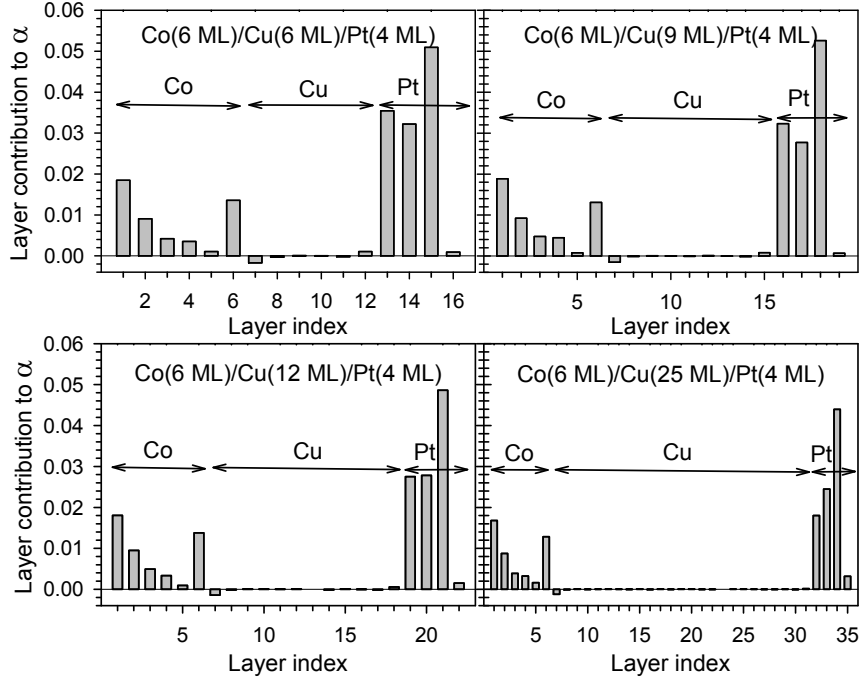
Figure 4.6: Layer contributions to the Gilbert damping constant in Co(6 ML)/Cu(N ML)/Pt(4 ML) trilayers ($N = 6, 9, 12, 25$); $\Gamma = 0.01$ eV.

is significantly smaller than the values $\lambda_{\text{sd}}^{\text{Pd}} = 2.0 \pm 0.09$ nm [167] and $\lambda_{\text{sd}}^{\text{Pd}} = 2.6 \pm 0.12$ nm [58] found experimentally for Pd.

The layer contributions to the Gilbert damping are also obtained for Co/NM/Pt (NM=Cu, Ag) and Pt/Co/Pt trilayers; see Figs. 4.6, 4.7 and 4.8, respectively. Figures 4.6 and 4.7 present layer contributions for Co(6 ML)/Cu/Pt(4 ML) and Co(6 ML)/Ag/Pt(4 ML) trilayers with different thicknesses of Cu and Ag spacers. It is seen that the layer contributions in the Co part are similar for different Cu or Ag spacer thicknesses and there are almost no contributions from the Cu or Ag spacer whilst large contributions from the Pt part are found. Thus, it is visualised that the magnetisation that precesses in the Co part is damped mainly in the distant Pt layer which implies that the magnetic damping is highly nonlocal. As the Cu spacer get thicker the contributions from Pt get smaller although the decay is very slow. The results of present quantum-mechanical calculations confirm the prediction of the spin pumping theory (partly based on phenomenological approach) that there is a nonlocal damping in the second nonmagnetic layer which is a good spin sink (Pt here) due to transferring spin angular momentum from the Co part, through a nonmagnetic spacer which has low spin-flip rate. This effect can be interpreted in the presently applied SO torque-correlation model as arising from d states which form nonzero magnetisation in the Co part but can penetrate to the Pt part through, almost ineffective, the Cu or Ag spacer.

Another system that the layer contributions have been calculated for is symmetric Pt/Co/Pt
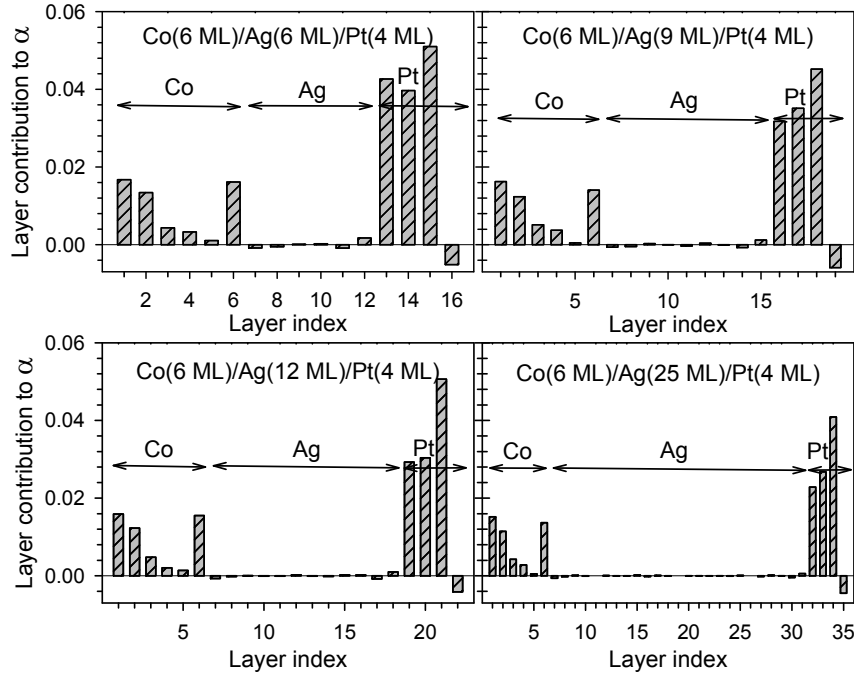
Figure 4.7: Layer contributions to the Gilbert damping constant in Co(6 ML)/Ag(N ML)/Pt(4 ML) trilayers ($N = 6, 9, 12, 25$); $\Gamma = 0.01$ eV.

trilayers. The results of such calculations for Pt/Co(6 ML)/Pt with different thicknesses of Pt are shown in Fig. 4.8. The obtained contributions in both the Pt parts are the same, due to the mirror symmetry with respect to the central plane of the trilayer. They are predominant in atomic layers of the Pt parts closest to both Co/Pt interfaces, whereas the contributions from Co atomic layers are marginal. As seen, some layer contributions α_l to the Gilbert damping have significantly large negative values. This is possible because the obtained formula (4.5) for the layer contributions does not guarantee their positivity, as already mentioned above. On the other hand, as it has been checked for the considered layered systems, the sum (4.4) of contributions α_l from all atomic layers, with negative values at some layers, gives the correct value of the total damping constant α which is a positive quantity.

The shape of the spatial distribution of the Gilbert damping in the Pt layer near the Co/Pt interfaces of Pt/Co/Pt trilayers is similar as in Co/Pt bilayers (Fig. 4.5). However, the contributions from Pt atomic layers near the Co/Pt interfaces are smaller, more than twice, in Pt/Co(6 ML)/Pt trilayers than in Co(6 ML)/Pt bilayers. Thus, it is predicted that adding a Pt underlayer to the Co/Pt bilayer dramatically changes the damping in Pt caps that governs the spin relaxation in Co/Pt bilayers. This can be argued to be a consequence of very small thickness of the considered Co film (6 ML, i.e., about 1 nm) so that the presence of the second Pt layer strongly affects amplitude of quantum states throughout the system, including the first Pt layer. It is expected that this effect becomes weak for sufficiently thick Co films so that the spatial
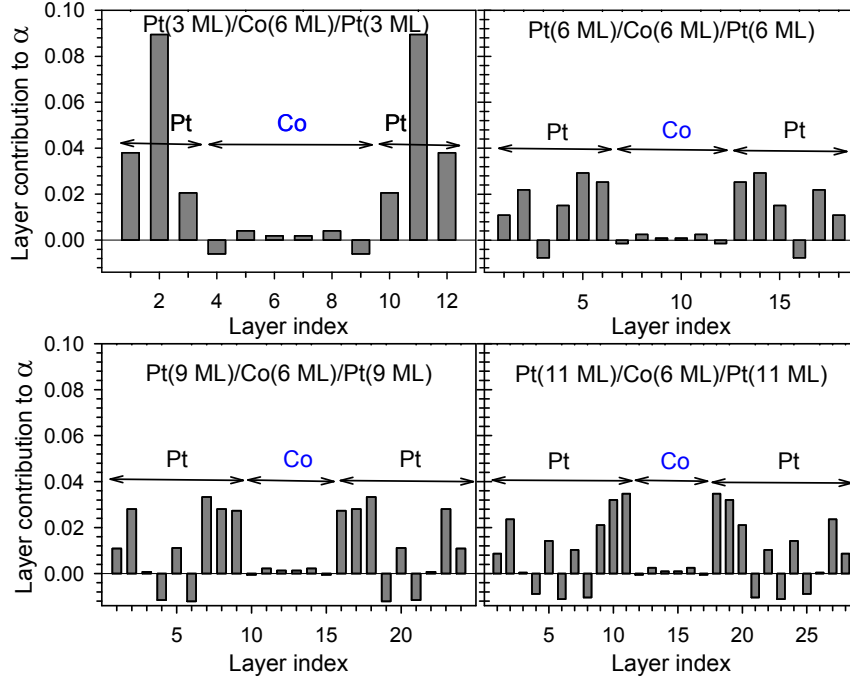
Figure 4.8: Layer contributions to the Gilbert damping constant in Pt(N ML)/Co(6 ML)/Pt(N ML) trilayers ($N = 3, 6, 9, 11$); $\Gamma = 0.01$ eV.

distribution of the Gilbert damping in the Pt layers becomes ultimately the same in Pt/Co/Pt trilayers and Co/Pt bilayers. In such a case, the additional damping, i.e., its enhancement $\alpha - \alpha_{\mathrm{b}}$ due to Pt layers in the trilayers should be twice as in the bilayers. Such is the prediction of the spin pumping theory [6, 7]. Thus, the present results imply that spin pumping theory can break down in layered metallic structures with ultrathin ferromagnetic layers which are several ML thick.

4.2 k-point contributions to Gilbert damping

This section seeks to probe more deeply the nature of the Gilbert damping by analysing its distribution in the momentum space. It is shown that it is feasible to find $\boldsymbol{k}$-points in the BZ that give the main contributions to the Gilbert damping constant α. To determine how different $\boldsymbol{k}$-points in the BZ contribute to the Gilbert damping, it is sufficient to note that the obtained expression (2.103) for α has the form of the integral over the BZ

$$\alpha = \frac{1}{N_{\mathrm{2D}}} \sum_{\boldsymbol{k} \in \mathrm{BZ}} g(\boldsymbol{k}) = \frac{1}{\Omega_{\mathrm{BZ}}} \int_{\boldsymbol{k} \in \mathrm{BZ}} d\boldsymbol{k} \, g(\boldsymbol{k}) \tag{4.8}$$

112

Figure 4.9: $\boldsymbol{k}$-point contributions to the Gilbert damping constant in Fe(N ML) films (N=1,...,10) with scattering rate $\Gamma = 0.01$ eV.

where Ω_{BZ} is the volume of the BZ. The damping contribution $g(\boldsymbol{k})$ from each $\boldsymbol{k}$-point is then given by

$$g(\boldsymbol{k}) = \frac{\pi}{N_{\mathrm{FM}}\,\mu_{\mathrm{FM}}} \sum_{n,n'} |A_{nn'}(\boldsymbol{k})|^2 \, F_{nn'}(\boldsymbol{k}) \tag{4.9}$$

which is a double sum over band indexes n, n' and includes all the coefficients appearing in Eq. (2.103) apart from the normalising factor $1/N_{\mathrm{2D}}$. The terms $A_{nn'}(\boldsymbol{k})$ and $F_{nn'}(\boldsymbol{k})$ are given in Eqs. (2.108) and (2.102), respectively.

Figures 4.9, 4.10 and 4.11 present $\boldsymbol{k}$-point contributions to the damping constant α for (001) bcc Fe, fcc Co and fcc Ni films, respectively. These plots for various film thicknesses show how the Gilbert damping in pure ferromagnetic films is affected by electronic quantum states with different $\boldsymbol{k}$-points in the 2D BZ. As it is clear from the figures there are some small regions in the 2D BZ that give dominant contributions in the $\boldsymbol{k}$-space distribution of the damping constant α. These hot spots, corresponding to peaks of the Gilbert damping distribution $g(\boldsymbol{k})$, move with the thickness of films but are located mostly near the corners of the 2D BZ although they also appear around its centre in some cases [e.g., in Co(1 ML), Ni(3 ML) and Ni(6 ML)]. The same conclusion is true for $\boldsymbol{k}$-point contributions in Co/NM bilayers, in which the corners of the 2D BZ contain $\boldsymbol{k}$-points most effectively contributing to α (see Fig. 4.12). One may also notice the large magnitude of peaks in the damping distribution $g(\boldsymbol{k})$ and the increase of their number at some film thicknesses, in particular for Fe films with even numbers of layers, at $N = 1$ ML, 2
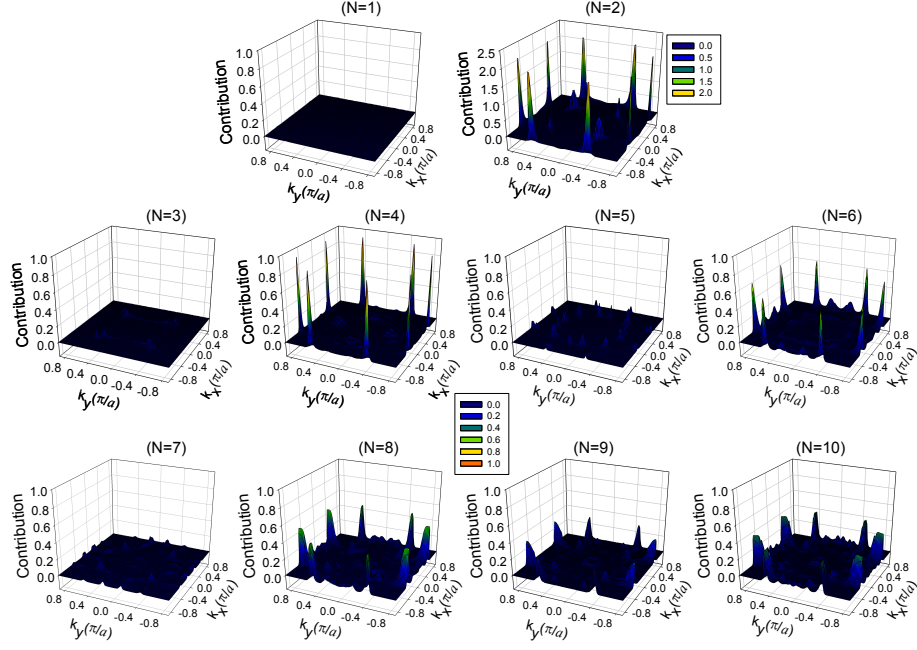
113

Figure 4.10: $\boldsymbol{k}$-point contributions to the Gilbert damping constant in Co(N ML) films (N=1,...,10) with scattering rate $\Gamma = 0.01$ eV. Here and in Figs. 4.11-4.14 below, the two components of the wave vector $\boldsymbol{k} = (k_x, k_y)$ correspond, respectively, to [110] and [1,-1,0] directions of the (001) fcc surface square lattice with the lattice constant $a_{2d} = a/\sqrt{2}$.
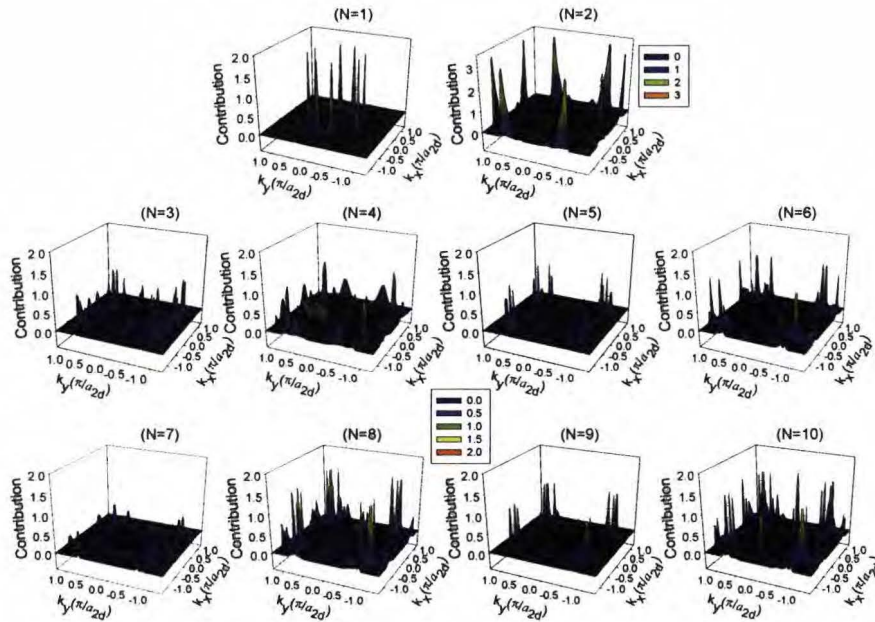

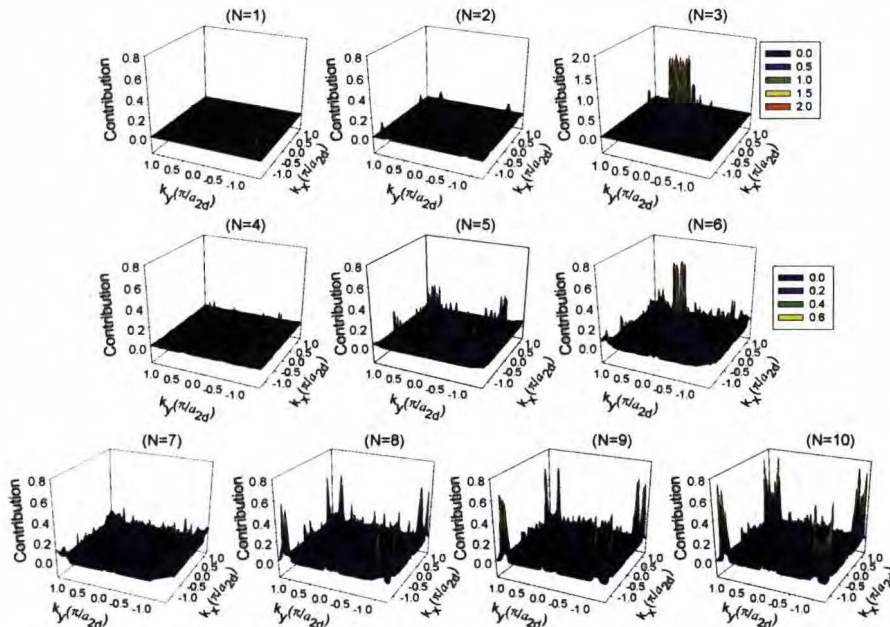Figure 4.11: $\boldsymbol{k}$-point contributions to the Gilbert damping constant in Ni(N ML) films (N=1,...,10) with scattering rate $\Gamma = 0.01$ eV.

114

ML, 6 ML, 8 ML, 10 ML for Co films, and at $N = 3$ ML, 6 ML, 10 ML for Ni films. These peaks lead to the occurrence of corresponding maxima in film thickness dependence of the total damping α for Fe, Co and Ni films (cf. Fig. 3.7, the right panel). On the other hand, the peaks of $g(\boldsymbol{k})$ for Fe films of 1 ML and 3 ML thicknesses as well as for Ni monolayer ($N = 1$) are not visible due to the scale of the respective figures; they are small in comparison with the maximum value of $g(\boldsymbol{k})$ at some other film thicknesses.

The $\boldsymbol{k}$-point contributions to the Gilbert damping in Co/NM bilayers, shown in Fig. 4.12, reflect the pronounced enhancement of the overall damping constant with respect to pure Co films, which is particularly strong for the Pt cap. To show this enhancement in the $\boldsymbol{k}$-space, the difference $\Delta g(\boldsymbol{k})$ of the damping contributions $g(\boldsymbol{k})$ in the Co(6 ML)/NM bilayers and the Co(6 ML) films are plotted in Fig. 4.13. In this figure one can see that much more $\boldsymbol{k}$-points, as compared to pure Co films, contribute to the Gilbert damping thus leading to larger damping in Co/NM bilyers. The distribution of the magnetic damping in the $\boldsymbol{k}$-space is much smoother for the Co(6 ML)/NM bilayers than the Co(6 ML) film in which there are only few sharp peaks of $g(\boldsymbol{k})$ at some $\boldsymbol{k}$-points near the corners of the 2D BZ (Fig. 4.10). Still, like in the Co(6 ML) film, it is the corner regions (close the $\overline{M}$ points) of the 2D BZ that contain $\boldsymbol{k}$-points most effectively contributing to α in the Co(6 ML)/NM bilayers (see Figs. 4.12, 4.13).

The change of damping distribution due to the NM cap, $\Delta g(\boldsymbol{k})$, does not come strictly from the region of the NM layer (especially for NM=Cu, Ag and Au) as it has been previously shown by discussing the atomic layer contributions to the Gilbert damping constant in Sec. 4.1. The obtained negative values of $\Delta g(\boldsymbol{k})$ at some $\boldsymbol{k}$-points imply that there is not only no contribution to enhancement of α from some $\boldsymbol{k}$-points but the change of the electronic structure, due to adding the NM cap, results in smaller damping contributions in a Co/NM bilayer than in pure Co film for these $\boldsymbol{k}$-points.

The hot spots, which are the regions where the contribution $g(\boldsymbol{k})$ has largest values (peaks), are located at the points where there are pairs of electron states with energies close to the Fermi level as it is clear from Eq. (2.102) which contains the factor $F_{nn'}(\boldsymbol{k})$ dependent on the states energies $\epsilon_n(\boldsymbol{k})$, $\epsilon_{n'}(\boldsymbol{k})$. Such pairs of states from different energy bands indexed with n and $n' \neq n$ in the expression (4.9) for $g(\boldsymbol{k})$, give off-diagonal (interband) terms of the Gilbert damping. The expression for $g(\boldsymbol{k})$ also includes diagonal (intraband) terms, which come from individual quantum states ($n = n'$) and thus can be expected to become largest along hot lines formed by $\boldsymbol{k}$-points where energy bands cross the Fermi level (a further discussion on diagonal and off-diagonal terms of the Gilbert damping can be found in Sec. 3.2). It should be noted that the hot spots can be regarded as the crossing points of hot lines corresponding to different
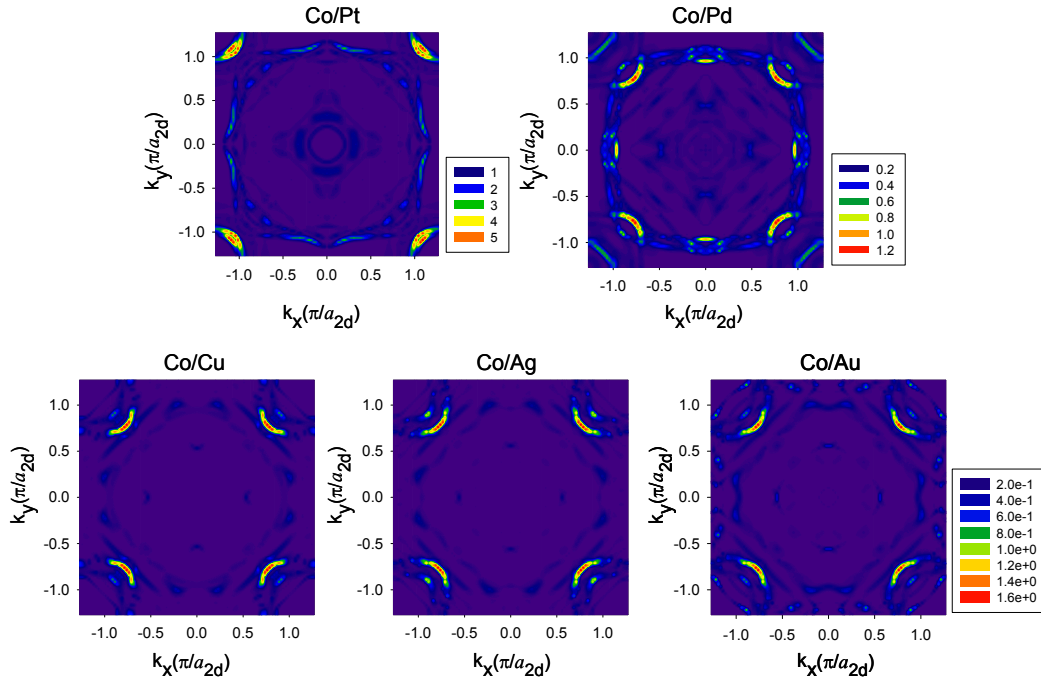
Figure 4.12: k-point contributions to the Gilbert damping constant in Co(6 ML)/NM(6 ML) bilayers, with scattering rate $\Gamma = 0.01$ eV.

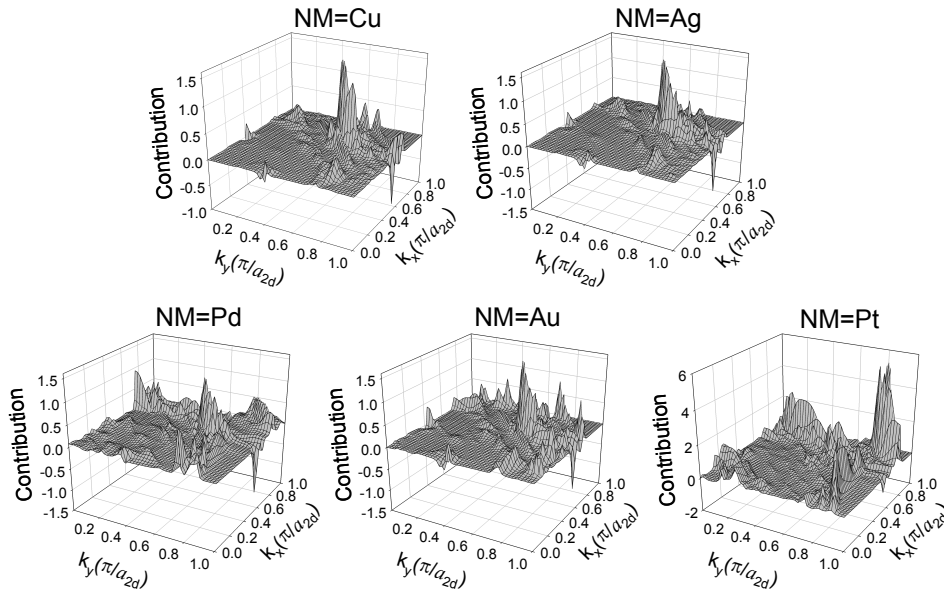Figure 4.13: Change $\triangle g(k)$ of k-point contributions to the Gilbert damping constant due to the presence of NM caps in Co(6 ML)/NM(6 ML) bilayers, with scattering rate $\Gamma = 0.01$ eV. The plots are shown in the 1/4 2D BZ only and they are symmetrical in other three quarters of the 2D BZ.

116

energy bands. The locations of the hot spots vary with the film thickness since the number of energy bands increases and they move as the thickness increases; this concerns QW states in particular. The importance of hot spots in spin flip processes, which contribute to the Gilbert damping, has been recognised in Refs. [131, 132].

It has been revealed that for all considered ferromagnetic films (Fe, Co and Ni) the $\boldsymbol{k}$-point contributions $g(\boldsymbol{k})$, and consequently the damping constant α, stem almost entirely from the off-diagonal (interband) terms. This can be clearly seen in Fig. 4.14, where diagonal (intraband) terms, off-diagonal terms and the total (diagonal + off-diagonal) are plotted for an (001) fcc Co(10 ML) film. Note that, due to the symmetry $g(k_x, k_y) = g(\pm k_x, \pm k_y)$ upon $(x, y) \to (x, \pm y)$ only one quarter of the BZ is shown in Fig. 4.14. For ferromagnetic films with even number of layers, like Co(10 ML), the obtained diagonal terms are finite only at the borders of the 2D BZ, whilst they turn out to completely vanish for the films with odd number of layers ($N = 1, 3, 5, ...$ ML). However, as shown later in this section, with an appropriate choice of eigenstates at $\boldsymbol{k}$-points where they are degenerate states (especially on the high-symmetry lines, including the borders of the BZ) the diagonal terms vanish throughout the whole BZ for (001) cubic monometallic films with any number (odd or even) of atomic layers. Thus, no contribution of the diagonal terms to the Gilbert damping makes such films different from bulk ferromagnetic metals in which both diagonal and off-diagonal terms are present and they are dominant for small and large scattering rates Γ, respectively (see Fig. 3.5). However, as explained below, this difference is rather apparent since the diagonal damping terms can also be made to vanish for bulk cubic metals if non-Bloch 3D eigenstates of the Hamiltonian are chosen owing to the $z \to -z$ symmetry. It is interesting to note that, due the absence of the aforementioned mirror symmetry in Co/NM bilayers, the *diagonal* terms do not vanish and in fact they are dominant in the case of Co/NM bilayers. The latter result requires further investigations.

In the following it will be proved that contributions from the diagonal terms to the Gilbert damping in ferromagnetic films vanish because the eigenstates of the Hamiltonian H (i) have (for a general $\boldsymbol{k}$-point) or (ii) can be chosen to have (for $\boldsymbol{k}$-points at the BZ edges or high-symmetry lines in the BZ) a definite symmetry under the reflection operation $R : z \to -z$. In fact, this proof is valid for any layered system with $z \to -z$ spatial mirror symmetry, like symmetric NM/FM/NM trilayers, but does not hold for FM/NM bilayers which lack such symmetry.

The actual symmetry operator $Q = 2S_z R = \sigma_z R$ has to include, besides the spatial part R, also the corresponding spin part σ_z (one of the Pauli matrices) to make the total Hamiltonian H, including the SO interaction H_{SO}, invariant if acted upon by Q. It means that H commutes with the so-defined operator, $[H, Q] = 0$, i.e., the relation $QHQ^{-1} = H$ holds. Indeed, the kinetic
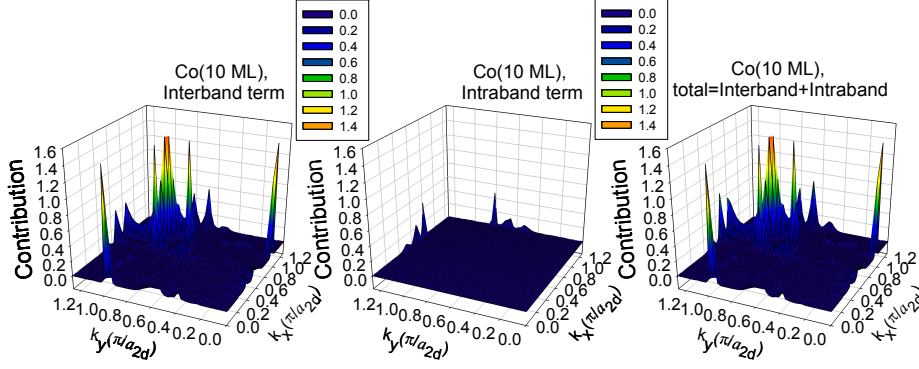
Figure 4.14: Diagonal (intraband), off-diagonal (interband) and the total $\boldsymbol{k}$-point contributions to the Gilbert damping constant in Co(10 ML) film, with scattering rate $\Gamma = 0.01$ eV. The plot are shown in 1/4 2D BZ are shown only and they are symmetrical in quarters of the 2D BZ.

$(p^2/2m)$ and potential $(V_\uparrow(\boldsymbol{r}), V_\downarrow(\boldsymbol{r}))$ parts of the Hamiltonian do not change if z is replaced with $-z$, whilst $H_{\mathrm{SO}} = \xi \sum_{lj} \boldsymbol{S} \cdot \boldsymbol{L}(\boldsymbol{r} - \boldsymbol{R}_{lj})$ remains unchanged under the action of the operator Q since orbital and spin angular momenta are both pseudovectors which transform in the same way. In particular, the orbital momentum $\boldsymbol{L} = \boldsymbol{r} \times \boldsymbol{p} = (L_x, L_y, L_z)$ transforms to $(-L_x, -L_y, L_z)$ under the mirror symmetry $z \to -z$ and the spin operator $\boldsymbol{S} = (S_x, S_y, S_z)$ becomes

$$\sigma_z \boldsymbol{S} \sigma_z^{-1} = (\sigma_z \boldsymbol{S}_x \sigma_z^{-1}, \sigma_z \boldsymbol{S}_y \sigma_z^{-1}, \sigma_z \boldsymbol{S}_z \sigma_z^{-1}) = (-S_x, -S_y, S_z) \tag{4.10}$$

if the operator σ_z is applied in the spin subspace. The transformation of the spin operator $\boldsymbol{S}$ is the result of the commutation rules satisfied by the Pauli matrices $\sigma_x, \sigma_y, \sigma_z$, i.e.,

$$\{\sigma_z, \sigma_x\} \;\; = \;\; \sigma_z \sigma_x + \sigma_x \sigma_z = 0 \,, \tag{4.11a}$$

$$\{\sigma_z, \sigma_y\} \;\; = \;\; \sigma_z \sigma_y + \sigma_y \sigma_z = 0 \,, \tag{4.11b}$$

$$\left[\sigma_z, \sigma_z\right] \;\; = \;\; 0 \,. \tag{4.11c}$$

It can also be proved that the choice of the spin operator (σ_z) corresponding to the reflection $z \to -z$ is unique (up to a constant phase factor); see appendix D where the mirror symmetry in spin space is briefly discussed.

The operation Q, which does not change the electron coordinates x, y and commutes with the Hamiltonian H, transforms an eigenstate $|n\boldsymbol{k}\rangle$ of H to a state $|n'\boldsymbol{k}\rangle = Q|n\boldsymbol{k}\rangle$ with the same $\boldsymbol{k}$ and also with the same eigenenergy $\epsilon_n(\boldsymbol{k})$ since $HQ|n\boldsymbol{k}\rangle = QH|n\boldsymbol{k}\rangle = \epsilon_n(\boldsymbol{k})Q|n\boldsymbol{k}\rangle$. Thus for a general $\boldsymbol{k}$-point, where the state $|n\boldsymbol{k}\rangle$ is usually non-degenerate, the transformed state $|n'\boldsymbol{k}\rangle = Q|n\boldsymbol{k}\rangle$ is equal to the original state $|n\boldsymbol{k}\rangle$. The only difference between $Q|n\boldsymbol{k}\rangle$ and $|n\boldsymbol{k}\rangle$

can be a constant factor $c_n(\boldsymbol{k})$ i.e.,

$$Q|n\boldsymbol{k}\rangle = c_n(\boldsymbol{k})|n\boldsymbol{k}\rangle. \tag{4.12}$$

Due to the relation $Q^2 = 1$ (as $R^2 = 1$, $\sigma_z^2 = 1$), which gives $|n\boldsymbol{k}\rangle = Q^2|n\boldsymbol{k}\rangle = c_n(\boldsymbol{k})^2|n\boldsymbol{k}\rangle$, one readily finds $c_n(\boldsymbol{k}) = 1$ or $c_n(\boldsymbol{k}) = -1$ so that non-degenerate states in ferromagnetic films have definite parity (even or odd) with respect to the symmetry operation $Q = \sigma_z R$.

Using this property of states $|n\boldsymbol{k}\rangle$ and $Q|n\boldsymbol{k}\rangle$ and the fact that

$$Q^\dagger H_{\text{SO}} Q = H_{\text{SO}}, \tag{4.13a}$$

$$Q^\dagger S^- Q = -S^- \tag{4.13b}$$

one can easily prove that

$$\langle n'\boldsymbol{k}|A^-|n\boldsymbol{k}\rangle = \langle n'\boldsymbol{k}|(-Q^\dagger A^- Q)|n\boldsymbol{k}\rangle = -c_{n'}^*(\boldsymbol{k})c_n(\boldsymbol{k})\langle n'\boldsymbol{k}|A^-|n\boldsymbol{k}\rangle \tag{4.14}$$

since the SO torque operator $A^- = [H_{\text{SO}}, S^-]$ anticommutes with Q,

$$QA^- Q^{-1} = [QH_{\text{SO}}Q^{-1}, QS^- Q^{-1}] = [H_{\text{SO}}, -S^-] = -A^-, \tag{4.15}$$

and the symmetry operator Q is unitary: $Q^{-1} = Q^\dagger$. From the relation (4.14) one finds with $n' = n$ that

$$\langle n\boldsymbol{k}|A^-|n\boldsymbol{k}\rangle = -|c_n(\boldsymbol{k})|^2\langle n\boldsymbol{k}|A^-|n\boldsymbol{k}\rangle = -\langle n\boldsymbol{k}|A^-|n\boldsymbol{k}\rangle \tag{4.16}$$

so that

$$\langle n\boldsymbol{k}|A^-|n\boldsymbol{k}\rangle = 0. \tag{4.17}$$

This proof also holds for $\boldsymbol{k} = (k_x, k_y)$ on high-symmetry lines in the 2D BZ even if there are two (or more) degenerate states $|n\boldsymbol{k}\rangle, |n+1, \boldsymbol{k}\rangle$ provided that the $|n\boldsymbol{k}\rangle, |n+1, \boldsymbol{k}\rangle$ are *chosen* to have a definite parity under the symmetry operation Q corresponding to the $z \to -z$ symmetry of the film, e.g.,

$$Q|n\boldsymbol{k}\rangle = -|n\boldsymbol{k}\rangle, \tag{4.18a}$$

$$Q|n+1, \boldsymbol{k}\rangle = +|n+1, \boldsymbol{k}\rangle. \tag{4.18b}$$

The states $|n\boldsymbol{k}\rangle, |n+1, \boldsymbol{k}\rangle$ determined in numerical calculations do *not* have this property automatically, and this is the reason why nonzero diagonal contributions are found at the edges of

the 2D BZ for some film thicknesses. However, one can appropriately choose such two combinations of the numerically obtained degenerate states $|n\boldsymbol{k}\rangle, |n+1, \boldsymbol{k}\rangle$ (by diagonalising Q in the subspace spanned by these two states) that these combinations have a definite parity under the operation Q.

Bulk cubic metals also have the $z \rightarrow -z$ symmetry. However, if the symmetry operation $Q = \sigma_z R$ is applied to an eigenstate $|n\boldsymbol{k}\rangle$ with $\boldsymbol{k} = (k_x, k_y, k_z)$ then the state $Q|n\boldsymbol{k}\rangle$ has the same energy as $|n\boldsymbol{k}\rangle$ (because $[H, Q] = 0$), but it corresponds to a different $\boldsymbol{k}$-point, namely $R\boldsymbol{k} = (k_x, k_y, -k_z)$ since the prefactor $e^{i\boldsymbol{k}\cdot\boldsymbol{r}}$ in a Bloch function becomes equal to $e^{i\boldsymbol{k}\cdot R\boldsymbol{r}} = e^{iR\boldsymbol{k}\cdot\boldsymbol{r}}$ after the transformation $R : z \rightarrow -z$. Thus, for a general $\boldsymbol{k}$-point the non-degenerate state $|n\boldsymbol{k}\rangle$ is transformed to a state $|n, R\boldsymbol{k}\rangle$ up to a constant factor $c_n(\boldsymbol{k})$. This phase factor can be included into a redefined states $|n, R\boldsymbol{k}\rangle$ so that we have

$$Q|n\boldsymbol{k}\rangle = |n, R\boldsymbol{k}\rangle. \tag{4.19}$$

Note, however, that this does not mean that the state $|n\boldsymbol{k}\rangle$ has a definite parity under the operation Q. In consequence, the relations (4.14) and (4.16) do not hold for a bulk system. Instead, in a similar way as for films, the following relations can be derived for bulk cubic metals

$$\langle n'\boldsymbol{k}|A^-|n\boldsymbol{k}\rangle = -\langle n', R\boldsymbol{k}|A^-|n, R\boldsymbol{k}\rangle, \tag{4.20a}$$

$$\langle n\boldsymbol{k}|A^-|n\boldsymbol{k}\rangle = -\langle n, R\boldsymbol{k}|A^-|n, R\boldsymbol{k}\rangle \tag{4.20b}$$

but the latter does *not* imply that the relation (4.17) holds. Accordingly, the element $\langle n\boldsymbol{k}|A^-|n\boldsymbol{k}\rangle$ and, consequently, the diagonal (intraband) contributions to the Gilbert damping do not vanish for bulk. However, even in this case the diagonal damping terms can be made to vanish by suitable redefinition of the Hamiltonian eigenstates.

The eigenstates of $|n\boldsymbol{k}\rangle$ and $|n, R\boldsymbol{k}\rangle$ have the same energy. As mentioned above, by choosing an appropriate phase factor in the states $|n, R\boldsymbol{k}\rangle$ [with $R\boldsymbol{k} = (k_x, k_y, -k_z)$] one obtains $Q|n\boldsymbol{k}\rangle = |n, R\boldsymbol{k}\rangle$ for any $\boldsymbol{k}$. Thus, one can construct a pair of new states which are also eigenstates of H [with the same energy $\epsilon_n(\boldsymbol{k}) = \epsilon_n(R\boldsymbol{k})$]

$$|n\boldsymbol{k}, +\rangle = \frac{1}{\sqrt{2}}(|n\boldsymbol{k}\rangle + |n, R\boldsymbol{k}\rangle), \tag{4.21a}$$

$$|n\boldsymbol{k}, -\rangle = \frac{1}{\sqrt{2}}(|n\boldsymbol{k}\rangle - |n, R\boldsymbol{k}\rangle) \tag{4.21b}$$

which have a definite parity under the operation Q

$$Q|n\boldsymbol{k}, +\rangle = |n\boldsymbol{k}, +\rangle\,, \qquad Q|n\boldsymbol{k}, -\rangle = -|n\boldsymbol{k}, -\rangle \tag{4.22}$$

if the relations (4.19) and $Q^2 = 1$ are applied. Then using such states, i.e., taking $\boldsymbol{k}$ from one half of the 3D BZ only and for each $\boldsymbol{k}$ taking the states $|n\boldsymbol{k}, +\rangle, |n\boldsymbol{k}, -\rangle$ one can use the argument applied for films and find the relation similar to Eq. (4.16) to hold for these states. As a result, the diagonal elements of the SO torque A^- vanish

$$\langle n\boldsymbol{k}, +|A^-|n\boldsymbol{k}, +\rangle = 0\,, \qquad \langle n\boldsymbol{k}, -|A^-|n\boldsymbol{k}, -\rangle = 0. \tag{4.23}$$

However, such procedure is at some cost: the new eigenstates $|n\boldsymbol{k}, +\rangle$ and $|n\boldsymbol{k}, -\rangle$ are no longer the Bloch states ! These states have the form of standing waves in the z direction whilst still being Bloch states in the x and y directions. They are labelled with $\boldsymbol{k}$ from one half of the 3D BZ but also with the additional label $w = +$ or $-$. This is a non-standard description of electronic structure. If we keep Bloch states $|n\boldsymbol{k}\rangle$ as the Hamiltonian eigenstates in bulk metals we will get nonzero diagonal terms in the Gilbert damping from the whole 3D BZ except for the $k_z = 0$ plane where Eq. (4.20b) reduces to (4.16). This discussion shows that distinguishing between the diagonal (intraband) and off-diagonal (interband) contributions to the Gilbert damping largely depends on the way the eigenstates are defined and calculated.

Chapter 5

Nonadiabatic spin-transfer torque in magnetic nanostructures

Displacement of DWs in magnetic nanowires by means of spin-polarised current is a fascinating topic in recent years due to their promising applications. DWs are at the heart of the idea of race track memories where each domain represents a bit of information and is moved by flowing current. The velocity of magnetic DWs in current-carrying ferromagnetic structures is affected by the value of nonadiabatic STT coefficient β, alongside the Gilbert damping α discussed in the previous chapters. Moreover, the coefficient β is one of the main factors affecting the threshold current required for depinning DWs. The existence of the nonadiabatic STT is also important in other magnetic phenomena at micro- and nanoscales. In Ref. [169], for instance, it has been shown that considering nonadiabaticity of the current driven STT affects the DW resonance frequency and the DW mass in a Permalloy (Py) nanowire sample. Also, a very recent research on STT based nanomagnonic devices suggests that the parameter β is of significant importance [170]. Thus, nonadiabatic STT represented by the coefficient β is vital for application of magnetic structures in spintronic devices such as magnetic racetrack memories [171].

The nonadiabatic STT enters the LLG equation [61, 62] which describes the dynamics of magnetisation in the presence of an external magnetic field and electric current flowing through the system. On the fundamental level, the nonadiabatic STT originates from the SO interaction which couples the spin and configurational degrees of freedom of electrons in a physical system.

An extended phenomenological LLG equation including the nonadiabatic STT term has been proposed by Zhang and Li [106, 107]. The new term added to the LLG equation, known as the β term, is perpendicular to the adiabatic STT term present in the extended LLG equation [Eq. (2.13)] and accompanies other terms due to the magnetic filed, exchange interaction and the

Gilbert damping. Therefore, the magnetisation dynamics in current-carrying magnetic structures is governed by the coefficients α and β. Though the two quantities refer to different aspects of the magnetisation dynamics, the same physical interaction, namely the SO coupling, is the source of the Gilbert damping constant α and the coefficient β. However, the Gilbert damping constant α essentially arises from d electrons, whilst its counterpart β stems mainly from conduction (s, p) electrons.

The value of β is usually compared to the Gilbert damping constant α, since the ratio β/α governs the DW velocity. Thus, the inclusion of the STT coefficient β, accompanying the Gilbert damping constant α, strongly affects the DW dynamics not only through the DW velocity, but also via the threshold current for the DW motion. Experimentally, β has been mostly reported for ferromagnetic semiconductors and magnetic multilayer nanowires [168], rather than magnetic films of transition metals, by investigation of the DW motion in such systems (see Ref. [172] for a comprehensive discussion). Ohno and Dietl have reported a value of the order of 0.01 in (Ga,Mn)As strips [173], whilst in Ref. [174] a range of $0.17 < \beta < 0.36$ has been obtained for an (Ga,Mn)As thin film.

The coefficient β is strongly affected by spin polarisation, material composition and geometrical structure. Thus, uncertainty about the spin polarisation in the system, the presence or absence of symmetry in the system also give rise to different values of β [172, 175]. That is the reason why different values of β are reported for the same system, as in Refs. [173, 174], due to unavoidable estimations during measurements.

Another factor affecting β is temperature. The values $\beta = 1.45 \pm 0.25$ and $\beta = 0.35 \pm 0.08$ have been estimated for [Co/Pt] multilayers at $T = 250$ K and $T = 300$ K, respectively [176]. Other reports on β in Co/Pt and Co/Ni spin valves result in $\beta \approx \alpha$ [177]. Different values of β has been reported for Py nanowires with different, transverse or vortex, DW structures [178]. Various ranges of values have also been reported in experiment for the ratio β/α [179, 180]. In particular, the value $\beta = 0.15 \pm 0.07$ has been found during measurement of vortex DWs' displacement in Py disk which is over an order of magnitude larger than α in similar systems [181].

The coefficient β has previously been calculated by several groups via different methods such as Green function method [182] and the Keldysh formalism [183] (see also [184]). As an extension of Kamberský's formula for α, a quantum-mechanical model for calculation of both α and β has been proposed by Gilmore *et al.* [67, 68]. However, there is no report, neither theoretical nor experimental, on β in magnetic layered systems. Despite various reports on the relation between α and β ($\beta = \alpha$ or $\beta \neq \alpha$), such a relation is still under debate and remains an open question.

Thus, the evaluation of β in magnetic structures is desirable.

In this chapter, the coefficient β is calculated for several magnetic systems utilising the expression proposed by Gilmore and co-workers in Ref. [67]. The attention is directed to bulk ferromagnetic metals (bcc Fe, fcc Co and fcc Ni) as well as ultrathin ferromagnetic metallic films, though the method presented here is general and can be used for various magnetic nanostructures. The calculations are performed within a realistic nine-band TB model [95] with the SO coupling included. The Hellmann-Feynman (HF) theorem is employed for the calculation of electron velocities defined as the derivatives of band energies with respect to the wave vector which appear in the expression for β. The dependence of β on the electron scattering rate Γ as well as on thicknesses of ferromagnetic films is investigated. The relation between the coefficients α and β is also investigated and the alleged equality ($\alpha = \beta$) is questioned.

5.1   Calculation method

According to the formalism in Refs. [67, 68] the coefficient β is given by the following ratio

$$\beta = \frac{\frac{\pi}{\Omega_{\mathrm{BZ}}} \sum\limits_{n,n'} \int \frac{d\boldsymbol{k}}{(2\pi)^D} \, \alpha_{nn'} \left(\boldsymbol{k}, \boldsymbol{q}\right) \left(\tau_{n',\boldsymbol{k}+\boldsymbol{q}} \, \boldsymbol{v}_{n',\boldsymbol{k}+\boldsymbol{q}} - \tau_{n\boldsymbol{k}} \, \boldsymbol{v}_{n\boldsymbol{k}}\right) \cdot \boldsymbol{E}}{\boldsymbol{q} \cdot \boldsymbol{v}_s} \tag{5.1}$$

in the limit of the vanishing wave vector $\boldsymbol{q}$ of a spin wave ($q \to 0$). Here Ω_{BZ} is the volume of the BZ, D is the system's dimensionality and $\boldsymbol{E}$ is the electric field that leads to the occurrence of electric and spin currents. The parameters $\boldsymbol{v}_{n\boldsymbol{k}} = \nabla_{\boldsymbol{k}} \epsilon_{n\boldsymbol{k}}$ and $\tau_{n\boldsymbol{k}}$ are the velocity and the lifetime of an electron, respectively, in the state $|n\boldsymbol{k}\rangle$ with the energy $\epsilon_{n\boldsymbol{k}} = \epsilon_n(\boldsymbol{k})$ (this modified notation for energies is used in this chapter for the sake of simplicity) and $\alpha_{nn'}(\boldsymbol{k}, \boldsymbol{q}) = |A_{nn'}(\boldsymbol{k}, \boldsymbol{q})|^2 F_{nn'}(\boldsymbol{k}, \boldsymbol{q})$. The matrix element of the SO torque $A^- = [S^-, H_{\mathrm{SO}}]$ (Eq. (2.105)) is given by

$$A_{nn'}^-(\boldsymbol{k}, \boldsymbol{q}) = \langle n\boldsymbol{k}|A^-|n', \boldsymbol{k}+\boldsymbol{q}\rangle. \tag{5.2}$$

which for $\boldsymbol{q} = 0$ reduces to $A_{nn'}(\boldsymbol{k})$ in Eq. (2.108). The factor $F_{nn'}(\boldsymbol{k}, \boldsymbol{q})$ is defined as

$$F_{nn'}(\boldsymbol{k}, \boldsymbol{q}) = \int d\epsilon \, \eta(\epsilon) L(\epsilon - \epsilon_{n\boldsymbol{k}}) L(\epsilon - \epsilon_{n',\boldsymbol{k}+\boldsymbol{q}}). \tag{5.3}$$

which extends the definition (2.102) of the $F_{nn'}(\boldsymbol{k}) = F_{nn'}(\boldsymbol{k}, \boldsymbol{q} = 0)$ to finite $\boldsymbol{q}$ (see Refs. [62, 83]). The quantity $\boldsymbol{v}_s$ is the drift velocity of the conduction electron spins which corresponds to the parameter v_0 in the LLG equation (2.13). By replacing $\boldsymbol{v}_s$ in Eq. (5.1) with the expression given

by Eq. (7) of Ref. [67] one obtains

$$\beta \;=\; \frac{\sum\limits_{n,n'} \int \frac{d\boldsymbol{k}}{(2\pi)^D}\, \alpha_{nn'}\left(\boldsymbol{k},\boldsymbol{q}\right) \left(\tau_{n',\boldsymbol{k}+\boldsymbol{q}} \frac{\partial \epsilon_{n',\boldsymbol{k}+\boldsymbol{q}}}{\partial \boldsymbol{k}} - \tau_{n,\boldsymbol{k}} \frac{\partial \epsilon_{n\boldsymbol{k}}}{\partial \boldsymbol{k}}\right) \cdot \boldsymbol{E}}{\sum\limits_{n} \int \frac{d\boldsymbol{k}}{(2\pi)^D}\, \langle n_{n\boldsymbol{k}}^z \rangle \left(\boldsymbol{q} \cdot \frac{\partial \epsilon_{n\boldsymbol{k}}}{\partial \boldsymbol{k}}\right)\left(\frac{\partial \epsilon_{n\boldsymbol{k}}}{\partial \boldsymbol{k}} \cdot \boldsymbol{E}\right) F_{nn}\left(\boldsymbol{k},\boldsymbol{q}\right)}. \tag{5.4}$$

where $n_{n\boldsymbol{k}}^z = \langle n\boldsymbol{k}|S_z|n\boldsymbol{k}\rangle$ is the z component of spin in the state $|n\boldsymbol{k}\rangle$. It is dimensionless since the $\boldsymbol{S}$ operator is assumed to represent the physical electron spin in units of the Planck constant $\hbar$. It has to be noted that, the factor n_s (the dimensionless spin density) is missing in Eqs. (1) and (2) of Ref. [67] though it presumably has been considered in the numerical calculations therein. Inclusion of this factor in necessary to get agreement with the earlier work [68] by the same authors (cited as the reference [48] in Ref. [67]), in which expressions for α and β have been proposed. The former corresponds to Kamberský's formula for the Gilbert damping constant [44](see Eq. (2.43)). Accordingly, this correction is taken into account in Eq. (5.4) in the present calculations.

To evaluate the coefficient β the two following cases can be considered

$$\boldsymbol{E} \;=\; E_x \boldsymbol{i}\,, \quad \boldsymbol{q} = q_x \boldsymbol{i}\,; \tag{5.5a}$$

$$\boldsymbol{E} \;=\; E_y \boldsymbol{j}\,, \quad \boldsymbol{q} = q_x \boldsymbol{i} \tag{5.5b}$$

that define the orientation of the electric field $\boldsymbol{E}$ and the spin wave vector $\boldsymbol{q}$ with vectors $\boldsymbol{i} = (1,0,0)$ and $\boldsymbol{j} = (0,1,0)$ along the x and y axes, respectively. In the former case ($\boldsymbol{E} = E_x \boldsymbol{i}\,,\ \boldsymbol{q} = q_x \boldsymbol{i}$), one obtains

$$
\begin{aligned}
\beta = \beta_x \;&=\; \frac{E_x \sum\limits_{\boldsymbol{k}} \sum\limits_{n,n'} \alpha_{nn'}\left(\boldsymbol{k},\boldsymbol{q}\right)\left(\tau_{n',\boldsymbol{k}+\boldsymbol{q}} \frac{\partial \epsilon_{n',\boldsymbol{k}+\boldsymbol{q}}}{\partial k_x} - \tau_{n,\boldsymbol{k}} \frac{\partial \epsilon_{n\boldsymbol{k}}}{\partial k_x}\right)}{q_x E_x \sum\limits_{\boldsymbol{k}} \sum\limits_{n} \langle n_{n\boldsymbol{k}}^z \rangle \left(\frac{\partial \epsilon_{n\boldsymbol{k}}}{\partial k_x}\right)^2 F_{nn}\left(\boldsymbol{k},\boldsymbol{q}\right)} \\[2mm]
&=\; \left(\frac{1}{\Gamma q_x}\right) \frac{\sum\limits_{\boldsymbol{k}} \sum\limits_{n,n'} \alpha_{nn'}\left(\boldsymbol{k},\boldsymbol{q}\right)\left(\frac{\partial \epsilon_{n',\boldsymbol{k}+\boldsymbol{q}}}{\partial k_x} - \frac{\partial \epsilon_{n\boldsymbol{k}}}{\partial k_x}\right)}{\sum\limits_{\boldsymbol{k}} \sum\limits_{n} \langle n_{n\boldsymbol{k}}^z \rangle \left(\frac{\partial \epsilon_{n\boldsymbol{k}}}{\partial k_x}\right)^2 F_{nn}\left(\boldsymbol{k},\boldsymbol{q}\right)}
\end{aligned}
\tag{5.6}
$$

where lifetimes of all electron states $\tau_{n,\boldsymbol{k}} = \tau_{n',\boldsymbol{k}+\boldsymbol{q}} = 1/\Gamma$ are approximated with the average electron scattering rate Γ. Note that, the integration over $\boldsymbol{k}$ in Eq. (5.4) has been replaced by summation over $\boldsymbol{k}$-points (used in numerical implementation).

For the latter case ($\boldsymbol{E} = E_y \boldsymbol{j}\,,\ \boldsymbol{q} = q_x \boldsymbol{i}$), one obtains

$$\beta = \beta_y \;=\; \frac{\sum\limits_{\boldsymbol{k}} \sum\limits_{n,n'} \alpha_{nn'}\left(\boldsymbol{k},\boldsymbol{q}\right)\left(\tau_{n',\boldsymbol{k}+\boldsymbol{q}} \frac{\partial \epsilon_{n',\boldsymbol{k}+\boldsymbol{q}}}{\partial k_y} - \tau_{n,\boldsymbol{k}} \frac{\partial \epsilon_{n\boldsymbol{k}}}{\partial k_y}\right) E_y}{\sum\limits_{\boldsymbol{k}} \sum\limits_{n} \langle n_{n\boldsymbol{k}}^z \rangle \left(q_x \frac{\partial \epsilon_{n\boldsymbol{k}}}{\partial k_x}\right)\left(\frac{\partial \epsilon_{n\boldsymbol{k}}}{\partial k_y} E_y\right) F_{nn}\left(\boldsymbol{k},\boldsymbol{q}\right)}$$

125

$$= \left(\frac{1}{\Gamma q_x}\right) \frac{\sum\limits_{\boldsymbol{k}} \sum\limits_{n,n'} \alpha_{nn'}(\boldsymbol{k}, \boldsymbol{q}) \left(\frac{\partial \epsilon_{n',\boldsymbol{k}+\boldsymbol{q}}}{\partial k_y} - \frac{\partial \epsilon_{n\boldsymbol{k}}}{\partial k_y}\right)}{\sum\limits_{\boldsymbol{k}} \sum\limits_{n} \langle n_{n\boldsymbol{k}}^z \rangle (\frac{\partial \epsilon_{n\boldsymbol{k}}}{\partial k_x})(\frac{\partial \epsilon_{n\boldsymbol{k}}}{\partial k_y}) F_{nn}(\boldsymbol{k}, \boldsymbol{q})}. \tag{5.7}$$

However, β is infinite for this configuration of the $\boldsymbol{E}$ and $\boldsymbol{q}$ directions since the denominator in Eq. (5.7) vanishes as a consequence of the product $(\frac{\partial \epsilon_{n\boldsymbol{k}}}{\partial k_x})(\frac{\partial \epsilon_{n\boldsymbol{k}}}{\partial k_y})$ present in the sum over the BZ. The divergence of β_y has been confirmed in the numerical calculations based on Eq. (5.7). However, this problem has not been discussed in Ref. [68] and one should assume that the values of β reported therein correspond to the case of convergent $\beta = \beta_x$. Thus, in the present thesis $\beta = \beta_x$, given by the Eq. (5.6) and corresponding to both $\boldsymbol{E}$ and $\boldsymbol{q}$ oriented along the x direction, is calculated. Electron velocities, defined as the derivatives of band energies, and the spin expectation values $\langle n_{n\boldsymbol{k}}^z \rangle$ present in the (5.6) are calculated as follows.

Hellmann-Feynman theorem

In the following, the Hellmann-Feynman (HF) theorem is employed to find an analytical expression for the derivatives of eigenenergies $\frac{\partial \epsilon_{n\boldsymbol{k}}}{\partial k_x}, \frac{\partial \epsilon_{n\boldsymbol{k}}}{\partial k_y}$ appearing in the expression (5.6) for β. Although originally the HF theorem is proved for a Hamiltonian *operator* that depends on a scalar parameter λ, it also applies to any $M \times M$ Hermitian *matrix* $\mathcal{H} = \mathcal{H}(\lambda)$ dependent on a scalar parameter λ (e.g., $\lambda = k_x$ or $\lambda = k_y$ in the present case) and its eigenstate $\boldsymbol{x}_n = \boldsymbol{x}_n(\lambda) = (\boldsymbol{x}_{n1}, ..., \boldsymbol{x}_{nM})$ with an eigenvalue $\epsilon_n = \epsilon_n(\lambda)$. Indeed, one readily obtains

$$
\begin{aligned}
\frac{\partial \epsilon_n}{\partial \lambda} &= \frac{\partial}{\partial \lambda}(\boldsymbol{x}_n | \mathcal{H} \boldsymbol{x}_n) \\
&= (\frac{\partial}{\partial \lambda} \boldsymbol{x}_n | \mathcal{H} \boldsymbol{x}_n) + (\boldsymbol{x}_n | \frac{\partial \mathcal{H}}{\partial \lambda} | \boldsymbol{x}_n) + (\boldsymbol{x}_n | \mathcal{H} | \frac{\partial}{\partial \lambda} \boldsymbol{x}_n) \\
&= \epsilon_n(\frac{\partial}{\partial \lambda} \boldsymbol{x}_n | \boldsymbol{x}_n) + (\boldsymbol{x}_n | \frac{\partial \mathcal{H}}{\partial \lambda} | \boldsymbol{x}_n) + \epsilon_n(\boldsymbol{x}_n | \frac{\partial}{\partial \lambda} \boldsymbol{x}_n) \\
&= \epsilon_n \frac{\partial}{\partial \lambda}(\boldsymbol{x}_n | \boldsymbol{x}_n) + (\boldsymbol{x}_n | \frac{\partial \mathcal{H}}{\partial \lambda} | \boldsymbol{x}_n) \\
&= \sum_{ij} x_{ni}^* (\frac{\partial \mathcal{H}}{\partial \lambda})_{ij} x_{nj} = \sum_{ij} x_{ni}^* \frac{\partial \mathcal{H}_{ij}}{\partial \lambda} x_{nj}
\end{aligned}
\tag{5.8}
$$

since the vector $\boldsymbol{x}_n$ is normalised (for any λ) with the scalar product $(\boldsymbol{x}_n | \boldsymbol{x}_n) = 1$. The last step in the above derivation is valid because here the indexes i, j refer to the basis states $\boldsymbol{e}_i = (0, ..., 1, ..., 0)$, $\boldsymbol{e}_j = (0, ..., 1, ..., 0)$ in $\mathcal{R}^M$, which do not depend on λ , so that

$$(\frac{\partial \mathcal{H}}{\partial \lambda})_{ij} = (\boldsymbol{e}_i | \frac{\partial \mathcal{H}}{\partial \lambda} | \boldsymbol{e}_j) = \frac{\partial}{\partial \lambda}(\boldsymbol{e}_i | \mathcal{H} \boldsymbol{e}_j) = \frac{\partial \mathcal{H}_{ij}}{\partial \lambda}. \tag{5.9}$$

This issue and the whole proof shown in Eq. (5.8) become even more clear if, at all its steps, the

126

M-dimensional vector $\boldsymbol{x}_n$ is represented by its coordinates and the matrix $\mathcal{H}$ by its elements.

The original KS Hamiltonian operator H (given by Eq. (2.47)) does not depend on the wave vector $\boldsymbol{k}$. However, when the eigenstates $|\boldsymbol{x}) = |n\boldsymbol{k}\rangle$ are represented in the Bloch basis the resultant matrix elements $\mathcal{H}_{ij} = \langle i|\mathcal{H}|j\rangle$ of the operator H, with $|i\rangle = |\boldsymbol{k}l\mu\sigma\rangle$ and $|j\rangle = |\boldsymbol{k}l'\nu\sigma'\rangle$, are $\boldsymbol{k}$-dependent. This makes us able to use the HF theorem in the form of Eq. (5.8) to find $\frac{\partial\epsilon_{n\boldsymbol{k}}}{\partial\lambda}$, where $\lambda = k_x$ or k_y. Within the TB model (see Sec. 2.4.3), the eigenstates of Hamiltonian are written in terms of the Bloch basis as

$$|n\boldsymbol{k}\rangle = \sum_{l\mu\sigma} a_{nl\mu}^{\sigma}(\boldsymbol{k})|\boldsymbol{k}l\mu\sigma\rangle \tag{5.10}$$

with the eigenvalues $\epsilon_n(\boldsymbol{k})$ obtained from the matrix equations

$$\sum_{l'\nu\sigma} H_{l\mu,l'\nu}^{\sigma\sigma'}(\boldsymbol{k})\, a_{nl'\nu}^{\sigma'}(\boldsymbol{k}) = \epsilon_n(\boldsymbol{k})\, a_{nl\mu}^{\sigma}(\boldsymbol{k}). \tag{5.11}$$

Matrix elements of Hamiltonian are given by

$$\mathcal{H}_{ij} = H_{l\mu,l'\nu}^{\sigma\sigma'}(\boldsymbol{k}) = \sum_{j'}^{\text{n.n.}} \langle l0\mu\sigma|\, H\, |l'j'\nu\sigma'\rangle\, e^{i\boldsymbol{k}\cdot(\boldsymbol{R}_{l'j'}-\boldsymbol{R}_{l0})}\delta_{\sigma\sigma'} + \epsilon_\mu^\sigma\delta_{\mu\nu}\delta_{\sigma\sigma'}\delta_{ll'} + H_{\text{SO};\,l\mu,l'\nu}^{\sigma\sigma'} \tag{5.12}$$

where ϵ_μ^σ is the on-site energy of orbital μ with spin σ, $H_{\text{SO};\,l\mu,l'\nu}^{\sigma\sigma'}$ are the matrix elements of the SO interaction and j' numbers nearest neighbours of atom at the position $\boldsymbol{R}_{l0}$. The TB eigenvalue matrix (5.11) can then be written as $\mathcal{H}\boldsymbol{x} = \epsilon_n\boldsymbol{x}_n$ where $x_{ni} = a_{nl\mu}^{\sigma}(\boldsymbol{k})$ and i correspond to the composite index $(l\mu\sigma)$. Thus, invoking the HF theorem in the form (5.8) and using the expression (5.12) one obtains

$$\begin{aligned}
\frac{\partial\epsilon_{n\boldsymbol{k}}}{\partial k_x} &= \sum_{ll',\mu\nu,\sigma\sigma'} (a_{nl\mu}^{\sigma}(\boldsymbol{k}))^* \, a_{nl'\nu}^{\sigma'}(\boldsymbol{k})\, \frac{\partial}{\partial k_x} H_{l\mu,l'\nu}^{\sigma\sigma'}(\boldsymbol{k}) \\
&= \sum_{ll',\mu\nu,\sigma} (a_{nl\mu}^{\sigma}(\boldsymbol{k}))^* \, a_{nl'\nu}^{\sigma}(\boldsymbol{k}) \sum_{j'} \langle l0\mu\sigma|\, H\, |l'j'\nu\sigma\rangle\, i(x_{l'j'} - x_{l0})\, e^{i\boldsymbol{k}\cdot(\boldsymbol{R}_{l'j'}-\boldsymbol{R}_{l0})}
\end{aligned} \tag{5.13}$$

since $\frac{\partial\epsilon_\mu^\sigma}{\partial k_x} = 0$, $\frac{\partial H_{\text{SO};\,l\mu,l'\nu}^{\sigma\sigma'}}{\partial k_x} = 0$. Here the x coordinates of the atomic position vectors $\boldsymbol{R}_{l0} = (x_{l0}, y_{l0}, z_{l0})$, $\boldsymbol{R}_{l'j'} = (x_{l'j'}, y_{l'j'}, z_{l'j'})$ appear as the result of the differentiation over k_x. A similar expression is obtained for $\frac{\partial\epsilon_{n\boldsymbol{k}}}{\partial k_y}$ with $x_{l'j'} - x_{l0}$ replaced by $y_{l'j'} - y_{l0}$. It should be noted that the derivatives of electronic energies $\epsilon_{n\boldsymbol{k}}$ can be easily evaluated since all necessary ingredients are obtained during calculation of the Hamiltonian and its diagonalisation.

In this way, by taking the advantage of the HF theorem, explicit expressions for the derivatives of eigenenergies (Eq. (5.13)) are found. Thus, the calculation of the band velocities, which is required in evaluation of β, is performed analytically in the present thesis. In the pre-

127

viously reported *ab initio* calculations in Ref. [67] the band velocities were found by numerical differentiation of band energies within the centred finite difference approximation.

The other parameter needed in the calculation of β is the dimensionless z component of spin in the state $|n\boldsymbol{k}\rangle$, i.e., $\langle n_{n\boldsymbol{k}}^z \rangle$. In the Bloch representation (Eqs. (2.49), (2.50)) the factor $\langle n_{n\boldsymbol{k}}^z \rangle$ is calculated as

$$
\begin{aligned}
\langle n_{n\boldsymbol{k}}^z \rangle &= \langle n\boldsymbol{k}|S_z|n\boldsymbol{k}\rangle \\
&= \sum_{lj\mu\sigma,\, l'j'\nu\sigma'} (a_{nl\mu}^{\sigma}(\boldsymbol{k}))^* \, a_{nl'\nu}^{\sigma'}(\boldsymbol{k}) \, e^{i\boldsymbol{k}\cdot(\boldsymbol{R}_{l'j'}-\boldsymbol{R}_{lj})} \langle lj\mu\sigma|S_z|l'j'\nu\sigma'\rangle \\
&= \sum_{l\mu\sigma} (a_{nl\mu}^{\sigma}(\boldsymbol{k}))^* \, a_{nl\mu}^{\sigma}(\boldsymbol{k}) \, \langle \sigma|S_z|\sigma\rangle \\
&= \frac{1}{2}\left(\sum_{l,\mu} (a_{nl\mu}^{\uparrow}(\boldsymbol{k}))^* \, a_{nl\mu}^{\uparrow}(\boldsymbol{k}) - \sum_{l,\mu} (a_{nl\mu}^{\downarrow}(\boldsymbol{k}))^* \, a_{nl\mu}^{\downarrow}(\boldsymbol{k}) \right)
\end{aligned}
\tag{5.14}
$$

since $\langle lj\mu\sigma|S_z|l'j'\nu\sigma'\rangle = \langle \sigma|S_z|\sigma\rangle \delta_{ll'}\delta_{jj'}\delta_{\mu\nu}\delta_{\sigma\sigma'}$.

It is found that in the case of β, unlike for the Gilbert damping constant α, the integration over $\boldsymbol{k}$-points in Eq. (5.6) cannot be limited to the irreducible BZ. Thus, the summation over $\boldsymbol{k}$ in Eq. (5.6) or Eq. (5.7) must be evaluated by integration over the full 3D BZ for bulk and the full 2D BZ for ferromagnetic films. The factor $F_{nn'}(\boldsymbol{k}, \boldsymbol{q})$ given by an integral over energy ϵ (Eq. (5.3)) can be calculated efficiently with an analytical expression obtained with the aid of the residue theorem and subsequent summation over the Matsubara frequencies (see Appendix A). Thus, having determined all parameters appearing in Eq. (5.4) one can evaluate β for various magnetic structures.

To find a reliable value of the nonadiabatic STT coefficient β, the length of the spin wave vector $\boldsymbol{q}$ must be sufficiently small. It is found that the value $|\boldsymbol{q}| = q_x \simeq 10^{-4}\, \pi/a$ leads to converged results for the whole range of the considered values of the electron scattering rate Γ. Therefore, the value $q_x = 10^{-4}\, \pi/a$ has been used in Eq. (5.5) in evaluation of β for bulk ferromagnets and ferromagnetic films.

To challenge the alleged equality $\alpha = \beta$ the dependence of the nonadiabatic STT β on the electron scattering rate in bulk ferromagnets and ferromagnetic films is investigated, as it was previously performed in the case of the Gilbert damping constant α.

5.2   Bulk ferromagnets

In this section the nonadiabatic STT coefficient β is calculated for bcc Fe, fcc Co and fcc Ni bulk ferromagnets using the expression (5.6). In particular, the coefficient β for bulk Co, which
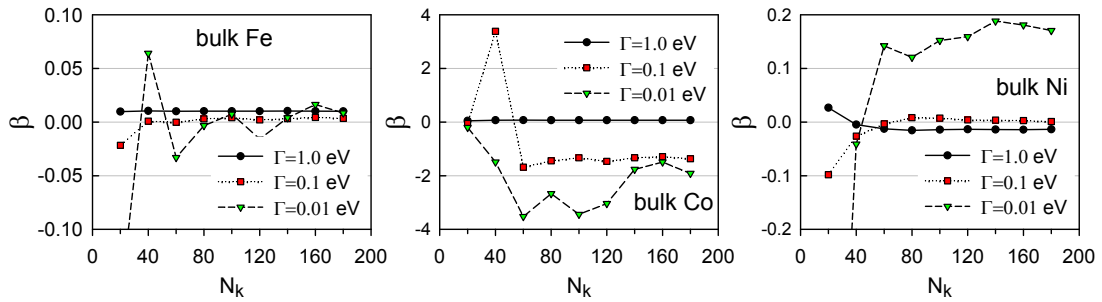
Figure 5.1: Convergence of the nonadiabatic STT coefficient β with the number $(2N_k + 1)^3$ of $\boldsymbol{k}$-points in BZ for bulk Fe, Co and Ni.

has not been reported by Gilmore *et al.* [67], is addressed.

Calculation of the nonadiabatic STT coefficient β is more intensive than the Gilbert damping constant α, especially for very small scattering rate Γ, due to the presence of energy derivative in the expression (5.6) for β. The results obtained with different numbers of $\boldsymbol{k}$-points in the full 3D BZ for bulk Fe, Co and Ni with various scattering rates Γ are shown in Fig. 5.1. A satisfactory convergence of β is obtained with as many as $(360)^3$ $\boldsymbol{k}$-points for bulk Fe, Co and Ni with $\Gamma \geqslant 0.01$ eV, compared to $(100)^3$ $\boldsymbol{k}$-points for α in the same bulk metals (see Fig. 3.1). These numbers are similar to the previously reported for bulk Fe and Ni $[(370)^3$ $\boldsymbol{k}$-points$]$ in the *ab initio* calculations in Ref. [67] using the same expression for β (Eq. (5.4)). The convergence for bulk Fe and Ni with $\Gamma \geqslant 0.1$ eV is obtained with $(200)^3$, whilst slightly larger number of $\boldsymbol{k}$-points, about $(240)^3$, is needed to obtain convergence in bulk Co with $\Gamma \geqslant 0.1$ eV. For all these bulk ferromagnets, one may need more than $(400)^3$ $\boldsymbol{k}$-points to obtain satisfactory results for $\Gamma < 0.01$ eV.

Figure 5.2 depicts the nonadiabatic STT coefficient β, accompanied by the damping constant α, versus the scattering rate Γ for bulk Fe, Co and Ni. The value obtained for β in bulk Fe is positive in the whole range of considered scattering rates $(0.001\,\text{eV} \leqslant \Gamma \leqslant 2\,\text{eV})$, whilst some negative values of β are found in bulk Co and Ni. This is possible because the applied expression (5.6) allows, in principle, for any sign of β (unlike the formula (2.103) giving positive α) since it includes electron velocities (derivatives of band energies) which can be either positive or negative depending on $\boldsymbol{k}$. The obtained values of β for bulk Fe and Ni partly agree (are of the same order) with the results of *ab initio* calculations [67], especially at small scattering rates for bulk Fe and at large scattering rates for bulk Ni. The disagreement in some range of scattering rates is explained in the following. Note that, the dependence of the damping constant α on the scattering rate Γ [62, 67] is similar to its dependence on the electrical resistivity ρ [88]. In particular, the minima of α in bulk ferromagnets occur at $\Gamma \simeq 0.1$ eV [62] which corresponds
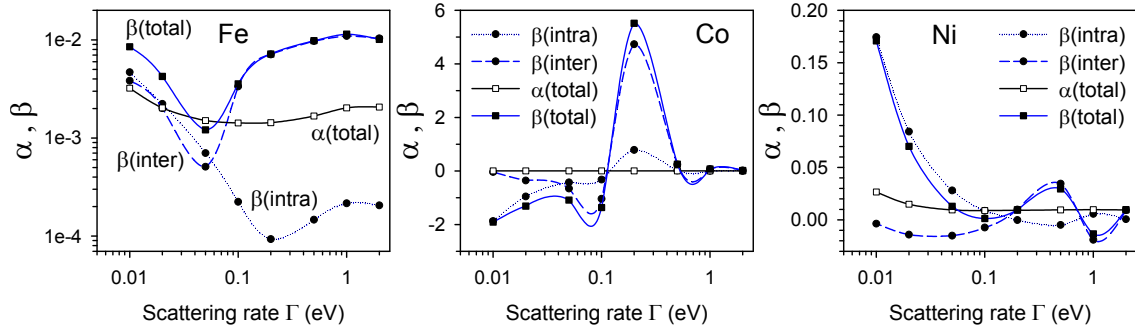
Figure 5.2: Nonadiabatic STT coefficient β and the Gilbert damping constant α vs scattering rate Γ for bulk Fe, Co and Ni. Solid, dotted and dashed curves show the total β as well as intraband and interband contributions to it, respectively.

to $\rho \simeq 1.5 \times 10^{-8}\,\Omega\text{m}$ [67]. Thus, one can estimate the correspondence between Γ and ρ which allows us to compare the results for β obtained here with those reported in Ref. [67].

In the case of bulk Fe, the coefficient β follows roughly similar trend as α when plotted as a function of Γ. In particular, the characteristic minimum occurs for both α and β in bulk Fe, though the minimum of β at $\Gamma = 0.05$ eV is much deeper than the minimum of α at Γ close to 0.1 eV. The coefficient β is larger than α in the whole considered range of scattering rate Γ, except for Γ very close to 0.05 eV at which the minimum of β occurs.

In the case of bulk Ni, the only negative value occurs at $\Gamma = 1$ eV (among several considered values of scattering rate) at which $\beta \simeq -1.4\,\alpha$. As a general trend, β in bulk Ni decreases with increasing the scattering rate Γ, though this decrease is not strictly monotonic, with two minima: at $\Gamma = 0.1$ eV and $\Gamma = 1$ eV. As Γ increases, the difference between α and β declines so that the two curves representing α and β cross each other at $\Gamma \simeq 0.07, 0.2, 0.7$ eV giving rise to $\beta \simeq \alpha$. In particular, one obtains $\beta \simeq 6\,\alpha, 0.5\,\alpha, -1.4\,\alpha$ for $\Gamma = 0.01, 0.1, 1$ eV, respectively. Thus, for bulk Ni one finds $|\beta/\alpha| < 1$ in the range of $0.07\,\text{eV} \lesssim \Gamma \lesssim 0.2$ eV only. At the largest considered value of $\Gamma = 2$ eV the positive value of $\beta \simeq \alpha$ is obtained, though such a large Γ seems quite unphysical.

Except the point at Γ close to 1 eV in bulk Ni, β is positive in bulk Fe and Ni in the whole considered range of scattering rate $(0.001\,\text{eV} \leqslant \Gamma \leqslant 2\,\text{eV})$. The coefficient β reported in Ref. [67] is positive at high electrical resistivity $\rho \geqslant 5 \times 10^{-8}\,\Omega\text{m}$, corresponding to $\Gamma > 0.1$ eV, in bulk Fe and at low resistivity $\rho < 0.7 \times 10^{-8}\,\Omega\text{m}$, corresponding to $\Gamma < 0.02$ eV, in bulk Ni.

In the case of bulk Co the strong dependence of β on the scattering rate leads to a complicated behaviour for β in comparison with α. The relation $\beta \simeq \alpha$ in bulk Co holds for Γ very close to (slightly larger than) 0.1 eV. A large peak occurs for β with $\Gamma = 0.2$ eV at which $\beta \simeq 3660\,\alpha$. One may notice that some negative values of β are also found in the range $\Gamma \leqslant 0.1$ eV where

130

$-830\,\alpha \lesssim \beta \lesssim -1150\,\alpha$. For small scattering rates $\Gamma \leqslant 0.1$ eV, the β curve falls below the α curve and subsequently β obtains negative values reaching its minimum at $\Gamma = 0.01$ eV.

To summarise the obtained results, it is found that $0.8 \lesssim \beta/\alpha \lesssim 5.9$ for bulk bcc Fe, $-1150 < \beta/\alpha < 3660$ for bulk fcc Co and $-1.4 \lesssim \beta/\alpha \lesssim 6$ for bulk bcc Ni with the scattering rate within the range $0.01\,\mathrm{eV} \leqslant \Gamma \leqslant 1$ eV. In particular, the following values of β have been obtained in the three bulk metals with $\Gamma = 0.01$, 0.1 and 1 eV: $\beta \simeq 2.6\,\alpha$, $2.5\,\alpha$ and $5.6\,\alpha$ for Fe; $\beta \simeq -830\,\alpha$, $-1150\,\alpha$ and $26\,\alpha$ for Co; and $\beta \simeq 6\,\alpha$, $0.5\,\alpha$ and $-1.4\,\alpha$ for Ni, respectively.

Unlike the Gilbert damping constant α in bulk ferromagnets for which a compromise between the intraband and interband contributions results in a minimum in the dependence of α on Γ (cf. Fig. 3.5), in the case of STT coefficient β its minima arise due to different distributions of the terms coming from intraband and interband transitions (see Fig. 5.2). In bulk Fe the obtained minimum in β is only due to the interband contribution. In other words, similar minimum occurs in the interband term which plays the dominant role at large Γ. At large scattering rates, $\Gamma \geqslant 0.1$ eV, the intraband contribution plays a minor role and β comes almost entirely from the interband terms, whilst at $\Gamma \leqslant 0.05$ eV both the interband and intraband terms share almost the same contributions to β. In bulk Co, apart from the point at $\Gamma \geqslant 0.2$ eV at which a maximum occurs, the intraband and interband transitions give similar contributions to β whilst β comes almost entirely from the interband contributions at $\Gamma = 0.2$ eV. In bulk Ni with $\Gamma < 0.2$ eV and $\Gamma \geqslant 0.2$ eV, however, β comes almost entirely from the intraband and interband contributions, respectively, giving rise to a maximum in β at $\Gamma = 0.5$ eV and a minimum at $\Gamma = 1$ eV.

It is found that the presently calculated β in bulk Ni behaves similarly to that obtained in the *ab initio* calculations [67] as a function of electrical resistivity ρ (with the same trend and in the same range ($-0.1 < \beta < 0.2$)), though it takes negative values for $\rho > 0.7 \times 10^{-8}\,\Omega$m. However, in the case of bulk Fe the present results for β are in contradiction with those reported in Ref. [67] where β possesses negative value at low resistivities (at $\rho \lesssim 5 \times 10^{-8}\,\Omega$m corresponding to $\Gamma < 0.1$ eV). The discrepancy between the present results and those of *ab initio* calculations (Ref. [67]) is accounted for as follows.

As mentioned above, the convergence of β for bulk ferromagnets is problematic at small scattering rates Γ. That prompted us to investigate convergence of β with much more care. As shown in Figs. 5.1 and 5.2 for bulk metals, β takes very small values for some ranges of Γ. In such a case, β oscillates, with the number of $\boldsymbol{k}$-points, between positive and negative values which result in totally different behaviour of β as a function of Γ depending on the number of $\boldsymbol{k}$-points before a full convergence is reached. Moreover, the coefficient β reported in Ref. [67] is affected by spin current polarisation and it is diverges as the current polarisation approaches
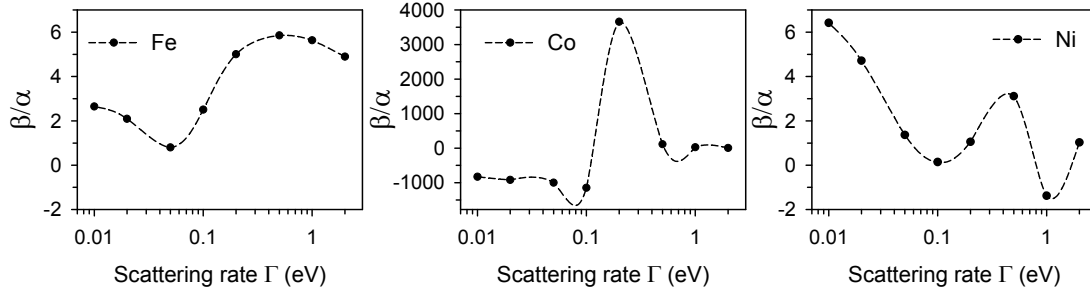
131

Figure 5.3: Ratio of the nonadiabatic STT coefficient and the Gilbert damping constant, β/α, vs scattering rate Γ for bulk Fe, Co and Ni.

zero.

All in all, the present author has serious doubts about the convergence of β with $\rho < 5 \times 10^{-8}\,\Omega\text{m}$ (corresponding to $\Gamma \lesssim 0.4$ eV), which covers almost the whole region in which β is physically defined and calculated for the electron's lifetime ratio $r = 1$, reported for bulk Fe in Ref. [67], since its convergence gets worse with decreasing resistivity (see Fig. 1 therein). Note that, the electron lifetime is considered to be the same for spin up and spin down electrons in the present calculations (i.e., spin-independent scattering rates are assumed) and, thus, the results obtained here have to be compared with plots for $r = \tau^{\downarrow}/\tau^{\uparrow} = 1$ in Ref. [67]). They have reported the values of β within ± 0.2 for small resistivities (small Γ), corresponding to negative values for β in Ref. [67]. This is called "worse convergence" therein. Similar, but a few times smaller, uncertainty, namely ± 0.005, occurs in the present calculations for bulk Fe with $\Gamma < 0.1$ eV. The small resistivities (small Γ) is the range that there is a doubt about because β oscillates between positive and positive values and, with the considered number of $\boldsymbol{k}$-points, it is hard to decide which value β ultimately converges to. That is the reason why the present author believes that β eventually converges to positive values at most scattering rates, as presented here.

Figure 5.3 presents the ratio β/α as a function of scattering rate Γ for bulk Fe, Co and Ni. This ratio is of particular importance because it determines the DW velocity in current-carrying ferromagnetic systems. In the case of bulk Fe, the ratio β/α changes as $0.8 \lesssim \beta/\alpha < 6$ and attains its extrema at $\Gamma = 0.05$ eV and $\Gamma = 0.5$ eV corresponding to $\beta/\alpha \simeq 0.8$ and $\beta/\alpha \simeq 5.9$, respectively.

In the case of bulk Ni, the ratio β/α stays within the range $0.5 \lesssim |\beta/\alpha| \lesssim 6$ with two minima at $\Gamma = 0.1, 1$ eV corresponding to $\beta/\alpha \simeq 0.5$ and $\beta/\alpha \simeq -1.4$ and with two maxima at $\Gamma = 0.01, 0.5$ eV corresponding to $\beta/\alpha \simeq 6$ and $\beta/\alpha \simeq 3$, respectively. The obtained ranges of the ratio β/α in bulk Fe and Ni are similar to those reported in Ref. [67].

The most surprising behaviour occurs for the ratio β/α in bulk Co in which this ratio changes within the range $-1150 \lesssim \beta/\alpha \lesssim 3660$. The ratio β/α in bulk Co is negative for $\Gamma \leqslant 0.1$

eV and positive for $\Gamma > 1$ eV. The smallest value of $|\beta/\alpha|$ is obtained for $\Gamma = 1, 2$ eV with values $\beta/\alpha \simeq 26, 6.8$, respectively. This ratio increases with decreasing the scattering rate Γ down to $\Gamma = 0.2$ eV at which it reaches its *giant* peak presenting $\beta/\alpha \simeq 3660$. It changes as $-830 \lesssim \beta/\alpha \lesssim -1150$ within the range $0.01\,\mathrm{eV} \leqslant \Gamma \leqslant 0.1$ eV. However, one should not be worried about very large values of the obtained ratio $|\beta/\alpha|$ in bulk Co since the DW velocity is, in fact, affected not only by this ratio, but by the combination of $(\beta/\alpha)P$ where $P = \sigma_{\mathrm{P}}/\sigma$ is defined with the spin conductivity σ_{P} and the electric conductivity σ. This fact is pointed out by the authors of Ref. [67] who note that β is inversely proportional to σ_{P} so that it diverges for $\sigma_{\mathrm{P}} \approx 0$, whilst at the same time the product $\sigma_{\mathrm{P}}\beta$ remains finite. The latter result requires further investigations.

The coefficient β takes negative values in some ranges of Γ resulting in negative ratio β/α. The negative β/α imply that DWs move in the opposite direction than the spin current for that range of Γ. This rather unexpected result is discussed in Ref. [67] and it is claimed to be just a particular case of $\beta \neq \alpha$ that leads to the DW velocity different from the spin drift velocity v_0.

5.3 Ferromagnetic films

Evaluation of the nonadiabatic STT coefficient β invokes much more computational effort than the Gilbert damping constant α also in ferromagnetic films. As it was discussed in 3.1, in the case of the damping constant α in ferromagnetic films, the convergence requires a large number of $\boldsymbol{k}$-points as the scattering rate decreases regardless of film thickness. In the case of β in ferromagnetic films the convergence varies with film thickness and it gets worse for the small range of the considered scattering rate, namely for $\Gamma < 0.01$ eV. Due to numerically demanding calculations, the results for β in Fe, Co and Ni films only of a few ML thick are presented. Convergence of β with the number of $\boldsymbol{k}$-points in 2D BZ for various thicknesses of Fe, Co and Ni films of 1-4 ML thicknesses is shown in Figs. 5.4 and 5.5.

For Fe and Co monolayers ($N = 1$) (Fig. 5.4) it is found that the convergence of β is reached with $(200)^2$ $\boldsymbol{k}$-points for $0.01\,\mathrm{eV} \leqslant \Gamma \leqslant 1\,\mathrm{eV}$, whilst for Ni monolayers the convergence is obtained with this number of $\boldsymbol{k}$-points for the whole range of considered scattering rate ($0.001\,\mathrm{eV} \leqslant \Gamma \leqslant 2$ eV). As for the Gilbert damping constant α, in the case of β one also needs a larger number of $\boldsymbol{k}$-points to obtain convergence for smaller Γ. In particular, more than $(400)^2$ $\boldsymbol{k}$-points are needed for $0.002\,\mathrm{eV} \leqslant \Gamma < 0.01$ eV in the case of Fe(1 ML) and for $\Gamma = 0.005$ eV in the case of Co(1 ML). For thicker films with $0.01\,\mathrm{eV} \leqslant \Gamma < 1$ eV the number of $\boldsymbol{k}$-points which is required for convergence varies $[(300)^2\text{-}(600)^2]$ with film thicknesses and the metal that the film is made
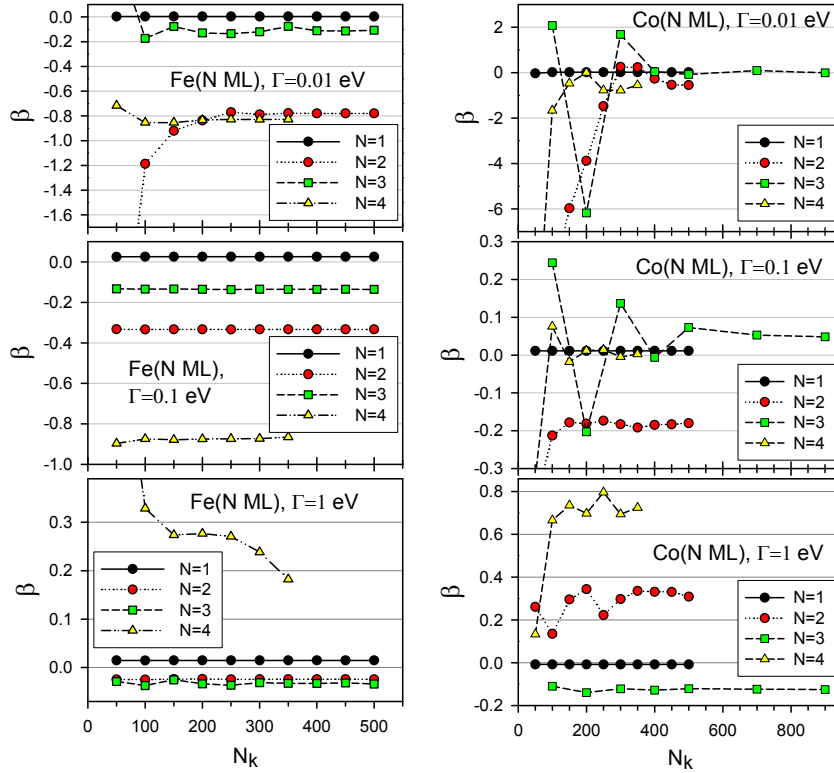
Figure 5.4: Convergence of the nonadiabatic STT coefficient β with the number $(2N_k + 1)^2$ of $\boldsymbol{k}$-points in the 2D BZ for FM(N ML) films [FM=Fe, Co] with different scattering rates Γ.

of. The exception is the Co(3 ML) film for which even summing over $(1800)^2$ $\boldsymbol{k}$-points hardly results in a satisfactory convergence for $\Gamma \leqslant 0.02$ eV. As mentioned above, the convergence of β in ferromagnetic films with small scattering rate, namely $\Gamma < 0.01$ eV, is not satisfactory. Thus, only the reliable results of the calculated nonadiabatic STT coefficient β (in the range of the scattering rates $0.01\,\text{eV} \leqslant \Gamma \leqslant 1$ eV) are presented here.

Figures 5.9-5.8 present the calculated nonadiabatic STT coefficient β in ferromagnetic films for various thicknesses of Fe, Co and Ni films with different values of the scattering rate Γ. Although the films considered here are too thin to allow one to find a general trend for the
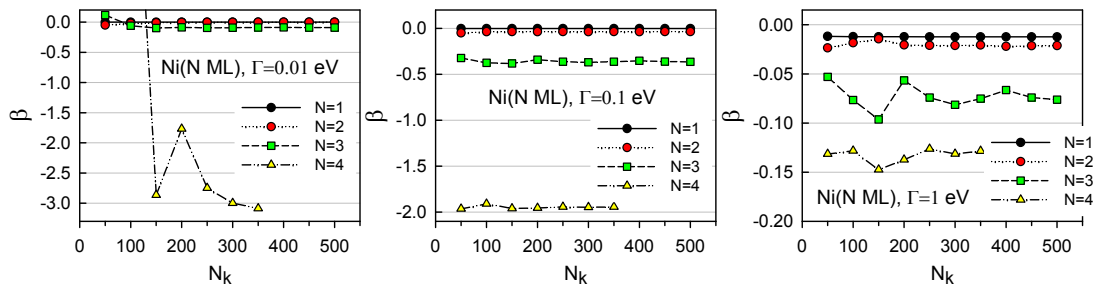

Figure 5.5: Convergence of the nonadiabatic STT coefficient β with the number $(2N_k + 1)^2$ of $\boldsymbol{k}$-points in the 2D BZ for Ni(N ML) films with different scattering rates Γ.
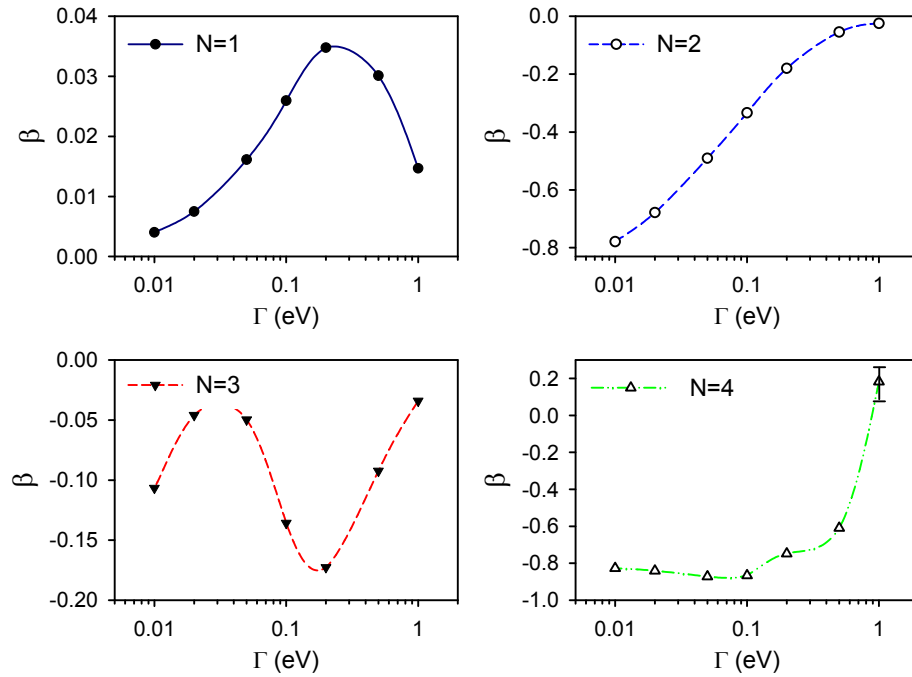
Figure 5.6: Nonadiabatic STT coefficient β vs the scattering rate Γ in bcc Fe(N ML) films.

film thickness dependence of β, they lead one to the conclusion that β strongly depends on the film thickness and scattering rate Γ. The coefficient β is even found to change the sign upon increasing the film thickness, especially in Co films, or value of Γ. As seen, β in Fe and Co films oscillates with the film thicknesses (with maxima at odd thicknesses N and minima at even N) whilst it is a monotonic decreasing function of the film thickness in the case of Ni films.

In the considered films of Fe and Ni, except for their mololayers in which β is positive, β takes negative values almost in the whole range of considered scattering rates, in contrary to β in their bulk counterparts. In the case of films, the sign of β may change with the scattering rate Γ. In general, one finds larger absolute value of β in Fe films than Co films.

The coefficient β is also plotted as a function of scattering rate Γ (see Figs. 5.6-5.8) for different ferromagnetic film thicknesses. As seen, Γ dependence of β strongly depends on film thickness. For the Fe(2 ML) and Fe(4 ML) films β is an increasing function of Γ whilst it has extrema for Fe(1 ML) and Fe(3 ML); see Fig. 5.6. One may also notice the negative sign of β [except in Fe(1 ML)].

This pattern changes for the Co films in which β decreases in Co(1 ML) and increases in Co(2 ML) with increasing Γ; the aforementioned extrema appears for Co(3 ML) and Co(4 ML); see Fig. 5.7. The error bar in the case of Co shown at $\Gamma = 0.02$, 0.01 eV reflects the not fully converged summation over the BZ with $N_k = 900$ for Co(3 ML).

In the case of the Ni films (Fig. 5.8) decreasing and increasing trend of β with increasing Γ

135
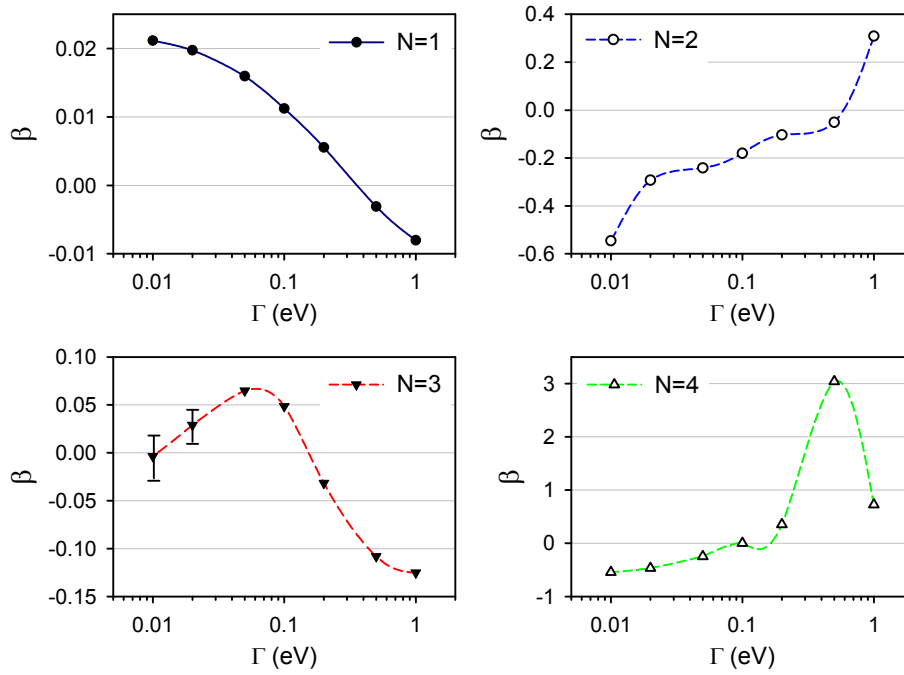
Figure 5.7: Nonadiabatic STT coefficient β vs the scattering rate Γ in fcc Co(N ML) films.
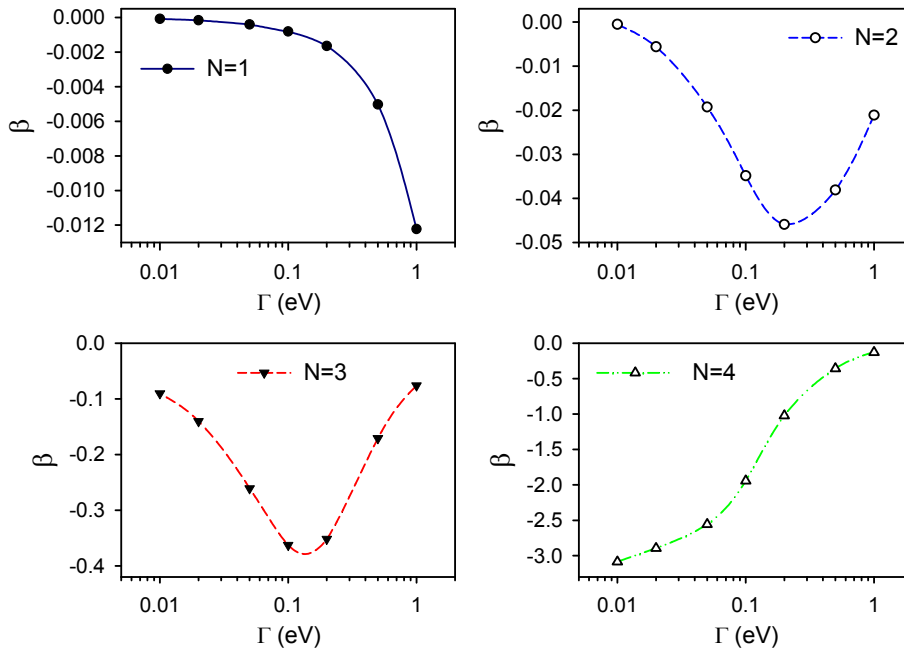
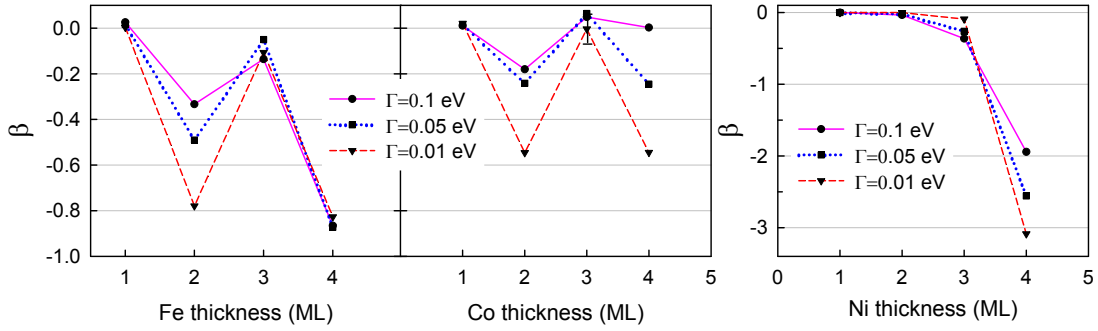Figure 5.8: Nonadiabatic STT coefficient β vs the scattering rate Γ in fcc Ni(N ML) films.

Figure 5.9: Nonadiabatic STT coefficient β vs film thicknesses in Fe, Co and Ni films with various scattering rates Γ.
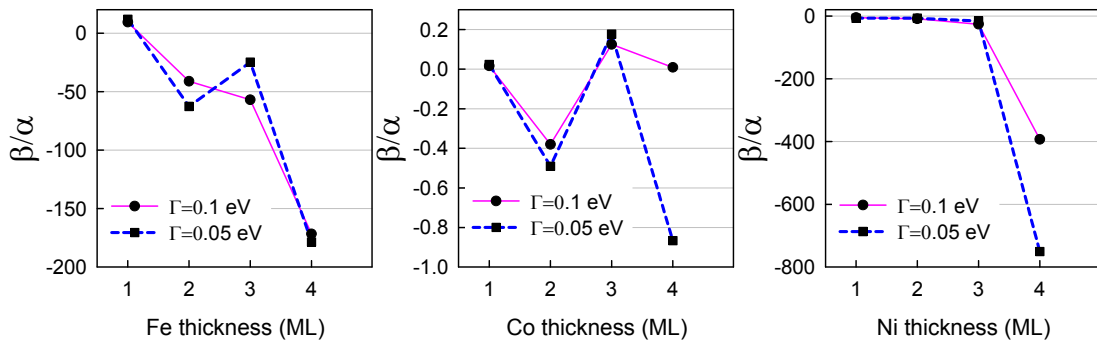

Figure 5.10: Ratio of the nonadiabatic STT coefficient and the Gilbert damping constant, β/α, vs film thickness for Fe, Co and Ni films.

occurs in Ni(1 ML) and Ni(4 ML), respectively, whilst two minima appear in Ni(2 ML) and Ni(3 ML) at Γ close to 0.2 eV. As seen β is negative over the whole range of considered Γ and Ni thicknesses.

In Fig. 5.10 the ratio β/α as a function of film thickness for Fe, Co and Ni films with two values of $\Gamma = 0.05,\ 0.1$ eV is shown. This ratio is of particular important because it determines the DW velocity in current-carrying ferromagnetic systems. Since the Gilbert damping α is a positive quantity, the sign of the ratio β/α is the same as that of β which is found to change with the scattering rate and and film thickness in some films. The ratio β/α changes within the range $-0.9 \lesssim \beta/\alpha < 0.2$ for Co up to 4 ML thickness whereas it drops drastically in Fe and Ni films, attaining large negative values, with the thicknesses increasing from 1 ML to 4 ML.

As already discussed for bulk ferromagnets the negative values of β obtained in most of the considered ultrathin Fe, Co and Ni films are fully allowable by the expression (5.6) applied in the present calculations. However, the negative sign of β, corresponding to the DW motion in the direction opposite to the spin current (though observed in few specific systems [186, 187, 188]), is not usually found in experiment for layered nanostructures. In particular, the positive values $\beta = 0.022 \pm 0.002$ and $\beta = 0.06 \pm 0.03$ (leading to $\beta/\alpha \approx 0.6, 0.7$) have been found for Fe/Pt

alloy films and Co/Ni multilayers, respectively [189] whilst $\beta = 0.35 \pm 0.08$ has been reported for Co/Pt multilayers at room temperature. Also, the values of $\beta = 0.040 \pm 0.005$ [190] and $\beta = 0.016$ (with $\alpha = 0.008$, leading to $\beta/\alpha = 2$) [171] have been reported for Py nanowires.

The obtained values of (β) in Fe and Ni films are very large, at least an order of magnitude larger in some cases, than reported experimentally. However, the present prediction can still be plausible to be definite since, in fact, it is the product of the spin conductivity σ_P and β/α (with $\beta \sim 1/\sigma_P$) that determines the DW velocity observed experimentally as a response to an external electric field (due to applied voltage).

The discrepancy in sign and magnitude of β between theory and experiment needs serious consideration. It might be attributed to inaccuracies in the description of the electronic structure in films composed of just a few atomic layers with the TB parameters (particularly on-site energies) obtained by fitting *ab initio* energy bands of bulk metals. Another possible reason could be associated with the form of the nonadiabatic STT, which was proposed in Refs. [106, 107] and is commonly accepted, but has recently been questioned by the results of the first-principle calculations [191] of the out-of-plane and in-plane torques in Fe, Co and Ni DWs. Finally, the sign and magnitude of β can be significantly changed if the presence of substrate and overlayer is accounted for in the calculations. Such systems better correspond to experimental sample than the free-standing films considered in this chapter. Moreover, the enhancement of the Gilbert damping in FM/NM layered systems can lead to a substantial reduction of the ratio β/α. Thus, the present results for a few ML films cannot be directly compared with experiment and further theoretical investigations are required.

Chapter 6

Summary

The applied theoretical models and the methods developed in this thesis have provided effective tools for investigating spin relaxation in bulk ferromagnetic metals and magnetic layered nanostructures built of transition metals with overall thickness of up to 50 ML (about 10 nm). The main calculations are done for the Gilbert damping constant α given by Kamberský's SO torque correlation formula. Following Ref. [113], it is shown how this formula can be rederived by comparing long-wave spin-wave frequency obtained from the phenomenological LLG equation, describing the dynamics of magnetisation, with that determined from the quantum-mechanical expression for the transverse magnetic susceptibility. In addition, the nonadiabatic STT coefficient β has been calculated, though for a much smaller range of systems than α, using the expression proposed by Gilmore *et al.* [68, 67].

To carry out the calculations for systems of such considerable thickness at moderate computational effort, their electronic structure is described using the TB model with the basis of nine (s, p, d) orbitals of each spin per atom and including the SO interaction with site-specific coupling strength. Consequently, explicit expressions for α and β in terms of the energies of electron states and their amplitudes (defined as projections on orbitals at different atoms, or Bloch basis states composed of such orbitals) have been obtained within the TB model for both bulk and layered systems. It has turned out that, employing finite temperature as well as replacing the involved energy integral by the derived equivalent analytical expression including a summation over Matsubara frequencies lead to a faster convergence of the numerical integration over the BZ required in the calculation of the Gilbert damping constant and the nonadiabatic STT coefficient.

Additionally, an equivalent, but novel, expression for α in terms of the Green function is derived in two alternative forms, which are not limited to the TB model. Such expression can

be particularly useful in systems with reduced symmetry for which the Green function can be efficiently determined with specific techniques like the recursion method. However, for presently considered layered systems, with 2D or 3D translational symmetry, the Hamiltonian was diagonalised and the resulting eigenstates and their energies were used directly in calculation of α and β.

The Gilbert damping constant has been calculated for bulk ferromagnets (bcc Fe, fcc Co and fcc Ni), purely ferromagnetic (FM=Fe, Co and Ni) films, Co/NM bilayers, NM/Co/NM and Co/NM1/NM2 trilayers as well as $L1_0$ Co/NM superlattices and $[Co/NM]_N$ binary multilayers. The dependence of α on the FM and NM cap thicknesses and the effect of the nonmagnetic caps, for various electron scattering rate Γ, has been investigated and compared with recent experiments. It has been found that, the Gilbert damping in Fe, Co and Ni films behaves differently with changing film thickness, often in a non-monotonic way. The calculated damping constant in ferromagnetic films converges to the bulk value α_b for large enough film thicknesses, depending on metal and the electron scattering rate Γ. In some cases the convergence is so slow that α does not saturate to α_b for the thickest considered films. In the case of Ni films with $\Gamma \leqslant 0.01$ eV, for instance, such convergence to α_b does not occur within the investigated range of thicknesses and one may need as many as a few hundred ML to reach α_b. The damping constant α is found to oscillate in FM films, Co/NM bilayers and Co/NM1/NM2 trilayers with the thicknesses N_{FM} and N_{NM} of FM films and NM caps, respectively. These characteristic oscillations, attributed to the QW states with energies close to the Fermi level, die away at N_{FM} and N_{NM} larger than 20 ML.

The Gilbert damping appears to be largely modified in pure ferromagnetic films, in comparison with their bulk counterparts, so that α is reduced or enhanced depending on the value of Γ. However, the Gilbert damping is found to be really remarkably enhanced in Co/NM bilayers due to adding the nonmagnetic caps, even 1 ML thick, to Co films, particularly strongly for Pd and Pt caps. Similar results are also obtained for the investigated Co-based trilayers and multilayers. The obtained large enhancement is successfully explained by attributing it to the combined effect of the large SO coupling and simultaneous presence of d states at the Fermi level ϵ_F in the NM. This effect is in agreement with numerous experiments on magnetic damping in FM/NM structures and predictions of the semiphenomenological theory based on spin pumping [6, 7]. The Gilbert damping in Co/NM bilayers is found to decrease as the Co thickness increases, also in accord with experiment. However, it is not very sensitive to change of the nonmagnetic cap thickness. In the latter case, the Gilbert damping saturates at a final value after adding just a few ML of nonmagnetic cap if small QW oscillations are disregarded. Furthermore, an extra and

highly nonlocal contribution to the Gilbert damping in Co/NM1/NM2 trilayers, due to adding the second nonmagnetic cap (NM2), is obtained which is also consistent with the spin pumping theory and recent experiments. The present calculations predict correctly that the Gilbert damping constant in Co/NM/Pt trilayers declines as the thickness of the nonmagnetic spacer increases. Thus, the applied quantum-mechanical model is capable of well describing the Gilbert damping and its thickness dependence in a wide variety of magnetic layered systems.

The calculations have been generalised to the case of arbitrary direction of magnetisation which allows one to investigate the angular dependence of the Gilbert damping in bulk ferromagnets and ferromagnetic films. For this purpose the angle-dependent expression for the Gilbert damping constant has been derived. Thus, in particular, one is able to make a comparison of the damping constants in magnetic layered systems with out-of-plane and in-plane directions of magnetisation. The Gilbert damping constant has been found to depend on the magnetisation orientation, weakly for bulk ferromagnets (with the same α for the magnetisation along different principal axes) but much stronger for ultrathin FM films. In bulk Fe, Co and Ni, the change of α with changing the magnetisation direction is relatively small, but increases for small Γ, though not exceed 13% , 3% and 18%, respectively, for $\Gamma = 0.01$ eV. The Gilbert damping is particularly strongly enhanced (by even more than 50%) in ferromagnetic films with magnetisation orientation intermediate between in-plane and out-of-plane directions, corresponding to no symmetry axis.

To shed light on the obtained results, analysis of the Gilbert damping in the real space (atomic layer contributions) and momentum space ($\boldsymbol{k}$-point contributions) has also been performed. In the former case, thanks to the obtained novel analytical expression, layer contributions from various atomic layers to the Gilbert damping are obtained. It has been found that, for layered systems including Co/NM bilayers with NMs possessing d bands at ϵ_F (i.e., Pd and Pt) the major contributions stem from a few atomic layers in the NM close to the Co/NM interfaces, whilst for NMs with no such d bands at ϵ_F the main contributions originate from the Co part of the system. The nonlocal nature of the Gilbert damping in Co/NM1/NM2 trilayers, with NM2=Pd and Pt caps considered to be perfect spin sinks, is clearly visualised by the dominating contributions from atomic layers in the nonmagnetic capping layer. The $\boldsymbol{k}$-point contributions, on the other hand, reveal that there are several *hot* spots in the BZ, mostly near its corners, which give the most significant contributions to the Gilbert damping. These analyses provide a better understanding of the Gilbert damping mechanism in magnetic layered structures.

Finally, the nonadiabatic STT coefficient β has been calculated for bulk ferromagnets as well as ferromagnetic films and the ratio β/α, related to the DW velocity, has been discussed.

Calculations of β are based on the quantum-mechanical expression given in Ref. [67], implemented in the TB model and slightly modified by employing the Hellmann-Feynman theorem for calculation of electron velocities which appear in the expression for β. It has been found that, in the case of bulk Fe and Co the coefficient β is larger than α for the whole considered range of the scattering rate Γ. For bulk Ni, this result holds merely for small scattering rate Γ and β takes negative values in a wide range of Γ. The calculations for ferromagnetic films of a few ML thickness have shown a strong dependence of β on the film thickness and the scattering rate, including oscillations and even leading to the change of its sign. The discrepancy between experimental values of β/α and the obtained large negative values of this ratio is discussed and possible explanations are given.

In each part of the present thesis, the obtained results are compared with predictions of other theoretical models, such as *ab initio* calculations and the spin pumping theory, as well as experimental reports.

In summary, the applied quantum-mechanical model and presented theoretical methods have proved to be efficient in investigating the relaxation of magnetisation in bulk and magnetic materials with layered structure. The theoretical description of the Gilbert damping, its distribution in real space and the nonadiabatic STT has been formulated within the TB model. Methods for faster and more accurate calculation of α and β, including the analytical expression for the involved integrals over energy, have been proposed and successfully applied. The results obtained for a variety of magnetic nanostructures have given a new insight into the mechanism of spin relaxation, and the Gilbert damping, in particular.

Appendix A

Derivatives of Fermi-Dirac function

The function $\eta(z) = -\frac{\partial f_{\mathrm{FD}}}{\partial z}$ and its derivatives enter the calculation of the Gilbert damping constant α through their appearance in the analytical expression for the factor $F_{nn'}(\boldsymbol{k})$ defined as the integral over energy in Eq. (2.102). Equation (2.136) presents a recursion relation for the derivatives of $\eta(z)$ of arbitrary order m.

The derivatives of the first, second and third order are given in Eq. (2.137). The $(m+1)$-th order derivative of $\eta(z)$ is expressed in terms of its derivatives of lower orders or the corresponding derivatives, of the Fermi-Dirac distribution function f_{FD},

$$\eta' = \frac{d\eta(z)}{dz} = -\frac{\partial^2 f_{\mathrm{FD}}}{\partial z^2}, \qquad \ldots, \quad \eta^{(m)} = \frac{d^m \eta(z)}{dz^m} = -\frac{\partial^{m+1} f_{\mathrm{FD}}}{\partial z^{m+1}}. \tag{A.1}$$

The obtained expressions for all the derivatives $\eta^{(m)}$ up to the order $m = 10$ are listed below.

$$
\begin{aligned}
\eta &= -f_{\mathrm{FD}}' = \beta f_{\mathrm{FD}}\left(1 - f_{\mathrm{FD}}\right) = -\beta\eta\left(1 - f_{\mathrm{FD}}\right), \\
\eta' &= -f_{\mathrm{FD}}'' = -\beta\eta\left(1 - 2f_{\mathrm{FD}}\right), \\
\eta'' &= -f_{\mathrm{FD}}^{(3)} = \beta\left(-2\eta^2 + (1 - 2f_{\mathrm{FD}})f_{\mathrm{FD}}''\right) = -\beta\left(-2\eta^2 + (1 - 2f_{\mathrm{FD}})\eta'\right), \\
\eta^{(3)} &= -f_{\mathrm{FD}}^{(4)} = \beta\left(6\eta f_{\mathrm{FD}}'' + (1 - 2f_{\mathrm{FD}})f_{\mathrm{FD}}^{(3)}\right) = -\beta\left(6\eta\eta' + (1 - 2f_{\mathrm{FD}})\eta''\right), \\
\eta^{(4)} &= -f_{\mathrm{FD}}^{(5)} = \beta\left(-6(f_{\mathrm{FD}}'')^2 + 8\eta f_{\mathrm{FD}}^{(3)} + (1 - 2f_{\mathrm{FD}})f_{\mathrm{FD}}^{(4)}\right) = -\beta\left(6\eta'^2 + 8\eta\eta'' + (1 - 2f_{\mathrm{FD}})\eta^{(3)}\right), \\
\eta^{(5)} &= -f_{\mathrm{FD}}^{(6)} = \beta\left(-20 f_{\mathrm{FD}}'' f_{\mathrm{FD}}^{(3)} + 10\eta f_{\mathrm{FD}}^{(4)} + (1 - 2f_{\mathrm{FD}})f_{\mathrm{FD}}^{(5)}\right) \\
&= -\beta\left(20\eta\eta'' + 10\eta\eta^{(3)} + (1 - 2f_{\mathrm{FD}})\eta^{(4)}\right), \\
\eta^{(6)} &= -f_{\mathrm{FD}}^{(7)} = \beta\left(-20(f_{\mathrm{FD}}^{(3)})^2 - 30 f_{\mathrm{FD}}'' f_{\mathrm{FD}}^{(4)} + 12\eta' f_{\mathrm{FD}}^{(5)} + f_{\mathrm{FD}}^{(6)} + (1 - 2f_{\mathrm{FD}})f_{\mathrm{FD}}^{(6)}\right) \\
&= -\beta\left(20\eta'\eta'' + 30\eta'\eta^{(3)} + 12\eta\eta^{(4)} + (1 - 2f_{\mathrm{FD}})\eta^{(5)}\right), \\
\eta^{(7)} &= -f_{\mathrm{FD}}^{(8)} = -\beta\left(70\eta^{(2)}\eta^{(3)} + 42\eta'\eta^{(4)} + 14\eta\eta^{(5)} + (1 - 2f_{\mathrm{FD}})\eta^{(6)}\right),
\end{aligned}
$$

$$\eta^{(8)} \;=\; -f_{\mathrm{FD}}^{(9)} = -\beta\left(70(\eta^{(3)})^2 + 12\eta''\eta^{(4)} + 56\eta'\eta^{(5)} + 16\eta\eta^{(6)} + (1 - 2f_{\mathrm{FD}})\eta^{(7)}\right),$$

$$\eta^{(9)} \;=\; -f_{\mathrm{FD}}^{(10)} = -\beta\left(252\eta^{(3)}\eta^{(4)} + 168\eta''\eta^{(5)} + 72\eta'\eta^{(6)} + 18\eta\eta^{(7)} + (1 - 2f_{\mathrm{FD}})\eta^{(8)}\right),$$

$$\eta^{(10)} \;=\; -f_{\mathrm{FD}}^{(11)} = -\beta\left(252(\eta^{(4)})^2 + 420\eta^{(3)}\eta^{(5)} + 420\eta''\eta^{(6)} + 90\eta'\eta^{(7)} + 20\eta\eta^{(8)} + (1 - 2f_{\mathrm{FD}})\eta^{(9)}\right).$$

$$(\mathrm{A.2})$$

Appendix B

Dynamical magnetic susceptibility: relation with spin-orbit torque correlation function

In section 2.3, the Gilbert damping constant $\alpha = \frac{\omega_2(\boldsymbol{q}=0)}{\omega_1(\boldsymbol{q}=0)}$ is expressed with the real and imaginary parts of the spin-wave energy $\omega(\boldsymbol{q}) = \omega_1 - i\omega_2$ determined as the pole of the transverse dynamical magnetic susceptibility $\chi_\perp(\boldsymbol{q}, \omega)$ at $\boldsymbol{q} = 0$ (corresponding to uniform precession of magnetisation). This is done by starting from the relation (2.19) for $\chi_\perp(\omega) = \chi_\perp(\boldsymbol{q} = 0, \omega)$ which includes the correlation function $\chi_A(\omega)$ of the SO torque $A^- = [S^-, H_{\mathrm{SO}}]$. This relation, given for arbitrary $\boldsymbol{q}$ in Ref. [61], can be derived following the general method introduced by Edwards and Fisher [114] and based on the equation of motion for the spin operator $S^-(t)$ in the Heisenberg representation.

Making use of the definition of the susceptibility, Eqs. (2.17), (2.18), one obtains

$$
\begin{aligned}
\chi(\boldsymbol{q}, \omega) &= \frac{i}{\hbar} \int_0^\infty dt \, \langle [S_{\boldsymbol{q}}^-(t), S_{-\boldsymbol{q}}^+(0)] \rangle \, e^{-i\omega_- t} \\
&= \frac{i}{\hbar} \int_0^\infty dt \, \langle [S_{\boldsymbol{q}}^-(t), S_{-\boldsymbol{q}}^+(0)] \rangle \, (\frac{-1}{i\omega_-}) \frac{d}{dt} \, e^{-i\omega_- t} \\
&= \frac{-1}{\hbar\omega_-} \int_0^\infty dt \, \langle [S_{\boldsymbol{q}}^-(t), S_{-\boldsymbol{q}}^+(0)] \rangle \, \frac{d}{dt} \, e^{-i\omega_- t}.
\end{aligned}
\tag{B.1}
$$

where $\omega_- = \omega - i\eta$ with $\eta \to 0^+$. The latter integral in Eq. (B.1) can be calculated, with

integration by parts, as follows

$$
\begin{aligned}
\chi(\boldsymbol{q},\omega) &= \frac{-1}{\hbar\omega_-}\left(\langle[S_{\boldsymbol{q}}^-(t),S_{-\boldsymbol{q}}^+]\rangle\, e^{-i(\omega-i\eta)t}|_0^\infty - \int_0^\infty dt\,\langle[\frac{dS_{\boldsymbol{q}}^-(t)}{dt},S_{-\boldsymbol{q}}^+]\rangle\, e^{-i\omega_- t}\right) \\
&= \frac{-1}{\hbar\omega_-}\left(0 - \langle[S_{\boldsymbol{q}}^-,S_{-\boldsymbol{q}}^+]\rangle - \int_0^\infty dt\,\langle[\frac{dS_{\boldsymbol{q}}^-(t)}{dt},S_{-\boldsymbol{q}}^+]\rangle\, e^{-i\omega_- t}\right).
\end{aligned}
\tag{B.2}
$$

Note that, the argument (0) is skipped in $S_{-\boldsymbol{q}}^+(0)$ (and similar operators in this section) since at $t=0$ the operator $S_{-\boldsymbol{q}}^+(t)$ is equal to the original, time-independent, operator $S_{-\boldsymbol{q}}^+$ used in the Schrödinger representation. In the next step one can take advantage of the Heisenberg equation of motion

$$
i\hbar\frac{dS_{\boldsymbol{q}}^-(t)}{dt} = [S_{\boldsymbol{q}}^-(t),H]
\tag{B.3}
$$

for the spin operator $S_{\boldsymbol{q}}^-(t) = e^{iHt/\hbar}S_{\boldsymbol{q}}^-\, e^{-iHt/\hbar}$. This leads us to

$$
\begin{aligned}
\chi(\boldsymbol{q},\omega) &= \frac{1}{\hbar\omega_-}\left(\langle[S_{\boldsymbol{q}}^-,S_{-\boldsymbol{q}}^+]\rangle + \frac{1}{i\hbar}\int_0^\infty dt\,\langle[[S_{\boldsymbol{q}}^-(t),H],S_{-\boldsymbol{q}}^+]\rangle\, e^{-i\omega_- t}\right) \\
&= \frac{1}{\hbar\omega_-}\left(-2\hbar\langle S_z\rangle + \frac{1}{i\hbar}\int_0^\infty dt\,\langle[C_{\boldsymbol{q}}^-(t),S_{-\boldsymbol{q}}^+] + [[S_{\boldsymbol{q}}^-(t),H_Z],S_{-\boldsymbol{q}}^+]\rangle\, e^{-i\omega_- t}\right)
\end{aligned}
\tag{B.4}
$$

where $C_{\boldsymbol{q}}^- = [S_{\boldsymbol{q}}^-,H_{\text{kin}}+H_{\text{SO}}]$. The first term in the right-hand side (RHS), the commutator $[S_{\boldsymbol{q}}^-,S_{-\boldsymbol{q}}^+]$, has been evaluated as follows

$$
\begin{aligned}
[S_{\boldsymbol{q}}^-,S_{-\boldsymbol{q}}^+] &= [\sum_n e^{i\boldsymbol{q}\cdot\boldsymbol{r}_n}S_n^-,\sum_n e^{i(-\boldsymbol{q})\cdot\boldsymbol{r}_n}S_n^+] \\
&= \sum_{n,n'} e^{i\boldsymbol{q}\cdot(\boldsymbol{r}_n-\boldsymbol{r}_{n'})}[S_n^-,S_{n'}^+]\delta_{n,n'} \\
&= \sum_n [S_n^-,S_n^+] = -2\hbar\sum_n S_n^z = -2\hbar S_z.
\end{aligned}
\tag{B.5}
$$

The integral in the RHS of Eq. (B.4) can be split into two parts, called χ_2 and χ_3, respectively. Thus, one is left with

$$
\chi(\boldsymbol{q},\omega) = \frac{-1}{\hbar\omega_-}\left(2\langle S_z\rangle + \chi_2 + \chi_3\right)
\tag{B.6}
$$

where

$$
\chi_2(\boldsymbol{q},\omega) = \frac{i}{\hbar}\int_0^\infty dt\,\langle[C_{\boldsymbol{q}}^-(t),S_{-\boldsymbol{q}}^+]\rangle\, e^{-i\omega_- t},
\tag{B.7}
$$

146

$$\chi_3(\boldsymbol{q},\omega) \quad = \quad \frac{i}{\hbar} \int_0^\infty dt \, \langle [[S_{\boldsymbol{q}}^-(t), H_{\mathrm{Z}}], S_{-\boldsymbol{q}}^+] \rangle \, e^{-i\omega_- t}. \tag{B.8}$$

Using the equation of motion for the operator $C_{\boldsymbol{q}}^-(t)$, in a similar way as it is done for $S_{\boldsymbol{q}}^-(t)$ in Eq. (B.2), one obtains

$$
\begin{aligned}
\chi_2(\boldsymbol{q},\omega) &= \frac{1}{\hbar\omega_-} \left(\langle [C_{\boldsymbol{q}}^-, S_{-\boldsymbol{q}}^+] \rangle + \frac{1}{i\hbar} \int_0^\infty dt \, \langle [[C_{\boldsymbol{q}}^-, H], S_{-\boldsymbol{q}}^+] \rangle \, e^{-i\omega_- t} \right) \\
&= \frac{1}{\hbar\omega_-} \left(\langle [C_{\boldsymbol{q}}^-, S_{-\boldsymbol{q}}^+] \rangle + \frac{1}{i\hbar} \int_0^\infty dt \, \langle [C_{\boldsymbol{q}}^-, [H, S_{-\boldsymbol{q}}^+]] \rangle \, e^{-i\omega_- t} \right)
\end{aligned} \tag{B.9}
$$

where the relation $[[C_{\boldsymbol{q}}^-(t), H], S_{-\boldsymbol{q}}^+] = [C_{\boldsymbol{q}}^-(t), [H, S_{-\boldsymbol{q}}^+]] - [[C_{\boldsymbol{q}}^-(t), S_{-\boldsymbol{q}}^+], H]$ has been used and it is taken into account that $\langle [X, H] \rangle$ vanishes for any operator X (in particular, it is equal to $\langle 0|XH - HX|0 \rangle = (E_0 - E_0)\langle 0|X|0 \rangle = 0$ at $T = 0$).

The second term in the RHS of Eq. (B.9) can be split into two parts, where the second part is nothing but χ_2 (up to a constant factor) since $[H, S_{-\boldsymbol{q}}^+] = C_{\boldsymbol{q}}^+ - 2\mu_{\mathrm{B}} B_{\mathrm{ext}} S_{-\boldsymbol{q}}^+$. Thus, one obtains

$$\chi_2 = \frac{1}{\hbar\omega_-} \left(\langle [C_{\boldsymbol{q}}^-, S_{-\boldsymbol{q}}^+] \rangle + \frac{1}{i\hbar} \left\{ \int_0^\infty dt \, \langle [C_{\boldsymbol{q}}^-(t), C_{\boldsymbol{q}}^+] \rangle \, e^{-i\omega_- t} - 2\mu_{\mathrm{B}} B_{\mathrm{ext}} \int_0^\infty dt \, \langle [C_{\boldsymbol{q}}^-(t), S_{\boldsymbol{q}}^+] \rangle \, e^{-i\omega_- t} \right\} \right) \tag{B.10}$$

which finally yields

$$\chi_2 \quad = \quad \frac{1}{\hbar\omega_-} \left(\langle C_{\boldsymbol{q}}^-(t), S_{-\boldsymbol{q}}^+ \rangle - \chi_C + 2\mu_{\mathrm{B}} B_{\mathrm{ext}} \chi_2 \right), \tag{B.11}$$

if the definition of χ_2 and

$$\chi_C = \frac{i}{\hbar} \int_0^\infty dt \, \langle [C_{\boldsymbol{q}}^-(t), C_{\boldsymbol{q}}^+] \rangle \, e^{-i\omega_- t} \tag{B.12}$$

are used. The latter is the correlation function for $C_{\boldsymbol{q}}^- = [S_{\boldsymbol{q}}^-, H_{\mathrm{kin}}] + A_{\boldsymbol{q}}^-$ where $A_{\boldsymbol{q}}^- = [S_{\boldsymbol{q}}^-, H_{\mathrm{SO}}]$ is the SO torque operator generalised to arbitrary $\boldsymbol{q}$. The relation (B.11) is a linear equation in terms of χ_2. Solving this linear equation for χ_2 leads to

$$\chi_2 = \frac{\langle [A_{\boldsymbol{q}}^-, S_{-\boldsymbol{q}}^+] \rangle - \chi_C(\boldsymbol{q}, \omega)}{\hbar(\omega_- - b_{\mathrm{ext}})} \tag{B.13}$$

where $b_{\mathrm{ext}} = \frac{2\mu_B B_{\mathrm{ext}}}{\hbar}$.

The next task is evaluation of χ_3 defined by Eq. (B.8). Solving this integral gives rise to

$$\chi_3 = -\hbar \, b_{\mathrm{ext}} \, \chi(\boldsymbol{q}, \omega). \tag{B.14}$$

Substituting this relation into Eq. (B.6) results in the following equation linear in $\chi(\boldsymbol{q}, \omega)$

$$\chi(\boldsymbol{q}, \omega) \;\; = \;\; \frac{-2\langle Sz \rangle}{\hbar\omega_-} - \frac{\chi_2}{\hbar\omega_-} + \frac{b_{\mathrm{ext}}}{\omega_-}\chi(\boldsymbol{q}, \omega) \tag{B.15}$$

where χ_2 is given by Eq. (B.13). After solving Eq. (B.15) for $\chi(q, \omega)$ one ends up with the formula

$$
\begin{aligned}
\chi(\boldsymbol{q}, \omega) \;\; &= \;\; \frac{-2\langle S_z \rangle}{\omega_- - b_{\mathrm{ext}}} + \frac{\chi_2}{\hbar(\omega_- - b_{\mathrm{ext}})} \\
&= \;\; \frac{-2\langle S_z \rangle}{\omega - b_{\mathrm{ext}}} + \frac{1}{\hbar^2(\omega - b_{\mathrm{ext}})^2}\big\{\chi_C(\boldsymbol{q}, \omega) - \langle[C_{\boldsymbol{q}}^-, S_{-\boldsymbol{q}}^+]\rangle\big\}
\end{aligned}
\tag{B.16}
$$

that is exactly Eq. (A.6) in Ref. [61]. In Eq. (B.16) the infinitesimally small η is dropped in ω_- which is correct for complex spin-wave frequencies $\omega = \omega_1 - i\omega_2$ with a finite imaginary part ω_2. In this way, one finds the expression (B.16) for the dynamical susceptibility whose poles, equal to the spin wave energies $\omega = \omega_1 - i\omega_2$ (complex if damping is present), can then be determined as shown for $\boldsymbol{q} = 0$ in Sec. 2.3. In the latter case, the formula (B.16) reduces to Eq. (2.19) where $\chi_A(\omega)$ replaces $\chi_C(\boldsymbol{q}, \omega)$ since the relation $[S_{\boldsymbol{q}}^-, H_{\mathrm{kin}}] = 0$, and consequently, $C_{\boldsymbol{q}}^- = A_{\boldsymbol{q}}^- = A^- = [S^-, H_{\mathrm{SO}}]$ hold for $\boldsymbol{q} = 0$.

Appendix C

Slater-Koster formulas for hopping integrals

As discussed in section 2.4.5 the expressions for the hopping integrals (interatomic matrix elements of the Hamiltonian) in terms of the two-centre SK parameters were formulated by Slater and Koster for s, p, d orbitals back in 1954 [122]. A method to obtain such expressions for arbitrary orbital numbers L, L' is reported in Ref. [124]. The general formula (2.79) for the hopping integral, for orbitals μ and ν centred at two atoms connected by the vector $\boldsymbol{R}$, includes the products of the two-centre SK parameters $T^{\sigma}_{LL'm'}$ and the function $F^{LL'm'}_{\mu\nu}(\theta_{\boldsymbol{R}}, \phi_{\boldsymbol{R}})$ dependent on the direction of $\boldsymbol{R}$. In the following, it is shown, in a few examples, how the angular dependence of the functions $F^{(LL'm')}_{\mu\nu}(\theta_{\boldsymbol{R}}, \phi_{\boldsymbol{R}})$ can be derived using the definition of the cubic harmonics and the explicit form of the coordinate transformation $\boldsymbol{r}_i = Q\,\boldsymbol{r}''_i$.

In particular, one immediately finds from Eq. (2.65) [with (x, y, z) and (x'', y'', z'') superseded by (x_i, y_i, z_i) and (x''_i, y''_i, z''_i), respectively], multiplied by $N_p/r_i = N_p/r''_i$ (see Eq. (2.60)), that

$$p_{x_i} = p_{x''_i} \cos\theta_{\boldsymbol{R}} \cos\phi_{\boldsymbol{R}} - p_{y''_i} \sin\phi_{\boldsymbol{R}} + p_{z''_i} \sin\theta_{\boldsymbol{R}} \cos\phi_{\boldsymbol{R}}, \qquad \text{(C.1a)}$$

$$p_{y_i} = p_{x''_i} \cos\theta_{\boldsymbol{R}} \sin\phi_{\boldsymbol{R}} - p_{y''_i} \cos\phi_{\boldsymbol{R}} + p_{z''_i} \sin\theta_{\boldsymbol{R}} \sin\phi_{\boldsymbol{R}}. \qquad \text{(C.1b)}$$

Thus, one obtains

$$
\begin{aligned}
\langle l0p_{x_1}\sigma|H^{\sigma}_{2c}|l'j'p_{x_2}\sigma\rangle &= \cos^2\theta_{\boldsymbol{R}} \cos^2\phi_{\boldsymbol{R}} \langle l0p_{x''_1}\sigma|H^{\sigma}_{2c}|l'j'p_{x''_2}\sigma\rangle \\
&+ \sin^2\phi_{\boldsymbol{R}} \langle l0p_{y''_1}\sigma|H^{\sigma}_{2c}|l'j'p_{y''_2}\sigma\rangle \\
&+ \sin^2\theta_{\boldsymbol{R}} \cos^2\phi_{\boldsymbol{R}} \langle l0p_{z''_1}\sigma|H^{\sigma}_{2c}|l'j'p_{z''_2}\sigma\rangle \qquad \text{(C.2)}
\end{aligned}
$$

since other terms, involving pairs of orbitals like $p_{x''_1}, p_{y''_2}$ or $p_{y''_1}, p_{z''_2}$, vanish due to symmetry. For

instance for the first of these orbital pairs the integrand function is proportional to $x_1'' y_2'' = x_1'' y_1''$ (as $y_2'' = y_1''$) so that it is antisymmetrical in x_1'' (and also in y_1'') which implies the integral over x_1'' vanishes. Note that $H_{2c}^\sigma = H_{2c}^\sigma(\rho_1'', z_1'')$ remains unchanged if x_1'' is replaced with $-x_1''$. Further, it can be easily shown that the matrix elements $\langle l0p_{x_1''}\sigma|H_{2c}|l'j'p_{x_2''}\sigma\rangle$ and $\langle l0p_{y_1''}\sigma|H_{2c}|l'j'p_{y_2''}\sigma\rangle$ are equal to each other, each of them is equal to

$$|C_\mu^1|^2 \, T_{111}^\sigma + |C_\mu^{-1}|^2 \, T_{11,-1}^\sigma = \left(|C_\mu^1|^2 + |C_\mu^{-1}|^2\right) T_{111}^\sigma = 1 \cdot T_{pp\pi}^\sigma = T_{pp\pi}^\sigma \qquad (C.3)$$

if the orbitals $p_{x_i''}$ and $p_{y_i''}$ $(i = 1, 2)$ are represented in spherical harmonics and the relation

$$T_{11,-1}^\sigma = T_{111}^\sigma = T_{pp\pi}^\sigma \qquad (C.4)$$

is taken into account. The relation $\langle l0p_{z_1''}\sigma|H_{2c}^\sigma|l'j'p_{z_2''}\sigma\rangle = T_{pp\sigma}^\sigma$ also holds. Finally, within the applied two-centre approximation for the one-electron Hamiltonian (its non-relativistic part, without H_{SO}) $H_0^\sigma \approx H_{2c}^\sigma$, one finds

$$
\begin{aligned}
\langle l0p_{x_1}\sigma|H_0^\sigma|l'j'p_{x_2}\sigma\rangle &= \left(\cos^2\theta_{\boldsymbol{R}}\cos^2\phi_{\boldsymbol{R}} + \sin^2\phi_{\boldsymbol{R}}\right) T_{pp\pi} + \sin^2\theta_{\boldsymbol{R}}\cos^2\phi_{\boldsymbol{R}} T_{pp\sigma} \\
&= \left(\cos^2\phi_{\boldsymbol{R}} - \sin^2\theta_{\boldsymbol{R}}\cos^2\phi_{\boldsymbol{R}} + \sin^2\phi_{\boldsymbol{R}}\right) T_{pp\pi} + \left(\sin\theta_{\boldsymbol{R}}\cos\phi_{\boldsymbol{R}}\right)^2 T_{pp\sigma} \\
&= \alpha_x^2 \, T_{pp\sigma} + \left(1 - \alpha_x^2\right) T_{pp\pi} \qquad (C.5)
\end{aligned}
$$

where the definitions of the directional cosines $\alpha_x = \sin\theta_{\boldsymbol{R}}\cos\phi_{\boldsymbol{R}}$, $\alpha_y = \sin\theta_{\boldsymbol{R}}\sin\phi_{\boldsymbol{R}}$, $\alpha_z = \cos\theta_{\boldsymbol{R}}$ of the interatomic vector $\boldsymbol{R}$ are used. In a similar way, one can show that

$$
\begin{aligned}
\langle l0p_{x_1}\sigma|H_{2c}^\sigma|l'j'p_{y_2}\sigma\rangle &= \cos^2\theta_{\boldsymbol{R}}\cos\phi_{\boldsymbol{R}}\sin\phi_{\boldsymbol{R}} \, \langle l0p_{x_1''}\sigma|H_{2c}^\sigma|l'j'p_{x_2''}\sigma\rangle \\
&\quad - \cos\phi_{\boldsymbol{R}}\sin\phi_{\boldsymbol{R}} \, \langle l0p_{y_1''}\sigma|H_{2c}^\sigma|l'j'p_{y_2''}\sigma\rangle \\
&\quad + \sin^2\theta_{\boldsymbol{R}}\cos\phi_{\boldsymbol{R}}\sin\phi_{\boldsymbol{R}} \, \langle l0p_{z_1''}\sigma|H_{2c}^\sigma|l'j'p_{z_2''}\sigma\rangle \\
&= \left(1 - \sin^2\theta_{\boldsymbol{R}}\right)\cos\phi_{\boldsymbol{R}}\sin\phi_{\boldsymbol{R}} \, T_{pp\pi}^\sigma \\
&\quad - \cos\phi_{\boldsymbol{R}}\sin\phi_{\boldsymbol{R}} \, T_{pp\pi}^\sigma \\
&\quad + \sin^2\theta_{\boldsymbol{R}}\cos\phi_{\boldsymbol{R}}\sin\phi_{\boldsymbol{R}} \, T_{pp\sigma}^\sigma \\
&= \alpha_x\alpha_y\left(T_{pp\sigma}^\sigma - T_{pp\pi}^\sigma\right). \qquad (C.6)
\end{aligned}
$$

It is also possible to use this method for matrix elements between d orbitals though the

derivation is more cumbersome. For instance, one can show that

$$
\begin{aligned}
d_{yz} = \frac{N_d}{r^2} yz \;\; = \;\; & \frac{N_d}{r''^2} \big[\, (z''^2 - x''^2) \cos\theta_{\boldsymbol{R}} \sin\theta_{\boldsymbol{R}} \sin\phi_{\boldsymbol{R}} - x''y'' \sin\theta_{\boldsymbol{R}} \cos\phi_{\boldsymbol{R}} \\
& + z''x''(\cos^2\theta_{\boldsymbol{R}} - \sin^2\theta_{\boldsymbol{R}}) \sin\phi_{\boldsymbol{R}} + y''z'' \cos\theta_{\boldsymbol{R}} \cos\phi_{\boldsymbol{R}} \,\big] \\
= \;\; & \sqrt{3}\, d''_{3z^2-r^2}\, \alpha_y \alpha_z - d''_{x^2-y^2}\, \alpha_y \alpha_z - d''_{xy} \alpha_x \\
& - d''_{zx} \left(\cos^2\theta_{\boldsymbol{R}} - \sin^2\theta_{\boldsymbol{R}} \right) \sin\phi_{\boldsymbol{R}} + d''_{yz} \cos\theta_{\boldsymbol{R}} \cos\phi_{\boldsymbol{R}} \quad\quad (C.7)
\end{aligned}
$$

where the definition of cubic harmonics in the rotated frames $x''_i y''_i z''_i$ is used. These harmonics are denoted as d''_μ for short (with index $i = 1, 2$ skipped and $''$ shifted to superscript). With such representation of d_{yz} and using the symmetry properties of the orbitals d''_μ under the translations: $x''_1 \to -x''_1$ and $y''_1 \to -y''_1$, one can find the following expression

$$
\begin{aligned}
\langle l 0 d_{yz} \sigma | H_0^\sigma | l' j' d_{yz} \sigma \rangle \;\; = \;\; & 3\, \alpha_y^2 \alpha_z^2\, T_{dd\sigma}^\sigma + \left(\alpha_y^2 \alpha_z^2 + \alpha_x \right) T_{dd\delta}^\sigma \\
& + \big[\, \left(\cos^2\theta_{\boldsymbol{R}} - \sin^2\theta_{\boldsymbol{R}} \right)^2 \sin^2\phi_{\boldsymbol{R}} + \cos^2\theta_{\boldsymbol{R}} \cos^2\phi_{\boldsymbol{R}} \big]\, T_{dd\pi}^\sigma \\
= \;\; & 3\, \alpha_y^2 \alpha_z^2\, T_{dd\sigma}^\sigma + \left(\alpha_y^2 + \alpha_z^2 - 4\alpha_y^2 \alpha_z^2 \right) T_{dd\pi}^\sigma + \left(\alpha_x^2 + \alpha_y^2 \alpha_z^2 \right) T_{dd\delta}^\sigma . \;\; (C.8)
\end{aligned}
$$

These three derived exemplary formulas for the matrix elements of Hamiltonian coincide with the ones given in Ref. [122]. Thus, here it has been shown how the well-known hopping integrals can be derived in a direct way based on the transformation of coordinates and the explicit forms of orbitals given by cubic harmonics.

Appendix D

Mirror symmetry in spin space

In the following it is shown how to find the operator R_s which acts, in the spin space, on spin operators S_x, S_y, S_z of an electron spin states in the same way as the reflection operator $R : (x, y, z) \to (x, y, -z)$ acts in the configurational space. Spin $\boldsymbol{S} = (S_x,\, S_y,\, S_z)$ is an angular momentum which has to transform as a pseudovector under symmetry operations. Therefore, the quantum operator $\boldsymbol{S} = (S_x,\, S_y,\, S_z)$ should be transformed to $(-S_x,\, -S_y, S_z)$ under the unitary operator R_s (in the spin space) corresponding to the operator R of the mirror symmetry (in the configurational space). Thus, in particular one obtains

$$R_\mathrm{s} S_x R_\mathrm{s}^{-1} \;=\; -S_x \,, \tag{D.1a}$$

$$R_\mathrm{s} S_y R_\mathrm{s}^{-1} \;=\; -S_y \,, \tag{D.1b}$$

$$R_\mathrm{s} S_z R_\mathrm{s}^{-1} \;=\; S_z \,. \tag{D.1c}$$

By acting with R_s on the following two equations

$$S_z |\uparrow\rangle \;=\; \frac{1}{2} |\uparrow\rangle \,, \tag{D.2a}$$

$$S_z |\downarrow\rangle \;=\; -\frac{1}{2} |\downarrow\rangle \,, \tag{D.2b}$$

which define the spin-up and spin-down basis states, and subsequently using Eq. (D.1b), i.e. $R_\mathrm{s} S_z = S_z R_\mathrm{s}$, one finds

$$S_z (R_\mathrm{s} |\uparrow\rangle) \;=\; \frac{1}{2} (R_\mathrm{s} |\uparrow\rangle) \,, \tag{D.3a}$$

$$S_z (R_\mathrm{s} |\downarrow\rangle) \;=\; -\frac{1}{2} (R_\mathrm{s} |\downarrow\rangle) \,. \tag{D.3b}$$

Thus the states $R_\mathrm{s}|\uparrow\rangle$ and $R_\mathrm{s}|\downarrow\rangle$ are also eigenstates of S_z which implies that

$$R_\mathrm{s}|\uparrow\rangle \;=\; C_\uparrow|\uparrow\rangle\,, \tag{D.4a}$$

$$R_\mathrm{s}|\downarrow\rangle \;=\; C_\downarrow|\downarrow\rangle \tag{D.4b}$$

where $C_\uparrow$ and $C_\downarrow$ are two constants. With $S_x = \frac{1}{2}\sigma_x$ defined with the Pauli matrix σ_x one finds

$$S_x|\downarrow\rangle = \frac{1}{2}|\uparrow\rangle\,. \tag{D.5}$$

Acting on Eq. (D.4b) with S_x and using, consecutively, Eqs. (D.1), (D.4b) and (D.5) one readily finds $C_\uparrow + C_\downarrow = 0$. This gives rise to

$$R_\mathrm{s}|\uparrow\rangle = C|\uparrow\rangle\,, \tag{D.6a}$$

$$R_\mathrm{s}|\downarrow\rangle = -C|\downarrow\rangle\,. \tag{D.6b}$$

From Eq. (D.6a) one obtains

$$\langle\uparrow|R_\mathrm{s}^\dagger R_\mathrm{s}|\uparrow\rangle = CC^*\langle\uparrow|\uparrow\rangle \tag{D.7}$$

which leads to $|C| = 1$ because R_s is an unitary operator ($R^{-1}R^\dagger = 1$). Thus, relations (D.6a) and (D.6b) with $|C| = 1$ define R_s up to an phase factor $C = e^{i\varphi}$. Its phase cannot be determined uniquely since for any ϕ the operator R_s defined in Eq. (D.6a) and (D.6b) satisfies the transformation rules of the spin operators, Eqs. (D.1a) and (D.1b), which were the starting point, as the only condition imposed on R_s. In fact we can choose $C = e^{i\varphi}$ arbitrarily, e.g., $C = 1$ so that $R_\mathrm{s}|\uparrow\rangle = |\uparrow\rangle$ and $R_\mathrm{s}|\downarrow\rangle = -|\downarrow\rangle$. This defines the action of R_s on the spin basis states and means that $R_\mathrm{s} = 2S_z = \sigma_z$ as it was assumed in Sec 4.2. Accordingly, the total mirror symmetry operator, acting in both configurational and spin spaces has the form $Q = R_\mathrm{s}R = \sigma_z R$.

Bibliography

[1] G. E. Uhlenbeck and S. Goudsmit, Naturwissenschaften **47**, 95 (1925).

[2] W. Gerlach, O. Stern, Zeitschrift für Physik **9**, 353 (1922).

[3] S. A. Wolf, Science **294**, 5546 (2001).

[4] A. Brataas, A. D. Kent, and H. Ohno, Nat. Mat. **11**, 372 (2012).

[5] M. H. D. Guimarães, A. Veligura , P. J. Zomer , T. Maassen , I. J. Vera-Marun , N. Tombros , and B. J. van Wees, Nano Lett. **12** (7), 3512 (2012).

[6] Y. Tserkovnyak, A. Brataas, and G. E. W. Bauer, Phys. Rev. Lett., **88**, 117601 (2002).

[7] Y. Tserkovnyak, A. Brataas, and G. E. W. Bauer, Phys. Rev. B **66**, 224403 (2002).

[8] T. L. Gilbert, Phys. Rev. **100**, 1243 (1955).

[9] T. L. Gilbert, IEEE Trans. Mag. **40**, 3443 (2004).

[10] S. Mizukami, Y. Ando, T. Miyazaki, Phys. Rev. B **66**, 104413 (2002).

[11] X. R. Wang, P. Yan, J. Lu, and C. He, Annals of Physics **324**, 1815 (2009).

[12] S. S. P. Parkin, M. Hayashi, and L. Thomas, Science **320**, 190 (2008).

[13] V. E. Demidov, S. Urazhdin, H. Ulrichs, V. Tiberkevich, A. Slavin, D. Baither, G. Schmitz, and S. O. Demokritov, Nature Mater. **11**, 1028 (2012).

[14] X. G. Luo, X. H. Chen, X. Liu, R. T. Wang, Y. M. Xiong, C. H. Wang, G. Y. Wang, and X. G. Qiu, Phys. Rev. B **70**, 054520 (2004).

[15] P. Grünberg, R. Schreiber, Y. Pang, M. B. Brodsky, and H. Sowers, Phys. Rev. Lett. **57**, 2442 (1986).

[16] A. Fert, F. Nguyen Van Dau, F. Petroff, P. Etienne, G. Creuzet, A. Friederich, J. Chazelas, Phys. Rev. Lett. **61** (21), 2472 (1988).

[17] G. Binasch, P. Grünberg, F. Saurenbach, W. Zinn, Phys. Rev. B **39** (7) 4828 (1989).

[18] R. E. Camley, and J. Barnaś, Phys. Rev. Lett. **63** (6), 664 (1989).

[19] J. Barnaś and P. Grünberg, J. Magn. Magn. Mat. **82**, 186 (1989).

[20] J. Barnaś and A. Fert, Phys. Rev. Lett. **80**, 1058 (1998).

[21] P. Bruno and C. Chappert, Phys. Rev. Lett. **67**, 1602 (1991).

[22] P. J. H. Bloemen, H. W. van Kesteren, H. J. M. Swagten, and W. J. M. de Jonge, Phys. Rev. B **50**, 13505 (1994).

[23] M. Tsoi, A. G. M. Jansen, J. Bass, W.-C. Chiang, M. Seck, V. Tsoi, and P. Wyder, Phys. Rev. Lett. **80**, 4281 (1998).

[24] E. B. Myers, D. C. Ralph, J. A. Katine, R. N. Louie, and R. A. Buhrman, Science **285**, 867 (1999).

[25] W. P. Pratt, Jr., S.-F. Lee, J. M. Slaughter, R. Loloee, P. A. Schroeder, and J. Bass, Phys. Rev. Lett. **66**, 3060 (1991).

[26] S. S. P. Parkin, Z. G. Li, and David J. Smith, Appl. Phys. Lett. **58**, 2710 (1991).

[27] E. E. Fullerton, M. J. Conover, J. E. Mattson, C. H. Sowers, and S. D. Bader, Appl. Phys. Lett. **63**, 1699 (1993).

[28] M. Jullière, Phys. Lett. **54A**, 225 (1975).

[29] S. Ikeda, J. Hayakawa, Y. Ashizawa, Y. M. Lee, K. Miura, H. Hasegawa, M. Tsunoda, F. Matsukura and H. Ohno, Appl. Phys. Lett. **93** (8), 0825 (2008).

[30] J. Mathon and A. Umerski, Phys. Rev. B **63**, 220403(R) (2001).

[31] J. Majewski,"*Basics of Spintronics: From Metallic to All-Semiconductor Magnetic Tunnel Junctions*" in Condensed Matter Physics in the Prime of the 21st Century, 159 (World Scientific Publishing, 2015).

[32] P. F. Carcia, A. D. Meinhaldt and A. Suna, Appl. Phys. Lett. **47**, 178 (1985).

[33] H. J. G. Draaisma, W. J. M. de Jonge and F. J. A. den Broeder, J. Magn. Magn. Mat. **66**, 351 (1987).

[34] F. J. A. den Broeder, D. Kuiper, A. P. van de Mosselaer and W. Hoving, Phys. Rev. Lett. **60**, 2769 (1988).

[35] P. F. Carcia, J. Appl. Phys. **63**, 5066 (1988).

[36] T. Sugimoto, T. Katayama, Y. Suzuki and Y. Nishihara, Jpn. J. Appl. Phys. **28**, L2333 (1989).

[37] W. Platow, A. N. Anisimov, G. L. Dunifer, M. Farle, and K. Baberschke, Phys. Rev. B **58**, 5611 (1998).

[38] S. Mizukami, F. Wu, A. Sakuma, J. Walowski, D. Watanabe, T. Kubota, X. Zhang, H. Naganuma, M. Oogane, Y. Ando, and T. Miyazaki, Phys. Rev. Lett. **106**, 117201 (2011).

[39] Th. Gerrits, M. L. Schneider, and T. J. Silva, J. Appl. Phys. **99**, 023901 (2006).

[40] D. Weller, Y. Wu, J. Stöhr, M. G. Samant, B. D. Hermsmeier, and C. Chappert, Phys. Rev. B **49**, 12888 (1994).

[41] S. Uba, L. Uba, A. N. Yaresko, A. Ya. Perlov, V. N. Antonov, and R. Gontarz, Phys. Rev. B **53**, 6526 (1996).

[42] B. Hu, N. Amos, Y. Tian, J. Butler, D. Litvinov, S. Khizroev, J. Appl. Phys. **109**, 034314 (2011).

[43] S. X. Wang and G. Li, IEEE Trans. Magn. **44**, 1687 (2008).

[44] V. Kamberský, Czechoslovak Journal of Physics, Section **26**, 1366 (1976).

[45] L. Berger, Phys. Rev. B **54**, 9353 (1996).

[46] R. Arias and D. L. Mills, Phys. Rev. B **60**, (1999) 7395; J. Appl. Phys. **87**, 5455 (2000).

[47] P. Landeros, R. E. Arias, and D. L. Mills, Phys. Rev. B **77**, 214405 (2008).

[48] A. V. Nazarov, D. Menard, J. J. Green, C. E. Patton, G. M. Argentina, and H. J. Van Hook, J. Appl. Phys. **94**, 7227 (2003).

[49] G. Woltersdorf and B. Heinrich, Phys. Rev. B **69**, 184417 (2004).

[50] R. Arias and D. L. Mills, Phys. Rev. B **60**, 7395 (1999).

[51] J-M. L. Beaujour, J. H. Lee, A. D. Kent, K. Krycka, and C-C. Kao, Phys. Rev. B **74**, 214405 (2006).

[52] S. J. Yuan, L. Sun, H. Sang, J. Du, and S. M. Zhou, Phys. Rev. B **68**, 134443 (2003).

[53] Y. Tserkovnyak, A. Brataas, G. E. W. Bauer, and B. I. Halperin, Rev. Mod. Phys. **77**, 1375 (2005).

[54] T. Yoshino, K. Ando, K. Harii, H. Nakayama, Y. Kajiwara, and E. Saitoh, Appl. Phys. Lett. **98**, 132503 (2011).

[55] M. Charilaou, K. Lenz, and W. Kuch, J. Magn. Magn. Mater. **322**, 2065 (2010).

[56] S. Mizukami, X. Zhang, T. Kubota, H. Naganuma, M. Oogane, Y. Ando, and T. Miyazaki, Appl. Phys. Express **4**, 013005 (2011).

[57] S. Mizukami, E. P. Sajitha, D. Watanabe, F. Wu, T. Miyazaki, H. Naganuma, M. Oogane, and Y. Ando, Appl. Phys. Lett. **96**, 152502 (2010).

[58] C. T. Boone, Hans T. Nembach, Justin M. Shaw, and T. J. Silva, J. Appl. Phys. **113**, 153906 (2013).

[59] M. Zwierzycki, Y. Tserkovnyak, P. J. Kelly, A. Brataas, and G. E. W. Bauer, Phys. Rev. B **71**, 064420 (2005).

[60] L. Landau, E. Lifshitz, Phys. Z. Sowjetunion **8**, 153 (1935).

[61] D. M. Edwards and O. Wessely, J. Phys.: Condens. Matter **21**, 146002 (2009).

[62] E. Barati, M. Cinal, D. M. Edwards, and A. Umerski, EPJ Web of Conferences **40**, 18003 (2013).

[63] J. Xiao, A. Zangwill, and M. D. Stiles, Phys. Rev. B **73**, 054428 (2006).

[64] S. E. Barnes and S. Maekawa, Phys. Rev. Lett. **95**, 107204 (2005).

[65] M. D. Stiles, W. M. Saslow, M. J. Donahue, and A. Zangwill, Phys. Rev. B **75**, 214423 (2007).

[66] M. Hayashi, L. Thomas, Ya B. Bazaliy, C. Rettner, R. Moriya, X. Jiang and S. S. P. Parkin, Phys. Rev. Lett. **96**, 197207 (2006).

[67] K. Gilmore, I. Garate, A. H. MacDonald, and M. D. Stiles, Phys. Rev. B **84**, 224412 (2011).

[68] I. Garate, K. Gilmore, M. D. Stiles, and A. H. MacDonald, Phys. Rev. B **79**, 104416 (2009).

[69] B. Heinrich, F. Cochran, and R. Hasegawa, J. Appl. Phys. **57**, 3590 (1985).

[70] J.-M. Beaujour, D. Ravelosona, I. Tudosa, E. E. Fullerton, and A. D. Kent, Phys. Rev. B **80**, 180415(R) (2009).

[71] H-S Song, K-D Lee, J-W Sohn, S-H Yang, S. S. P. Parkin, Ch-Y You, and S-Ch Shin, Appl. Phys. Lett. **102**, 102401 (2013).

[72] G. Malinowski, K. C. Kuiper, R. Lavrijsen, H. J. M. Swagten, and B. Koopmans, Appl. Phys. Lett. **94**, 102501 (2009).

[73] B. Heinrich, K. B. Urquhart, A. S. Arrott, J. F. Cochran, K. Myrtle, and S. T. Purcell, Phys. Rev. Lett. **59**, 1756 (1987); Z. Celinski and B. Heinrich, J. Appl. Phys. **70**, 5935 (1991).

[74] Kh. Zakeri, J. Lindner, I. Barsukov, R. Meckenstock, M. Farle, U. von Hörsten, H. Wende, W. Keune, J. Rocker, S. S. Kalarickal, K. Lenz, W. Kuch, K. Baberschke, and Z. Frait, Phys. Rev. B **76**, 104416 (2007).

[75] F. Schreiber, J. Pflaum, Z. Frait, Th. Mühge, and J. Pelzl, Solid State Commun. **93**, 965 (1995).

[76] A. Barman, S. Wang, O. Hellwig, A. Berger, E. E. Fullerton, and H. Schmidt, J. Appl. Phys. **101**, 09D102 (2007).

[77] P. He, X. Ma, J. W. Zhang, H. B. Zhao, G. Lüpke, Z. Shi, and S. M. Zhou, Phys. Rev. Lett. **110**, 077203 (2013).

[78] R. Urban, G. Woltersdorf, and B. Heinrich, Phys. Rev. Lett. **87**, 217204 (2001).

[79] S. Mizukami, T. Miyazaki, J. Magn. Magn. Mater. **226**, 1640 (2001).

[80] P. Lubitz, S. F. Cheng, and F. J. Rachford, J. Appl. Phys. **93**, 8283 (2003).

[81] J. Walowski, M. Djordjevic Kaufmann, B. Lenk, C. Hamann, J. McCord and M. Münzenberg, J. Phys. D: Appl. Phys. **41**, 164016 (2008).

[82] X. Liu, W. Zhang, M. J. Carter, and G. Xiao, J. Appl. Phys. **110**, 033910 (2011).

[83] V. Kamberský, Can. J. Phys., **48**, 2906 (1970).

[84] N. Nakabayashi, A. Takeuchi, K. Hosono, K.Taguchi, and G. Tatara, Phys. Rev. B **82**, 014403 (2010).

[85] A. T. Costa, R. B. Muniz, S. Lounis, A. B. Klautau, and D. L. Mills, Phys. Rev. B **82**, 014428 (2010).

[86] D. L. R. Santos, P. Venezuela, R. B. Muniz, and A. T. Costa, Phys. Rev. B **88**, 054423 (2013).

[87] I. Garate and A. MacDonald, Phys. Rev. B **79**, 064403 (2009); Phys. Rev. B **79**, 064404 (2009).

[88] K. Gilmore, Y. U. Idzerda, and M. D. Stiles, Phys. Rev. Lett. **99**, 027204 (2007).

[89] H. Ebert, S. Mankovsky, D. Ködderitzsch, and P. J. Kelly, Phys. Rev. Lett. **107**, 066603 (2011).

[90] S. Mankovsky, D. Ködderitzsch, G. Woltersdorf, and H. Ebert, Phys. Rev. B **87**, 014430 (2013).

[91] D. Thonig and J. Henk, New J. Phys. **16**, 013032 (2014).

[92] Ch. Liu, C. K. A. Mewes, M. Chshiev, T. Mewes, W. H. Butler, Appl. Phys. Lett. **95**, 022509 (2009).

[93] I. Barsukov, S. Mankovsky, A. Rubacheva, R. Meckenstock, D. Spoddig, J. Lindner, N. Melnichak, B. Krumme, S. I. Makarov, H. Wende, H. Ebert, and M. Farle, Phys. Rev. B **84**, 180405(R) (2011).

[94] E. Barati, M. Cinal, D. M. Edwards, and A. Umerski, Phys. Rev. B **90**, 014420 (2014).

[95] M. Cinal, D. M. Edwards, and J. Mathon, Phys. Rev. B **50**, 3754 (1994).

[96] S.-Y. Huang, D. Qu, and Ch.-L. Chien, in "*Recent Advances in Magnetic Insulators-From Spintronics to Microwave Applications*", Academic Press, Vol **64**, (2013).

[97] A. L. Smirl, M. J. Stevens, R. D. R. Bhat, A. Najmaie, J. E. Sipe, and H. M. van Driel, Semicond. Sci. Technol. **19**, S369 (2004).

[98] C. Heide, Phys. Rev. Lett. **87**, 197201 (2001).

[99] S. J. Lloyd, J. C. Loudon, and P. A. Midgley, J. Microsc. **207**, 118 (2002).

[100] M. Hayashi, L. Thomas, Ch. Rettner, R. Moriya, and S. S. P. Parkin, Nature Phys. **3**, 21 (2007).

[101] A. J. Schellekens, A. van den Brink, J. H. Franken, H. J. M. Swagten and B. Koopmans, Nature Commun. **3**, 847 (2012).

[102] Leonard I. Schiff, "*Quantum Mechanics*" (McGraw-Hill 1968).

[103] Z. Z. Sun and X. R. Wang, Phys. Rev. Lett. **97**, 077205 (2006).

[104] X. R. Wang and Z. Z. Sun, Phys. Rev. Lett. **98**, 077201 (2007).

[105] N. L. Schryer and L. R. Walker, J. Appl. Phys. **45**, 5406 (1974).

[106] Z. Li, S. Zhang, Phys. Rev. Lett. **92**, 207203 (2004).

[107] Z. Li, S. Zhang, Phys. Rev. Lett. **93**, 127204 (2004).

[108] D. A. Papaconstantopoulos and M. J. Mehl, J. Phys.: Condens. Matter **15**, R413 (2003).

[109] K. Shen, G. Tatara, and M. W. Wu, Phys. Rev. B **81**, 193201 (2010).

[110] J. M. Lock, Br. J. Appl. Phys. **17**, 1645 (1966).

[111] K. Lenz, H. Wende, W. Kuch, K. Baberschke, K. Nagy, and A. Janossy, Phys. Rev. B **73**, 144424 (2006).

[112] R. Marshall and S. U. Lovesey, "*Theory of Thermal Neutron Scattering: The Use of Neutrons for the Investigation of Condensed Matter (Monographs on Physics)*", Clarendon Press. Oxford (1971).

[113] D. M. Edwards, unpublished (2010).

[114] D. M. Edwards and B. Fisher, J. Physique **32**, C1 697 (1971).

[115] B. Velický, S. Kirkpatrick, and H. Ehrenreich, Phys. Rev. **175**, 747 (1968).

[116] V. Kamberský, Czechoslovak Journal of Physics, Section B **34**, 1111 (1984).

[117] C. Fiolhais, F. Nogueira, and M. Marques (Eds.), "*A Primer in Density Functional Theory*", Lecture notes in physics, vol. **620**, Springer, Berlin (2003).

[118] P. Hohenberg and W. Kohn, Phys. Rev. **136**, B864 (1964).

[119] W. Kohn and L. J. Sham, Phys. Rev. **140**, A1133 (1965).

[120] J. Korringa, Physica **XIII**, 392 (1947).

[121] W. Kohn and N. Rostoker, Phys. Rev. **94**, 1111 (1954).

[122] J. C. Slater and G. F. Koster, "*Simplified LCAO method for the Periodic Potential Problem*", Physical Review **94** (6), 1498 (1954).

[123] D. A. Papaconstantopoulos, "*Handbook of the Band Structure of Elemental Solids*" (Plenum Press, New York 1986).

[124] A. K. McMahan, Phys. Rev. B **58**, 4293 (1998).

[125] K. Takegahara, Y. Aoki, and A. Yanase, J. Phys. C: Solid St. Phys. **13**, 583 (1980).

[126] L. T. Thomas, Phil. Mag. **3**, 1 (1927).

[127] J. D. Jackson, "*Classical Electrodynamics*", second edition, John Wiley & Sons Inc. (1975).

[128] A. R. Mackintosh and O. K. Andersen, "*Electrons at Fermi surface*" (Cambridge university press, Cambridge 1980).

[129] M. Cinal and D. M. Edwards, Phys. Rev. B **55**, 3636 (1997).

[130] M. Gradhand, M. Czerner, D. V. Fedorov, P. Zahn, B. Yu. Yavorsky, L. Szunyogh, and I. Mertig, Phys. Rev. B **80**, 224413 (2009).

[131] J. Fabian and S. Das Sarma, Phys. Rev. Lett. **81**, 5624 (1998).

[132] M. Pickel, A. B. Schmidt, F. Giesen, J. Braun, J. Minár, H. Ebert, M. Donath, and M. Weinelt, Phys. Rev. Lett. **101**, 066402 (2008).

[133] E. Abate and M. Asdente, Phys. Rev. **140**, A1303 (1965).

[134] Ch. Li, A. J. Freeman, H. J. F. Jansen, and C. L. Fu, Phys. Rev. B **42**, 5433 (1990).

[135] P. E. Blöchl, O. Jepsen and O. K. Andersen, Phys. Rev. B **49**, 16223 (1994).

[136] M. Cinal and A. Umerski, Phys. Rev. B **73**, 184423 (2006).

[137] R. Haydock, Solid State Physics **35**, 215 (1980).

[138] V. Kamberský, Phys. Rev. B **76**, 134416 (2007).

[139] K. Gilmore, Y. U. Idzerda, and M. D. Stiles, J. Appl. Phys. **103**, 07D303 (2008).

[140] S. M. Bhagat and P. Lubitz, Phys. Rev. B **10**, 1974 (1974).

[141] S. Mizukami, Y. Ando, and T. Miyazaki, J. Magn. Magn. Mater. **239**, 42 (2002).

[142] E. Barati, M. Cinal, D. M. Edwards, and A. Umerski, in *Ultrafast Magnetism I - Proceedings of Ultrafast Magnetism Conference (UMC 2013), Strasbourg, France, October 28 - November 1, 2013*, Series: Springer Proceedings in Physics, Vol. 159, edited by J.-Y. Bigot, W. Hübner, T. Rasing and R. Chantrell, (Springer International Publishing, Cham, 2015).

[143] S. Fukami, T. Suzuki, N. Ohshima, K. Nagahara, and N. Ishiwata, J. Appl. Phys. **103** 07E718 (2008).

[144] D. M. Edwards, J. Mathon, R. B. Muniz, and M. S. Phan, J. Phys.: Condens. Matter **3**, 4941 (1991).

[145] S. S. P. Parkin, N. More, and K. P. Roche, Phys. Rev. Lett. **64**, 2304 (1990).

[146] M. Cinal and D. M. Edwards, Phys. Rev. B **57**, 100 (1998).

[147] J. Li, M. Przybylski, F. Yildiz, X.-D. Ma, and Y. Wu, Phys. Rev. Lett. **102**, 207206 (2009).

[148] L. Szunyogh, B. Újfalussy, and P. Weinberger, Phys. Rev. B **54**, 9883 (1996).

[149] M. Cinal, J. of Phys.: Condens. matter **15**, 29 (2003).

[150] U. Bauer, M. Dabrowski, M. Przybylski, and J. Kirschner, Phys. Rev. B **84**, 144433 (2011).

[151] M. Przybylski, M. Dabrowski, U. Bauer, M. Cinal, and J. Kirschner, J. Appl. Phys. **111**, 07C102 (2012).

[152] M. Cinal, A. Umerski, and D. M. Edwards, J. Inoue, Surf. Sci. **493**, 744 (2001).

[153] J. C. Slonczewski, J. Magn. Magn. Mater. **159**, L1 (1996).

[154] A. M. N. Niklasson, S. Mirbt, H. L. Skriver, and B. Johansson, Phys. Rev. B **56**, 3276 (1997).

[155] A. Ghosh, J. F. Sierra, S. Auffret, U. Ebels, and W. E. Bailey, Appl. Phys. Lett. **98**, 052508 (2011).

[156] A. Ghosh, S. Auffret, U. Ebels, and W. E. Bailey, Phys. Rev. Lett. **109**, 127202 (2012).

[157] P. J. Metaxas, J. P. Jamet, A. Mougin, M. Cormier, J. Ferré, V. Baltz, B. Rodmacq, B. Dieny, and R. L. Stamps, Phys. Rev. Lett. **99**, 217208 (2007).

[158] M. G. Samant, J. Stöhr, S. S. P. Parkin, G. A. Held, B. D. Hermsmeier, F. Herman, M. Van Schilfgaarde, L.-C. Duda, D. C. Mancini, N. Wassdahl, and R. Nakajima, Phys. Rev. Lett. **72**, 1112 (1994).

[159] R. Urban, B. Heinrich, and G. Woltersdorf, J. Appl. Phys. **93**, 8280 (2003).

[160] S. Mizukami, Y. Ando, and T. Miyazaki, Jpn. J. Appl. Phys. **40**, 580 (2001).

[161] J. Bass and W. P. Pratt Jr, J. Phys.: Condens. Matter **19**, 183201 (2007).

[162] S. Mizukami, S. Iihama, N. Inami, T. Hiratsuka, G. Kim, H. Naganuma, M. Oogane, and Y. Ando, Appl. Phys. Lett. **98**, 082501 (2011).

[163] S. Pal, B. Rana, O. Hellwig, T. Thomson, and A. Barman, Appl. Phys. Lett. **98**, 082501 (2011).

[164] S. Mizukami, X. Zhang, T. Kubota, H. Naganuma, M. Oogane, Y. Ando, and Terunobu Miyazaki, Appl. Phys. Express **4**, 013005 (2011).

[165] M. Haertinger, C. H. Back, S-H Yang, S. S. P. Parkin, and G. Woltersdorf, J. Phys. D: Appl. Phys. **46**, 175001 (2013).

[166] T. Kato, Y. Matsumoto, S. Kashima, S. Okamoto, N. Kikuchi, S. Iwata, O. Kitakami, and S. Tsunashima, IEEE Trans. Magn. **48**, 3288 (2012).

[167] K. Kondou, H. Sukegawa, S. Mitani, K. Tsukagoshi, and S. Kasai, Appl. Phys. Express **5**, 073002 (2012).

[168] L. S. E. Alvarez, K. Wang, S. Lepadatu, S. Landi, S. J. Bending, C. H. Marrows, Phys. Rev. Lett. **104**, 137205 (2010).

[169] M. Jamali, K.-J. Lee, and H. Yang, Appl. Phys. Lett. **98**, 092501 (2011).

[170] S. Urazhdin, V. E. Demidov, H. Ulrichs, T. Kendziorczyk, T. Kuhn, J. Leuthold, G. Wilde, and S. O. Demokritov, Nat. Nanotechnol. **9**, 509 (2014).

[171] M. Hayashi, L. Thomas, C. Rettner, R. Moriya, and S. S. P. Parkin, Appl. Phys. Lett. **92**, 162503 (2008).

[172] O. Boulle, G. Malinowski, M. Kläui, Mater. Sci. Eng. R **72**, 159 (2011).

[173] H. Ohno and T. Dietl, J. Magn. Magn. Mater. **320**, 1293 (2008).

[174] J.-P. Adam, N. Vernier, J. Ferré, A. Thiaville, V. Jeudy, A. Lemaître, L. Thevenard, and G. Faini, Phys. Rev. B **80**, 193204 (2009).

[175] I. M. Miron, P.-J. Zermatten, G. Gaudin, S. Auffret, B. Rodmacq, A. Schuhl, Phys. Rev. Lett. **102**, 137202 (2009).

[176] O. Boulle, J. Kimling, P. Warnicke, M. Kläui, U. Rüdiger, G. Malinowski, H.J.M. Swagten, B. Koopmans, C. Ulysse, G. Faini, Phys. Rev. Lett. **101**, 216601 (2008).

[177] C. Burrowes, A. P. Mihai, D. Ravelosona, J.-V. Kim, C. Chappert, L. Vila, A. Marty, Y. Samson, F. Garcia-Sanchez, L. D. Buda-Prejbeanu, I. Tudosa, E. E. Fullerton, and J.-P. Attané, Nature Phys. **6**, 17 (2010).

[178] M. Eltschka, M. Wötzel, J. Rhensius, S. Krzyk, U. Nowak, M. Kläui, T. Kasama, R. E. Dunin-Borkowski, L. J. Heyderman, H. J. van Driel, and R. A. Duine, Phys. Rev. Lett **105**, 056601 (2010).

[179] R. Moriya, L. Thomas, M. Hayashi, Y. B. Bazaliy, Ch. Rettner, and S. S. P. Parkin, Nature Phys. **4**, 368 (2008).

[180] E. Martinez, L. Lopez-Diaz, O. Alejos, and L. Torres, Phys. Rev. B **77**, 144417 (2008).

[181] L. Heyne, J. Rhensius, D. Ilgaz, A. Bisig, U. Rüdiger, M. Kläui, L. Joly, F. Nolting, L. J. Heyderman, J. U. Thiele, F. Kronast, Phys. Rev. Lett. **105**, 187203 (2010).

[182] H. Kohno, G. Tatara, and J. Shibata, Phys. Soc. Jap **75**, 113706 (2006).

[183] R. A. Duine, A. S. Núñez, J. Sinova, A. H. MacDonald, Phys. Rev. B **75**, 214420 (2007).

[184] Y. Tserkovnyak, H. J. Skadsem, A. Brataas, G. E. W. Bauer, Phys. Rev. B **74**, 144405 (2006).

[185] P. Baláž, V. K. Dugaev, and Barnaś, Phys. Rev. B **85**, 024416 (2012).

[186] K.-S. Ryu, L. Thomas, S.-H. Yang, and S. Parkin, Nat. Nanotechnol. **8**, 527 (2013).

[187] S. Emori, U. Bauer, S.-M. Ahn, E. Martinez, and G. S. D. Beach, Nat. Mat. **12**, 611 (2013).

[188] A. Thiaville, S. Rohart, É. Jué, V. Cros, and A. Fert, Europhys. Lett. **100**, 57002 (2012).

[189] C. Burrowes, A. P. Mihai, D. Ravelosona, J.-V. Kim, C. Chappert, L. Vila, A. Marty, Y. Samson, F. Garcia-Sanchez, L. D. Buda-Prejbeanu, I. Tudosa, E. E. Fullerton, and J.-P. Attané, Nat. Phys. **6**, 17 (2009).

[190] S. Lepadatu, M. C. Hickey, A. Potenza, H. Marchetto, T. R. Charlton, S. Langridge, S. S. Dhesi, and C. H. Marrows, Phys. Rev. B **79**, 094402 (2009).

[191] L. Tang, Zh. Xu, and Z. Yang, Int. J. Mod. Phys. B **27**, 1350092 (2013).